



**Control Analysis for Grid Tied Battery Energy  
Storage System for SOC and SOH Management**

**Burcu MANTAR GUNDOGDU**

A thesis submitted for the degree of

**DOCTOR OF PHILOSOPHY**

Department of Electronic and Electrical Engineering

The University of Sheffield, UK

**April 2019**

## Abstract

Frequency regulation is an important part of grid ancillary services in the UK power system to mitigate the impacts of variable energy resources and uncertainty of load on system frequency. The National Grid Electricity Transmission (NGET), the primary electricity transmission network operator in the UK, is introduced various frequency response services such as firm frequency response (FFR) and the new fast enhanced frequency response (EFR), which are designed to provide real-time response to deviations in the grid frequency. Flexible and fast response capabilities of battery energy storage systems (BESSs) make them an ideal choice to provide grid frequency regulation. This thesis presents control algorithms for a BESS to deliver a charge/discharge power output in response to deviations in the grid frequency with respect to the requisite service specifications, while managing the state-of-charge (SOC) of the BESS to optimize the availability of the system. Furthermore, this thesis investigates using the BESS in order to maximize triad avoidance benefit revenues while layering UK grid frequency response services. Using historical UK electricity prices, a balancing service scheduling approach is introduced to maximize energy arbitrage revenue by layering different types of grid balancing services, including EFR and FFR, throughout the day. Simulation results demonstrate that the proposed algorithm delivers both dynamic and non-dynamic FFR and also EFR to NGET required service specifications while generating arbitrage revenue as well as service availability payments in the balancing market. In this thesis, a new fast cycle counting method (CCM) considering the effect of current rate (C-rate), SOC and depth-of-discharge (DOD) on battery lifetime for grid-tied BESS is presented. The methodology provides an approximation for the number of battery charge-discharge cycles based on historical microcycling SOC data typical of BESS frequency regulation operation. The EFR and FFR algorithms are used for analysis. The obtained historical SOC data from the analysis are then considered as an input for evaluating the proposed CCM. Utilizing the Miner Rule's degradation analysis method, lifetime analysis based on battery cycling is also provided for a lithium-titanate (LTO) and lithium-nickel-manganese-cobalt-oxide (NMC) battery. The work in this thesis is supported by experimental results from the 2MW/1MWh Willenhall Energy Storage System (WESS) to validate the models and assess the accuracy of the simulation results.

## List of Publications

Parts of the work presented in this thesis have been enclosed in the following internationally-respected publications.

### Journal Publication

- [J1] **B. Gundogdu**, S. Nejad, D. T. Gladwin, M. P. Foster, and D. A. Stone, "A battery energy management strategy for U.K. enhanced frequency response and triad avoidance," *IEEE Trans. Ind. Electron.*, vol. 65, no. 12, pp. 9509-9517, Dec. 2018.
- [J2] **B. Gundogdu**, D. T. Gladwin, S. Nejad, M. P. Foster, and D. A. Stone, "Scheduling of grid tied battery energy storage system participating in frequency response services and energy arbitrage", *IET Gener. Transm. Dis.*, published, 26 Feb 2019.
- [J3] **B. Gundogdu**, D. T. Gladwin, and D. A. Stone, "Battery energy management strategies for UK firm frequency response service and energy arbitrage," in *IET J. Eng.* vol. 2019, no. 17, pp. 4152-4157, June 2019.

### Conference Proceedings

- [C1] **B. Gundogdu**, D. T. Gladwin, and D. A. Stone, "Battery energy management strategies for UK firm frequency response service and energy arbitrage," in *IET Int. Conf. Power Electron. Mach. Drives (PEMD'18)*, Liverpool, UK, 2018, pp. 1-6.
- [C2] **B. Gundogdu**, D. T. Gladwin, M. P. Foster, and D. A. Stone, "A forecasting battery state of charge management strategy for frequency response in the UK system," in *IEEE Int. Conf. Ind. Technol. (ICIT'18)*, Lyon, France, 2018, pp. 1726-1731.
- [C3] **B. Gundogdu** and D. T. Gladwin, "A fast battery cycle counting method for grid-tied battery energy storage system subjected to microcycles," in *IEEE Int. Elect. Eng. Cong. (iEECON'18)*, Krabi, Thailand, 2018, pp. 1-6.
- [C4] **B. Gundogdu** and D. T. Gladwin, "Bi-directional power control of grid-tied battery energy storage system operating in frequency regulation," in *IEEE Int. Elect. Eng. Cong. (iEECON'18)*, Krabi, Thailand, 2018, pp. 1-6. (Best Paper Awarded)
- [C5] **B. Gundogdu**, D. T. Gladwin, and D. A. Stone, "Battery SOC management strategy for enhanced frequency response and day-ahead energy scheduling of BESS for

energy arbitrage," in *IEEE Ind. Electron. Soc. Annu. Conf. (IECON'17)*, Beijing, China, 2017, pp. 7635-7640.

- [C6] **B. Gundogdu**, D. T. Gladwin, and D. A. Stone, "A battery energy management strategy for UK enhanced frequency response," in *IEEE Int. Symp. Ind. Electron. (ISIE'17)*, 2017, Edinburg, Scotland, pp. 1-6.

### **Manuscript in Preparation**

- [M1] **B. Gundogdu**, D. T. Gladwin, and D. A. Stone, "Battery lifetime analyses for large scale grid-tied battery energy storage system operating in frequency regulation," *IEEE Trans. Ind. Electron.*, (2019).

## **Acknowledgment**

With the sincerest gratitude in my heart, I would like to thank to my doctorate supervisor and truly dedicated mentor, Dr Daniel Thomas Gladwin, and my co-supervisor, Prof David Stone, for their patient guidance, continuous support, encouragement, technical advices, direction and constructive criticism throughout the course of my doctoral degree. I could not have imagined having a better advisor and mentor for my PhD study.

I would like to thank the Turkish Ministry of National Education for funding my PhD.

I would like to give my special thanks to my husband Dr Tayfun Gundogdu, who was my colleague in the University of Sheffield, for his endless love, moral support, encouragement, motivation, and great technical discussions throughout my PhD. He has been a true and great supporter in my general life. I would like to thank my family: my parents Mr Tahsin Mantar and Mrs Nilgun Mantar, and to my brother Mr Tayfun Mantar for their unconditional love, everlasting moral support and encouragement, without whom, this journey would have not been possible.

I would like to thank Dr Shahab Nejad, Prof Martin Foster and Mr Peter Barton for their encouragement and technical advices on my PhD. I wish to give my special thanks to Prof Zi-Qiang Zhu, who is my husband's PhD supervisor, for his kind encouragement, support and motivation during my PhD. I also thank to other academic members at The University of Sheffield who have blessed me with their technical and moral support throughout my research.

I would like to thank Dr Petrica Taras for his technical advices and great discussions on my PhD; and thanks to my colleagues and officemates in for the stimulating discussions and all the fun we have had in the last four years. I would like to thank all my friends, who created a positive environment for me to complete my PhD studies in. I also thank my colleagues, who have been a pleasure to work with during the four years in the Centre for Research into Electrical Energy Storage & Applications, CREESA.

Finally, I would like to thank Prof Guven Komurgoz Kiris and Prof Okan Ozgonenel for their kind encouragement and moral support throughout my PhD.

# Content

<b>Abstract.....</b>	<b>1</b>
<b>List of Publications .....</b>	<b>2</b>
<b>Acknowledgment.....</b>	<b>4</b>
<b>Nomenclature .....</b>	<b>12</b>
<b>Abbreviation.....</b>	<b>16</b>
<b>1 General Introduction.....</b>	<b>22</b>
<b>1.1 Thesis Organizations.....</b>	<b>22</b>
<b>1.2 Introduction .....</b>	<b>26</b>
<b>1.3 Energy Storage Systems (ESSs) .....</b>	<b>29</b>
1.3.1 Importance of Energy Storage in Power Systems.....	29
1.3.2 Classification of Energy Storage Technologies .....	30
1.3.3 ESS Applications used for Supporting Power System .....	35
<b>1.4 Battery Energy Storage Systems (BESSs).....</b>	<b>39</b>
1.4.1 Battery Terminologies .....	40
1.4.2 Types of Batteries .....	42
1.4.3 Functions of Grid Scale BESS for Grid Support .....	44

1.4.4	Some Examples of Installed Battery Energy Storage Systems in Power System	45
1.4.5	Grid-Tied Battery Energy Storage System Configuration	47
1.4.6	Battery Management System (BMS)	47
<b>1.5</b>	<b>Future of UK Power System and National Grid Product Strategies</b>	<b>51</b>
1.5.1	Comparison of Traditional and Future UK Power System	51
1.5.2	UK Grid Flexibility	54
1.5.3	Future UK Power System Needs	55
1.5.4	Future of National Grid Balancing Services Product Strategy Consultation – Implications for Energy Storage	58
<b>1.6</b>	<b>Grid Storage Services and Applications</b>	<b>61</b>
1.6.1	Frequency Response Services	61
1.6.2	Triad Avoidance	63
1.6.3	Energy Arbitrage	64
<b>1.7</b>	<b>Literature Review</b>	<b>65</b>
1.7.1	Frequency Regulation	65
1.7.2	Grid Storage Applications	66
1.7.3	Distributed Generation (DG) System	68
1.7.4	Energy Storage Systems (ESSs)	69
1.7.5	Battery Energy Storage Systems (BESSs)	70
1.7.6	Power Management & Energy Management System (EMS)	73
1.7.7	Battery Management System (BMS) and State-of-Charge (SOC) Estimation	74
1.7.8	Battery Lifetime Analyses	75

<b>2</b>	<b>Control of Grid Tied Battery Energy Storage System for Frequency Response Services.....</b>	<b>77</b>
<b>2.1</b>	<b>Introduction .....</b>	<b>77</b>
<b>2.2</b>	<b>BESS Control for Firm Frequency Response (FFR) Service.....</b>	<b>79</b>
2.2.1	BESS Control for Dynamic FFR Service with No Battery SOC Management ....	80
2.2.2	Simulation Results of the BESS Control for DFFR Service.....	84
2.2.3	BESS Control for Static FFR Service .....	86
2.2.4	Simulation Results of the BESS Control for SFFR Service .....	88
2.2.5	BESS Control for DFFR Service with Battery SOC Management.....	90
2.2.6	Simulation Results of the BESS Control for DFFR with SOC Management.....	95
<b>2.3</b>	<b>BESS Control for Pre-Enhanced Frequency Response (Pre-EFR) Service ....</b>	<b>101</b>
2.3.1	Pre-EFR Service Specifications .....	102
2.3.2	Pre-EFR Control Algorithm Design .....	103
2.3.3	Simulation Results of Pre-EFR Control Algorithm .....	105
<b>2.4</b>	<b>BESS Control for Enhanced Frequency Response (EFR) Service .....</b>	<b>113</b>
2.4.1	NGET required EFR Service Specifications.....	114
2.4.2	Standard EFR Control Algorithm (EFR-A1) Design.....	116
2.4.3	Advanced EFR Control Algorithms (EFR-A2 and EFR-A3) Design.....	121
2.4.4	Standard EFR Algorithm with SOC-based Proportional Control (EFR-A4).....	122
2.4.5	Simulation Results of the Standard EFR Control Algorithm (EFR-A1) .....	125
2.4.6	Simulation Results of the Advanced EFR Control Algorithm (EFR-A2) .....	129
2.4.7	Simulation Results of the Advanced EFR Control Algorithm (EFR-A3) .....	130



2.4.8	Simulation Results of the Standard EFR Control Algorithm with Proportional Control (EFR-A4).....	132
2.4.9	Analyses of Simulation Results of the all EFR Control Algorithms .....	138
<b>2.5</b>	<b>Conclusion.....</b>	<b>140</b>
<b>3</b>	<b>BESS Control for Grid Scale Energy Storage Applications through Frequency Response Services.....</b>	<b>143</b>
<b>3.1</b>	<b>Introduction .....</b>	<b>143</b>
<b>3.2</b>	<b>Triad Avoidance .....</b>	<b>148</b>
3.2.1	Triad Avoidance Strategy through EFR service .....	151
3.2.2	Simulation Results of the Triad Avoidance Strategy.....	152
<b>3.3</b>	<b>Energy Arbitrage.....</b>	<b>161</b>
3.3.1	Investigation of the General UK Electricity Price Pattern.....	161
3.3.2	Scheduling Approach of Grid Tied BESS Participating in Frequency Response for Energy Arbitrage.....	162
3.3.3	Simulation Results of the Scheduling Approach .....	165
<b>3.4</b>	<b>Conclusion.....</b>	<b>172</b>
<b>4</b>	<b>Willenhall Energy Storage System .....</b>	<b>173</b>
<b>4.1</b>	<b>WESS Control .....</b>	<b>175</b>
<b>4.2</b>	<b>WESS Design .....</b>	<b>178</b>
4.2.1	Battery Pack Information .....	179
4.2.2	Power Converter Control .....	180

4.2.3	Transformer.....	181
<b>4.3</b>	<b>WESS Grid Scale Applications .....</b>	<b>182</b>
<b>4.4</b>	<b>WESS Experimental Results .....</b>	<b>183</b>
4.4.1	Experimental Verification with WESS for EFR-A1 Control Algorithm.....	183
4.4.2	Experimental Verification with WESS for DFFR Control Algorithm .....	185
<b>5</b>	<b>Lifetime Analyses of BESS Operating in Grid Frequency Regulation.....</b>	<b>189</b>
<b>5.1</b>	<b>Introduction .....</b>	<b>189</b>
<b>5.2</b>	<b>Review on CCMs and Battery Degradation Methodologies.....</b>	<b>195</b>
5.2.1	CCMs .....	195
5.2.2	Battery Degradation Analyses Methodology .....	198
<b>5.3</b>	<b>A New Fast CCM Considering Various Effects on Battery Lifetime.....</b>	<b>199</b>
5.3.1	A Basic Fast CCM .....	200
5.3.2	Simulation Results of the Basic Fast CCM.....	203
5.3.3	Fast CCM considering only C-rate Effect on Battery Lifetime .....	210
5.3.4	Simulation Results of the Fast CCM considering C-rate Effect .....	211
5.3.5	Fast CCM considering both C-rate and SOC Effect on Battery Lifetime .....	215
5.3.6	Simulation Results of the Fast CCM considering both C-rate and SOC effect ..	217
5.3.7	Fast CCM considering Effect of DOD in Partial Charge/Discharge Cycling ....	226
<b>5.4</b>	<b>Conclusion.....</b>	<b>235</b>
<b>6</b>	<b>Conclusions and Future Work.....</b>	<b>239</b>

<b>6.1</b>	<b>Conclusion.....</b>	<b>239</b>
6.1.1	BESS Control for Dynamic and Static Firm Frequency Response Services .....	240
6.1.2	BESS Control for Pre Enhanced Frequency Response Services .....	240
6.1.3	BESS Control for Enhanced Frequency Response Services.....	241
6.1.4	Triad Avoidance Strategy through Enhanced Frequency Response.....	242
6.1.5	Scheduling of Grid Tied BESS Participating in UK Frequency Response Services and Energy Arbitrage.....	242
6.1.6	Battery State of Health Analysis.....	242
<b>6.2</b>	<b>Scope for Future Works .....</b>	<b>243</b>
<b>References .....</b>		<b>244</b>
<b>Appendix A General Definitions .....</b>		<b>265</b>
<b>A.1</b>	<b>Important Components of the UK Electricity System.....</b>	<b>265</b>
<b>A.2</b>	<b>Definition of Demand Side Sources .....</b>	<b>265</b>
<b>A.3</b>	<b>Definition of Distribution Network Operator (DNO) and Distribution System Operator (DSO).....</b>	<b>266</b>
<b>Appendix B Simulation Findings of Fast CCM .....</b>		<b>267</b>
<b>B.1</b>	<b>Fast Battery CCM Considering No Other Effect.....</b>	<b>267</b>
<b>B.1</b>	<b>Fast Battery CCM Considering SOC and C-rate effect on Battery Lifetime.....</b>	<b>277</b>
<b>Appendix C LabVIEW Software Coding of EFR-A1 used in WESS .....</b>		<b>281</b>



## Nomenclature

$SOC_t$	Present state-of-charge value	%
$APR_d$	Total daily arbitrage revenue	£/MWh
$APR_y$	Total yearly arbitrage revenue	£/kWh.yr
$A_{t\_buy}$	System electricity buy price	£/MWh
$A_{t\_sell}$	System electricity sell price	£/MWh
$C_C$	Cost of BESS charging	£/MWh
$C_{DC}$	Cost of BESS discharging	£/MWh
$Cycle_{chg}$	Number of charging cycles in cycle counting	cycle
$Cycle_{dischg}$	Number of discharging cycles in cycle counting	cycle
$Cycle_{total}$	Number of full charge-discharge cycles in cycle counting	cycle
$E_t$	Energy stored in the BESS at hour t	Wh
$N_{cyc}$	Number of cycles	number
$N_{max}$	Maximum number of cycles	number
$P_{meas}$	EFR measured power	kW
$P_{out}$	EFR output power	kW
$P_{set}$	EFR power set point	kW
$P_t$	Delivered bi-directional power	W
$SOC_0$	Initial state-of-charge value	%

$SOC_{chg}$	Sum of charging indexes in cycle counting	%
$SOC_{dischg}$	Sum of discharging indexes in cycle counting	%
$SOC_{max}$	Maximum state of charge	%
$SOC_{min}$	Minimum state of charge	%
$\eta_C$	Battery charging efficiency	%
$\eta_D$	Battery discharging efficiency	%
$\eta_{dc}$	BESS charge/discharge efficiency in Pre-EFR control	%
$\Delta E$	Change of energy in battery	Wh
$\Delta SOC$	Change in state of charge	%
C	Battery charge power in Pre-EFR control	kW
C <sub>Power</sub>	DFFR power set-point	kW
D	Battery discharge power in Pre-EFR control	kW
DB	Dead-band frequency	Hz
DN	Battery doing nothing in Pre-EFR control	-
<i>Down</i>	Discharging indexes in cycle counting	%
E	Battery export power in Pre-EFR control	kW
E/P	Energy/Power ratio	number
f	Grid frequency	Hz
F	Grid frequency in SFFR control	Hz
F <sub>high</sub>	High trigger frequency in SFFR control	Hz

Flow	Low trigger frequency in SFFR control	Hz
I	Battery import power in Pre-EFR control	kW
P <sub>batt</sub>	Instantaneous battery power	W
P <sub>c</sub>	Calculated power dictated by Pre-EFR	kW
P <sub>out</sub>	Output power in Pre-EFR control	kW
PowerOut	DFFR output power	kW
P <sub>s</sub>	Set charge/discharge power in Pre-EFR control	kW
Q	Battery watt-hour capacity	Wh
RampL	Lower ramp rate limit set in EFR control	MW/s
RampU	Upper ramp rate limit set in EFR control	MW/s
SOC	Available state-of-charge	%
SOC <sub>high</sub>	DFFR high operational state-of-charge limit	%
SOC <sub>init</sub>	Initial state-of-charge	%
SOC <sub>l</sub>	Lower SOC band in Pre-EFR control	%
SOC <sub>low</sub>	DFFR low operational state-of-charge limit	%
SOC <sub>low</sub>	Lower SOC operational limit in Pre-EFR control	%
SOC <sub>low</sub>	Lower SOC operational limit in EFR control	%
SOC <sub>u</sub>	Higher SOC band in Pre-EFR control	%
SOC <sub>up</sub>	Upper SOC operational limit in Pre-EFR control	%
SOC <sub>up</sub>	Upper SOC operational limit in EFR control	%
SPM	Service performance measurement	%

$SPower$	Maximum SFFR power response	kW
$Up$	Charging indexes in cycle counting	%
$\eta$	Inverter efficiency	%
$C$	Total battery capacity	Wh
$Kp$	Proportional controller gain	number
$PD$	Amount of delivered power in arbitrage control	kW
$Q$	Size of battery	Wh
$SDT$	Service delivery time	hr
$SP$	Service price	£/hr
$dSOC/dt$	Change in state-of-charge	%



## Abbreviation

AC	Alternative current
ANN	Artificial Neural Network
AR	Arbitrage revenue
B2G	Building-to-Grid
BES	Battery energy storage
BESS	Battery energy storage system
BM	Balancing Mechanism
BMS	Battery management system
CAES	Compressed-air energy storage
CAN	Controller area network
CCM	Cycle counting method
CCT	Coulomb counting technique
CE	Continental Europe
CES	Cryogenics energy storage
C-rate	Current rate
CSI	Current Source Inverter
DB	Dead-band frequency
DC	Direct current
DFFR	Dynamic firm frequency response

DG	Distributed generation
DNO	Distribution Network Operator
DOD	Depth-of-discharge
DSM	Demand side management
DSO	Distribution System Operator
DSR	Demand side response
DUoS	Distribution network use-of-service charges
EAR	Energy arbitrage revenue
EDLC	Electrochemical double-layer capacitors
EFR	Enhanced frequency response
EFR-A1	Enhanced frequency response control algorithm-1
EFR-A2	Enhanced frequency response control algorithm-2
EFR-A3	Enhanced frequency response control algorithm-3
EFR-A4	Enhanced frequency response control algorithm-4
EIS	Electrochemical impedance spectroscopy
EPSRC	Engineering and Physical Sciences Research Council
ES	Energy storage
ESSs	Energy storage systems
EU	European Union
EVs	Electric vehicles
FC	Fuel cell

FES	Flywheel energy storage
FFR	Firm frequency response
GHG	Greenhouse gas
HES	Hydrogen energy storage
HESS	Hybrid energy storage system
HFR	High frequency response
HHM	Half-hourly metered
LCO	Lithium-cobalt-oxide battery
LiFePO <sub>4</sub> /C	Lithium iron phosphate battery (referred as LFP)
Li-ion	Lithium-ion battery
LiMO <sub>2</sub> /Li <sub>4</sub> Ti <sub>5</sub> O <sub>12</sub>	Lithium Titanate battery (referred as LTO)
LMO	Lithium-manganese-oxide battery
LTO	Lithium-titanate-oxide battery
MAPE	Mean absolute percentage error
MFR	Mandatory Frequency Response
NaS	Sodium-sulphur battery
NCA	Lithium-nickel-cobalt-aluminium battery
NG	National Grid
NGET	National Grid Electricity Transmission System
NiCd	Nickel-cadmium battery
NiMH	Nickel metal hydride battery

NISM	Insufficient system margin
NMC	Lithium-nickel-manganese-cobalt-oxide battery
NPV	Net present value
OCV	Open circuit voltage
P/Q	Active/reactive power
PbA	Lead-acid battery
PCS	Power conversion system
PFR	Primary frequency response
PHS	Pumped hydroelectric storage
PI control	Proportional-Integral control
PJM	Pennsylvania-New Jersey-Maryland
Pre-EFR	Pre-enhanced frequency response
PSB	Polysulfide bromine flow battery
PV-BES	Photovoltaic battery energy systems
RCCM	Rainflow cycle counting method
RESs	Renewable energy sources
RMSE	Root mean square error
RO	Robust optimisation
RoCoF	Rate of change of frequency
SAP	Service availability payment
SC	Supercapacitor energy storage

SFFR	Static firm frequency response
SFFR <sub>high</sub>	Static firm frequency – high response
SFFR <sub>low</sub>	Static firm frequency – low response
SFR	Secondary frequency response
SMES	Superconductive magnetic energy storage
SOC	State-of-charge
SOH	State-of-health
SPM	Service performance measurement
SW	Switch mode in triad avoidance control strategy
TAB	Triad avoidance benefit
TES	Thermal energy storage
TNUoS	Transmission Network Use of Service
UK	United Kingdom
UoL	University of Lancaster
UoS	University of Sheffield
V2G	Vehicle-to-grid
VPP	Virtual Power Plant
VRB	Vanadium redox flow battery
VSI	Voltage Sourced Inverter
WESS	Willenhall energy storage system
WPP	Wind Power Plant

ZnBr	Zinc bromide battery
$\Delta/\Delta$	Transformer delta-delta connection

# 1 General Introduction

## 1.1 Thesis Organizations

The work in this thesis began in Jan 2015 at a time when there was only a handful of small grid connected batteries and the commercial interest in grid storage was just starting to ramp up. Over the last four years battery systems have been commercialised and there are now a number of large (>20MW) BESS installed throughout the UK. The work in this thesis has been published in three journals and six conference proceedings and has been delivered through workshops to a number of industrial partners that have used this knowledge to aid their commercialisation.

The works provided in this thesis are summarised below.

- Development of a BESS model that has been experimentally verified using a 2MW/1MWh system in which both static and dynamic firm frequency response control algorithms have been implemented with state-of-charge (SOC) management. Based on historical frequency data, results are presented showing the obtainable performance for a BESS delivering these services.
- During the development of the UK enhanced frequency response (EFR) specification the maximum power allowed during dead band (DB) was undefined. A sensitivity analysis was carried out on both the SOC target range and maximum power in the DB for both the wide and narrow services. In the work the service performance measurement (SPM) is used as a metric to select the best combination for maximum delivery with minimal power.
- For the final UK EFR specification with a defined DB, four control algorithms are presented and the SPM of each compared. The first algorithm implements the basic service specification, whilst the second includes an optional 30-min non-delivery window following a 15-min event that is shown to increase the availability of the BESS. The third algorithm utilises the 30-min non-delivery window to manage the SOC of the BESS and is demonstrated to both improve the SPM and ability to manage the SOC. The fourth algorithm implements a proportional controller for power selection based on the EFR envelope that is shown successfully to reduce peak powers of the battery.

- A method is introduced using SOC target management whilst delivering EFR to prepare the BESS, by maximising the stored energy, for Triad Avoidance and participate in generating Triad Avoidance Benefit (TAB). A sensitivity analysis is carried out on the effects of acting upon different early morning Triad warning times.
- An approach for layering frequency response services and generating arbitrage revenues is presented that maximises system profitability. This method utilises SOC target management for both arbitrage and service preparation, and using historical frequency and electricity pricing data a scheduling method is demonstrated. A total of 18 different scenarios are analysed across week/weekend and different seasons of the year.
- A new fast cycle counting method (CCM) is introduced for counting battery cycles that is suited for frequency service applications where micro cycling is typical. The new method is further developed to group cycles by C-rate, SOC level, and depth of discharge (DOD). The metrics are considered to be the primary factors in grid level storage cycling aging and hence levels of degradation can be estimated.
- The CCM is used to study the frequency response service control algorithms presented in the thesis to publish typical cycle information. It is demonstrated how the method can be used to extract the required information to estimate the degradation based on techniques in literature. However, the new way in which the cycles can be attributed to different metrics (C-rate, SOC, DOD) means that new techniques based on experimental data can be used for more accurate prediction. It is proposed in the work how this can be achieved using both c-rate and SOC.

The main contribution of this thesis is to present a control algorithm that enables BESSs to provide a bi-directional power in response to changes in the grid frequency, whilst managing the SOC of the BESS to optimise availability of the system. Moreover, this thesis introduces a strategy to generate additional revenues from grid storage applications such as Triad Avoidance only available during the winter season. This thesis also considers layering different UK grid balancing services, EFR and FFR, for Energy Arbitrage to make extra money in order to maximise the system's availability and profitability. Finally, a new fast cycle counting method (CCM) considering the effect of current rate (C-rate), SOC and depth-of-discharge (DOD) on



battery lifetime for grid-tied BESS is presented. The method helps to analyse the effect of delivering frequency response services on battery lifetime.

This thesis is organised into several chapters, each contributing a part to the overall objective of the thesis. A list of publications corresponding to each chapter is made available in the beginning of thesis. A brief description of each chapter is provided below.

**Chapter 1** reviews the structure of the UK power system needs and the requirement for grid flexibility. Energy storage systems (ESS) are investigated in detail with the importance of ESS in the power system, types of ESS technologies, and ESS applications. One of the most important types of ESS, battery energy storage system (BESS), is reviewed in detail with the state-of-art of BESS, types of batteries, functions of grid scale BESS, existing BESS installations and grid-tied BESS configurations. Chapter 1 also investigates the future of UK power system needs and the National Grid (NG) balancing service product strategies. Finally, this chapter provides an overall literature review on power system analysis for grid scale ESSs, power and energy management strategies, battery management methods, and battery lifetime analysis.

**Chapter 2 (J1, J2, C4)** presents the UK's largest 2MW/1MWh Lithium-Titanate (LTO) based BESS, operated by the University of Sheffield (UoS), with its battery pack structure, power electronic design and BESS operation and control.

**Chapter 3 (J1, J2, J3, C1, C2, C4, C5, C6)** presents a dynamic firm frequency response (DFFR) control algorithm that enables BESSs to deliver dynamic power in response to deviation the grid frequency with respect to the National Grid Electricity Transmission (NGET) DFFR specifications. A static firm frequency response high (SFFR<sub>high</sub>) and low (SFFR<sub>low</sub>) frequency response control algorithm are also developed to deliver a non-dynamic power.

NGET prepared a Pre Enhanced Frequency Response (Pre-EFR) specification to facilitate a tender competition between potential energy storage providers in late 2015. Using the pre-published enhanced frequency response specification, a generalised UK frequency response control algorithm is developed to evaluate control strategies for delivering a real-time response to deviations in the grid frequency. At the time of this work BESS focused frequency response services were still being developed and therefore any anticipated service specific constraints around control in DB had been ignored. This allowed this study to explore forecasting of

battery SOC levels and to propose battery charge/discharge management methods in order to maximise BESS availability.

Finally, this chapter introduces four EFR control algorithms that enables BESSs to provide a bi-directional power in response to changes in the grid frequency, whilst managing the SOC of the BESS to optimise availability of the system. The first EFR control algorithm, called EFR-A1, introduces a standard control algorithm designed to meet the technical requirements of NGET specifications. The advanced EFR algorithm, called EFR-A2, addresses the EFR service design with an extended 15-minute frequency event control, in order to optimise the use of the available stored energy. The third algorithm, called EFR-A3, extends the EFR control algorithm to include a dynamic SOC target to maximise the energy stored. Finally, the last EFR algorithm, called EFR-A4, includes a SOC-based proportional controller in the standard EFR control algorithm (EFR-A1) to optimize the power delivery in order to reduce the battery degradation and hence extend the battery lifetime. The developed DFFR and EFR control algorithms have been experimentally validated with the WESS 2MW/1MWh battery.

**Chapter 4 (J1, J2, J3, C1, C5)** begins by introducing a technique using SOC target management to combine EFR service with Triad Avoidance. A new effective Triad strategy layering grid frequency response service is developed to increase battery storage availability to maximize Triad avoidance benefit (TAB) revenues. The performance of the EFR service delivery through TAB is quantified. The Chapter 3 presented the EFR control methodologies with their simulation results; and this chapter extends to show how this can be used to maximise profits from other services such as Triad Avoidance.

Chapter 4 also introduces a scheduling method for BESS participating in frequency response services and energy arbitrage. The focus of this chapter is related to not only energy arbitrage, but also the scheduling of grid balancing services such as frequency response for additional benefit. In this chapter, by using the historical electricity price profiles, a grid balancing service scheduling method is developed to achieve maximum energy arbitrage revenues that can be generated from the grid balancing services by layering EFR, DFFR, SFFR<sup>high</sup> and SFFR<sup>low</sup> throughout the day. The proposed approach is not only providing arbitrage revenue but also generating further income through balancing service availability payments; this maximizes the system's profitability and availability. In this chapter, the UK daily electricity price pattern has been forecasted by observing the real electricity price of several week/weekend days across different seasons along with the grid frequency profiles of those days.

**Chapter 5 (C3, M1) :** This chapter introduces a new fast battery cycle counting method (CCM) for a grid-tied BESS, operation in grid frequency regulation and hence subjected to microcycling. In this chapter, all frequency response control algorithms developed in Chapter 3 are simulated to produce battery SOC data for a given time period using historical frequency data, those are then used to demonstrate the battery cycle counting method. This chapter quantifies the microcycling in terms of full cycles to aid in the approximation of the degradation of a battery and the battery lifetime analyses using the Miner's Rule life prediction method, whilst providing ancillary services such as frequency response. Secondly, the CCM algorithm is improved by considering C-rate and SOC effect on battery state-of-health (SOH). The proposed algorithm determines the number of full charge-discharge cycles experienced by the BESS operating in EFR service at different C-rate values grouped in steps of 0.2 C (C-rate) for each SOC range grouped by 10%. Thirdly, this chapter provides a new fast CCM considering the effect of DOD in partial charge and discharge cycling. The proposed method approximates the number of partial charge and discharge cycles a battery subjected under different DOD ranges.

Finally, **Chapter 6** draws a number of conclusions and summaries the contributions that this thesis work has made to the control of large scale grid-tied battery energy storage system. The scope for the future work which can expand on this thesis is set out.

## 1.2 Introduction

The greenhouse effect, worldwide population growth and sustainable policies demand an increasing use of renewable energy sources (RESs) around the world. The deployment of hydropower, solar and wind resources has been incredible and is still rising. This century is expected to see remarkable growth and challenges in power generation, delivery and usage. Environmentally friendly renewable power generation technologies will play a vital role in future power supply owing to increased global public awareness of the need for environmental protection and the need for less dependence on fossil fuels for energy generation. These technologies involve power generation from renewable energy (RE) resources, such as photovoltaic (PV), wind, geothermal, micro hydro (MH), biomass, ocean and wave tides [NEH11].

The UK government has ambitious targets to deploy RESs and reduce greenhouse gas (GHG) emissions from the energy sector. According to the European Union (EU) 2020 target, the share of electrical energy produced from renewables needs to increase to around 30% [MEY15]; having 15% renewable energy on the grid by 2020 [PAT16]. Moreover, the UK is committed to reduce its GHG emissions by 80% by 2050. The current UK electricity generation mix is shown in Fig. 1.1 [ONL19f].

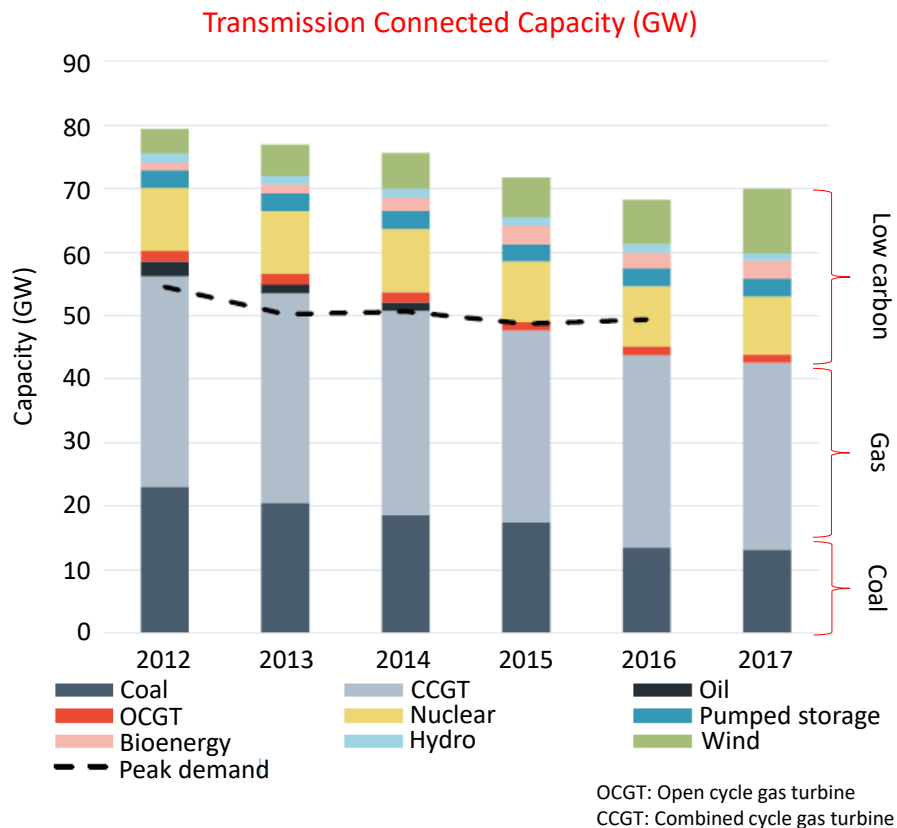


Fig. 1.1 UK electricity generation mix [ONL19f].

Distributed generation (DG) is going to play an important role in modernization of power system structure due to its promises to supply environmental friendly, reliable and cost-effective electricity to the customer. DG is small scale, self-contained generating plants that can be tied directly with load centre or near to load in distribution network. DG includes renewable technologies (photovoltaic, wind and biomass power) and high efficiency non-renewable power (gas turbine, fuel cell, internal combustion engine, micro turbine). Among various types of DG technologies, renewable DGs are becoming popular due to abundant availability of resources and almost zero emission in environment. Although the effects of renewable DGs are considered as completely favourable for distribution network, individual DG application may cause high distribution power losses and poor voltage stability of the

network. Therefore, type, optimal location and size selection of renewable DGs in the distribution network is a very important aspect of energy system planning [KAY14].

However, RESs have two significant drawbacks beside their invaluable benefits: RESs greatly depend on weather conditions, and they have unsynchronized generation peaks with the demand peaks [HUS13]. In the last 20 years wind and photovoltaic generation has been studied extensively and has led to large installations of both. Since the distributions of output power of these renewables it is difficult for them to be used locally. If they are linked to the main grid at scale, it may result in a large-scale surplus power flowing which may cause the power stability problems. Furthermore, integrating massive amount of intermittent RESs into power systems poses various technical and economic challenges. Variable RESs are difficult to predict and provide a highly fluctuating power output, hence adding variability and uncertainty to the planning and operation of power systems. Furthermore, the potential of RESs is generally spatially distributed and barely correlates in time with the load profiles. These characteristics of RESs challenge the adequacy of the power system (power and energy balance) and frequency and voltage regulation. Therefore, in order to successfully integrate a greater share of RESs, the planning and operation of power systems are required to become more flexible than they are today [HAA17], [COC14], [LAN11].

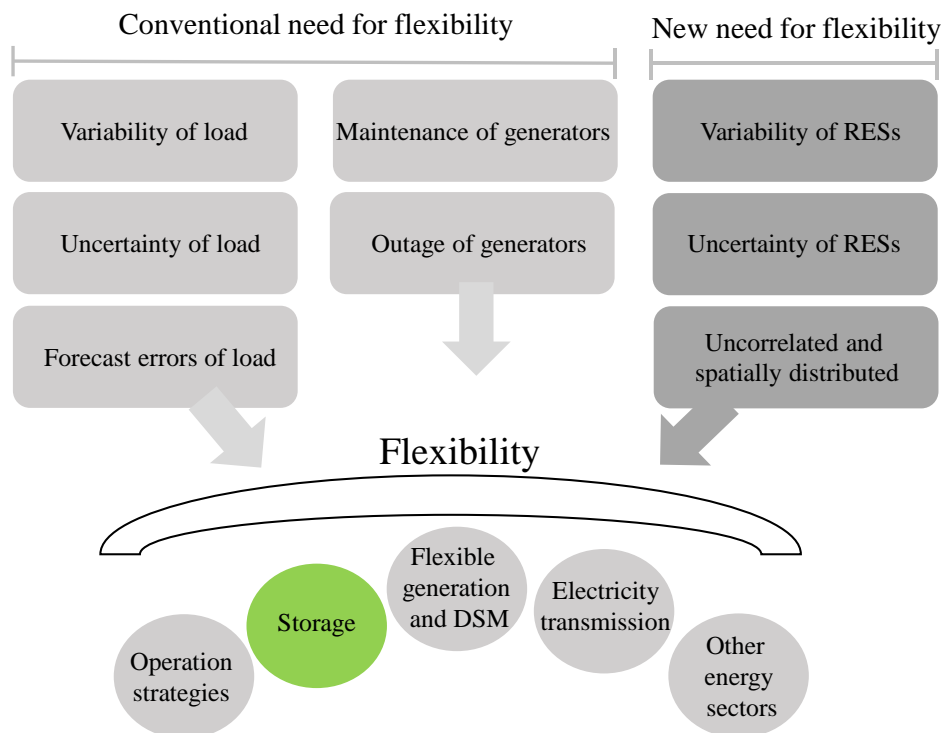


Fig. 1.2 Need for flexible power systems and flexibility sources.

The needed flexibility can be provided through various approaches as shown in Fig. 1.2. These involve operational strategies (e.g energy curtailment [BOU08], power output controls [RAH16], more frequent dispatches [DEA14], and residential and industrial demand side management (DSM) [JON11]), new market structures, integration between various energy sectors such as the transport, power and heat sectors [POU06], [POU12], [PIE14]. Additionally, it is possible to modify the power system infrastructure by reinforcing transmission infrastructure, adding flexible generation devices such as gas turbines [MAT14], and the inclusion of energy storage systems (ESSs) [FAI12], [HAO15], [HAA17].

To overcome these issues, renewable DGs are generally backed up with energy storage (ES) to minimize fluctuations in their produced power and to synchronize the generation peaks with the demand peaks. However, ES devices are expensive [HUS13]. More details about ES will be given in the following section.

### **1.3 Energy Storage Systems (ESSs)**

ES plays an essential role in power distribution systems. ES can store excess power in the valley load period and then releases the stored energy during the peak load period. Not only can it increase the efficiency of the utilization of the RES, but also can effectively lessen the load and the load pressure of the grid. Optimised usage of ES device promises the efficient utilization of RES [CHE15].

#### **1.3.1 Importance of Energy Storage in Power Systems**

ES technologies can provide numerous benefits to the power system, listed as following:

- ES technologies can decrease the use of fossil fuels, allowing a greener energy supply mix.
- RESs cannot be the sole provider of energy without an ES facility due to the variable output. ES can allow the integration of more RESs, especially wind and solar PV, in the energy mix [WHI12].
- ES technologies could reduce the requirement to invest in new traditional generation capacity, leading to financial savings and reduced emissions particularly from electricity generation [BAR04].

- ES could improve the energy security by optimising the demand and supply, thus reducing the requirement to import electricity via interconnectors [BAR04].
- ES can provide system stability during electricity blackouts by providing energy at these times and decreasing the financial cost of power blackouts [BAR04].
- Energy can be stored when electricity prices are low and used on site when the prices are high to save businesses and consumers money on their electricity bills. Alternatively, the stored energy can also be sold [FER13].
- Large scale ES can substantially reduce energy losses on transmission and distribution. Electricity transmission losses usually run at below 10% of the total energy first generated in the UK [ONL18c].
- ESS is an essential technology for the future electricity power network by maintaining storage and reserve facilities and will have an important impact on the market; for instance ESS will contribute to reduce the volatility of electricity market price, to increase market efficiency, to promote the qualification of grid ancillary services and to improve power system security [FER13].

### 1.3.2 Classification of Energy Storage Technologies

There are different methods for classification of various ESS technologies, such as, in terms of their response time, functions and suitable storage durations [LUO15]. The most widely used methods is based on the form of energy stored in the system, as shown in Fig. 1.3.

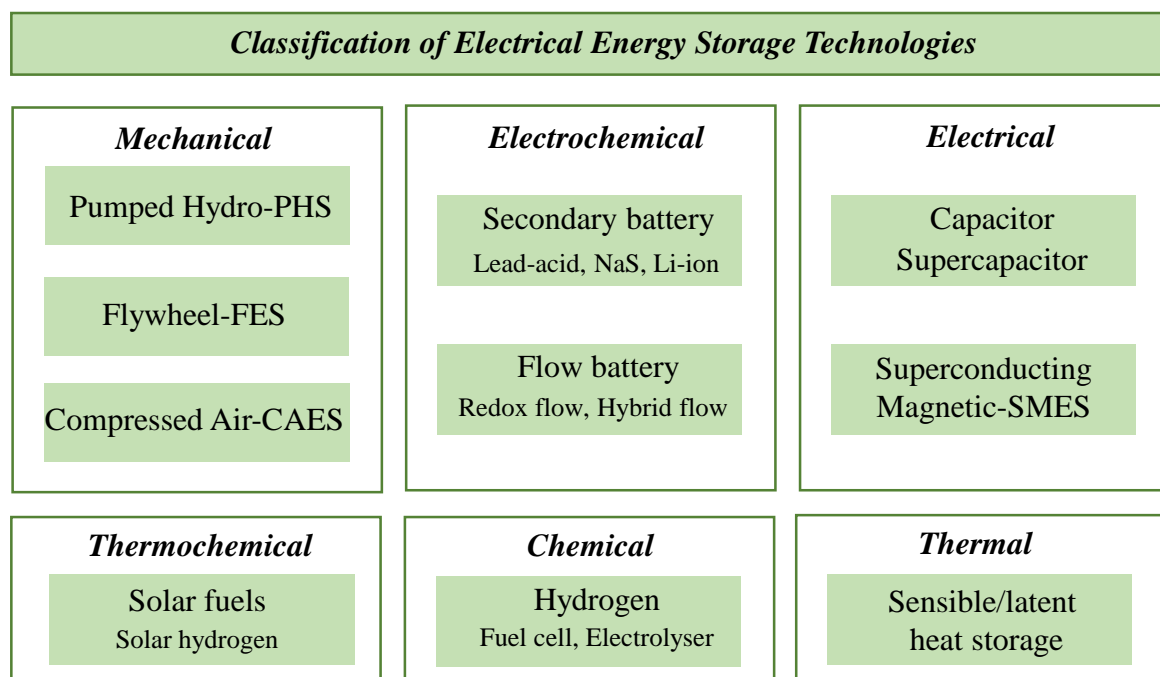


Fig. 1.3 Classification of energy storage technologies by the form of stored energy.

#### *A. Pumped Hydroelectric Storage (PHS)*

Pumped hydroelectric storage (PHS) is an ES technology with a long history, large energy capacity and high technical maturity. With an installed capacity of 153 GW in 2018 [ONL18b], PHS represents 99% of worldwide bulk storage capacity and contributed to around 3% of global generation [LUO15]. A standard PHS plant includes two water reservoirs, separated vertically. At off-peak electricity demand hours, the water is pumped into the higher level reservoir at peak hours, the water can be send back into the lower level reservoir. In this process, the water powers turbine units that drive the electrical machines to produce electricity. Many PHS plants exist with power rating ranging between 1MW-3003MW, with ~70-85% cycle efficiency and around 40 years lifetime [CHE09], [LUO15]. PHS applications mainly involve frequency control, energy management in the fields of energy arbitrage, non-spinning reserve and supply reserve. However, with the restriction of area selection (mountainous areas preferred), PHS plants suffer high capital investment and long construction. Solar and wind power generation coupled with PHS has been developed. This helps the adoption of renewable energy in distributed or isolated networks. For instance, in Greece, the Ikaria Island power station was integrated with 3x900 kW wind farms and a PHS (2MW) facility [PAP10].

#### *B. Battery Energy Storage (BES)*

Rechargeable battery is one of the most broadly used ES technologies in daily and industry life. Fig. 1.4 illustrates the simplified operational principle of a standard battery energy storage system (BESS). A BESS consists of some electrochemical cells connected in series or parallel, which generates electricity with a desired voltage from an electrochemical reaction. Each battery cell has two electrodes (one anode and one cathode) with an electrolyte that can be at liquid, solid or ropy states [LOU15]. A battery cell can bi-directionally convert energy between chemical and electrical energy. When discharging, the electrochemical reactions happen at the anodes and the cathodes simultaneously; to the external circuit, electrons are supplied from the anodes and are collected at the cathodes. When charging, the reverse reactions occur and the battery is recharged by applying an external voltage to the two electrodes (Fig. 1.4). The location for BESS installation is quite flexible, either close to the facilities where required, or housed inside a building. Currently, relatively short life times has been considered as the major barriers to implementing large scale facilities. The issues are high capex costs which are not



supported by long term contracts and potentially short lifetimes. The recycling or disposal of dumped batteries must be considered if toxic chemical materials are used [9]. Moreover, various types of battery cannot be fully discharged owing to their lifetime depending on depth of discharge [LUO15].

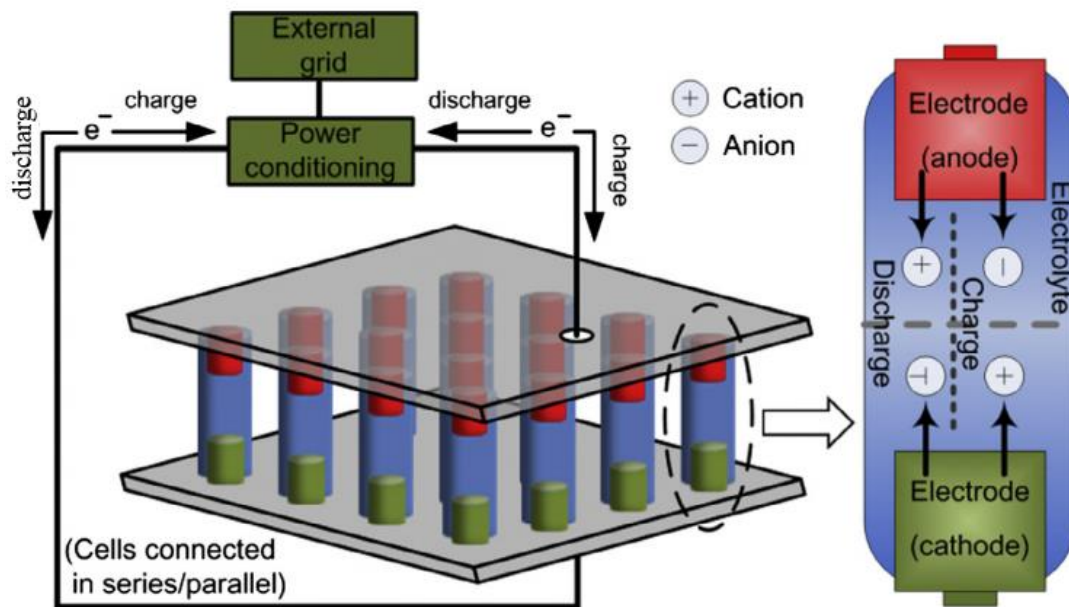


Fig. 1.4 Schematic diagram of a battery energy storage system operation [LUO15].

### C. Compressed Air Energy Storage (CAES)

In a compressed-air energy storage system (CAES), electrical compressors are used to compress air and store it in either an above-ground system of consisting of a vessel or pipes, or underground structure (abandon mines, salt cavern, rock structures). When required, the compressed air is released and mixed with natural gas, burned and expanded in a modified gas turbine. Current studies on the CAES are focused on the enhancement of systems with fabricated storage tanks that will remove the geological dependency and also the storage of compressed air at a higher pressure. There are currently only two CAES units in operation, they are placed in Macintosh in Alabama, USA and Huntorf, Germany. CAES has a high power (5-300 MW) and energy capacity rating; this makes the CAES another alternative for wind farms for energy management purposes. The storage period can be over a year because of very small self-discharge losses. However, the installation of a CAES is currently limited by topographical conditions [ZHA15].

#### *D. Flywheel Energy Storage (FES)*

In a flywheel energy storage system (FESS), the rotational energy is stored in an accelerated rotor, a large rotating cylinder. The system components are a rotating cylinder (consists of a rim attached to a shaft) in a compartment, a shaft and bearings. The whole structure is located in a vacuum enclosure to decrease windage losses. On charging, the rotor is accelerated to a very high speed which can typically reach anyway from 5,000 to 80,000 rpm depending on size. The energy is stored in the flywheel by maintaining the rotating body at a constant speed. On discharging, the flywheel uses its energy and drives the machine as a generator [ZHA15]. The main benefits of flywheels are its great cycling capability, a long life of supplying full charge-discharge cycles, high efficiency, high power density and low maintenance cost. The FESS is mostly applied as a power quality device to suppress fast wind power changes. The major disadvantages are the high self-discharge losses and short operation duration due to comparably low energy densities [ZHA15].

#### *E. Supercapacitor Energy Storage (SCs)*

Supercapacitor energy storage system (SCs) also known as ultra-capacitors, electrochemical capacitors or electric double layer capacitors were drawing less attention until very recently when faster ESSs were required in a number of applications to replace Li-ion batteries which suffer from comparably slow charge/discharge and suffer from limited lifetime. This renewed interest has led to significant progress in its development and use in ES technologies. SCs store energy in two series capacitors of the electric double layer that is formed between each of the electrodes and the electrolyte ions. They are capable of storing massive power density and can respond to any change in power demand in tens to hundreds of milliseconds. The number of charge and discharge cycles of SCs is potentially unlimited, however the energy throughput in fast cyclic operation is limited. They have an efficiency of 95% and 5% per day self-discharge; this means that the stored energy must be used quickly [PAT10], [ANE16].

#### *F. Cryogenic Energy Storage (CES)*

Cryogenics energy storage systems (CES) are a more recently developed low-temperature thermo-electric ES approach that enables grid operators to charge excess electricity to liquefaction of a gas that is subsequently stored in a thermally insulated storage tank at a cryogenic temperature (below  $-190^{\circ}\text{C}$ ), at near-ambient pressure. At the discharge process, the liquid gas (cryogen) is pressurised, evaporated and superheated. Cryogen is a new term

introducing a gas in a liquid state that has a boiling temperature below  $-150^{\circ}\text{C}$  at a pressure of 1 bar; examples include liquid hydrogen, liquid air, liquid nitrogen etc. The high pressure gas is then expanded to produce electricity in a gas turbine system. CES is a promising technology due to the high potential for bulk energy storage with a substantially larger volumetric energy density compared to CAES and PHS. CES is highly competitive compared to other grid scale ES technologies due to the following: (a) There are no geological constraints; (b) the theoretical number of charge and discharge cycles is infinite; (c) CESS is cost competitive with other low-carbon technologies; (d) the periods of storage are relatively long. With a discharge duration of several hours and a power rating above 100MW, CES is applicable to energy management [HAM17]. However, the CES unit has a very low round trip efficiency of 46.7% and the overall plant efficiency is only 24.4% [CET19]. Allowing synergies with other processes such as cooling or recovering waste cold/heat enables system efficiency to be increased.

### *G. Hydrogen Energy Storage (HES)*

Electricity can be converted to hydrogen by electrolysis, the hydrogen can be stored and ultimately re-electrified. Today, the round trip efficiency is quite low (~30% to 40%), but could increase up to 50% if more efficient technologies are designed. Despite its low efficiency, the interest in HES is growing owing to the much higher storage capacity compared to PHS, BES (small scale) and CAES (large scale) [ONL19j]. Hydrogen can be re-electrified in fuel cells with efficiencies up to 50%, or as an alternative, burned in combined cycle gas power plants with efficiency ~60% [ONL19j].

### *H. Summary of ES Technologies*

The above ES technologies are, owing to, their different characteristics, suitable for different applications. Generally, electrochemical storage systems (batteries, flow batteries, fuel cells) respond on very short timescales and hence are suitable for ancillary services (e.g grid frequency regulation). Flow batteries are emerging, however only few MW systems have been installed so far. Only batteries and PHS can be regarded as mature storage technologies with many commercial installations worldwide. CAES and PHS are slower, but have relatively low costs of the storage capacity, and hence more suitable for storing large amount of energy to be delivered over a longer duration. CAES systems have been worked for many years, however only two CAES systems have been installed and in both the power generation is dominated by combustion of natural gas. Both CAES and large scale reversible fuel cell technology still

require important research and development before they can be fully commercialized [EKM10]. Fig. 1.5 illustrates a comparison of power ratings and rated energy capacities of ES technologies. The nominal discharge time duration at the rated power is also illustrated within the range from seconds to months. From Fig. 1.5, ES technologies can be classified by the nominal discharge time at rated power; (1) discharge time less than 1 hour: flywheel, SMES, supercapacitor; (2) discharge time up to 10 hours; over ground small-scale CAES, PbA, Li-ion, ZnBr, NiCd and PSB; (3) discharge time longer than 10 hour: underground large-scale CAES, PHS, liquid air energy storage, solar fuel, VRB, fuel cell and TES [LUO15].

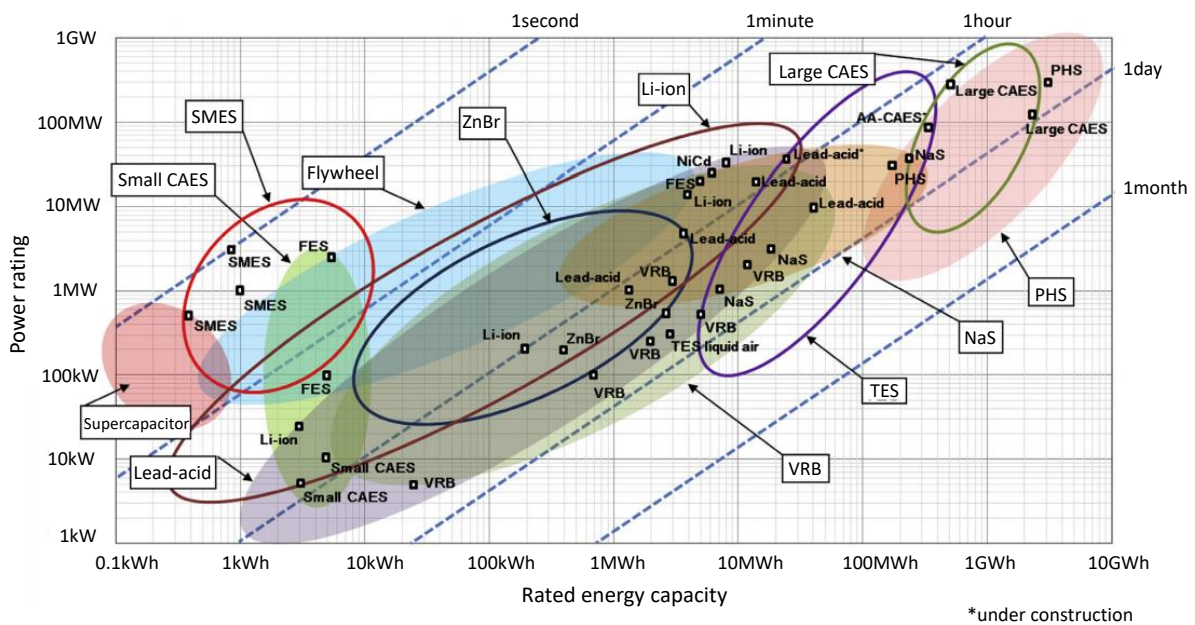


Fig. 1.5 Comparison of ES technologies' power rating and rated energy capacity with discharge time duration at power rating [LUO15].

### 1.3.3 ESS Applications used for Supporting Power System

Energy storage systems (ESSs) are continuously gaining importance owing to integration of RESSs into the distribution network. In addition to provide of bulky stored electricity, ESSs are suitable choices for various power system applications. Major types of ESS and their applications, priorities and challenges are given in Table 1.1. These involve increasing penetration of intermittent sources, improving power quality by mitigating voltage oscillations and improving network reliability by increasing transmission line capacities. ESSs are a cost effective candidate as compared to conventional fuel based system restorers such as diesel generators. ESSs do not have rotating parts, hence their operational and maintenance costs are lower and easier to troubleshoot within a short time [JAM15]. There are two major areas for

power system applications, including power quality and energy management. Power quality applications involve voltage support, frequency regulation, flicker compensation, spinning reserve, and low voltage ride through. Energy management applications can be composed of time shifting, energy arbitrage, load levelling, peak shaving and capacity firming [BHU12].

#### *A. Renewable Intermittency Mitigation*

DG is considered as new concept of electricity delivery in future grids primarily contributed by RESs. ESS can also be integrated into grids to provide electricity and cover a certain fraction of demand [JAM15].

#### *B. Load levelling*

When an ESS is located on a load bus of a power system, the change of load can be levelled by storing energy at peak periods and releasing the energy at off-peak times. Load levelling approach is based on charging at off-peak times and discharging at peak times, in order to secure a uniform load for generation, transmission and distribution system, thus maximizing the power system's efficiency [FER13].

#### *C. Peak shaving/valley filling*

Although the principle is the same for these two approaches, the purpose is slightly different. Peak shaving concerns the minimisation of peak power, and hence the use of more costly power plants, whilst valley filling focuses on improving the plants efficiency by increasing the load at those moments [FER13].

#### *D. Unbalance load compensation*

An unbalanced load can be compensated using a three-phase converter system along with ES. The control of the ES is configured in such a way so that absorbing and injecting energy can be managed on independent phases [BHU12].

#### *E. Energy arbitrage*

ESSs can be used to purchase energy from the power grid when the time-of-use pricing is lower, and later sell back the energy to the grid when the time-of-use price is higher. Revenue can be achieved using the energy arbitrage. If energy storage is located in a feeder which supplies to a local load, then grid flow can be regulated based on load changes [BHU12]. Energy arbitrage

function is traditionally implemented by PHS, CAES and BESSs. Energy arbitrage study is similar to peak shaving functions; which covers the optimum ESS scheduling for maximizing the profits, ESS sizing, implementation of distributed ESSs and economic assessment [CHA17].

#### *F. Frequency and voltage regulation*

ESSs can absorb active power when the grid frequency increases from a predefined upper frequency threshold, whereas it can release power when the frequency drops below the predefined lower frequency threshold. Hence, ESSs can contribute to stabilize the grid frequency. BESSs, FESs and Supercapacitors are generally adopted for grid frequency and voltage regulation due to their fast response [CHA17], [CHO17].

#### *G. Voltage support*

Providing required reactive power to a load can maintain system voltage at its nominal value. Generators are responsible to supply both real and reactive power. If there is a high demand for both real and reactive power, an ESS can share the real power with the generators, hence, the generators can deliver required reactive power for the load. Therefore, ESS can support a power system to prevent from voltage sag [BHU12].

#### *H. Spinning reserve*

Spinning reserve can be described as the amount of generation capacity that can be used to generate active power over a given period of time and which has not yet been committed to the generation of energy during this period. Spinning reserve indicates standby unused generation. ESSs are fast and hence can be used as a spinning reserve [BHU12].

#### *I. Black start*

If a power system is down due to a fault, the process of restoring the system is called black start. Typically, diesel generator systems are used for starting the power stations. However, an ESS along with a converter is capable to supply power to the grid, consequently, recover the power stations by energizing the field-coils of the synchronous generators [BHU12]. An example is the Huntorf CAES that supplies black-start power to nuclear units placed near to the North Sea [LUO15].

Table 1.1 Specifications of ESS technologies [DEH19], [ONL18f]

<b>Technology</b>	<b>Primary Application</b>	<b>Priorities</b>	<b>Challenges</b>
Flywheel energy storage (FESS)	<ul style="list-style-type: none"> <li>• Frequency regulation</li> <li>• Peak shaving</li> <li>• Load levelling</li> <li>• Transient stability</li> </ul>	<ul style="list-style-type: none"> <li>• Rapid response</li> <li>• Modular technology</li> <li>• Suitable for utility scale</li> <li>• High peak power without overheating concerns</li> <li>• Long cycle life</li> <li>• High round trip energy efficiency</li> </ul>	<ul style="list-style-type: none"> <li>• Rotor tensile strength limitations</li> <li>• Limited energy storage time because of high frictional losses</li> </ul>
Pumped hydro energy storage (PHS)	<ul style="list-style-type: none"> <li>• Backup and reserve</li> <li>• Energy management</li> <li>• Regulation service through variable speed pumps</li> </ul>	<ul style="list-style-type: none"> <li>• Mature and developed technology</li> <li>• Cost effective</li> <li>• Very high ramp-rate</li> </ul>	<ul style="list-style-type: none"> <li>• Geographically limited</li> <li>• Environmentally impacts</li> <li>• Plants site</li> <li>• High overall project cost</li> </ul>
Compressed air energy storage (CAES)	<ul style="list-style-type: none"> <li>• Backup and reserve</li> <li>• Energy management</li> <li>• Renewable integration</li> </ul>	<ul style="list-style-type: none"> <li>• Established technology in operation since 1970</li> <li>• Better ramp-rates than gas turbine plants</li> </ul>	<ul style="list-style-type: none"> <li>• Geographically limited</li> <li>• Slower response than batteries or flywheels</li> <li>• Lower efficiency owing to round trip conversion</li> <li>• Environmental impact</li> </ul>
Superconductive magnetic energy storage (SMES)	<ul style="list-style-type: none"> <li>• Frequency regulation</li> <li>• Power quality</li> </ul>	<ul style="list-style-type: none"> <li>• Highest round trip efficiency from discharge</li> </ul>	<ul style="list-style-type: none"> <li>• Material and manufacturing cost prohibitive</li> <li>• Low energy density</li> </ul>
Capacitors	<ul style="list-style-type: none"> <li>• Frequency regulation</li> <li>• Power quality</li> </ul>	<ul style="list-style-type: none"> <li>• Highly reversible and fast discharge</li> <li>• Very long life</li> </ul>	<ul style="list-style-type: none"> <li>• Currently cost prohibitive</li> </ul>
Thermochemical energy storage (TES)	<ul style="list-style-type: none"> <li>• Grid stabilization</li> <li>• Load levelling and regulation</li> </ul>	<ul style="list-style-type: none"> <li>• Extremely high energy densities</li> </ul>	<ul style="list-style-type: none"> <li>• Currently cost prohibitive</li> </ul>
Hydrogen Energy Storage (HES)	<ul style="list-style-type: none"> <li>• Load levelling</li> </ul>	<ul style="list-style-type: none"> <li>• Distributed storage</li> <li>• Other uses for produced hydrogen</li> <li>• Minor environmental issues</li> </ul>	<ul style="list-style-type: none"> <li>• Low efficiency</li> <li>• High investment costs</li> <li>• Raw material's limits</li> <li>• Environmental impacts</li> </ul>
Battery Energy Storage System (BESS)	<ul style="list-style-type: none"> <li>• Frequency regulation</li> <li>• Peak shaving</li> <li>• Power quality</li> </ul>	<ul style="list-style-type: none"> <li>• Distributed storage</li> <li>• Good configurability</li> <li>• Fast response time</li> <li>• High energy efficiency and density</li> </ul>	<ul style="list-style-type: none"> <li>• High investment costs</li> <li>• Short life span</li> </ul>

Table 1.2 Technical characteristics of the ESSs [WON19], [KYR16]

Type of ES	Storage Duration	Efficiency (%)	Lifetime (years)	Power Rating (MW)
SMES	Minutes-hours	95-98	20+	0.1-10
FES	Seconds-minutes	85-95	15	0-0.25
SC	Seconds-hours	84-97	10-30	0-0.3
<b>BES</b>				
PbA	Minutes-days	63-90	5-15	0-20
NaS	Seconds-hours	75-90	10-15	0.05-8
Li-ion	Minutes-days	75-97	5-15	0-0.1
ZnBr	Hours-months	65-85	5-10	0.05-2
CAES	Hours-months	50-89	20-60	5-300
HES	Hours-months	20-66	5-15	0-50
PHS	Hours-months	65-87	40-60	100-5000

This thesis focuses on the control of battery storage; therefore more detail about BESSs will be given in the following section.

#### 1.4 Battery Energy Storage Systems (BESSs)

There are various types of existing ESSs, as discussed in Section 1.3.2. In comparison to such ESSs, BESSs have numerous advantages including faster response time compared to conventional energy generation sources, energy efficiency, storage size, low self-discharge rate, high charging/discharging rate capability, and low maintenance requirements [SAW16], [FEE16]. BESS has a significant disadvantage such as low cycle life. The cost of batteries has been decreasing in recent years and therefore there is now a potential for profitable large-scale grid application. BESSs mostly participate in balancing demand and supply through frequency response services, voltage support and peak power lopping [CHE16], [XU16]. BESSs using various battery chemistries are installed around the world for grid support [GUN17a]. A BESS is becoming superior for the purpose of grid support owing to its benefits such as its fast response time, flexibility in locations, construction time, and low operation costs. There are numerous works dealing with different aspects of grid scale BESS on energy management [TAN15], control strategies [ZAL13], battery management [LAW14] and life cycle cost analysis [ZAK15].



### 1.4.1 Battery Terminologies

In literature, various terminologies are used to define different characteristics of BESSs. Those terms [ZHA17], [NEJ16] relevant to this chapter are provided in the following parts, which will later help on developing the BESS control algorithms, evaluating the cycle counting algorithms and battery lifetime analysis.

#### *A. Battery Cell, Module, Pack*

The term battery is associated with one or more cell(s) connected in a series and/or parallel configuration in order to provide the desired voltage and ampere-hour rating. A ‘string’ of cells often consists of a number of series or parallel connected cells. A string (or strings) of cells connected physically and electrically together is called a ‘module’, whereas a number of modules connected electrically and operated as single unit, is called a ‘battery pack’.

#### *B. Capacity*

Battery capacity can be defined using two terms. Ampere-hour (Ah) capacity is the total amount of releasable charge stored in a battery under some predefined conditions. It is usual to use Watt-hour (Wh) instead of Ah to define a battery’s capacity. The rated Wh capacity is mathematically defined as in (1.1).

$$\text{Battery Wh Capacity} = \text{Rated Ah Capacity} \times \text{Rated Nominal Voltage} \quad (1.1)$$

#### *C. Current-Rate (C-rate)*

C-rate is an arbitrary metric used to define the current rate, at which the battery will take one hour to fully discharge under standard conditions. For example, a rated 3.3 Ah cell will take a current of 3.3 A to fully discharge in one hour.

#### *D. Specific Energy and Power*

Specific energy is used to quantify the amount of energy a battery can store per unit mass. It is expressed in Wh/kg as given in (1.2). Similarly, specific power represents the battery’s peak power per unit mass, expressed in W/kg as in (1.3).

$$\text{Specific Energy} = \text{Rated Wh Capacity} / \text{Battery Mass} \quad (1.2)$$

$$\text{Specific Power} = \text{Rated Peak Power} / \text{Battery Mass} \quad (1.3)$$

### E. Energy and Power Density

Energy density is the nominal battery energy stored in a given space per unit volume. This is expressed in Wh/l as in (1.4).

$$\text{Energy Density} = \text{Rated Wh Capacity} / \text{Battery Volume} \quad (1.4)$$

Specific power is the term referring to the peak-power per unit volume of a battery, expressed in W/l as in (1.5).

$$\text{Power Density} = \text{Rated Peak Power} / \text{Battery Volume} \quad (1.5)$$

### F. State of Charge (SOC)

SOC is defined as the remaining amount of releasable charge in a battery with respect to the maximum available capacity.

### G. Depth of Discharge (DOD)

DOD is an indicator of the battery discharge since the last change at the  $n$ th global dispatch interval as in (1.6) For instance, when the battery is charged from 30% to 50% of the SOC, the DOD is 0% and  $\Delta SOC$  is 20%. When the battery is then discharged from 50% to 40% of the SOC, the DOD is 10% and  $\Delta SOC$  is -10%. If the battery is discharged from 40% to 20% of the SOC straight of the first charge, the DOD will be updated to 30% [ZHA17].

$$DOD_{n+1} = \begin{cases} DOD_n - \Delta SOC_n & , \quad \text{if } \Delta SOC_n \leq 0 \\ 0 & , \quad \text{if } \Delta SOC_n > 0 \end{cases} \quad (1.6)$$

### H. State-of-Health (SOH)

SOH is a measurement that shows the general condition of a battery and its ability to deliver the specified performance compared with a new battery. The designer of a BMS may use any of the following parameters (or in combination) to determine the SOH: - number of charge-

discharge cycles, -internal resistance, - capacity, - voltage, 5) self-discharge, 6) ability to accept a charge.

#### *I. End-of-Life (EOL) Condition*

Conventionally, battery reaches its end of life when its available capacity decreases to 80% of the maximum capacity or the capacity fade increases to 20% of the maximum capacity.

#### *J. Calendar Life and Cycle Life*

The calendar lifetime is the elapsed time for an inactive battery before the battery reaches the EOL condition, 80% of its original capacity. The cycle life is the number of complete charge/discharge cycles that the battery is able to support before its capacity decreases to under the EOL.

#### *K. Life Dependence on the Average SOC and Temperature*

Generally, the lithium battery life will also depend on the average SOC and temperature.

### **1.4.2 Types of Batteries**

Various types of batteries are used for large scale ES. The characteristics of different types of batteries used for large scale battery energy storage such as lithium-ion (Li-ion), lead-acid (PbA), sodium-sulphur (NaS), nickel metal hydride (NiMH) and flow batteries etc., as well as their applications, are discussed in this section. Major types of BESS and their applications, priorities and challenges are shown in Table 1.3.

#### *A. Lead-acid (PbA)*

PbA battery, invented in 1859, is the oldest type of rechargeable battery, and it uses a liquid electrolyte. Deep-cycle lead acid batteries are suitable for small-cycle RES integration applications. PbA batteries can be discharged repeatedly by as much as 80% of their capacity; and hence they are ideal for grid scale applications. With low investment costs, lowest self-discharge and relatively ease of maintenance, they offer a proven and cost-competitive solution to a range of storage requirements [POU13]. Drawbacks of this technology cover limited cycle life, failure due to deep and continuous cycling, poor performance at low and high ambient temperatures, and environmentally unfriendly lead content and acid electrolyte [NIR10].

### *C. Nickel-cadmium (NiCd)*

NiCd battery consists of a positive electrode with nickel oxyhydroxide as the active material and a negative electrode consisted of metallic cadmium. Owing to its higher energy density and longer cycle life than those of PbA, relatively lower cost than other batteries and tolerance for deep discharge, the NiCd battery is mostly preferred for medium-term energy management. NiCd also provides various benefits in PV applications and factors; including its cycling ability, durability, and reliability make it suitable for operating under adverse conditions. NiCd batteries are a competitive replacement for PbA batteries owing to their ability to provide continuous power for long periods, and also their use in applications that need instantaneous power [NIR10]. Its main drawbacks are that cadmium is toxic, and the battery exhibits negative temperature coefficient that causes charging problems at higher temperatures [BHU12].

### *D. Nickel metal hydride (NiMH)*

NiMH battery is a feasible option to NiCd battery due to its performance and environmental benefit. In comparison to PbA and NiCd batteries, NiMH is environmentally friendly owing to the lack of toxic substances such as lead, cadmium or mercury. Energy density of NiMh cell is 25-30% higher than high performance NiCd cell. NiMh batteries suffer from severe self-discharge; making them inefficient for long-term energy management [NIR10].

### *B. Sodium-sulphur (NaS)*

NaS battery is a rechargeable high temperature battery technology that uses metallic sodium and provide attractive solutions for various large scale utility ES applications; including power quality, load levelling and peak shaving, as well as renewable energy management and integration. This battery has a high charge/discharge efficiency (75-86%), high energy density, and is produced from inexpensive materials [POU13].

### *D. Lithium-ion (Li-ion)*

In Li-ion batteries, the lithium ions move between the anode and cathode to generate a current flow. Main applications include portable equipment (e.g mobile phone, laptop). Due to its high energy density, Li-ion has become the most promising battery technology for grid scale, EV and plug-in-hybrid EV applications. Historically the price of Li-ion batteries has been high but due to the increase production for the EV market, prices have significantly reduced over the

past 10 years. There are many types of battery technologies, however the most used in power applications today are Li-ion batteries. The advancement of Li-ion technology in increasing the levels of ES capacity is owing to the characteristics of high efficiency (>90%), response time (in milliseconds), high energy density, self-discharge rate (5% per month) and relatively long cycle life [FAI18]. Li-ion batteries are manufactured in various types of technologies and named in accordance with the materials used in their electrodes; e.g Lithium-cobalt-oxide (LCO), Lithium-manganese-oxide (LMO), Lithium-nickel-manganese-cobalt-oxide (NMC), Lithium-nickel-cobalt-aluminium (NCA) and Lithium-titanate-oxide (LTO). Emerging Li-ion battery technologies provide potentially improved cost, cycle life, performance and safety. To determine which battery technologies are more suitable for BESS applications, it is required to test them and evaluate their performance and cycle life time under typical BESS operation [VAL18]. Among those different types of Li-ion batteries, this thesis focuses on LTO battery due to its superior performance. LTO can provide relatively long life cycles, rapid charging, large available capacity, wide effective SOC range, excellent low-temperature operation and high input/output power performance, all while maintaining a high level of safety [ONL18a].

#### *D. Flow battery*

Flow batteries are a promising technology that decouples the stored energy from the rated power. The total stored capacity depends on the auxiliary tank volume, whilst the rated power depends on the reactor size. These characteristics make the flow battery suitable for supplying large amounts of power and energy needed by electrical grids. The main benefits of this battery technology include the following: 1) fast recharge by replacing exhaust electrolyte, 2) high configurable power and energy capacity, 3) long life enabled by easy electrolyte replacement, 4) use of nontoxic materials, 5) full discharge capability and 6) low-temperature operation. The main drawbacks of the system is the requirement for moving mechanical parts such as pumping systems that make system miniaturization difficult. As a result, the commercial uptake to date has still been limited [CHA14], [VAZ10].

### **1.4.3 Functions of Grid Scale BESS for Grid Support**

In recent years the capital cost of battery storage technologies has significantly reduced. BESS can cover a wide range of applications from short term power quality support to long term energy management.

Table 1.3 Specifications of BESS technologies [ANE16], [ONL18f], [KIM17]

Technology	Primary Application	Priorities	Challenges
Lead-acid (PbA)	<ul style="list-style-type: none"> <li>• Grid stabilization</li> <li>• Load levelling and regulation</li> </ul>	<ul style="list-style-type: none"> <li>• Mature battery technology</li> <li>• Good battery life</li> <li>• Low cost</li> <li>• High recycled content</li> </ul>	<ul style="list-style-type: none"> <li>• Large footprint</li> <li>• Electrode corrosion limits life</li> <li>• Low energy density</li> <li>• Limited depth-of-discharge</li> </ul>
Lithium-ion (Li-ion)	<ul style="list-style-type: none"> <li>• Frequency regulation</li> <li>• Power quality</li> </ul>	<ul style="list-style-type: none"> <li>• Relatively good cycle life</li> <li>• High energy densities</li> <li>• High charge/discharge efficiency</li> <li>• Fast response</li> </ul>	<ul style="list-style-type: none"> <li>• Extremely sensitive to overcharge and over temperature</li> <li>• High production cost</li> <li>• Intolerance to deep discharges</li> </ul>
Sodium-sulphur (NaS)	<ul style="list-style-type: none"> <li>• Congestion relief</li> <li>• Power quality</li> <li>• Renewable source integration</li> </ul>	<ul style="list-style-type: none"> <li>• Fast response</li> <li>• Relatively long life</li> <li>• High energy density</li> <li>• Long discharge cycles</li> </ul>	<ul style="list-style-type: none"> <li>• Operating temperature need between 250°-300°C</li> <li>• Liquid containment issues</li> </ul>
Flow batteries	<ul style="list-style-type: none"> <li>• Peak shaving</li> <li>• Time shifting</li> <li>• Frequency regulation</li> <li>• Power quality</li> </ul>	<ul style="list-style-type: none"> <li>• Ability to provide high number of discharge cycles</li> <li>• Relatively long life</li> </ul>	<ul style="list-style-type: none"> <li>• Complicated design</li> <li>• Lower energy density</li> <li>• Lower charge/discharge efficiencies</li> <li>• Not suitable for commercial scale</li> </ul>

This is an important benefit of BESS technologies since it allows various applications to be running on the same device [OUD06], [SUL76] with fast response; including integration renewable smoothing intermittent, peak shaving, load levelling, spinning reserve, flicker compensation, black-start capability, voltage sag correction, transmission upgrade deferral, standing reserve and uninterruptable power supply (UPS) etc. Therefore, the BESS improves the power system stability and security that helps the integration of distributed renewable energies [MER09], [CHO17].

#### 1.4.4 Some Examples of Installed Battery Energy Storage Systems in Power System

This section introduces the BESS installations throughout the world, especially UK-based battery storage systems. Globally there are many BESSs in commercial operation, with most of them used to mitigate renewable power generation. BESS technology is mostly used in the USA and Japan [ROB11]. The existing commercial installations show a positive perspective on the economic viability of BESSs [FEE16]. Battery technologies used in power network applications with their application area are given in Table 1.3. In the UK, there are limited numbers of installed BESS facilities which are suitable for providing grid support. The 6MW/10MWh Leighton Buzzard BESS, once Europe’s largest grid-tied battery storage, was installed in Bedfordshire with 10MWh ES capability in order to protect the UK’s power

network from fluctuations in supply of renewable energy. Comprising 3000 lithium-ion battery cells it has been connected to the electricity distribution network in Leighton Buzzard. The purpose of the project is to balance overall supply and demand, analyse the battery support on the local distribution network by reducing peak demand and stabilizing voltage and evaluating the benefit for the wholesale market [ONL18e]. In 2013, the UK's first grid-tie LTO based BESS, the Willenhall Energy Storage System (WESS), was installed by the University of Sheffield (UoS) to enable research on large scale batteries and to create a platform for research into grid ancillary services [GUN17a], [FEE16]. A detailed explanation about the WESS is provided in Chapter 2.

Table 1.4 Some examples of installed BESS facilities with their grid support applications

Types of BESS	Installation Size	Facility Size Range	Potential/Actual Applications
Lithium-Titanate (LTO)	The University of Sheffield, (WESS), UK [FEE16]	2 MW, 1 MWh	<ul style="list-style-type: none"> <li>• Frequency regulation</li> <li>• Peak shaving</li> <li>• Arbitrage</li> </ul>
Lithium Iron Phosphate	Darlington, UK [ONL18d]	2.5 MW, 5 MWh	<ul style="list-style-type: none"> <li>• Load shifting</li> <li>• Commercial ancillary services</li> </ul>
Lithium-Nickel (NMC)	Leighton Buzzard, UK [FEE16], [ONL18d]	6 MW, 10 MWh	<ul style="list-style-type: none"> <li>• Frequency support</li> <li>• Load shifting</li> <li>• Peak shaving</li> </ul>
Valve-Regulated Lead acid	Lerwick Power Station, Shetland Island, UK [GAL17]	1 MW, 3 MWh	<ul style="list-style-type: none"> <li>• Peak shaving</li> </ul>
Lithium-ion (Li-ion)	Broxburn Energy Storage, UK [ONL19e]	20 MW	<ul style="list-style-type: none"> <li>• Grid support</li> <li>• Enhanced frequency response service</li> </ul>
Flooded Lead acid	Bewag, Germany [SPI91]	17 MW, 14 MWh	<ul style="list-style-type: none"> <li>• Frequency regulation</li> <li>• Spinning reserve</li> </ul>
Nickel Cadmium (NiCd)	Golden Valley, Alaska [SWI10]	40 MW, 4.7 MWh	<ul style="list-style-type: none"> <li>• Electric supply reserve</li> <li>• Spinning reserve</li> </ul>
Sodium-Sulphur (NaS)	Rokkasho, Japan [SWI10]	34 MW, 220 MWh	<ul style="list-style-type: none"> <li>• Renewables energy time-shift</li> <li>• Renewables capacity firming</li> </ul>
Sodium Nickel Chloride (ZEBRA battery)	ZEBRA battery plant, Stabio, Switzerland [SWI10]	40 MWh	<ul style="list-style-type: none"> <li>• Mainly used in EV/HEVs</li> </ul>
Vanadium- Redox Flow Batteries	GuoDian LongYuan Wind Power Co. China [LI16]	5 MW, 10 MWh	<ul style="list-style-type: none"> <li>• Smoothing of wind power</li> </ul>

### 1.4.5 Grid-Tied Battery Energy Storage System Configuration

Fig. 1.6 shows a simplified diagram of the Li-ion BESS showing the li-ion battery pack and associated battery management system (BMS), a bi-directional ac-dc converter, and the control unit which controls the operation mode and grid interface of the ESS. The BMS controller determines the SOC and SOH of each battery cell and employs active charge equalization to balance the charge of all the battery cells in the pack. The ac-dc converter is the interface between the battery pack and the ac power grid, that needs to meet the requirements of bi-directional power flow capability and to ensure high power factor and low harmonic distortion [QIA10]. Principle diagram of the BESS can also be seen in Fig. 1.7.

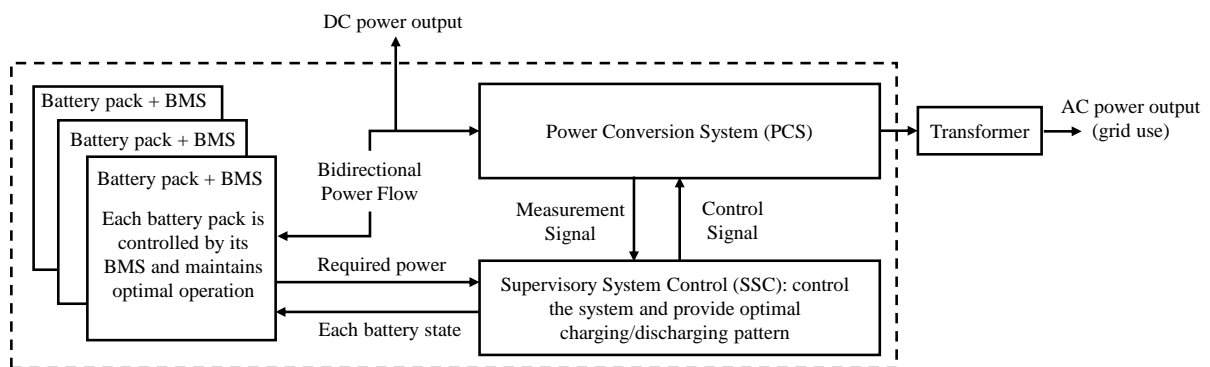


Fig. 1.6 Simplified diagram of a grid-tied BESS [WU19].

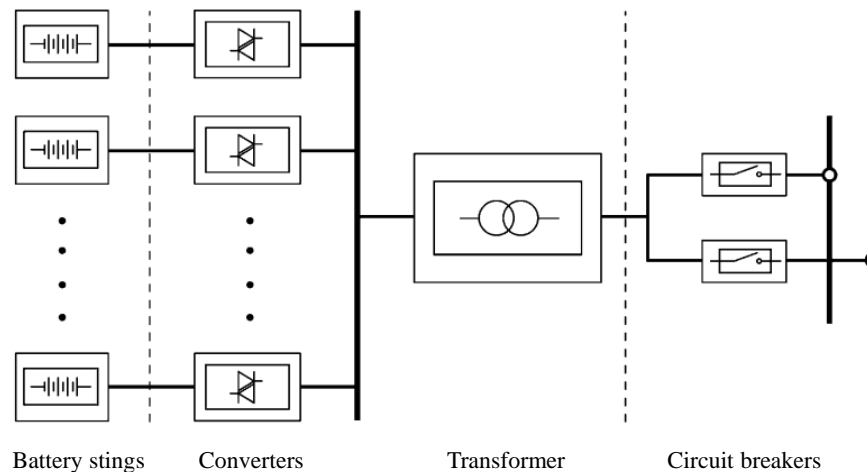


Fig. 1.7 Principle diagram of the BESS in [OUD07a].

### 1.4.6 Battery Management System (BMS)

In a grid-tied BESS, BMS is the essential component to ensure all battery cell voltages being maintained in boundaries for safety operation and battery cycle life. The BMS controller



monitors each battery cell parameters, including cell voltage, charge and discharge current, temperature, and estimates the SOC and SOH of each cell in the pack. Then, the SOC information is used to control the charge equalization circuits to reduce the imbalance between the series-connected battery cells.

### A. BMS Configuration

A typical BMS configuration shown in Fig. 1.8 [QIA11] comprises of module controllers that manage the series-connected battery cells, and a central controller that manages the series-connected battery modules, reports battery cell status, and control the contactors to protect the battery pack from undercharging and overcharging conditions. High voltage isolated controller area network (CAN) bus is used to communicate between the battery module controllers and central controller.

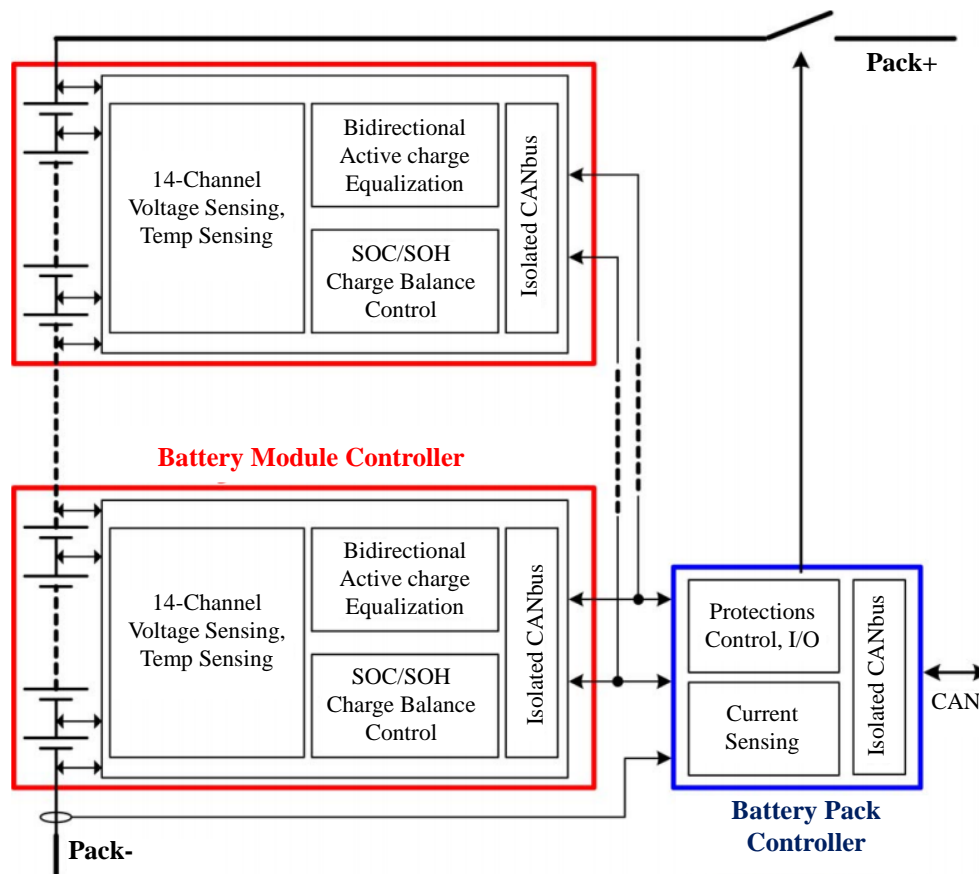


Fig. 1.8 A battery management system configuration [QIA11].

There are two important functions in the BMS given in Fig. 1.8. Firstly, the BMS monitors the condition of all the series-connected Li-ion battery cells in the system. The parameters being monitored include cell charging and discharging current, cell voltage and cell temperature.

These are processed by the BMS controller to estimate the SOC and SOH of the battery cell. Second, the BMS applies active balancing to equalize the battery cells in the pack. In a Li-ion battery system, all cell voltages need to be maintained to within manufacturer set limits to ensure safety operation. However, owing to production deviations, temperature difference within the battery pack and inhomogeneous aging, there will be SOC or capacity imbalance between cells. Minimising these imbalances is essential to guarantee the energy and power performance of the pack as they are limited by the first battery cell that goes beyond the voltage limits. An inductive-based active cell balancing method can be used to regulate the amount of charge in and out of each individual battery cell to balance the mismatches across the battery cell to keep the homogeneous status across the battery pack [QIA10].

### B. SOC Estimation

SOC is a measure of the electrochemical energy volume left in a cell or battery. It can be expressed as a proportion of the battery capacity and shows how much energy is stored in an energy storage device. For the battery industry, it is challenging to precisely estimate the SOC of Li-ion batteries as the electrochemical reaction inside a cell is complicated and difficult to model electrically in an accurate way. Table 1.5 compares various SOC estimation methods found in literature. Among all the techniques, the Coulomb counting technique (CCT) plus accurate open circuit voltage (OCV) approach is used in the BMS given in Fig. 1.8 to estimate the SOC. CCT aims to count how many Coulombs of charge are being pumped in or out of the battery cell. The Coulomb counter includes an accurate battery current sense analog front end and a digital signal processing unit to achieve the offset calibration and charge integration. CCT provides higher accuracy than most other SOC measurements, because it measures the charge flow in and out of battery cell directly. However, it depends on the current measurement accuracy and does not consider Coulomb efficiency of the battery cell. Due to polarization of the battery, power losses obviously occur during the charging and discharging process [CHA13], [QIA11]. In CCT, SOC is calculated by the equation (1.7) [CHA13].

$$SOC_t = SOC_0 - \frac{1}{C} \int_0^t i dt \quad (1.7)$$

where  $SOC_0$  is the initial SOC value, and  $SOC_t$  is the present value of SOC.  $C$  is the total capacity of the battery.  $\int_0^t i dt$  is the integral of discharge current during the discharging process. Several factors may affect the accuracy of CCT including battery history, temperature, discharge

current and cycle life [CHA13]. It should be noted that the Coulomb counting SOC estimation method is used to estimate the SOC of the 2MW/1MWh BESS used and presented in this thesis.

Table 1.5 Comparison of different SOC estimation methods [MEN17], [CHA13], [QIA11]

Method	Features	Advantages	Disadvantages
Discharge	Discharge and measure time to threshold	<ul style="list-style-type: none"> <li>• Most accurate</li> <li>• Easy</li> <li>• Independent of SOH</li> </ul>	<ul style="list-style-type: none"> <li>• Offline &amp; time consuming</li> <li>• Modifies battery state</li> </ul>
Open circuit voltage (OCV)	VOC-SOC look-up table	<ul style="list-style-type: none"> <li>• Accurate</li> <li>• One to one relationship between OCV and SOC;</li> <li>• Small amount of computation;</li> </ul>	<ul style="list-style-type: none"> <li>• Long relaxation time for OCV measurement;</li> <li>• Battery types, temperature and age affect the measurement of OCV.</li> </ul>
Coulomb counting (CCT)	Counting charges been injected/pumped	<ul style="list-style-type: none"> <li>• Easy to understand</li> <li>• Computational effectively</li> <li>• Direct SOC calculation</li> </ul>	<ul style="list-style-type: none"> <li>• Loss model &amp; need accuracy</li> <li>• Accurate initial SOC is needed;</li> <li>• Current sensor error accumulated during the process;</li> </ul>
Artificial network (ANN based method)	Adaptive artificial neural network system	<ul style="list-style-type: none"> <li>• Online</li> <li>• Do not need previous knowledge about battery;</li> <li>• Easy transplant to hardware after offline training</li> </ul>	<ul style="list-style-type: none"> <li>• Large amount of training samples is needed;</li> <li>• Hard to generalize to different driving cycles.</li> </ul>
DC resistance	R <sub>dc</sub>	<ul style="list-style-type: none"> <li>• Easy</li> </ul>	<ul style="list-style-type: none"> <li>• Only for low SOC</li> </ul>
Impedance Spectroscopy based Method	Impedance of the battery (RC combination)	<ul style="list-style-type: none"> <li>• SOC and SOH</li> <li>• Sensitive to SOC variation;</li> <li>• Diverse parameters indicate SOC</li> </ul>	<ul style="list-style-type: none"> <li>• Cost &amp; temp-sensitive</li> <li>• Hard for online measurement;</li> <li>• Different with battery type, experimental condition etc.</li> </ul>
Kalman filter	Get accurate information out of data using filter	<ul style="list-style-type: none"> <li>• Dynamic</li> </ul>	<ul style="list-style-type: none"> <li>• Large computing</li> </ul>
Fuzzy Logic		<ul style="list-style-type: none"> <li>• Online</li> </ul>	<ul style="list-style-type: none"> <li>• Complex and expensive to implement</li> </ul>

### C. Charge Equalization

Owing to inevitable differences in chemical and electrical characteristics from manufacturing, ambient temperatures and aging, there are SOC and capacity imbalances between cells. When

these unbalanced batteries are kept in use without any control (e.g cell equalization), the capacity of the ES decreases severely. Therefore, charge equalization for a series-connected battery string is required to minimize the imbalances between all the cells and prolong the battery life cycle. Charge balancing approaches are described in [QIA11].

## 1.5 Future of UK Power System and National Grid Product Strategies

This section introduces the future UK power system needs over the next five years, and how these system needs are evolving. Fig. 1.9 shows future of UK electricity function [ONL19f]. This section also describes the improvements required to balancing services to meet these needs. On Product Strategy provided by NG [ONL19g], NG is asking for providers' engagement and ideas to simplify and develop balancing services and the products that NG can use to handle these system needs. The System Needs and Product Strategy provided by NG is divided into two distinct parts, the UK power system needs and the product strategy consultation.

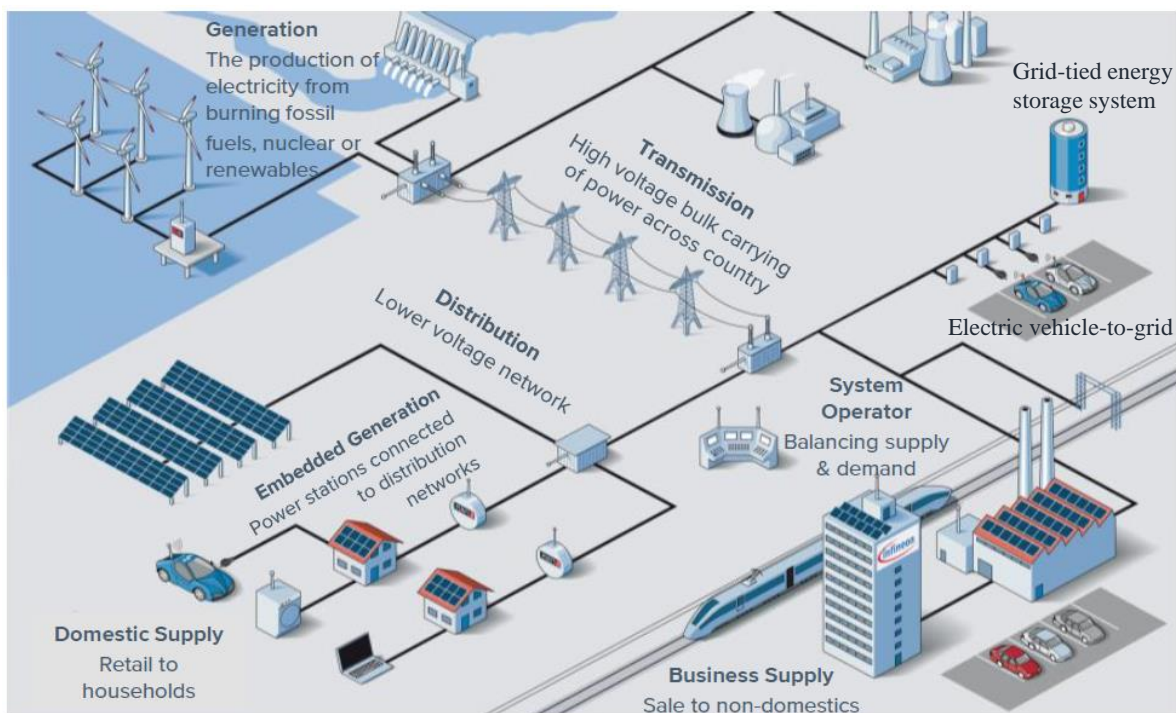


Fig. 1.9 Future of UK electricity function [ONL19f].

### 1.5.1 Comparison of Traditional and Future UK Power System

The UK electricity system is becoming increasingly decentralised, with more complex designs of power generation, transportation and consumption. New flexibility methods are being

developed to manage these changes. This section reviews approaches of developing flexibility, as well as economic and technical barriers to doing so. Fig. 1.10 shows traditional UK power system function [ONL19i]. The UK electricity system has historically developed over a ‘centralised’ system, where a few number of large power stations deliver the majority of electricity generation. Centralised power has been transported in one direction from generators to consumers via the transmission and distribution networks. The definition of generator, transmission and distribution networks are given in Appendix A.1. Distributed electricity generation is the opposite of centralised electricity generation, the mode which has dominated modern commercial electrical supplies for more than a century. Rather than depending on large central stations (fossil fuelled, hydro or nuclear) and high voltage transmission lines, distributed electricity generation relies on small-scale, local, on-site generation, preferably by tapping RESs. This arrangement avoids long-distance transmission losses, and, once organised in a web of smart micro grids, its design improves grid stability and reliability and offers more granular control. Since the cost of new renewable energy conversion continues to decrease, this form of electricity supply is expected to claim an increasing share of overall generation [SMI19].

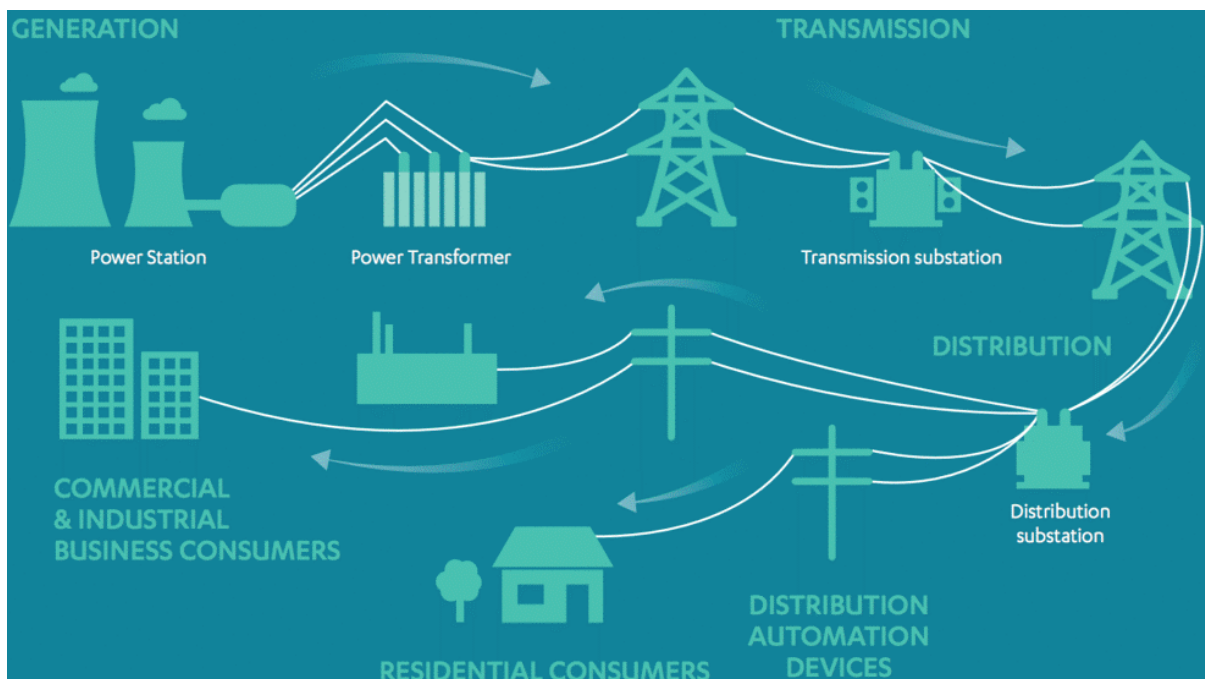


Fig. 1.10 Traditional UK power system [ONL19i].

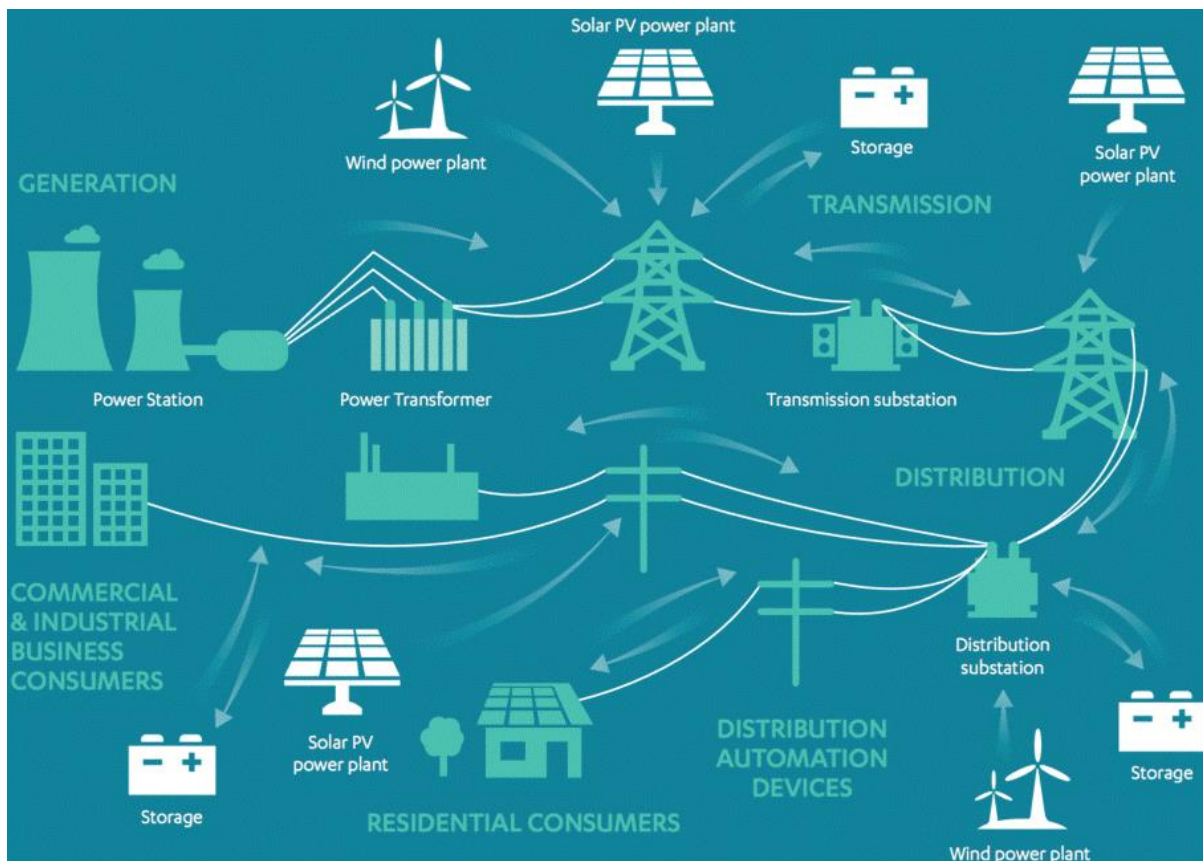


Fig. 1.11 Future of UK power system [ONL19i].

Fig. 1.11 shows the future of the UK power system. Three processes are providing new long-term changes in the UK power system [ONL19a]:

*Decentralisation:* Small power generation (e.g solar panels) situated close to consumers, are providing an increasing part of UK power supply.

*Decarbonisation:* In order to fulfil long-term GHG emissions reduction targets in the power sector, conventional fossil fuel use, especially coal, is lessening. This is in part being replaced by renewable energy generation which is decentralised.

*Digitisation:* Aging electricity networks and information and communication (ICT) infrastructure are being improved, significantly using data and automated processes to make the system operation more efficient. This covers the rollout of ‘smart’ electricity meters.

A substantial part of the new generation capacity is weather-dependent, meaning generation may not balance with demand. Decentralised power can flow in multiple directions over the power network between dispersed generators and consumers. These are causing challenges for

balancing demand and supply. Moreover, the use of electricity to provide heating and for transport is expected to increase. Therefore, parts of the network may need to be strengthened by increasing their capacity, or decreasing peak power flows. More details about the future of UK power system needs and the National Grid (NG) balancing service product strategies will be detailed in Section 1.5.

### **1.5.2 UK Grid Flexibility**

A more flexible power system is being developed to deal with these challenges. Grid flexibility is the ability to fast adjust generation or demand in response to a signal (e.g changing prices) to aid in managing the electricity system. Established and new technologies are increasingly providing grid flexibility, and the roles of power network operators are changing [ONL19a]. This section investigates these flexibility sources, changes to the power networks and potential associated policy challenges.

#### *A. Grid Balancing and Flexibility*

UK electricity demand broadly follows a daily pattern, with peaks in early evening and lows in early morning. Electricity demand and supply are matched on a second by second basis. NG, the primarily electricity transmission network operator in the UK, is responsible for grid balancing. Improving system flexibility will allow NG to balance at shorter timescales and will aid DNOs to manage their local networks more actively. There has been several UK projects which aim to develop more electricity flexibility [ONL19a].

#### *B. Supply Side Sources of Flexibility*

New sources of grid flexibility can act either by varying the electricity supply to the system or the amount of demand on the system. Supply side sources of flexibility adjust the electricity volume delivered to the system to match demand. This can be provided by flexible generators, interconnection to overseas networks or ES [ONL19a].

#### *C. Demand Side Sources of Flexibility*

Demand side flexibility provides financial and other incentives to consumers to adjust their demand, allowing it to coincide with times of high availability of renewables or low prices. Demand side flexibility sources cover demand side response (DSR) [ONL19b] and demand side management (DSM) [WAR14]. DSR and DSM are defined in Appendix A.2. They can be

obtained from energy-intensive commercial, or industrial consumers, or from more distributed sources such as electric vehicles (EVs) and residential consumers. NG aims to obtain 30-50% of grid balancing services from demand side sources by 2020, and it is expected that Distribution Network Operators (DNOs) will increasingly procure them in future. DSR in the UK is mostly operated by aggregator companies, defined in Appendix A.3. Aggregators adjust the demand of their customers to provide pooled flexibility in response to signals from system operators [ONL19a].

#### *D. Using Flexibility within Network*

Improvements in the electricity system will need changes to transmission and distribution network infrastructure. The increasing requirement for flexibility at the distribution level, and future electricity use for transport and heat, mean that the role of a DNO changes. They become more active distribution system operators (DSOs), whose role is similar to that of NG at the transmission level. Some network infrastructure may require network strengthening to contain changes in power flowing over them, and visibility is being increasing over the distribution network to track these power flows easily [ONL19a].

#### *E. Policy Challenges on Grid Flexibility*

Developing a more flexible electricity system improves the security of electricity supply whilst reducing carbon emissions and providing important savings for consumers. However, possible policy challenges of increasing flexibility cover the distribution benefits and costs, and concerns on cyber security and privacy [ONL19a].

### **1.5.3 Future UK Power System Needs**

The future of UK power system needs are described with five key future system needs; including inertia and rate of change of frequency (RoCoF), frequency response, reserve, reactive power/voltage support and black start. However, this section mostly focuses on frequency response. Table 1.6 presents a summary of how these needs are currently met and any potential improvements that could be made.



### *A. System inertia and Rate of Change of Frequency*

System inertia arise from the rotational energy stored in synchronous machines such as nuclear, gas, coal or hydro power plants. Inertia determines how quickly grid frequency will change when there is an imbalance between demand and supply; the higher the inertia, the slower the change in frequency. As levels of solar, wind and interconnection continue to grow, system inertia is expected to drop. Inertia stabilises grid frequency and decreases the RoCoF. Although faster acting frequency response helps to manage a greater RoCoF, some inertia is still needed to maintain frequency for long enough to allow even the fastest grid frequency response to be triggered.

### *B. Frequency Response*

Grid frequency response is an automatic change in demand or generation to respond to changes in system frequency. The amount of response required is directly influenced by system inertia, the largest generation size or demand loss. Frequency response can be summarized as following:

- Frequency response is needed to balance system frequency in real time.
- Response capacity is increasing and the requirement is greatest when the inertia is low.
- NG purchases a firm (stable) volume of response through Firm Frequency Response (FFR) ahead of time.
- The remaining, increasing or variable volume of response is accessed through Mandatory Frequency Response (MFR) in the BM closer to real time. Currently, this is economic and offers flexibility.
- Faster-acting response can decrease the overall volume of response required.
- The flexibility offered by MFR is needed for the volatility of the need, but the number of providers are reducing.
- Changes to respond products are needed that provide a route to market for fast-acting response and the flexibility which NG need closer to real time.
- This will be created using industry consultation and started by March 2018.

**How do NG manage frequency response today?** NG needs response which acts faster than the products which we use today and NG need flexibility closer to real time.

- The need is greatest when inertia is low. With lower system inertia, the frequency moves faster. This shows NG requires faster-acting response.
- ‘Dynamic’ response is used to continuously follow and control small deviations in frequency owing to small imbalances in demand and generation.
- ‘Static’ response initiates when a fixed frequency limit is breached. It is used along with dynamic response, to include a large frequency event such as generator or demand trips.
- The need certainty is less due to several factors such as transmission demands and output from solar and wind. This shows NG requires a market structure that enables procurement and access to flexibility closer to real time as requires become more certain.

### *C. Reserve*

Reserve is required to ensure imbalances which occur from forecasting errors or unexpected losses on the system can be managed. Reserve is instructed manually after automatic frequency response service have provided. Reserve can be either downward (a decrease in generation/increase in demand) or upward (an increase in generation/decrease in demand). Reserve is also used to describe the actions which NG take to ensure that sufficient downward and upward flexibility is available. NG uses a mix of balancing services products, the BM and trading to ensure that NG have access to reserve in the needed timescales.

### *D. Reactive Power*

Reactive power (in Mvar) is used to control voltage. Demand, generation and network equipment (e.g transformers, overhead lines and cables) can either absorb or generate reactive power. These contributions need to be maintained in balance to maintain the voltage at the right level. Voltage is a local property of the system hence needs vary from one region to another.

### *E. Black Start*

Black start is needed to allow electricity network restoration if the transmission system or a large part of the system shuts down. In this unlikely event, it is a requirement that NG is able to restore power in a timely manner.

Table 1.6 UK power system needs and future National Grid plans [ONL19h]

System Inertia and RoCoF	<ul style="list-style-type: none"> <li>• No standalone system inertia product is planned to be maintained.</li> <li>• Complete the plan to desensitize RoCoF.</li> <li>• Continue collaborating in Project Phoenix, which will design, deploy and show the advantages of a new hybrid synchronous compensator to improve grid stability.</li> </ul>
Frequency Response	<ul style="list-style-type: none"> <li>• Procure the design and implementation of an improved grid frequency response product, combining FFR and EFR service, by March 2018.</li> <li>• Until such launch, continue to contract for firm needs ahead of time in tendered markets and access close to real time flexibility through mandatory services.</li> </ul>
Reserve	<ul style="list-style-type: none"> <li>• Standardize present reserve products to increase transparency of their value.</li> <li>• Design and implement a new reserve product in 2018/2019.</li> <li>• Consider new European improvements that may affect the development of reserve products to ensure compatibility with pan-European reserve services.</li> </ul>
Reactive Power	<ul style="list-style-type: none"> <li>• Develop a new reactive market which values the reactive power support needed and provides location signals by the end of 2019.</li> <li>• Investigate how to lessen the number of technical barriers to distributed energy assets requiring to provide reactive power to the transmission system.</li> </ul>
Black Start	<ul style="list-style-type: none"> <li>• Consider alternative ways for system restoration in the event of a partial or total shut down.</li> <li>• Develop a more transparent way for black start procurement which allows greater competition.</li> </ul>

#### **1.5.4 Future of National Grid Balancing Services Product Strategy Consultation – Implications for Energy Storage**

In order to handle the limitations with the existing grid balancing services and better fulfil the challenges of the changing technology mix, NG will simplify the existing product range [ONL19g]. Therefore, NG has launched a consultation on the future of UK grid balancing

services markets. There is an importance on increasing the role of flexible balancing service providers to respond to the needs of the UK power system. This should offer opportunities for BESS providers.

Owing to the changing energy mix on the grid, especially the increasing amount of renewable and decentralized generation on the distribution network, there is more requirement to be able to respond intelligently and flexibly to the system demands. Motivating and making it easier for flexible service providers, such as operators of battery energy storage or demand side services, to participate in the grid balancing services markets can help to achieve this. The Consultations proposals aim to:

- Rationalize the existing proceeding of grid balancing services products by removing any obsolete products.
- Simplifying the remaining service products by standardising contract terms, the procurement process and technical needs.
- Improve the service products based on feedback received from industry.
- Improve the information that NG provided, to make it easier for participants to access grid balancing servicing products.

#### *A. Existing National Grid Balancing Services Markets*

The existing NG balancing services products have been build up over many years as NG needs have gradually shifted. There are currently more than 20 different balancing service products that providers can select from, each with different technical requirements and routes to market; more detail about each balancing service can be found in [ONL19g].

How NG purchases each product is different, however the purchase of each one is to ensure that NG has tools available to maintain the quality and security of the electricity generation at the lowest cost to consumers. This complexity produces a barrier to entry. This affects existing and new balancing service providers, new technologies and business models which may not fit into present product structures.

#### *B. Simplifying the Existing Balancing Services Products*

NG will address the issues described above through a three-stage programme of rationalisation, standardisation and improvement with important engagement with providers.

**Stage 1 – Rationalisation:** Some products are no longer needed in their present form or have been superseded by later products. Therefore, NG is proposing a review to decrease the suite of products that NG procure. Existing contracts for these products will still be respected, however the potential to move to market-based choices will be offered where possible. This does not mean that the requirement behind the product has lessened, just that there is or will be other possible route to market for those providing the product.

**Stage 2 – Standardisation:** Existing NG balancing services markets (e.g Fast Reserve, FFR and STOR) include some parameters which parties can change when submitting tenders. Besides the information on interactions and requirements detailed in [ONL19g], NG will also be looking to give more definition around these tendered parameters through standardising the products within each balancing service market. Approaches include:

- Daily availability windows, e.g 24-hour, 24-hour triad avoidance, evening peak, overnight.
- Contract periods, e.g 1 month, 6 months, 1 year, 2 years.
- Frequency response droop curve, e.g minimum MW power delivery at 0.2Hz, 0.5Hz and 0.5Hz deviations.
- Speed of reserve energy delivery, e.g 2 minutes, 5 minutes, 10 minutes, 20 minutes.

NG will also be reviewing NG contract periods to ensure that they are suitable for all technology types that could deliver the service. NG will keep working with industry to achieve the optimum way to standardise the existing balancing markets through the change proposal governance process.

**Stage 3 – Improvement:** NG wants to ensure that the products that NG purchases are fit for purpose today and in the future. Therefore, NG will work with the industry to improve the NG product suite beyond just standardising the existing balancing market products. NG will improve the product it purchases to better meet both changes in the technical abilities of the assets providing the balancing services, and changes in the commercial arrangements aiding the investment and operation of those assets.

## 1.6 Grid Storage Services and Applications

This section covers some important grid frequency response services and grid storage applications which are used in this thesis.

### 1.6.1 Frequency Response Services

In power distribution networks, the frequency changes continuously because of the imbalance between total generation and demand; if demand surpasses generation, a decrease in the frequency will occur and vice versa [ONL18g], [GUN18b]. Maintaining the grid at a nominal frequency (i.e. 50 Hz for the UK) requires the management of many disparate generation sources against varying loads. This is becoming ever more challenging because of the increased penetration of RESs and subsequent inertial level reduction [GUN17a]. To overcome this issue, the NGET has introduced various frequency response services, including FFR and EFR service, to assist with maintaining the grid frequency closer to 50 Hz under normal operation [ONL18g]. There are three response durations for FFR, including primary frequency response (PFR), secondary frequency response (SFR), and high frequency response (HFR). PFR requires a rapid generator response (see Fig 1.12).. The generator must be capable of increasing its power output within 10 second of predefined grid frequency excursions, and be capable of keeping this response for a further 20 seconds. Generators that deliver SFR services must be capable of increasing their power output within 30 seconds of predefined grid frequency excursions, and be able to keep this response for a further 30 minutes [ONL18h], [BAC07]. HFR must be provided within 10 seconds of a frequency event, which can be sustained indefinitely [ONL18h]. EFR is introduced as a new fast response service for grid balancing service that can provide 100% active power within 1 second of registering a frequency deviation, as shown in Fig 1.12. NG prepared an EFR specification to facilitate a tender competition between potential energy storage providers in 2016 [ONL16a].

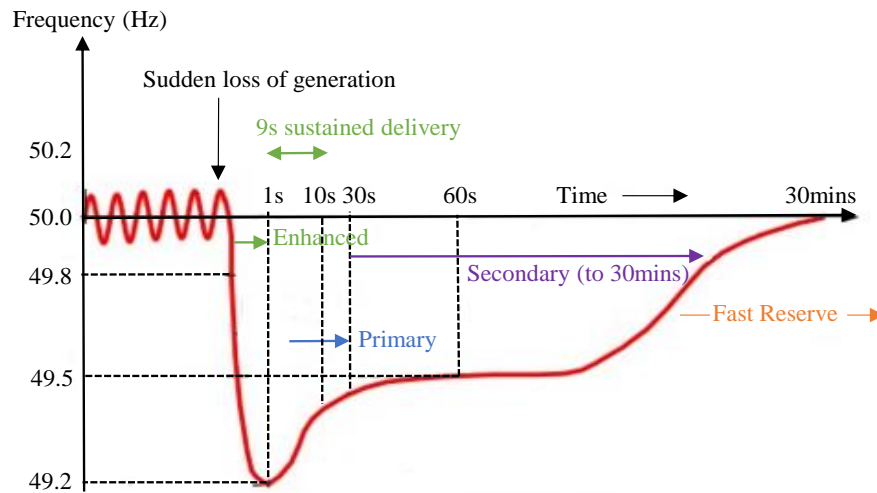


Fig. 1.12 Frequency response services used to limit grid frequency drops in the UK power system.

A BESS is an ideal choice for delivering such service to the power system due to its capability for a faster response time compared to conventional energy generation sources, high energy efficiency, flexible storage size and low maintenance requirements [FEE16], [SAW16]. BESS can reduce power demand variation by smoothing off-peak hours (charge) and shaving on-peak hours (discharge). Several benefits could be obtained from reducing demand variations, such as more reliable energy thanks to more ancillary services, congestion relief in main transmission network and more controllability in the case of unexpected disturbances [ANV17].

DFFR: Dynamic frequency response is continuously delivered and is used to manage second by second grid frequency variations. Dynamic response is automatically provided for all frequency changes outside of the DB ( $50\text{Hz} \pm 0.015\text{Hz}$ ) [ONL18n].

SFFR: Static frequency response is triggered at a defined frequency deviation that is specified in the providers Framework Agreement, which must be in qualified before tendering. There is no requirement to respond within the operating range [ONL18n].

EFR: EFR is introduced as a new fast frequency response service for grid balancing that can deliver full-scale active power within one second of registering a grid frequency deviation. NGET prepared final EFR specification to facilitate a tender competition for 200 MW of support provision to be distributed amongst potential energy storage providers in 2016 [ONL16a].

The amount of response provided by a provider is monitored from time to time during any sampled period. If the energy storage unit is deemed to be underperforming, this causes a reduction in all nomination and availability fees. The formula for calculating the Service Performance Measurement (SPM) is shown in (1.8) [ONL18o]. Availability rate based on SPM can be extracted using Table 1.7.

$$SPM = \text{Highest level of power generation} / \text{Contracted response} \quad (1.8)$$

Availability Fee (£/hr): This is the main fee that all energy storage providers will tender in. It is the number of hours availability from a storage provider for making the service available to the NG.

Nomination Fee (£/hr): Upon a tender being accepted, the NG can select to nominate all or part of the hours tendered in. This payment is generated by each hour nominated. This is a fee for being called upon to deliver the service.

Table 1.7 Availability rate based on SPM obtained from NGET frequency response service specification [ONL18o]

SPM (%)	Availability Rate (%)
<10	0
>10 & <60	50
>60 & <95	75
>95	100

The NG are continually reviewing the FFR service and hence all aspects are subject to change in the future. Existing provider arrangements will be maintained as they are, all new arrangements will be in line with updated current standard contract terms and framework arrangements [ONL18o].

### 1.6.2 Triad Avoidance

Triad refers to the three half-hours settlement periods with the highest system demand between the months of November and February, separated by at least ten clear days. The timing of these peaks is typically between 16:00 to 18:00. These three periods are not known in advance and therefore are determined from the measured data analysed in March of every year. Half hourly



metered (HHM) electricity customers in the UK pay charges proportional to their consumption during the Triad; this is called the Transmission Network Use of Service (TNUoS). The HHM customers can minimise their TNUoS charges by reducing their demand during Triad periods. Many commercial customers have an ES device or back-up generators to ensure the maintenance of critical supplies in case of a failure that can also be engaged to decrease Triad demand; this is known as ‘Triad avoidance’ [ONL18l], [MUL14], [GOU17]. It is also possible for generating assets such as BESSs to export power to the grid during the Triad, this results in a payment from the electricity supplier known as the TAB. It is a complex task to predict the Triad periods in advance, however, many electricity suppliers offer Triad prediction services based on insufficient system margin (NISM) provided by NG and other factors such as the weather forecast. The NG does not predict the Triads and they are not known in advance. Therefore, in order to avoid charges, HHM customers should avoid all potential peaks; this smooths the demand across the winter [ONL18u].

Triad is not a commercial service, however it does represent a benefit for substantial revenues from ESS. The mean energy demand within the three half-hours provide an important proportion of the annual network use charges imposed by the NG. By delivering energy during the Triad periods, ESS can make revenue by either absorbing the inverse of the charge directly or, if metered by an energy supply company, by decreasing the cost to the energy supply company and gaining an agreed proportion of the saving [GRE15].

### **1.6.3 Energy Arbitrage**

The electricity price tends to follow a daily pattern of a low price during off-peak night time hours and a high price during on-peak day-time hours. If the BESS stores energy at off-peak times with the lower price and then resells at on-peak times at a higher price, it can make profit from the price difference, this is referred to as arbitrage [GUN17]. The emergence of wholesale electricity markets in the UK, together with significant increases in prices, and price volatility of electricity have raised the interest in potential economic opportunities for electrical energy storage [SIO09]. One of the main profit streams for ES is temporal arbitrage opportunity obtained by price volatility in the wholesale market. Energy arbitrage refers to the participation of ES in the day-ahead energy market; and it involves utilizing ES to benefit from electricity price fluctuations by charging during low-price periods, discharging during high-price periods,

and profiting from the price differential [TEN17], [DUR14]. ES can also generate revenue through the delivery of ancillary services such as grid frequency regulation [XIN17].

## 1.7 Literature Review

This section provides a general literature review on grid storage services and applications, power system analysis, ESSs and BESSs. Note that each chapter in this thesis includes its own related literature review.

### 1.7.1 Frequency Regulation

Since the EFR is introduced as a new UK grid balancing service published in the late of 2016, in literature there are only a few papers about EFR service delivery for grid support. In [GRE17], a new EFR control algorithm implemented in the DC/AC converter of a BESS was developed to fulfil the NGET EFR service requirements, however in this thesis EFR control is achieved with battery energy management system rather than controlling the energy storage converter. The study [GRE17] compares the performance of the EFR Service-1 (wide dead-band) and Service-2 (narrow dead-band), and it was stated that the narrow service is technically more challenging, likely requiring four time the storage capacity of the wide service. That control algorithm does not cover the 15-mins frequency event control to be able to increase the availability of the BESS, especially with the narrow dead-band. However, this thesis extends the basic EFR control algorithm with the two different extended 15-mins frequency event controls to achieve a maximum BESS availability for delivering EFR service. In addition, in [GRE17], the algorithm manages the SOC of the BESS, maintaining at 49-51%. But, the SOC band should not be kept at less than 5% SOC band in order to reduce battery degradation and hence prolong its lifetime.

In [COO17], *Cooke et al.* present a method of providing the new EFR service to avoid the necessity of holding more FFR in reserve when system inertia falls. That study also introduced several alternative response curves which indicate that if arresting the fall in grid frequency in the event of a drop in generation is an important aspect of the control design, then a stepped response may provide a better service. An energy storage strategy based on PI control can help with restoration and damping of frequency. However, that response time will be slower than a stepped response so that stability can be ensured.

In [CAN17], the authors investigate the possible performance of a BESS in EFR provision, by simulating its response to grid frequency according to the EFR service requirements, and this evaluating its ability to exchange energy for the service, a service performance indicator, and the possible aging related to battery cycling. Different EFR power versus frequency characteristics, BESS technologies and BESS energy capacities are considered in [CAN17]. It was also assumed that the BESS are connected to the UK or to the Continental Europe (CE) synchronous area; therefore, for the CE system those requirements are adjusted according to the CE frequency behaviour. However, a major specification of the EFR service is to consider ramp-rate limits in the UK requirements, it was not considered in [CAN17] for simplicity; power exchange rate limits internal to the batteries was also neglected. In addition, that study did not cover an extended 15-min frequency event control in order to increase the batteries availability. In contrast to the above studies in the field; the main contribution of this thesis is to present a control algorithm that enables BESSs to provide a bi-directional power in response to changes in the grid frequency, whilst managing the SOC of the BESS to optimise availability of the system. This thesis also introduces a strategy to generate additional revenues from ancillary services such as Triad Avoidance only available during the winter season. Moreover, this thesis considers layering the new UK grid frequency balancing service, EFR, with Triad Avoidance or Energy Arbitrage in order to maximise the system's availability and profitability. This thesis also includes experimental validation with a 2MW/1MWh lithium-titanate BESS, called Willenhall Energy Storage System (WESS), commissioned and operated by the University of Sheffield, which is the largest research only platform for grid-tie energy storage applications.

### **1.7.2 Grid Storage Applications**

The emergence of wholesale electricity markets in the UK, together with significant increases in prices, and price volatility of electricity have raised the interest in potential economic opportunities for electrical energy storage [SIO09]. One of the main profit streams for energy storage (ES) is temporal arbitrage opportunity obtained by price volatility in the wholesale market. Energy arbitrage refers to the participation of ES in the day-ahead energy market; and it involves utilizing ES to benefit from electricity price fluctuations by charging during low-price periods, discharging during high-price periods, and profiting from the price differential [TEN17], [DUR14]. ES can also generate revenue through the delivery of ancillary services such as grid frequency regulation [XIN17]. Comparing those papers, this thesis investigates

two applications for BESS, grid frequency regulation and energy arbitrage in day-ahead spot markets, and how they be scheduled in a complimentary way such that revenues are maximised whilst meeting service compliance.

Numerous research studies around the world have been carried out to investigate the participation of large scale ESS in power grid and frequency regulation services. [BEV10] presents the concerns of the integration of new renewable power generation in power systems with a grid frequency regulation perspective. The study also covers a comprehensive overview on recent developments in the area of grid frequency regulation. ‘Energy management’ is a term that has several meanings, in this thesis we focus on an optimized utilization of the available stored energy in a grid-tied BESS operating in grid frequency regulation services. In literature, there are various research works that have dealt with the energy management issue in grid scale energy storage systems and also control strategies for grid-tied BESS operating in frequency regulation with regard to different points of functionality and objectives [ANV17]. Several methods in the smart grid environment have been developed to optimally manage the energy flowing on the smart system. [MBU17] presented a novel optimisation method of energy cost reduction in smart grid applications to include real-time electricity pricing and energy management. *Basaran et al.* [BAS17] introduced a novel power management strategy by designing a wind-PV hybrid system to operate both as a grid-tied system and an autonomous system. The proposed management unit implements measurements from various points in the system; providing an effective energy transfer to batteries, loads and grid. Considering the cost of batteries, adopting an effective charge/discharge management strategy for the efficient use of the battery in order to achieve high state-of-charge (SOC) and prolong battery lifetime is essential [EGH14]. *Gundogdu et al.* [GUN18b] presented a novel energy management strategy that enables grid-tied BESS to provide bi-directional power in response to changes in the grid frequency, whilst managing the SOC of the BESS to optimise utilisation of available energy and the availability of the system. The study also presented a strategy to generate additional revenues from ancillary services such as triad avoidance.

In literature, there are also many papers relating to the energy arbitrage application [26-31]. *Sioshansi et al.* [SIO09] presented one of the leading studies on energy arbitrage that analyses four key aspects of the economic value of electricity storage in the Pennsylvania-New Jersey-Maryland (PJM) markets: -The basic relationship among storage energy capacity, storage efficiency and the arbitrage value of energy storage; -The accuracy of theoretical ES dispatch

and the value of arbitrage using perfect foresight of future electricity prices; -The temporal and regional variation in the value of energy arbitrage, investigating natural gas price variations, transmission constraints and fuel mixes on energy storage economics. The impact of larger storage devices, investigating how the use of ES can decrease on-peak hourly prices and increase off-peak hourly prices diminishing the value of arbitrage, while producing welfare effects for generators and consumers. In comparison with this study [SIO09], the focus of this thesis is related to not only energy arbitrage, but also the scheduling of grid balancing services such as frequency response for additional benefit.

### **1.7.3 Distributed Generation (DG) System**

In the past, distribution systems were distinguished by the uni-directional power flow from centralized power generation stations to transmission and distribution networks. In recent years with the power system restructuring process, centralized energy sources are being replaced with decentralised ones. This has led to a new concept in electric power systems, especially in DG. Utilizing DG is essential for secure power generation and reducing power losses, however, the use of such technologies introduces challenges to power systems such as their optimal location, voltage regulation and power quality issues. Another important point which needs to be considered relates to specific DG technologies based on RESs, such as solar and wind, due to their uncertain power generation [ISM19]. Several types of renewable and non-renewable DG are available, including hydro power, wind turbines, PV, thermal solar, diesel generators, geothermal, fuel cells and microturbines [ROY15]. Recently, many DGs such as wind power generation have been installed into power systems. However, the fluctuations of these generator outputs affects the power system frequency. Therefore, in [ARI06], introduction of BESS to the power system was considered in order to suppress the fluctuation of the total power output of the DG.

*Razavi et al.* [RAZ19] provides a comprehensive review of various types of DG and investigates the new challenges arising in the presence of DG in electrical grids. In [YUK07], a method was developed to improve the power quality of a DG power system. The method uses an ESS with DG using RESs such as PV generation, wind power generation and FC. The paper demonstrated that the electric power quality is improved when the battery storage is introduced. *Obaid et al.* [OBA15] investigated the UK power system with FES and BESS alongside EVs for primary frequency control. The paper also presented an analysis of the simplified model of

the UK power system for 2030 projections. *Muttaqi et al.* [MUT19] provided a review of the state of art of future power grids, where new technologies will be integrated into the power distribution grid. *Mehigan et al.* [MEH18] also provide some predictions on what level of DG is expected, appropriate or optimal in future power systems. The paper investigated the factors that influence the role of DG in future electricity systems.

#### **1.7.4 Energy Storage Systems (ESSs)**

Owing to the great potential and the multiple functions of ESS, in literature there are many studies on ESS research, its developments, demonstrations and industrial applications. *Ibrahim et al.* [IBR08] investigated the need to store energy for improving power networks and maintaining load. A group of characteristics of various ESS technology is provided, which can help to improve performance and cost estimates for ESSs. The study provided a well-organized and comprehensive review on progress in ESSs, which included many types of ESS technologies and their applications and deployment status [CHE09].

In literature, there are a number of review articles focusing on several ESS technologies; including BESS [ZHA18], flywheels [MOU17], supercapacitors [BOY00], SMES [ALI10], TES [ALV18], CAES [BUD16] and PHS [REH15]. Battery, ultra-capacitor and fuel cell storage technologies were discussed and compared in [KHA10]. History, evaluation and future status of different ESS technologies were provided in [WHI12], [MAS10]; and a comprehensive review on ESS technologies, their roles, and impacts on future power system is given in [NAD19]. New technology and possible advances in energy storage technologies is evaluated in [BAK08]. According to *Baker et al.* [BAK08] the greatest potential for technological improvements probably lies in the incremental development of existing ES technologies facilitated by advances in engineering, material science, processing and fabrication. These factors are applicable to both thermal and electrical storage. Future ES technologies may be expected to offer increased power and energy densities, although, in practice, longevity, in reliability, cycle life expectancy and cost may be more important than increases in power/energy density. *Soloveichik et al.* [SOL14] provided a detailed review on the development of regenerative fuel cells (RFCs) and the current status of hydrogen-based RFCs for ES applications. RFCs are capable of both power generation and, in a reverse mode, a fuel production. The review study [SHA18] also provided an overview of different ES approaches and focused on hydrogen-based ES methods. The study presented the state-of-art

HES methods and addressed the technical challenges in this field. The various applications of hydrogen in load levelling and transportation are also presented in [ROH16].

*Greenwood et al.* [GRE17] published a leading study that provided new methods to analyse and assessing the performance of ESSs within existing service frameworks, using real-time network simulation and power hardware in the loop. New statistical approaches were devised to quantify the design and operational needs of ESS delivering EFR service. *Patsios et al.* [PAT17] introduced a case study, a 50 MW wind farm with hybrid ESS consist of NaS and SCs, and presented on Newcastle University research on hybrid ESSs; including hybrid systems sizing and technology selection, complementing renewables, industrial applications etc. The useful study also presented on ESSs technology selection and sizing and laboratory facilities dedicated to hybrid ESS integration.

*Jenkins et al.* [JEN17] provided a control methodology for the grid to consider a number of EVs in a similar way to more established ESS allowing existing ESS control algorithms to be utilised. The study [VAC16] built on established methods for sizing ES to complement wind generators on delivering grid frequency support and introduces considerations for hybrid ESS consists of more than one ES technology. The methodology was applied for a 60MW wind farm complemented by Vanadium Redox flow battery and supercapacitors for the provision of UK primary, secondary and high frequency response.

### **1.7.5 Battery Energy Storage Systems (BESSs)**

In the UK, a limited number of grid-tied BESS have been installed for delivering grid scale applications. A 2.5 MW/5MWh lithium iron phosphate ESS based in Darlington provides commercial ancillary services and load shifting to the power grid. A 6MW/10MWh lithium-nickel ESS based in Leighton Buzzard provides frequency support, load shifting, peak shaving and arbitrage applications to the grid. In 2013, the UK's first grid-tied lithium-titanate BESS; the Willenhall Energy Storage System (WESS), was installed by the University of Sheffield to enable research on large scale batteries and to create a platform for research into grid ancillary services such as fast frequency response [GUN17a], [GUN17b].

The study [OUD06] investigated the important potential of BESS for grid frequency regulation. Their value analyses is obtained by comparing frequency control reserve prices on the grid ancillary services market with standard BESS installation and maintenance costs. The BESS

can meet the technical requirements for primary frequency regulation by injecting power to the grid on low frequency excursions, below a nominal value, and absorbing power from the grid for high frequency periods, above a nominal set point. Moreover, since the BESS is composed only of static elements, it has a faster dynamic response compared to conventional generators or other storage devices.

In recent years, many BESSs have predominantly been installed worldwide for peak shaving and load levelling. Most early projects intended for grid frequency control were actual demonstrations for the feasibility of the technology and the economic feature was often left aside. For this reason, preceding BESS devices were usually over-dimensioned, thus eliminating any chances of high economic profitability [MER09]. A previous study [OUD07a] presented an optimisation strategy for the dimensioning of a BESS for primary frequency response using a control algorithm based on fixed state of charge limitations. The strategy developed enables sizing of the main parameters of a BESS; including battery capacity, minimum and maximum SOC, along with recharge and discharge powers, for primary frequency response control applied to a large interconnected power system. The study [LU95] derived a BESS dynamic model applied to power system stability; [KOT93] evaluated the effect of a 30MW battery device for grid frequency regulation in the Israeli isolated power system; [OUD06] performed a value analysis of various BESS applications; [OUD07b] examined the dimensioning and optimisation of the BESS applied to primary frequency control in interconnected networks; [ADI99] merged an incremental model of the BESS into the load frequency control of an isolated power system and evaluated the system performance improvement.

*Mercier et al.* [MER09] presented a method for optimal sizing and operation of a BESS used for spinning reserve in a small isolated power system. A new control algorithm using adjustable SOC limits is applied and tested on a BESS dynamic model. An optimal sizing method of the BESS is developed for an isolated power system in order to obtain highest profitability of the device. It was demonstrated that the BESS can significantly improve the power system stability, grid security and the flexibility for a small isolated power system with low grid inertia. It also meets the frequency control requirements with a high economic profitability.

BESSs inherently have a great flexibility for charging and discharging processes. Flexibility is likely to become an essential resource in the future power grid [BRA13]. Numerous studies investigated multi-purpose usage of BESS in the electric power system; most of them focusing



on the provision of local distribution grid services [BRA14], [OUD07b], [WEI14]. The use of battery unused capacity, in terms of power and energy, to provide primary control reserve (PCR) was investigated in [HOL16]. Cost-effectiveness in different regions [MIR15] such as Germany [HOL15], and the technical feasibility for this concept was presented in [THO13], [BOR13], [MEG13].

*Zhu et al.* [ZHU19] provided an optimal coordinated control of multiple BESS for primary regulation (PFR) service. The study proposed a profit-maximizing BESS coordination control strategy that is concerned with two operational phases, namely frequency regulation and SOC recovery. Regarding the frequency regulation phase, the study minimized the regulation failure penalty by optimally coordinating the operation of multiple BESSs in response to frequency deviations. For the SOC recovery phase, the study proposed to derive the optimal SOC target for the BESS. By adjusting the SOCs to the target during the SOC recovery phase, the expected regulation failure penalty is minimized for the upcoming grid frequency failure events. Comparing the single-BESS scenario, the major difficulty of multi-BESS control is the optimal coordination of BESSs at the frequency regulation. If not properly coordinated, some BESSs may exhaust their energy capacity before the others, which decreases the total power capacity available and may cause unwanted regulation failures [ZHU19].

*Patsios et al.* [PAT16] provided an important and leading study on control of grid-tied BESSs. The study also investigated the effect of SOC management on battery degradation and overall system efficiency. It was demonstrated in the study that on managing battery SOC, higher SOC bands increase the rate of battery degradation, whilst lower SOC bands decrease system efficiency owing to higher losses in the battery.

The well-known reference study [DIV09] investigated the current status of BES technology and methods of assessing their economic viability and impact on power system operation. A comprehensive discussion on the role of BESSs of electric hybrid vehicles in power system storage technologies was also provided.

Application and modelling of BESS in power systems was evaluated in [XU16]. The important study provided a useful guidelines in the use of new models to represent a BESS for power system analysis.

### 1.7.6 Power Management & Energy Management System (EMS)

Energy management is a term that has several meanings, in this paper we focus on an optimized utilization of the available stored energy in a grid-tied BESS operating in grid frequency regulation services. In literature, there are various research works that have dealt with the energy management issue in grid scale energy storage systems and also control strategies for grid-tied BESS operating in frequency regulation with regard to different points of functionality and objectives [MOG17]. Several methods in the smart grid environment have been developed to optimally manage the energy flowing on the smart system. [MBU16], [MBU17] presented a novel optimisation method of energy cost reduction in smart grid applications to include real-time electricity pricing and energy management. *Basaran et al.* [BAS17] introduced a novel power management strategy by designing a wind-PV hybrid system to operate both as a grid-tied system and an autonomous system. The proposed management unit implements measurements from various points in the system; providing an effective energy transfer to batteries, loads and grid. Considering the cost of batteries, adopting an effective charge/discharge management strategy for the efficient use of the battery in order to achieve high SOC and prolong battery lifetime is essential [EGH14]. *Bahloul et al.* [BAH18a] presented a hybrid power management method and investigated its impact on battery life extension on operating grid frequency regulation [BAH18a]. *Bahloul et al.* [BAH18b] also published another important study on a power management system for controlling a hybrid-supercapacitor hybrid ESS (HESS) on operating EFR service.

According to *Byrne et al.* [BYR18], EMSs and optimization methods are needed to safely and effectively utilize ES as a flexible grid asset that can deliver multiple grid services. The study provided a review of grid-scale ESS and overview of EMS architectures, and a summary of the existing leading applications for storage. The study also provided a comprehensive discussion of EMS optimization methods and design.

*Shen et al.* [SHE15] provided a supervisory EMS for real time implementation for a battery/ultracapacitor HESS. Furthermore, a rule-based EMS was also implemented in the work for comparison with the proposed EMS strategy. *Ke et al.* [KE15] presented an EMS control methods and sizing strategies for using ES to manage energy imbalance for variable generation resources.

The study [KHA17] presented a technical and economic model for the optimal sizing of a grid-tied photovoltaic-battery energy systems (PV-BES) for different battery technologies. An iterative analytical technique is used to determine the battery capacity, generate multiple combinations of PV-BES over a defined range of PV rated power, and apply a proper EMS.

### **1.7.7 Battery Management System (BMS) and State-of-Charge (SOC) Estimation**

An effective BMS using the Li-ion battery is essential so that battery can operate safely and reliably and to provide the full available power and energy capacity. Moreover, a BMS is important for collecting and processing data, detecting faults, equalizing battery voltage that are the significant factors for obtaining a good accuracy of SOC and SOH [HAN17]. SOC in BMS system is considered as one of the important and critical factors that has been researched in recent decades. The studies [HAN17], [HE12] discuss the Li-ion battery SOC estimation and management system in EV applications.

Various SOC estimation methods was proposed in literature [HUE98], [PIL01], [PEI06]. Among these, the internal resistance and the terminal voltage of a battery are two parameters than can be easily attained and hence are convenient for SOC estimation. However, these parameters not only change irregularly with the DOD, the ambient temperature and the charging/discharging rate, but also depend highly on SOH of the batteries which will decrease with time. The complex interrelationship of these factors brings into the difficulties in the research of an accurate SOC estimation method. [SOO09] proposes a SOC estimation method for Li-ion batteries on the basis of coulomb counting. The CCT calculates the remaining capacity simply by accumulating the charge transferred in or out of the battery. The recent applications of battery power in many portable devices and EVs [AFF05], [ROT05], are facilitating the realisation the application of CCT. The accuracy of this method reports mainly to an accurate measurement of the battery current and precise estimation of the initial SOC. With a pre-known capacity, which might be stored in the memory or initially estimated by the working conditions, the battery SOC can be calculated by integrating the charging and discharging currents over the working periods. However, the releasable charge is generally less than the stored charge in a charging and discharging cycle. This means, there are losses at charging and discharging process [COL07]. For more accurate SOC estimation, these factors has been taken into account in the CCT based SOC estimation method used in this thesis. There are various factors that affect the accuracy of Coulomb counting technique, including battery history, temperature, current measurement, and cycle life [SOO09].

### 1.7.8 Battery Lifetime Analyses

A key factor in BESS operational planning is the lifetime of battery. Therefore, a model which formulates the degradation mechanism as a function of battery operations is essential to account for the battery operating cost. Battery degradation models can be categorised as theoretical models and empirical models. Theoretical degradation researches [VET05], [NIN04], [NIN06], [SPO03], [ZHA08] have mostly investigated the loss of lithium ions and other active materials. These models provide comprehensive explanation of the different degradation mechanisms and how they are affected by the condition and use of the battery. At the planning stage one can only predict the BESS operating pattern, and no information is available on the cell conditions. Theoretical works linking operational-level observations to the molecular-level degradation processes are currently insufficient [SMI13], [LAR15]. Therefore, it is difficult to directly correlate the charging and discharging processes with the molecular-level processes occurring inside the cells.

Empirical models are more convenient to incorporate with storage planning and operations works [KOL13], [PET10], [ORT14]. Each of these empirical degradation models are developed for a particular BESS application, where the BESS operating region is narrow and model based degradation experiments can achieve an accuracy that is satisfactory. Empirical battery degradation models are limited by underlying experimental data. Therefore, a model designed for a specific application scenario may not be applicable to another. For instance, empirical models for EVs generally assume a regular daily charging scheme. Such a model is unlikely to be applicable to predict the performance of a battery used for grid frequency regulation, where the BESS follows a stochastic charging and discharging signal. Therefore, attaining an accurate empirical model of battery degradation needs that operation-specific battery aging experiments be performed for each new application. Such tests take a lot of time and would have to be performed in advance using costly test facilities. To overcome these difficulties, the study [XU18] proposes a semi-empirical battery degradation model intended for off-line battery life estimations. The model combines theoretical analyses with experimental observations, and gives a model that is accurate not only within the operating region covered by the experimental data, but is also suitable to other operating conditions.

Capacity fading in battery cells owing to charging and discharging is similar to the fatigue analyses of materials subjected to cyclic loading [VET05], [LAR15], [WAN11]. Each cycle generates an independent stress, and the loss of battery life is the result of the accumulation of

all cycles. Milner [MIL10] created an analytical cycle-based model based on Zhurkov's crack propagation theory [ZHU65] and the Arrhenius relationship [12]. [BEL16], [KAR13] implement the Rainflow cycle counting algorithm [MAT68], [DOW82] to count cycles in the battery's SOC profile. The Rainflow algorithm is broadly used for fatigue analyses and has been applied to battery cycle analysis in [DUF08], [MIS02], [CHA10].

## **2 Control of Grid Tied Battery Energy Storage System for Frequency Response Services**

Balancing the grid at 50 Hz requires managing many distributed generation sources against a varying load, which is becoming an increasingly challenging task due to the increased penetration of RESs such as wind and solar and loss of traditional generation which provide inertia to the system. In the UK, various frequency support services are available, which are developed to provide a real-time response to changes in the grid frequency. The NGET, the primary electricity transmission network operator in the UK, has introduced the FFR service which requires a response time of 2-30 seconds, depending on FFR service type; and the new fastest EFR service, which requires a response time of under one second. A BESS is a suitable candidate for delivering such service. Therefore, in this chapter a new DFFR control algorithm is presented which generates a charge/discharge power output with respect to deviations in the grid frequency and the NGET required DFFR specification. SFFR high and low frequency response control algorithms are also developed to deliver a non-dynamic service where an agreed amount of power is absorbed/generated if the grid frequency reaches a certain trigger point. Four EFR control algorithms are finally developed to provide a charge/discharge power output with respect to deviations in the grid frequency and the ramp-rate limits imposed by the NGET, whilst managing the SOC of the BESS for an optimised utilisation of the available stored energy. The simulation results of the FFR and EFR control algorithms developed in MATLAB/Simulink are experimentally validated by a 1MWh LTO battery based WESS, operated by the UoS.

### **2.1 Introduction**

In power distribution networks, the frequency changes continuously because of the imbalance between total generation and demand; if demand surpasses generation, a decrease in the frequency will occur and vice versa [ONL18g], [GUN18b]. Maintaining the grid at a nominal frequency (i.e. 50 Hz for the UK) requires the management of many disparate generation sources against varying loads. This is becoming ever more challenging because of the increased penetration of RESs and subsequent inertial level reduction [GUN17a]. To overcome this issue, the NGET has introduced various frequency response services, including FFR and EFR service, to assist with maintaining the grid frequency closer to 50 Hz under normal operation [ONL18g].

Various research studies around the world have been performed to investigate the participation of large scale BESS in power grid and FFR services [STR16] [STR17] [KNA16]. In [LIA17], a methodology for optimising BESS with respect to the control parameters for delivering FFR service and the size of the BESS is proposed under UK regulatory framework using historical grid frequency data. An economic analysis is also performed based on the estimated battery lifetime and the UK grid frequency regulation market. [BEV10] presents the concerns of the integration of new renewable power generation in power systems with the grid frequency regulation perspective. The study also covers a comprehensive overview on recent developments in grid frequency regulation area.

Since the EFR is introduced as a new UK grid balancing service published in 2016, in literature there are limited number of papers about EFR service delivery for grid support. *Greenwood et al.* [GRE17] published a leading study that provided novel methods to analyse and assessing the performance of ESSs within existing service frameworks, using real-time network simulation and power hardware in the loop. The study [GRE17] also compares the performance of the EFR Service-1 (wide DB) and Service-2 (narrow DB), and it was stated that the narrow service is technically more challenging, likely requiring four times the storage capacity of the wide service.

In [COO17], *Cooke et al.* considers different ES strategies for assisting with frequency response and compares these to the EFR and the more traditional FFR service. The study presents a method of providing the new EFR service to avoid the necessity of holding more FFR in reserve when system inertia falls.

In [CAN17], the authors investigate the possible performance of a BESS in EFR provision, by simulating its response to grid frequency according to the EFR service requirements, and evaluates its ability to exchange energy for the service, a service performance indicator, and the possible aging related to battery cycling. Different EFR power versus frequency characteristics, BESS technologies and BESS energy capacities are considered in [CAN17]. It was also assumed that the BESS are connected to the UK or to the Continental Europe (CE) synchronous area; therefore, for the CE system those requirements are adjusted according to the CE frequency behaviour. However, a major specification of the EFR service is to consider ramp-rate limits in the UK requirements, it was not considered in [CAN17] for simplicity; power exchange rate limits internal to the batteries was also neglected. In addition, the study did not cover an extended 15-min frequency event control in order to increase the BESS

availability. In [BAH18], a design framework for a power management system is presented to respond to the EFR service requirements with two storage system topologies; battery and hybrid ESS.

In contrast to other recent works in the field, the main contribution of this chapter presents a DFFR control algorithm that enables BESSs to deliver dynamic power in response to deviation the grid frequency with respect to the NGET DFFR specifications.  $SFFR_{high}$  and  $SFFR_{low}$  control algorithm are also developed to deliver a non-dynamic power if the grid frequency reaches a certain high and low grid frequency. This chapter also introduces four EFR control algorithms that enables BESSs to provide a bi-directional power in response to changes in the grid frequency, whilst managing the SOC of the BESS to optimise availability of the system. The first model introduces a standard control algorithm designed to meet the technical requirements of the NGET specifications. The advanced EFR algorithm addresses the EFR service design with an extended 15-minute frequency event control, in order to optimise the use of the available stored energy. The other advanced algorithm extends the EFR control algorithm to include a dynamic SOC target to maximise the energy stored. Finally, the last algorithm includes an SOC-based proportional controller to optimize the power delivery in order to reduce the battery degradation and hence extend the battery lifetime. The developed DFFR and EFR control algorithms have been experimentally validated with the WESS.

## **2.2 BESS Control for Firm Frequency Response (FFR) Service**

The NG has a statutory obligation to keep the frequency of the NGET within  $\pm 1\%$  of 50Hz (49.5Hz to 50.5Hz). The control room typically controls grid frequency within a tighter operational limit of 49.8Hz to 50.2Hz. Grid frequency is changing continuously, and it is determined and controlled by the balance between generation and demand. If generation is greater than demand, grid frequency increases; or if demand is greater than generation, frequency decreases. Therefore, the NG must ensure that sufficient demand and/or generation is held in readiness to respond to grid frequency deviations. Response represents the ability to adjust demand or generation to compensate for deviations in grid frequency within 2-30 seconds, depending on the type of FFR service [ONL18n].

In order to manage the grid system frequency NG relies on balancing service providers to adjust their active power output or consumption in order to minimise the imbalance between demand



and generation on the system. The extent of the required adjustment is determined by the system frequency deviation from 50Hz [ONL18h]. Therefore, NG purchases balancing services to manage the grid frequency; FFR is a frequency response service for grid balancing service that can supply a minimum of 1MW active power within a frequency deviation. FFR is open to all parties that can prequalify against the service requirements. Providers can provide other grid balancing services when they are not delivering FFR. Agreed loads, when summated, must be equal to or higher than 1MW. There must be a single point of dispatch or an approach in which the total output of the combined loads can be monitored to show to the NG that the service is available. FFR service is a proportional or continuous modulation of demand and generation; so FFR service can be either dynamic or static. There are three main dynamic service types, including primary (full output within 10 seconds sustained for further 20 seconds), secondary (full output within 30 seconds sustained for further 30 minutes) and high (requires to be achieved within 10 seconds and sustained indefinitely), as shown in Fig 1.12. In DFFR, power changes proportional to system frequency and in SFFR, a set power level is delivered at a defined frequency and remains at the set level for an agreed period [ONL18h], [ONL18i], [ONL18j].

A BESS model is developed in MATLAB/Simulink and verified against experimental operation of the WESS. Using the NGET required FFR service specifications, three FFR control algorithms, including DFFR, SFFR<sub>high</sub> and SFFR<sub>low</sub> are then implemented in the BESS model independently to deliver a grid frequency response service to their NGET service specifications [ONL18h]. The NGET required FFR service specifications and the proposed FFR control algorithms are detailed in the following sections.

### **2.2.1 BESS Control for Dynamic FFR Service with No Battery SOC Management**

In this section, a control algorithm is developed to meet the NGET required DFFR service specifications, as shown in Fig. 2.1 and Table 2.1.

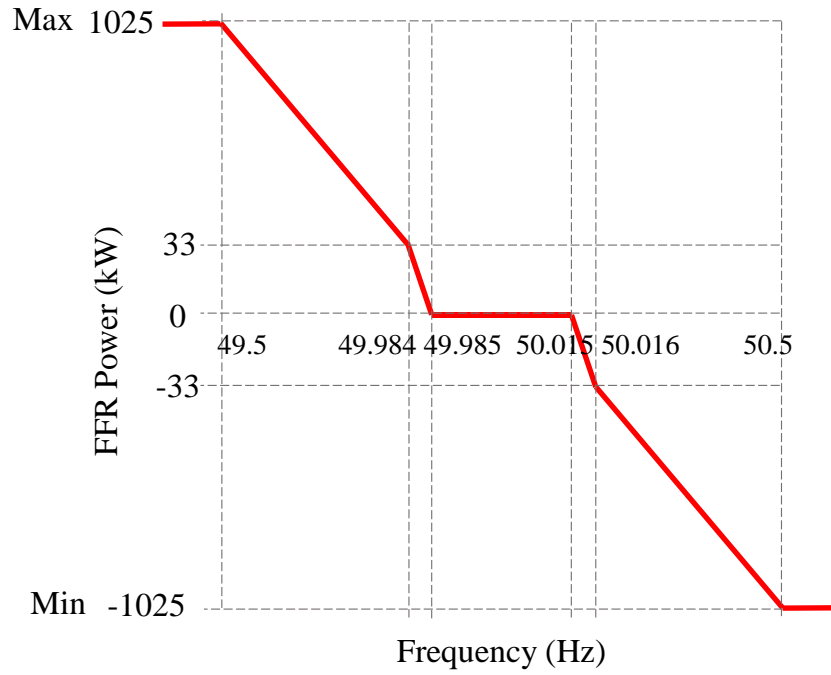


Fig. 2.1 NGET required DFFR power vs frequency envelope for a 1MW system [ONL18h].

Fig. 2.2 shows the proposed DFFR control scheme implemented in the BESS model, where the inputs are real-time grid frequency ( $f$ ) and battery SOC, with the output being the requested import/export power to deliver a frequency response according to the service specification. The algorithm starts by detecting the position of the measured frequency with respect to the zones bounded by frequency values ‘A’ to ‘R’ in Table 2.1 (left column). This is achieved by the ‘FFR Power Calculation’ (Block 1), where the required DFFR response envelope is calculated as a function of the limits given with their Table 2.1 (left and middle column). The calculation method of the proposed DFFR power envelope is described in the final column of the table. The required DFFR power is zero within the DB.

In this work, battery SOC is calculated using (2.1) where  $SOC_{init}$ ,  $Q$  and  $P_{batt}$  represent initial SOC, Watt-hour capacity and instantaneous battery power, respectively. Stored energy in the BESS is expressed in (2.2) and (2.3), where  $\eta_D, \eta_{DC}, E_t$  are battery discharging efficiency, battery charging efficiency, and energy stored in the BESS at hour  $t$ , respectively. Note that, if  $P_t > 0$  the BESS exports power at hour  $t$  and if  $P_t < 0$  the BESS imports power at hour  $t$ .

$$SOC_{out} = SOC_{init} + \frac{\int_0^t P_{batt} dt}{3600 \cdot Q} \quad (2.1)$$

$$\text{Discharge/Export: } P_t > 0 \quad E_t = \int_0^t \frac{P_t}{\eta_D} \cdot dt \quad (2.2)$$

$$\text{Charge/Import: } P_t < 0 \quad E_t = \int_0^t P_t \cdot \eta_C \cdot dt \quad (2.3)$$

Table 2.1 DFFR power vs frequency envelope limits [ONL18h] and the calculation of power set-points (CPower) in algorithm

<b>Freq. (Hz)</b>	<b>Contracted Power (kW)</b>	<b>CPower (kW)</b>
$A = 49.5$	$a = 1025$	$a$
$B = 49.6$	$b = 820$	$\left[\left(\frac{B-f}{B-A}\right) \cdot (a-b)\right] + b$
$C = 49.7$	$c = 615$	$\left[\left(\frac{C-f}{C-B}\right) \cdot (b-c)\right] + c$
$D = 49.8$	$d = 410$	$\left[\left(\frac{D-f}{D-C}\right) \cdot (c-d)\right] + d$
$E = 49.9$	$e = 205$	$\left[\left(\frac{E-f}{E-D}\right) \cdot (d-e)\right] + e$
$F = 49.984$	$f = 33$	$\left[\left(\frac{F-f}{F-E}\right) \cdot (e-f)\right] + f$
$G = 49.985$	$g = 0$	$g = 0$
$H = 50$	$h = 0$	$h = 0$
$J = 50.015$	$j = 0$	$j = 0$
$K = 50.016$	$k = -33$	$\left[\left(\frac{K-f}{K-J}\right) \cdot (j-k)\right] + k$
$L = 50.1$	$l = -205$	$\left[\left(\frac{L-f}{L-K}\right) \cdot (k-l)\right] + l$
$M = 50.2$	$m = -410$	$\left[\left(\frac{M-f}{M-L}\right) \cdot (l-m)\right] + m$
$N = 50.3$	$n = -615$	$\left[\left(\frac{N-f}{N-M}\right) \cdot (m-n)\right] + n$
$P = 50.4$	$p = -820$	$\left[\left(\frac{P-f}{P-N}\right) \cdot (n-p)\right] + p$
$R = 50.5$	$r = -1025$	$r$

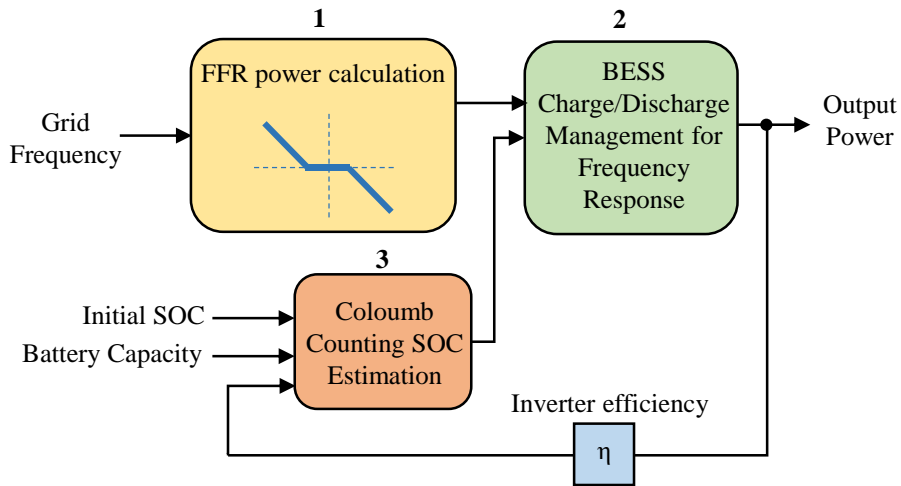


Fig. 2.2 Block diagram of the BESS control for DFFR service

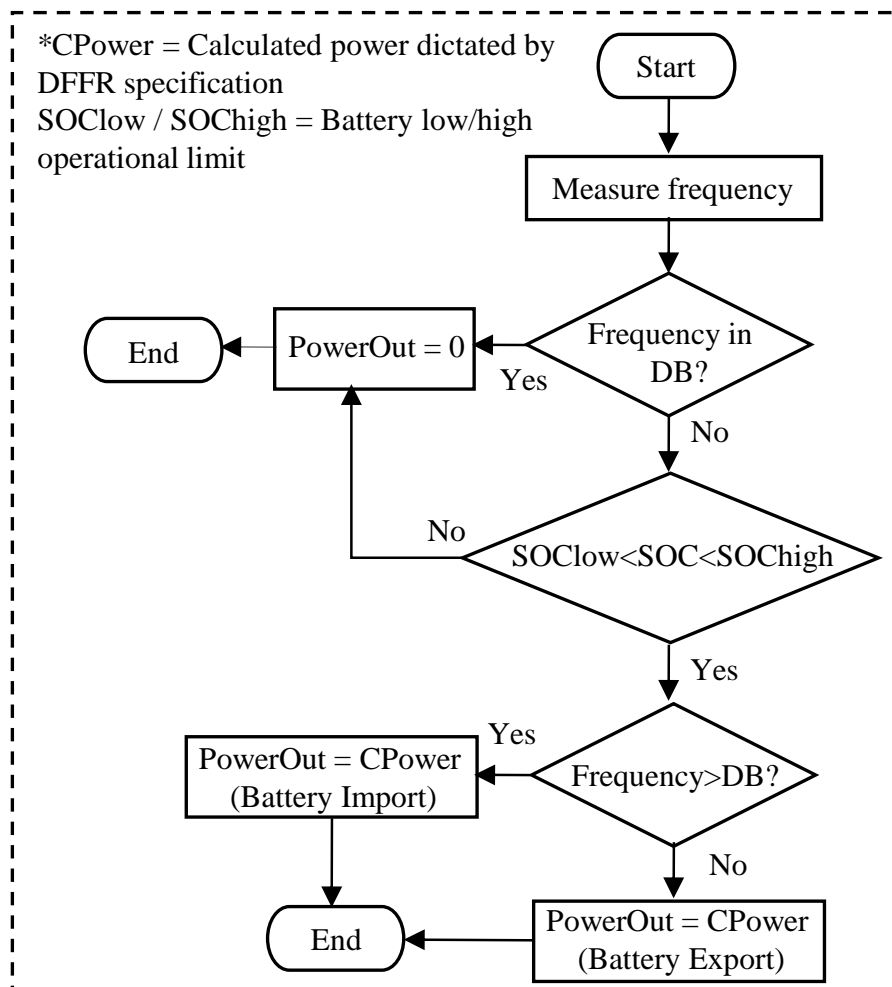


Fig. 2.3 Flow chart of the BESS charge/discharge management for DFFR (Fig. 2.2, Block 2).

DFFR is a continuously delivered service, a DB is defined where there is no requirement to import/export power to the grid but there is also no opportunity to charge/discharge the battery

to manage its SOC. Providers must deliver continuous import/export power as detailed in the DFFR service envelope in Table 2.1. The power level must remain at this required envelope at all times; power provided outside the envelope will decrease the SPM and hence the income revenue [ONL18i]. Operation principle of the proposed BESS charge/discharge management for delivering DFFR service (Fig. 2.2, Block 2) is described in Fig. 2.3. According to the logic of the DFFR charge/discharge management, BESS can only import/export power with respect to the required DFFR power envelope described in Table 2.1 to respond to grid frequency changes outside of DB ( $\pm 0.015\text{Hz}$ ). According to the NGET FFR requirements which were valid until 23th April 2018, [ONL18h], [ONL18i], [ONL18j], [ONL18o], the energy storage providers are not allowed to manage their SOC within DB. Therefore, in this section, the proposed DFFR control designed does not include a BESS SOC management strategy with respect to the recent NGET FFR specifications [ONL18h], [ONL18i], [ONL18j].

### 2.2.2 Simulation Results of the BESS Control for DFFR Service

BESS control for DFFR and SFFR services presented in 2.2.1 and 2.2.3 are simulated in MATLAB/Simulink using real frequency data set obtained from the NG. The simulation results presented in this section are all based on a 1MW/1MWh BESS model, which has been experimentally validated on the WESS. The parameters used in the BESS model with FFR control algorithms are shown in Table 2.2.

Table 2.2 Parameters used in the FFR control algorithms implemented in BESS model

<b>Parameter</b>	<b>Value</b>
Nominal grid frequency	50 Hz
Low/high DB	$\pm 0.015$ Hz (for DFFR)
High/low trigger frequency	$\pm 0.3$ Hz (for SFFR)
Max/min FFR power limit	$\pm 1$ MW
Battery power/capacity for FFR	1 MW/1 MWh
Battery initial SOC ( $\text{SOC}_{\text{init}}$ )	20%

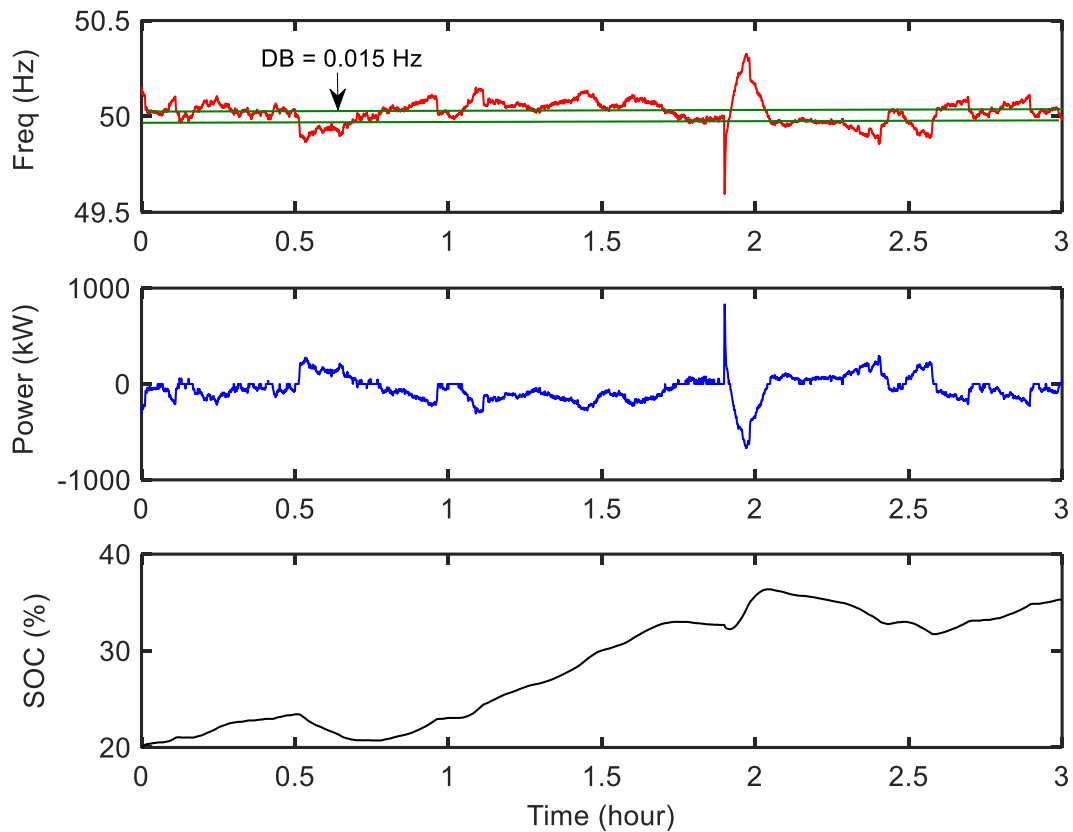


Fig. 2.4 Simulation results of the DFFR control algorithm for 11th Nov 2015 (first 3 hours).

In order to show the performance of the reported FFR control algorithms in Section 2.2.1 and Section 2.2.3, the real frequency data for the 11th November 2015 (first 3 hours data) is used herein, as this particular day is known to have both a low and high frequency event. Fig. 2.4 shows the simulation results of the DFFR control algorithm. On the frequency plot, the DB ( $\pm 0.015\text{Hz}$ ) is shown by the green lines. It is clear from the Fig. 2.4, the BESS continuously imports/exports power within the specified power envelope described in Fig. 2.1 and Table 2.1. It is clear from Fig. 2.5, the DFFR power (blue circles) does remain within the required envelope, meaning that the BESS achieved 100% availability and met the service requirements.

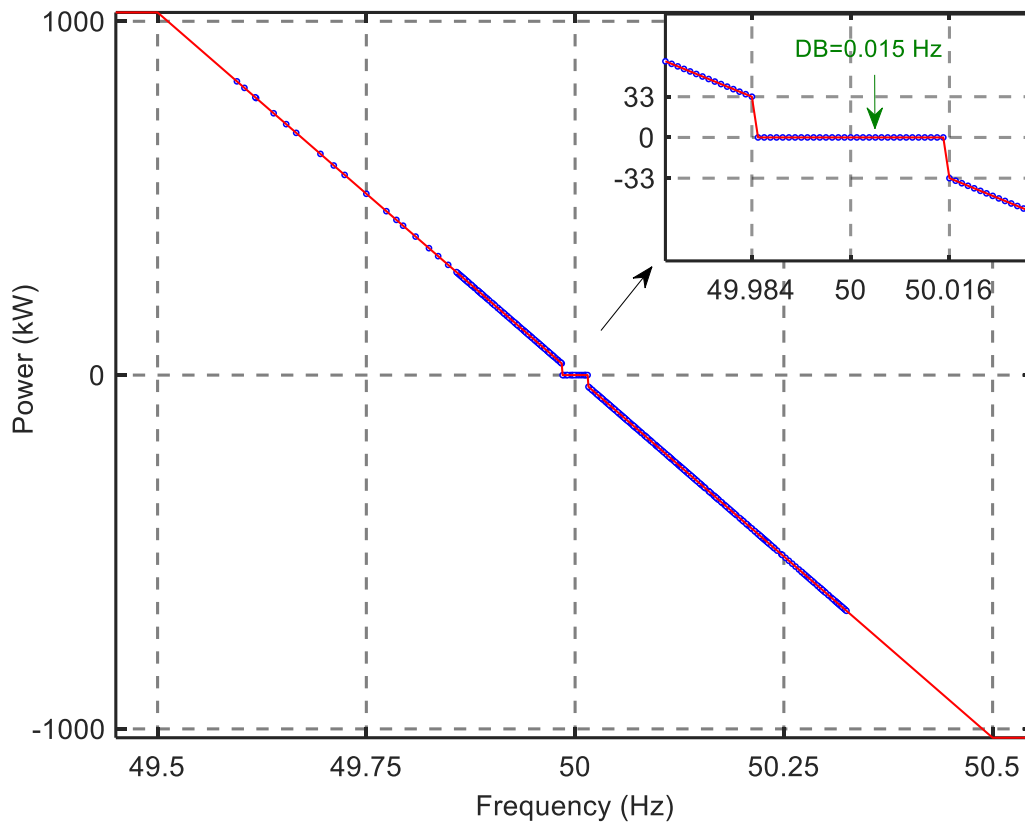


Fig. 2.5 DFFR power versus frequency response plot for 11th Nov 2015 (first 3 hours).

### 2.2.3 BESS Control for Static FFR Service

SFFR delivers a non-dynamic service where an agreed amount of power is delivered if the grid frequency reaches a certain trigger point (e.g 49.7Hz or 50.3Hz). The service providers monitor the grid frequency and adjust their generation or consumption power when the frequency goes below the specified frequency trigger. There are two modes of SFFR response, including high frequency response (SFFR<sub>high</sub>) and low frequency response (SFFR<sub>low</sub>). Fig. 2.6.a and Fig. 2.6.b show the logic of the low and high SFFR services respectively, which have to maintain their power output for 30 mins. NG specify a high reset frequency (50.3 Hz) and low reset frequency (49.7Hz) [ONL18h], [ONL18i]. The aim of the resets is to discontinue the frequency response if the grid frequency changes sharply for the period of the service.

According to the proposed BESS management for SFFR<sub>low</sub> shown in Fig. 2.6.a, when the grid frequency drops below the low trigger frequency ( $F_{low}$ ), the BESS starts to deliver a maximum power response ( $S_{Power} > 0$ ) until the grid frequency goes back above the specified high trigger frequency ( $F_{high}$ ); the response continuation must not be interrupted until it reaches the trigger reset or 30 mins. The logic is reversed for SFFR<sub>high</sub> control algorithm shown in Fig. 2.6.b.

According to the proposed BESS management for  $SFFR_{high}$ , when the frequency goes above the high trigger frequency ( $F_{high}$ ), the BESS starts to import a maximum power response ( $S_{Power} < 0$ ) until the grid frequency goes back below the specified low trigger frequency ( $F_{low}$ ); the response continuation must not be interrupted until it reaches the trigger reset or 30 mins.

Currently, the NG does not have a value for static high service. Overnight, the High requirement is small and the minimum dynamic need is equal to this so this shows that static high will already be fulfilled by the dynamic FFR service. There may be periods where a greater need is determined however this occurs relatively infrequently. It can be said that DFFR service is currently more valuable during the daytime because this service offsets margin costs which are not frequently incurred overnight [ONL18o].

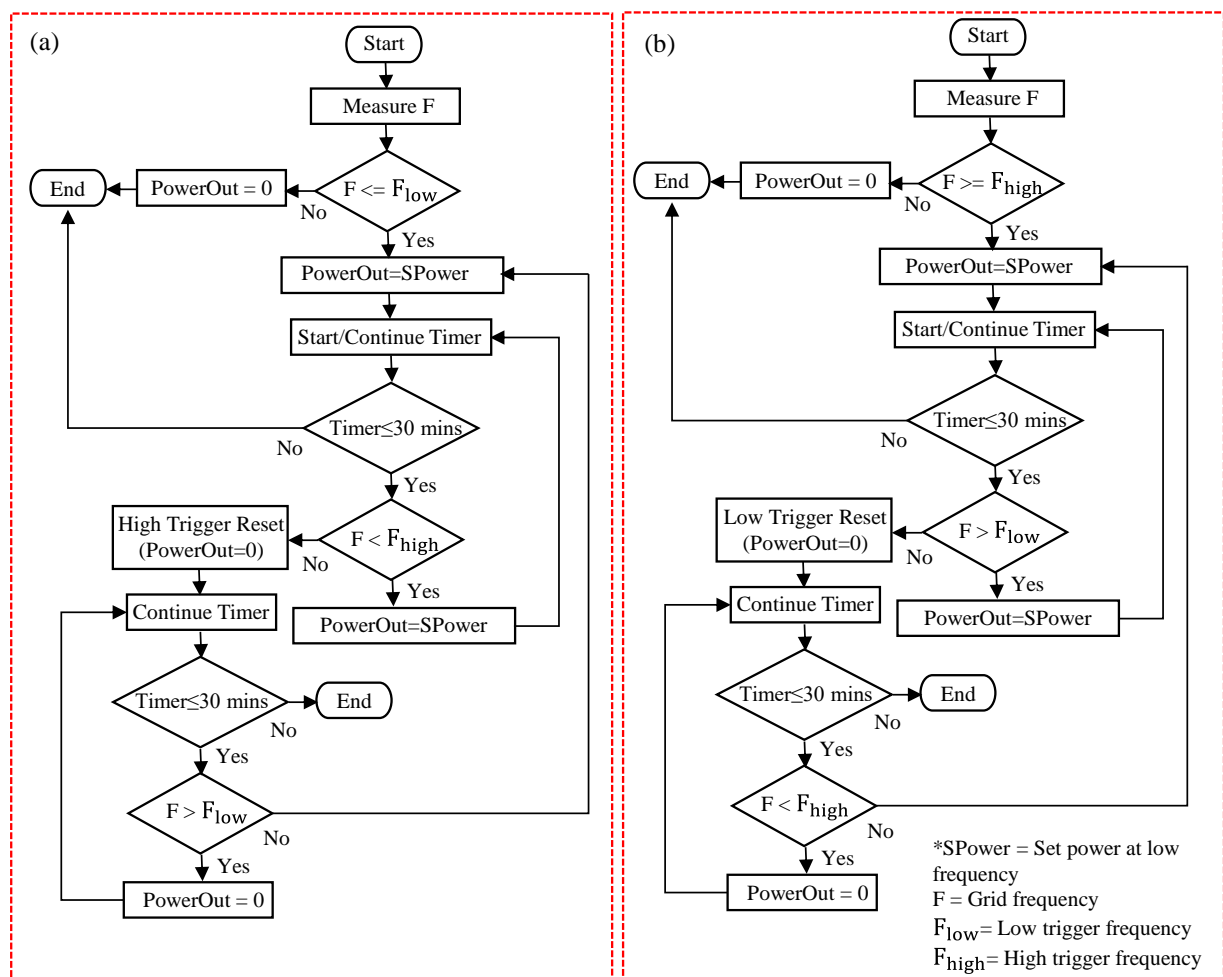


Fig. 2.6 Flow chart of the BESS charge/discharge management for static a) Low ( $SFFR_{low}$ ) and b) High ( $SFFR_{high}$ ) firm frequency response service.



## 2.2.4 Simulation Results of the BESS Control for SFFR Service

Fig. 2.7 and Fig. 2.8 show the simulation results for 11th Nov 2015 of the SFFR high and low frequency response control algorithms, respectively. On the frequency plot, the high and low trigger reset frequency set points are shown by the dotted green lines. Over the 3-hour profile the algorithms deliver to the  $SFFR_{low}$  and  $SFFR_{high}$  specification with no power being delivered until a frequency event occurs at 49.7Hz and 50.3Hz, respectively. As seen from the simulation results of the  $SFFR_{low}$  control algorithm (Fig. 2.8), the grid frequency drops below 49.7Hz, BESS starts to export 1 MW power response until the frequency goes back above 50.3Hz (trigger reset).

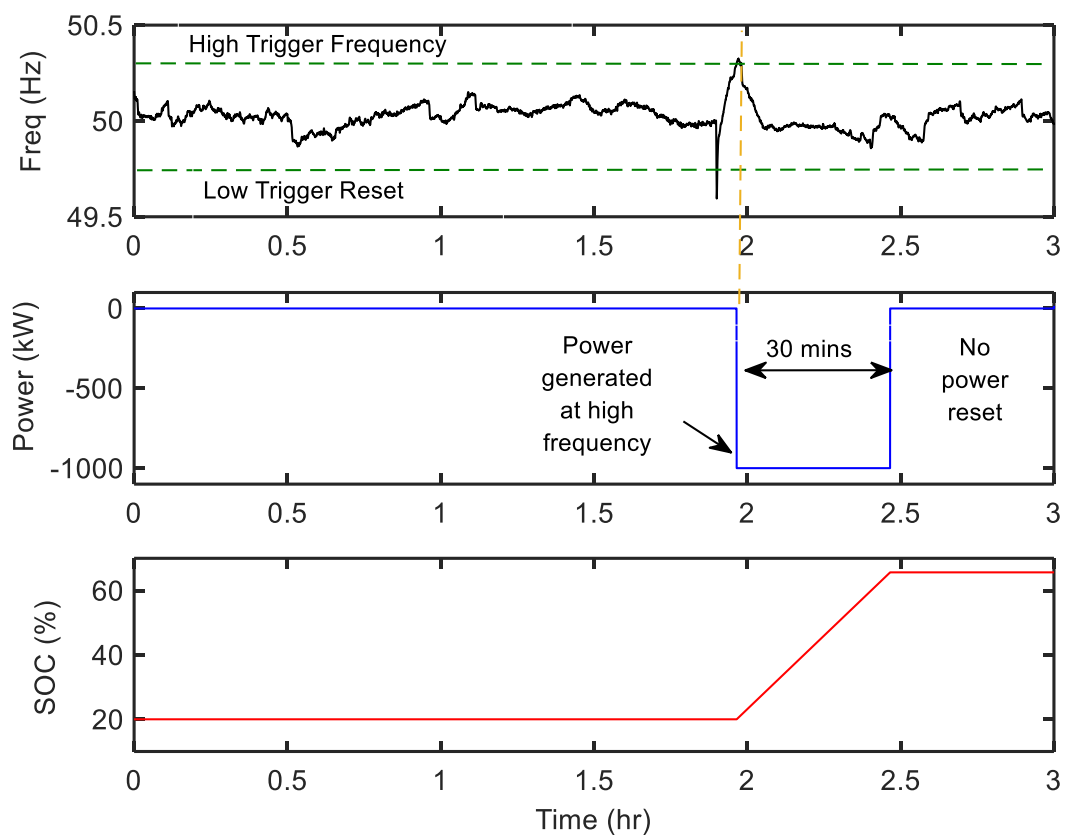


Fig. 2.7 Simulation results of the  $SFFR_{high}$  control for 11th Nov. 2015 (first 3 hours).

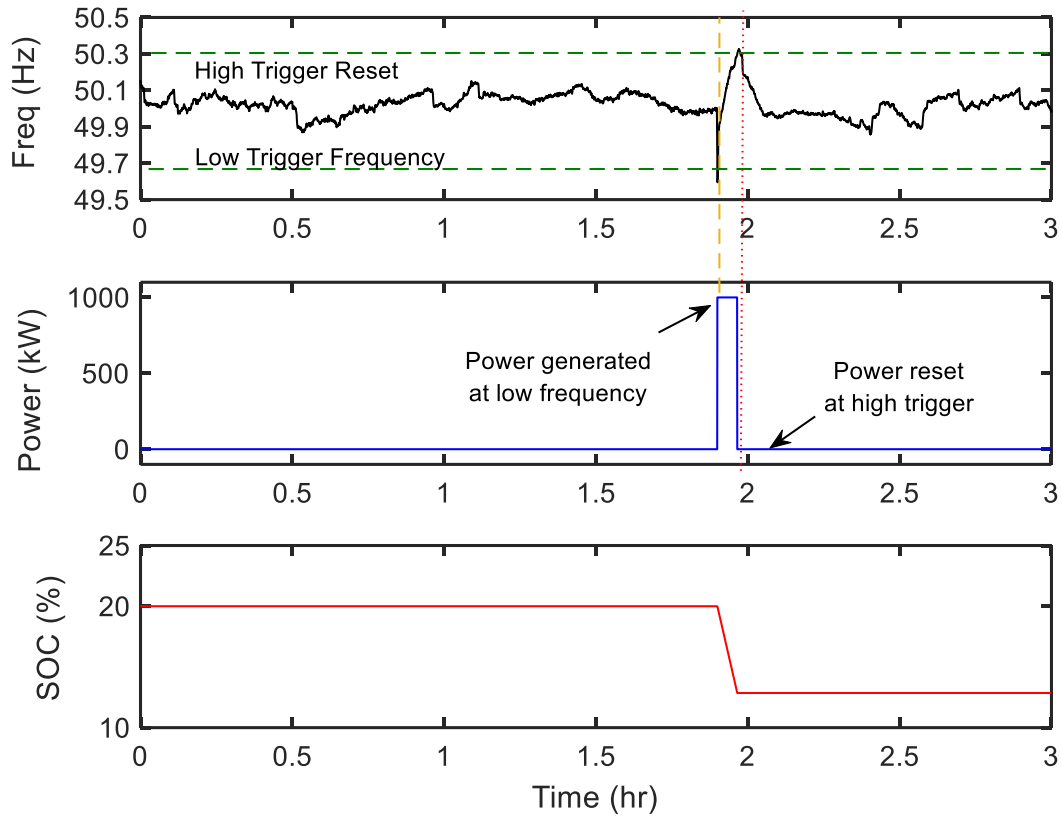


Fig. 2.8 Simulation results of the SFFR<sub>low</sub> control for 11th Nov 2015 (first 3 hours).

As seen from the results of SFFR<sub>high</sub> algorithm in Fig. 2.7, the grid frequency goes above 50.3Hz, BESS starts to import 1MW power response until 30 mins. The aim of the resets in the SFFR control algorithms is to discontinue the frequency response if the grid frequency changes sharply for the period of the service. Since there is no trigger reset here (Fig. 2.7), the power response must continue until 30 mins.

Table 2.3 presents the energy findings of the all FFR control algorithms for the 11 November 2015 (first 3 hours) frequency data. It can be seen that the DFFR control algorithm can continuously import and export power to the grid with 83.83kWh and 236.8 kWh energy output, respectively. However, when the grid frequency drops below the defined trigger frequency of 49.7Hz, the SFFR<sub>low</sub> algorithm can only import power until the high trigger reset, absorbing 65.56 kWh energy from the grid; and when the frequency sharply increase to the high frequency of 50.3Hz, the SFFR<sub>high</sub> algorithm can only export power until 30 minutes, delivering 500.6 kWh energy to the grid in order to balance the grid frequency.

Table 2.3 Energy output findings of the FFR algorithms for 11 Nov 2015 (first 3 hours data)

	<b>Actual Imp. (kWh)</b>	<b>Actual Exp. (kWh)</b>	<b>Potential Imp. (kWh)</b>	<b>Potential Exp. (kWh)</b>
<b>DFFR</b>	83.83	236.8	83.83	236.8
<b>SFFR<sub>high</sub></b>	500.6	-	500.6	-
<b>SFFR<sub>low</sub></b>	-	65.56	-	65.56

### 2.2.5 BESS Control for DFFR Service with Battery SOC Management

The NGET required DFFR service specifications [ONL18h], [ONL18i], [ONL18j], [ONL18o] was updated in 23th April 2018 and hence according to the current DFFR service requirements [ONL18p], the NGET demands from the energy storage providers to manage their SOC in the DB window; however the DFFR service control having SOC management must not negatively impact the power network in terms of losses, outages, frequency deviations or congestion problems; and hence requires an effective SOC management.

According to the updated DFFR specifications, the SOC modelling with modified DFFR envelopes to permit SOC management either by charging in the frequency DB or by over-delivery of response. The results of this analysis demonstrated that introducing these approaches could:

- 1) Reduce the maximum amount of response available in the event of a fault on the system.
- 2) Result in frequency disturbances following an event.
- 3) Cause an overall increase in frequency response requirements.

Therefore, the NG concluded that energy storage providers must continue to adhere to the DFFR envelope as given in their contracts, and should either [ONL18p]:

- 1) Withhold a fraction of the battery's total capacity from being contracted to use for battery SOC management; this capacity can then be used to charge or discharge the battery depending on its SOC.

- 2) The battery asset can be removed from delivering response entirely and use other assets (either another battery or alternative technology to provide response in its place while the battery SOC is restored to its optimum level).

The NG notes that the SOC management will continue to be investigated in the new service design process that is currently under development as part of the future of grid balancing services [ONL18p].

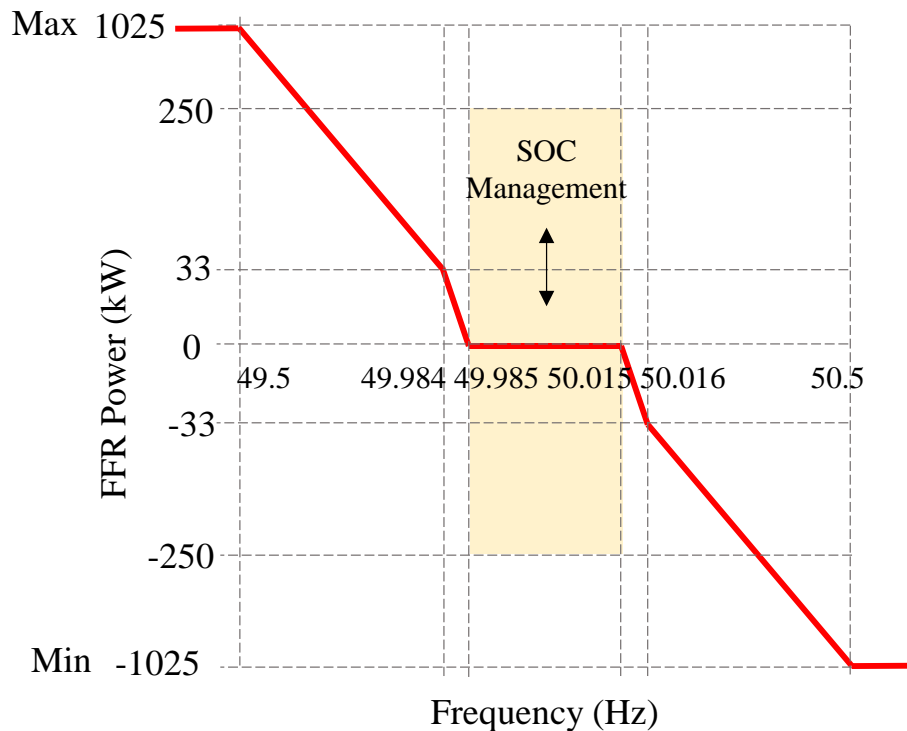
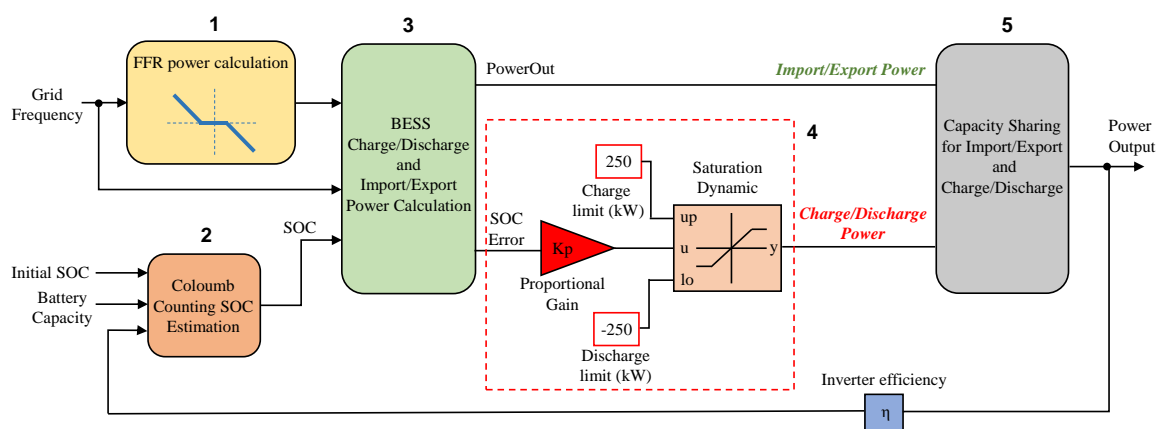
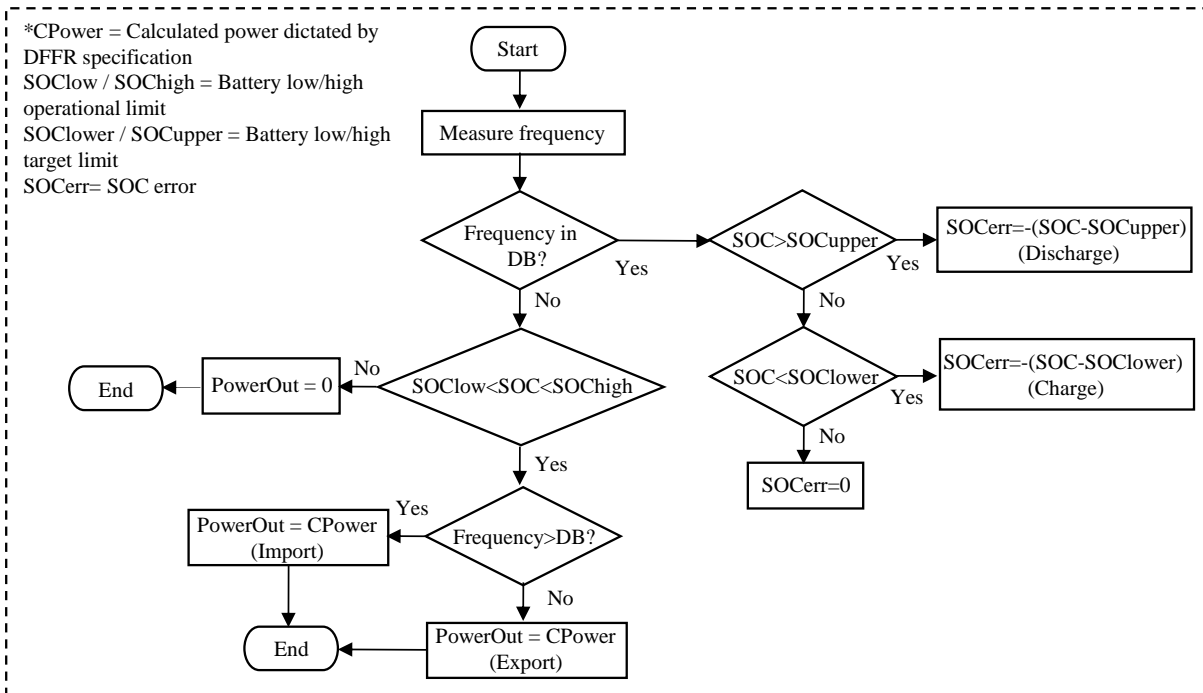


Fig. 2.9 Recent NGET required DFFR power vs frequency envelope, considering battery SOC management in DB of  $\pm 0.015$  Hz for a 1MW system [ONL18h].

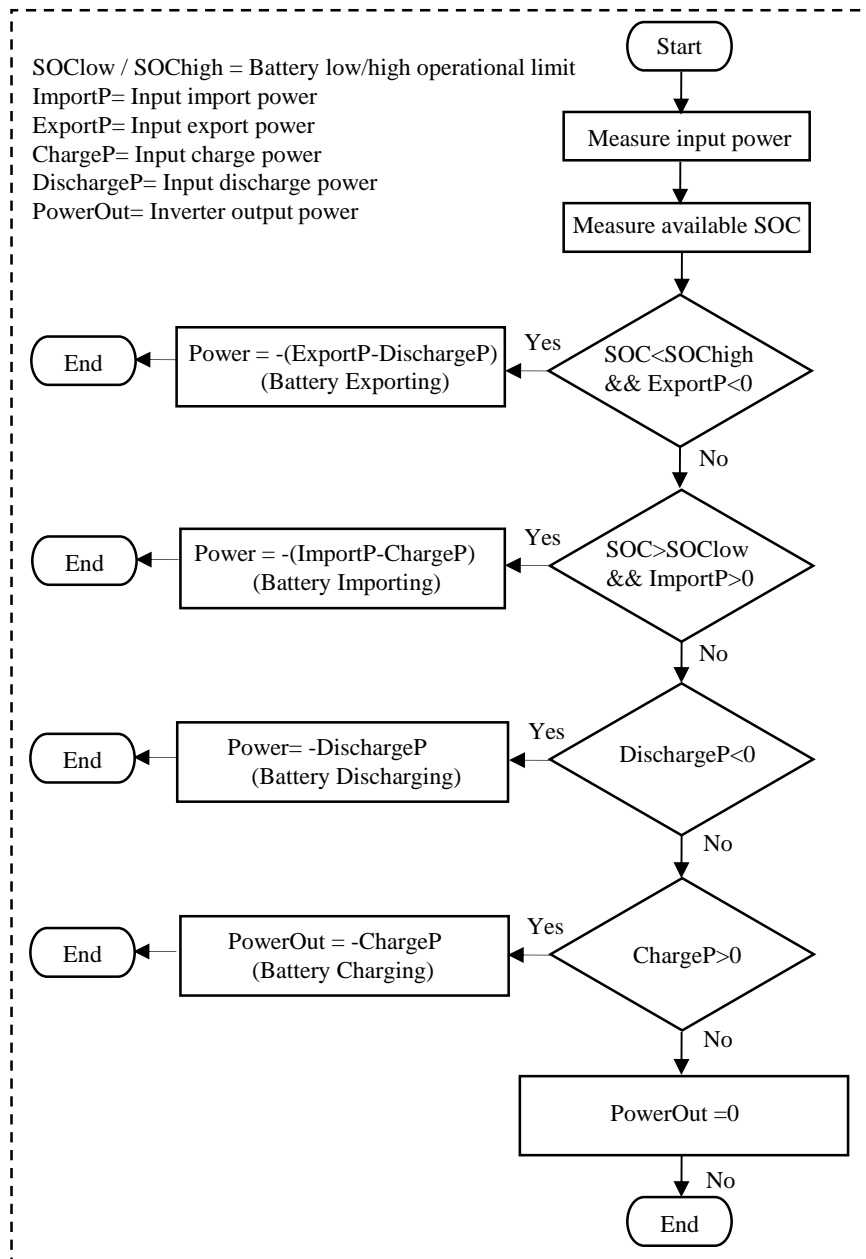


(a)



(b)

### Block 5



(c)

Fig. 2.10 BESS Control scheme for DFFR service with battery SOC management.

In this section, a control algorithm is developed to meet the NGET required DFFR service specifications, as shown in Fig. 2.9. Fig. 2.10 shows the proposed DFFR control scheme implemented in the BESS model, where the inputs are real-time grid frequency ( $f$ ) and battery SOC, with the output being the requested import/export power to deliver a frequency response according to the service specification or charge/discharge power to manage the battery SOC. The algorithm starts by detecting the position of the measured frequency with respect to the

zones bounded by frequency values ‘A’ to ‘R’ in Table 2.1 (left column). This is achieved by the ‘FFR Power Calculation’ (Block 1), where the required DFFR response envelope is calculated as a function of the limits given with their Table 2.1 (left and middle column). The calculation method of the proposed DFFR power envelope is described in the final column of the table. According to the recently updated DFFR specifications [ONL18p], the providers require to manage their SOC in the DB window, as shaded yellow in Fig. 2.9. Therefore, a proper SOC management control is implemented in the DFFR control design (Block 3) in MATLAB/Simulink (Fig. 2.10). In Fig. 2.10, the proposed DFFR algorithm withholds a fraction (1/4) of the battery’s total capacity (1000 kWh) from being contracted to use for the battery SOC management; hence this capacity (max 250 kWh) can be used to charge/discharge the battery depending on its SOC (Block 4 & Block 5). According to the proposed control algorithm, a proportional controller is implemented in the previously designed DFFR control algorithm, described in Section 2.2.1, to charge/discharge battery in order to manage the battery’s SOC (Block 4); hence this management will enable the providers reduce the likelihood of unavailability of the BESS on delivering the dynamic response service. As a result of this, the BESS will not only import/export power to the grid as in the previously designed DFFR control algorithm (Fig. 2.2 and Fig. 2.3); but also will do charging or discharging for managing the SOC of the battery, as seen in Fig. 2.10.

Proportional control is a type of linear feedback control system where a correction is applied to the controlled variable which is proportional to the difference between the desired value and the measured value [AST10]. In this section, a SOC-based proportional controller is applied to the standard DFFR control algorithm (Section 2.2.1) in order to control the output dynamic power as a proportional of battery SOC error in order to charge or discharge battery operating in dynamic frequency response service (Block 3). In the proposed proportional controller, the controller output is proportional to the error signal (SOC error), as shown in Block 4 Fig. 2.10. This means that the output of the proportional controller is the multiplication product of the SOC error and the proportional gain ( $K_p$ ). The aim of the proposed control algorithm is to share the battery’s capacity for charging/discharging and import/export, independently (Block 5). The aim of the use of the proportional controller in the DFFR control scheme is to utilize the partial capacity of the battery for charging and discharging to manage the battery’s SOC in order to avoid BESS unavailability, and prolong the battery lifetime. Simulation results of the DFFR control algorithm including SOC management will be presented in the next section.

## 2.2.6 Simulation Results of the BESS Control for DFFR with SOC Management

The simulation results of the DFFR control algorithm having the SOC management described in Section 2.2.5 is presented in this section. The results in this section are all based on a 1MW/1MWh BESS model, by sharing maximum 250 kWh battery capacity for charging/discharging; or the rest power for importing/exporting. The additional parameters used in the proposed model are shown in Table 2.4.

Table 2.4 Additional parameters used in the design of the SOC management in DFFR algorithm

Parameter	Value
Max capacity for charge/discharge	250 kWh
SOC band set in model	45-55%

Fig. 2.11 and Fig. 2.13 show the simulation results of the DFFR control algorithm having SOC management with setting the proportional gain  $Kp = 10$  and  $Kp = 2$ , respectively. As seen from Fig. 2.11 and Fig. 2.13, increasing the proportional gain  $Kp$  set in the controller, the BESS charging/discharging power dependently increases based on the battery SOC error. Comparing the battery SOC plot in Fig. 2.11 and Fig. 2.13, setting increased  $Kp$  value, the SOC of the battery reaches to the desired SOC band of 45-55% faster with increasing amount of charge/discharge power. The energy output findings of the DFFR control algorithms (see Table 2.5) show that due to the sharing of battery capacity for importing/exporting or charging/discharging, while increasing charging/discharging energy for faster SOC management; this leads to a faster SOC management in the algorithm.



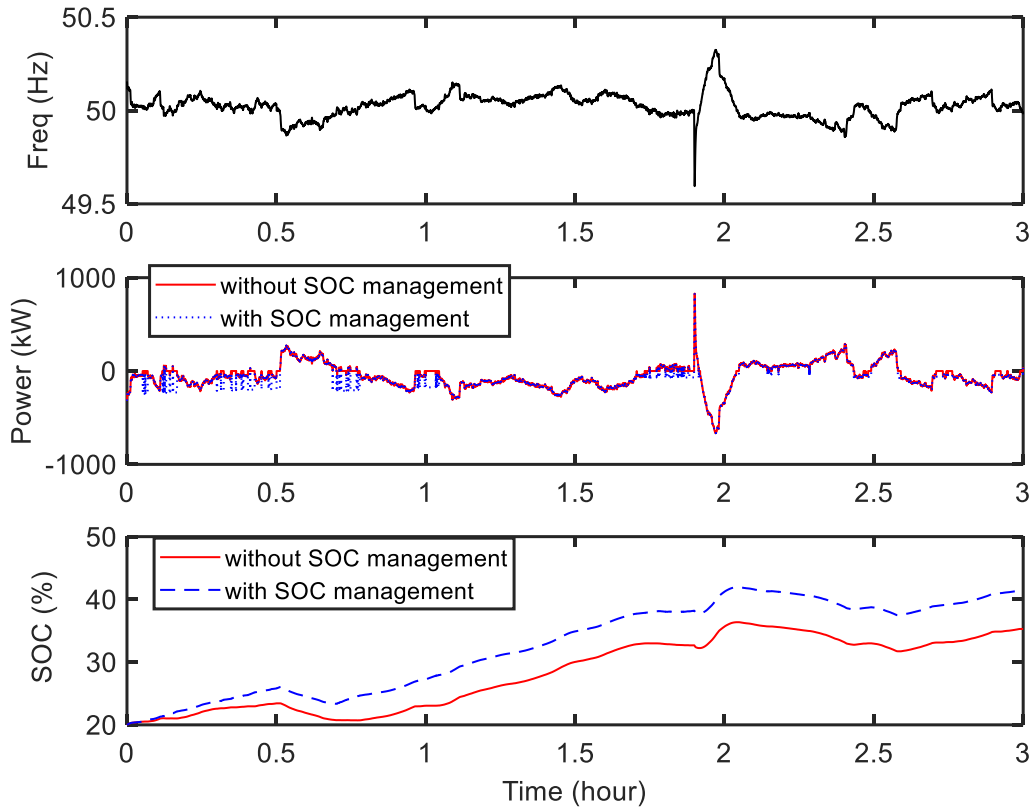


Fig. 2.11 Simulation results of DFFR algorithm with ( $K_p=10$ ) and without SOC management for 11 Nov 2015 (first 3 hours) frequency data.

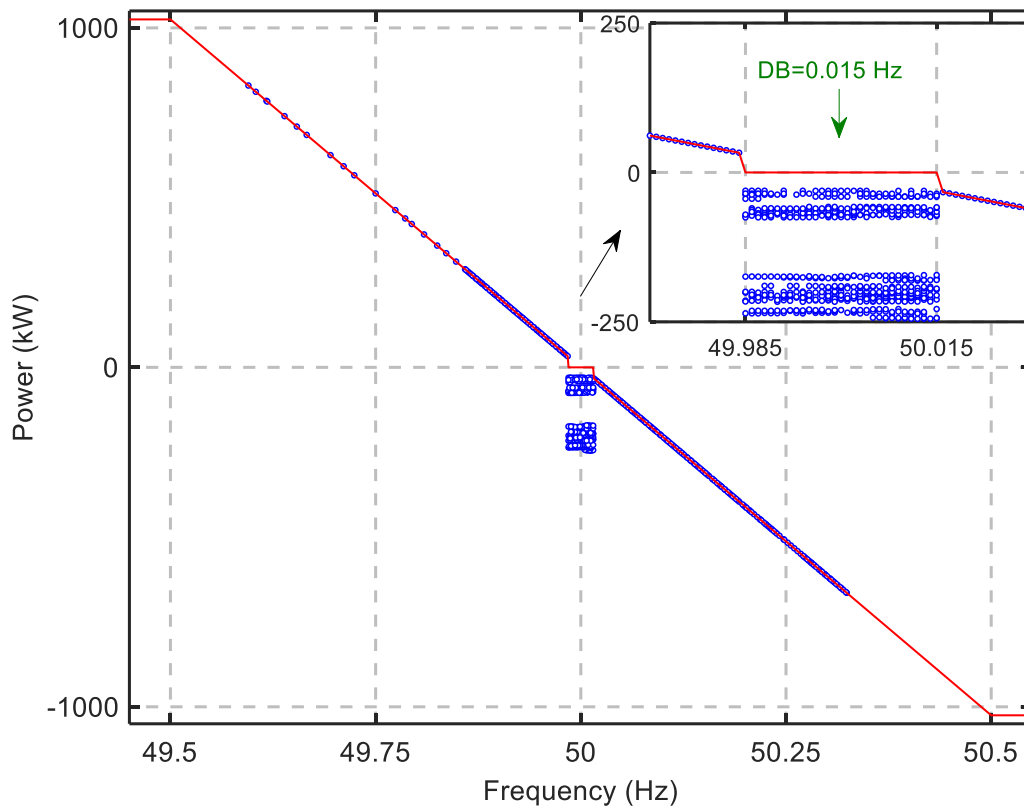


Fig. 2.12 Power versus frequency plot of measured DFFR algorithm with SOC management ( $K_p=10$ ) for 11 Nov 2015 (first 3 hours) frequency data.

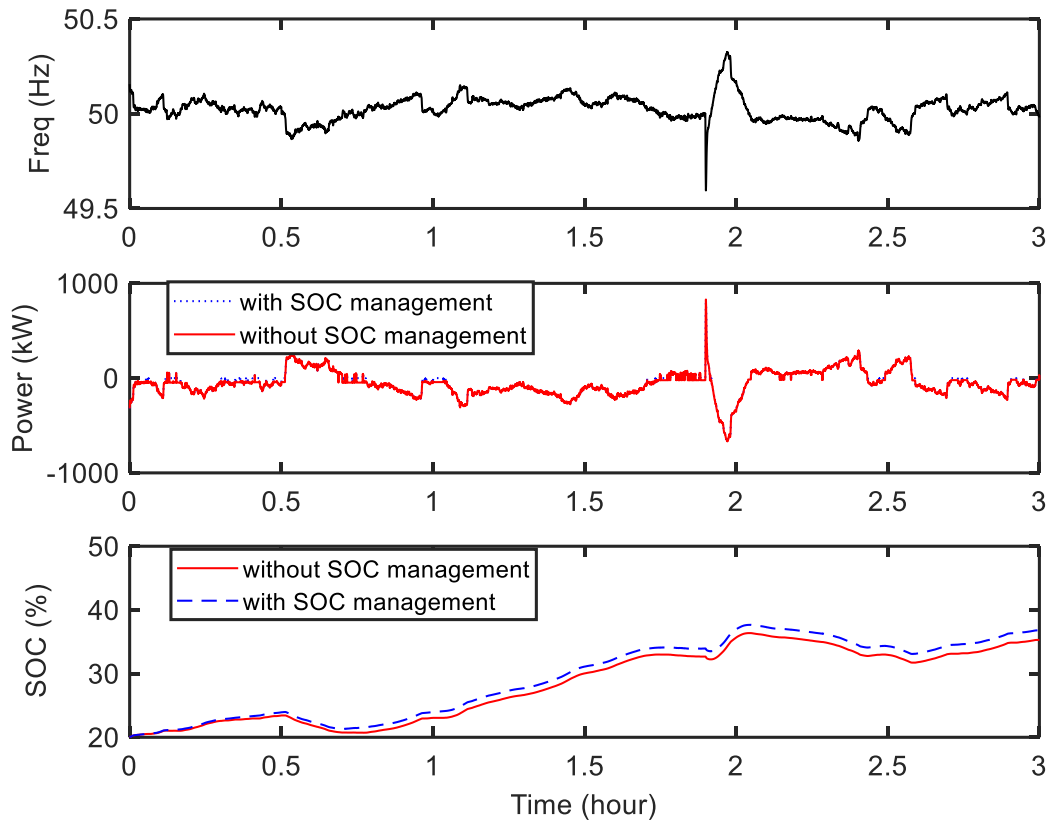


Fig. 2.13 Simulation results of DFFR algorithm with ( $K_p=2$ ) and without SOC management for 11 Nov 2015 (first 3 hours) frequency data.

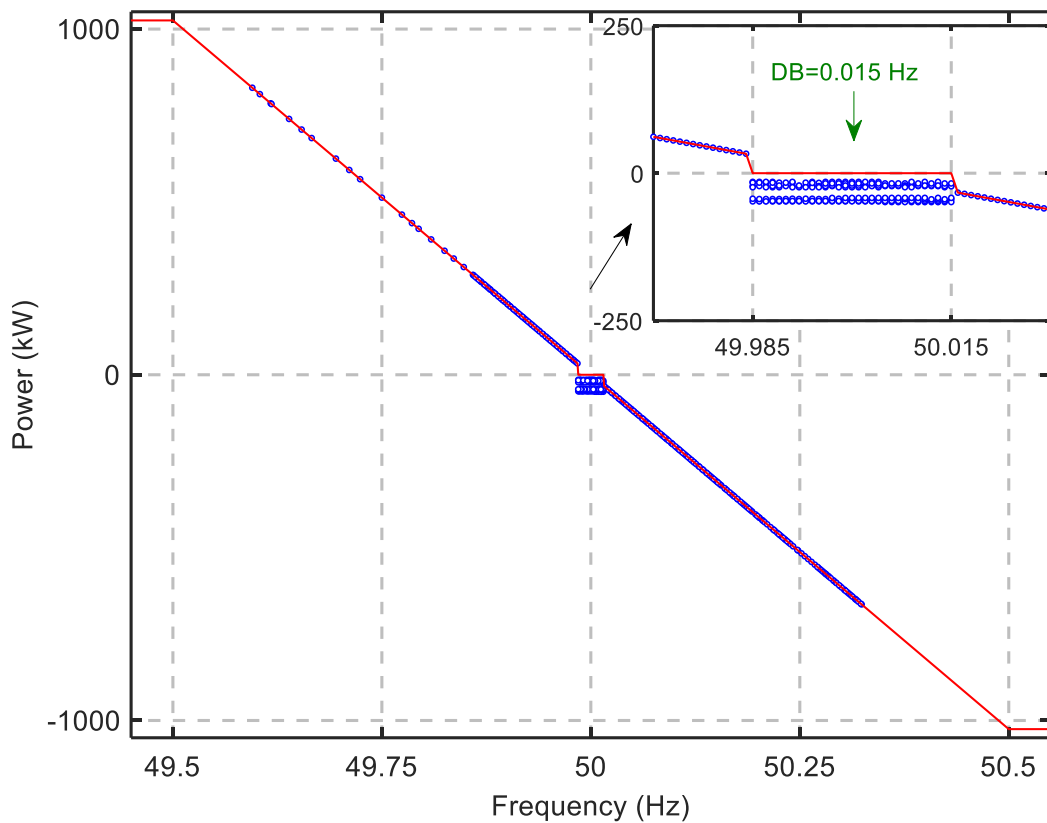


Fig. 2.14 Power versus frequency plot of measured DFFR algorithm with SOC management ( $K_p=2$ ) for 11 Nov 2015 (first 3 hours) frequency data.

Fig. 2.12 and Fig. 2.14 illustrate the power response versus grid frequency plot of DFFR control algorithm having SOC management by setting  $Kp = 10$  and  $Kp = 2$ , respectively for 11th Nov 2015 (first 3 hours). The red line represents the current NGET required DFFR power line described in Fig. 2.9. It is clear that the DFFR power (blue circles) does remain within the required envelope, meaning that the BESS achieved 100% availability and met the service requirements. Comparing the simulation findings in Fig. 2.12 and Fig. 2.14, increasing the  $Kp$  set in the proportional controller in model, the BESS charges/discharges itself with relatively increasing amount of power; this leads to a faster SOC management to stay the battery SOC in the desired SOC band.

Table 2.5 Energy output findings of DFFR Algorithm for 11 Nov 2015 (first 3 hours)

	<b>DFFR with NO management</b>	<b>DFFR with SOC management (<math>Kp = 10</math>)</b>	<b>DFFR with SOC management (<math>Kp = 5</math>)</b>	<b>DFFR with SOC management (<math>Kp = 2</math>)</b>	<b>DFFR with SOC management (<math>Kp = 1</math>)</b>
<b>Charging Energy (kW)</b>	-	61.76	35.09	15.18	7.796
<b>Discharging Energy (kW)</b>	-	0	0	0	0
<b>Import Energy (kW)</b>	83.83	22.07	48.74	68.65	76.04
<b>Export Energy (kW)</b>	236.8	236.7	236.7	236.7	236.7
<b>Potential Import (kW)</b>	83.83	83.83	83.83	83.83	83.83
<b>Potential Export (kW)</b>	236.8	236.7	236.7	236.7	236.7

Fig. 2.15 compares the simulation results of the DFFR algorithm with no SOC management and that with the proposed SOC management for whole October 2015 which is the worst month in 2015. As seen from the figure, applying the proposed SOC control into the basic DFFR algorithm, the battery's SOC can be successfully managed in the desired SOC band of 45-55%; therefore managing the battery SOC, the BESS availability increases significantly as observed from the comparison of the power versus frequency plots in Fig. 2.16 and Fig. 2.17.

The energy output findings of the DFFR control algorithms for the whole of October 2015 are shown in Table 2.6. It can also be seen that setting increased  $K_p$  in the proportional controller, the amount of charge/discharge power is increased on managing battery SOC while reducing the amount of power on importing or exporting. This leads to a faster SOC recovery, however, to reduce selling/buying power from/to grid. It can be seen from Fig. 2.15, applying the proposed SOC management into the DFFR algorithm, the battery's SOC can be successfully maintained in the desired SOC band of 45-55%; this results in an enhancement in the battery availability, as seen from the results.

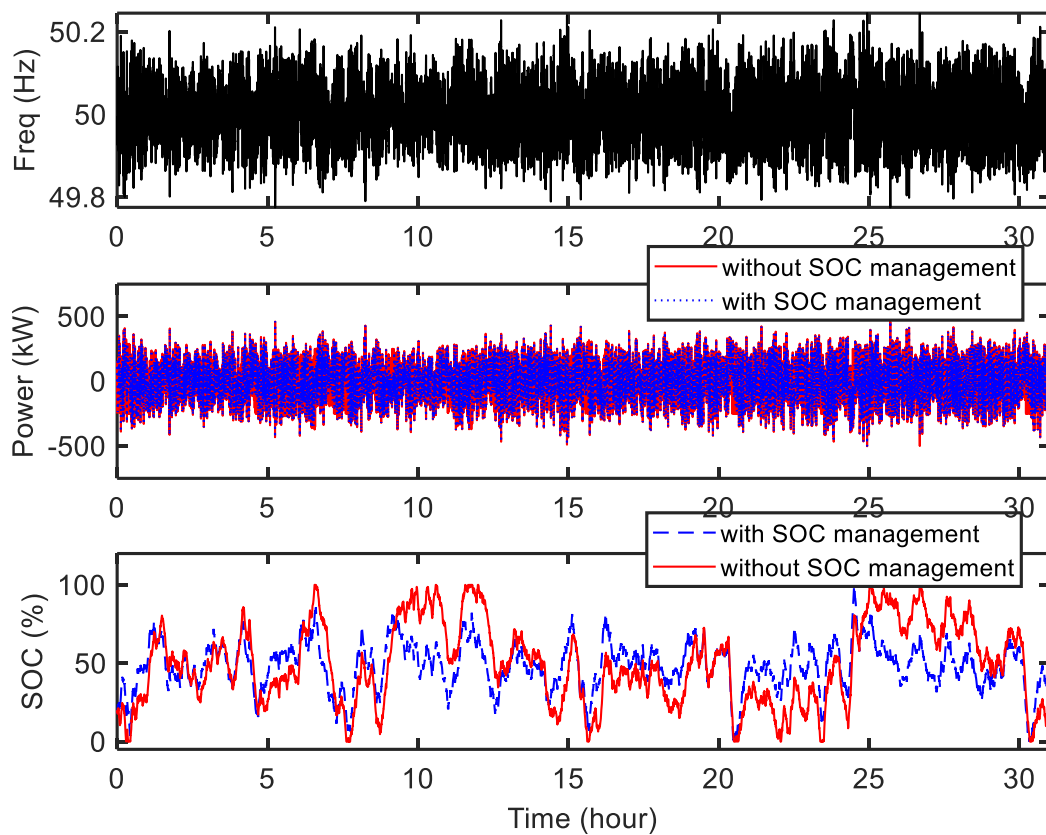


Fig. 2.15 Simulation results of DFFR algorithm with ( $K_p = 10$ ) and without SOC management for the whole October 2015 frequency data.

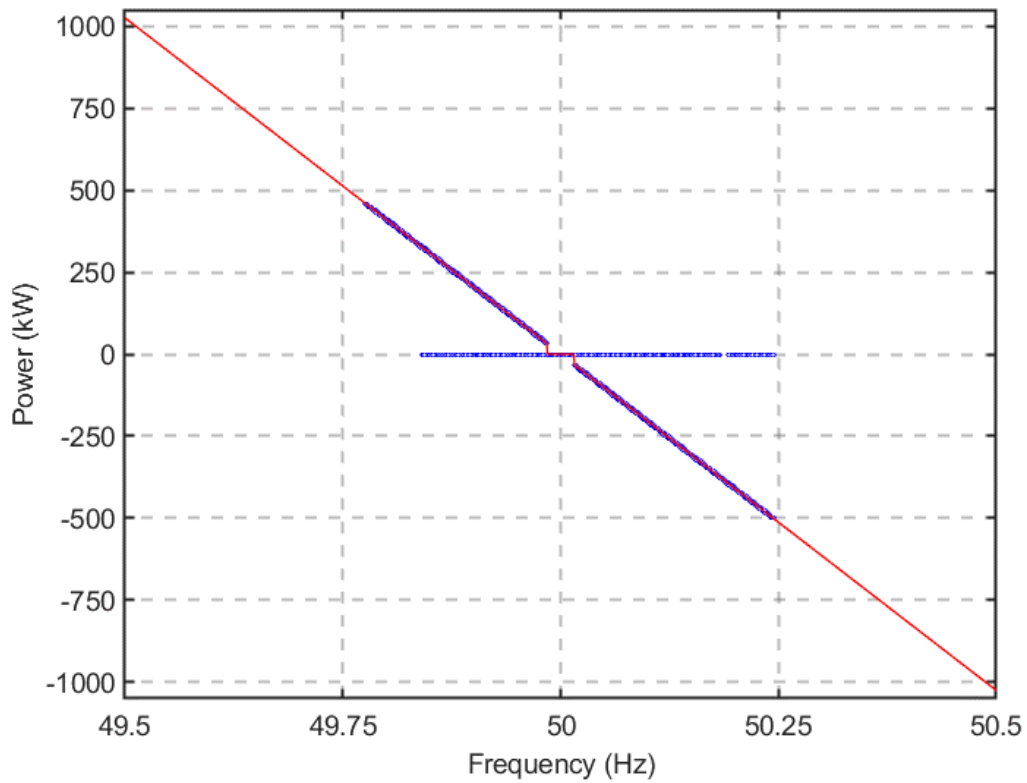


Fig. 2.16 Power versus frequency plot of DFFR algorithm with No SOC management for whole October 2015 frequency data.

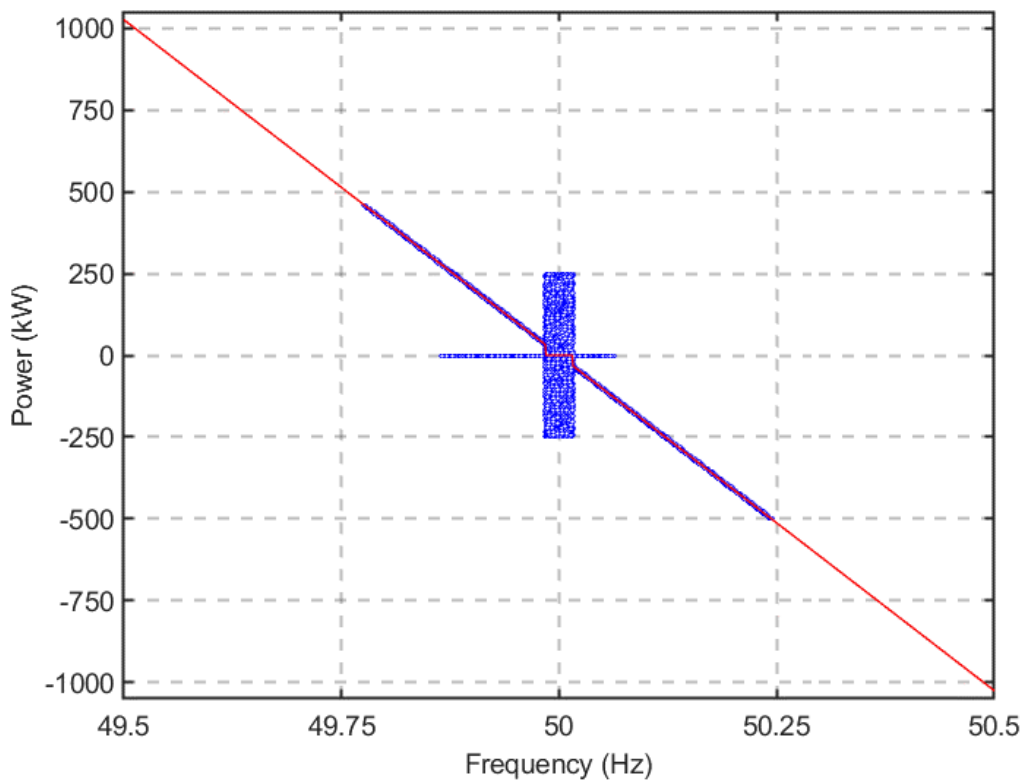


Fig. 2.17 Power versus frequency plot of DFFR algorithm with SOC management ( $K_p = 10$ ) for whole October 2015 frequency data.

Table 2.6 Energy output findings of DFFR Algorithm for whole October 2015 frequency data

	<b>Charging Energy (kW)</b>	<b>Discharging Energy (kW)</b>	<b>Import Energy (kW)</b>	<b>Export Energy (kW)</b>	<b>Potential Import (kW)</b>	<b>Potential Export (kW)</b>
<b>DFFR with NO management</b>	0	0	32520	32590	33490	33110
<b>DFFR with SOC management (<math>Kp = 50</math>)</b>	7627	6901	25740	26120	33490	33110
<b>DFFR with SOC management (<math>Kp = 10</math>)</b>	5137	4526	28260	28580	33490	33110
<b>DFFR with SOC management (<math>Kp = 5</math>)</b>	3587	3133	29710	29980	33490	33110
<b>DFFR with SOC management (<math>Kp = 2</math>)</b>	1794	1690	31150	31340	33490	33110
<b>DFFR with SOC management (<math>Kp = 1</math>)</b>	976.6	993.5	31790	31930	33490	33110

### 2.3 BESS Control for Pre-Enhanced Frequency Response (Pre-EFR) Service

The NGET prepared a pre EFR specification to facilitate a tender competition between potential energy storage providers in late 2015 [ONL15a]. Using the pre-published EFR specification, a generalised UK frequency response algorithm is developed to evaluate control strategies for delivering a real-time response to deviations in the grid frequency. At the time of this work BESS focused frequency response services were still being developed and therefore any anticipated service specific constraints around control in DB had been ignored. This allowed this study to explore forecasting of battery SOC levels and to propose battery charge/discharge management methods in order to maximise BESS availability.

### 2.3.1 Pre-EFR Service Specifications

According to NGET requirement of UK frequency response [ONL15a], energy storage providers must respond to deviations in nominal grid frequency of 50Hz by decreasing or increasing their power output. Devices specifically must supply power to the grid to respond to deviations in frequency outside the DB.

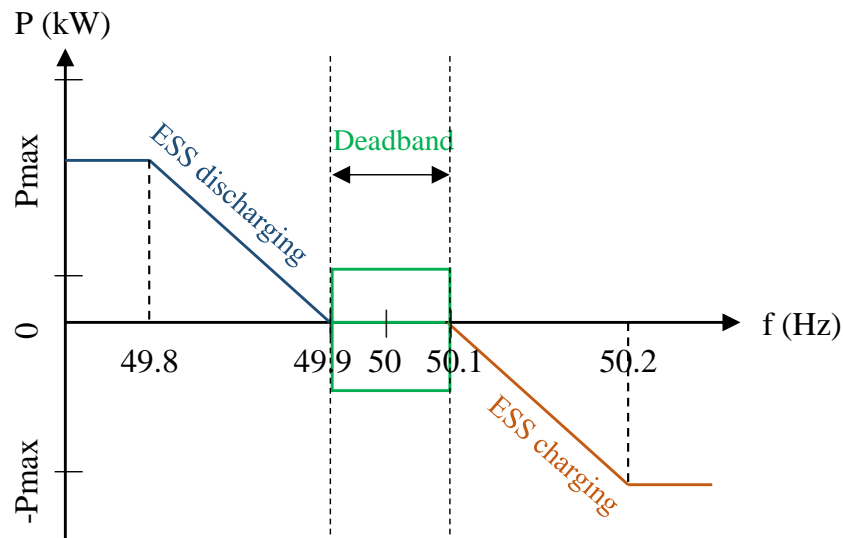


Fig. 2.18 Maximum allowable UK Pre-EFR frequency response envelope [ONL15a].

The maximum DB allowable is  $\pm 0.1$ Hz and it has been specified wide to enable flexibility, but it is allowed to be tighter. Within DB, there is no requirement to deliver power to the grid, however there is an opportunity to charge/discharge the battery with respect to the specified maximum power limit to achieve a target SOC range [ONL15a], [ONL15b]. For storage assets, devices should be capable of managing their SOC within an envelope, therefore minimising saturation and depletion. The storage providers must deliver continuous power at all times as shown in the required envelope in Fig. 2.18. Power delivered outside the specified envelope will reduce the SPM and hence availability payment [ONL15a], [ONL15b].

In this section, the SPM is calculated per settlement period as the sum of the second by second proportion of normalized response against the allowable envelope (Fig. 2.18) at a given frequency value. Normalized response is the ratio of actual response provided in that second against the operational capacity or tendered capacity in MW as shown in (2.4). If the normalized response is within the allowable envelope, the SPM is set at 100%. The calculation of the availability rate is described in Table 1.7, where the SPM rate of less than 95% will cause a penalty in the availability payment to the energy storage providers [ONL15a].

$$SPM = (Actual\ BESS\ Power / BESS\ Capacity) / (Allowable\ Power) \quad (2.4)$$

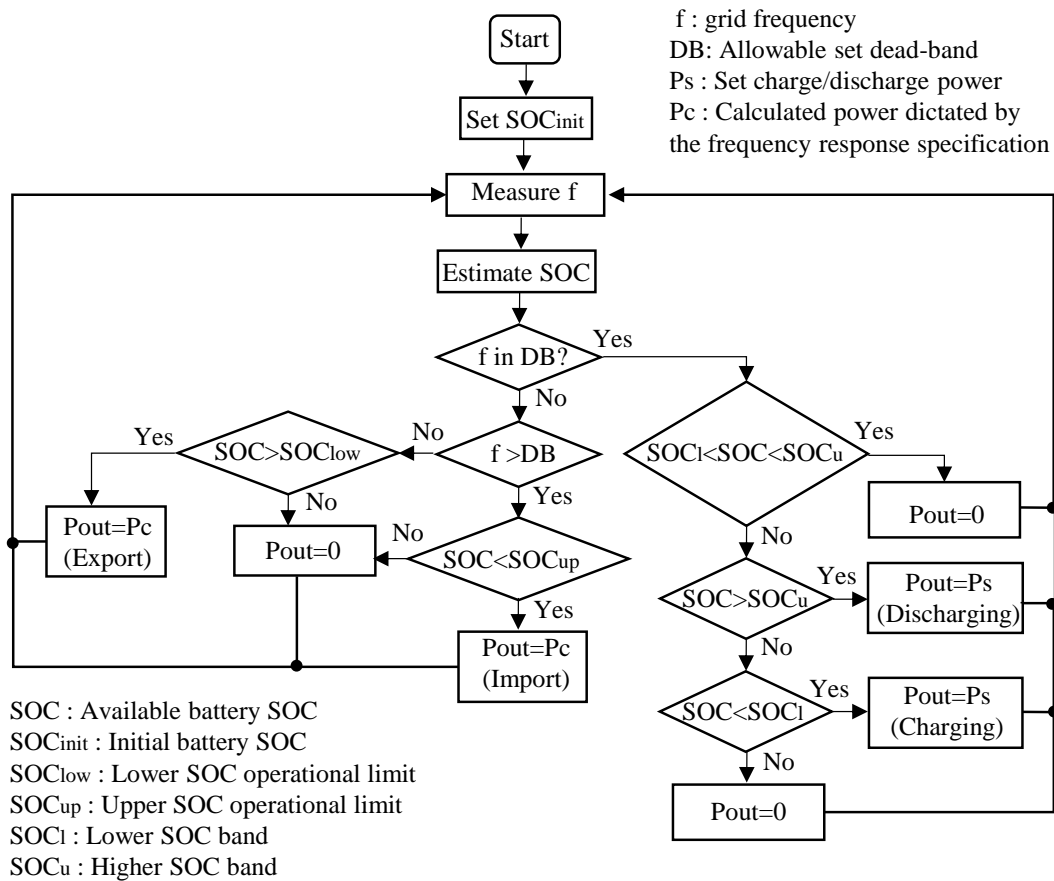
### 2.3.2 Pre-EFR Control Algorithm Design

A BESS model is developed in MATLAB/Simulink and verified against experimental operation of the WESS. A Pre-EFR frequency response control algorithm is then implemented in the model to deliver a grid frequency response service to the NGET specification. Fig. 2.19 shows the battery charge/discharge management for Pre-EFR service implemented in the BESS model, where the inputs are real grid frequency (f) and battery SOC, and the output is the required power. The control algorithm starts by detecting the position of the measured frequency with respect to the zones bounded by vertical lines in Fig. 2.18, and then the NGET required frequency response power [ONL15a], [ONL15b] is calculated.

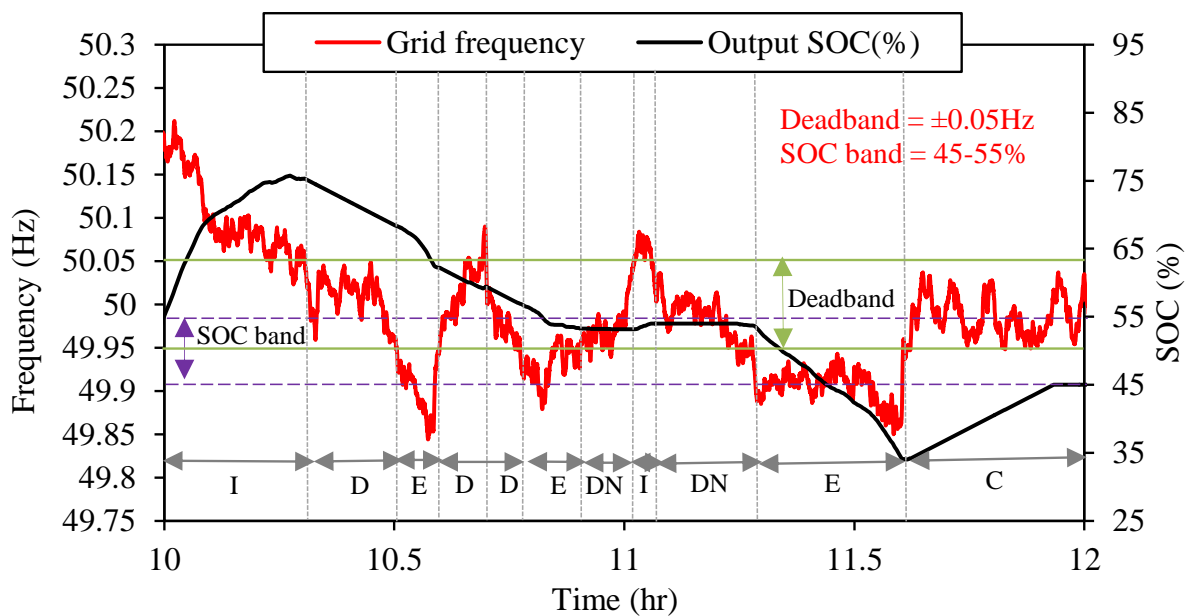
The logic of the proposed charge/discharge management is described in Fig. 2.19.a, where if frequency is outside the DB, the battery imports and exports power to the grid with respect to the set battery upper and lower operational limit [ONL15a], [ONL15b]. Within DB, the battery has an opportunity to charge/discharge in order to manage battery SOC. In this section, it is proposed that a desired SOC range is set in the control algorithm to maintain the battery SOC at a level to be able to achieve maximum battery availability and also prolong the battery lifetime. Operation principle of the proposed battery charge/discharge management in Fig. 2.19 (a) is demonstrated on the 2-hour profile of the real frequency of 19 Feb 2014 in Fig. 2.19 (b).

As seen from the profile Fig. 2.19 (b), if the grid frequency is greater than the DB, the battery imports power from the grid to maintain; when frequency returns to the DB, if the available battery SOC is greater than the set higher SOC band (55%), the battery discharges until the SOC is within the desired range (45-55%). If frequency is lower than the DB, the battery exports power to the grid; when frequency returns to the DB, if the SOC is lower than the set lower SOC band (45%), the battery charges to maintain the SOC within the desired range of 45-55%.





(a)



(b)

Fig. 2.19 Flow chart of the BESS charge/discharge management for Pre-EFR service (a), Demonstration of the management on the 2-hour profile of 3rd Feb 2014 (Battery import (I), export (E), charge (C), discharge (D), battery do nothing (DN) (b).

### 2.3.3 Simulation Results of Pre-EFR Control Algorithm

The proposed Pre-EFR control algorithm is simulated in MATLAB/Simulink using the real grid frequency data obtained from the NGET [ONL15a] using the validated WESS model. The parameters used in the frequency response algorithm are given in Table 2.7.

Table 2.7 Parameters used in the Pre-EFR control algorithm implemented in the BESS.

Parameter	Value
Allowable High/Low DB	$\pm 0.1$ Hz
Min/max EFR power limit	$\pm 2$ MW
Battery rated power/capacity	2 MW/1 MWh
Initial SOC ( $SOC_{init}$ )	40%
Operational SOC limit ( $SOC_{low}/SOC_{up}$ )	20% / 90%
Inverter efficiency ( $\eta$ )	97%
Battery charge/discharge efficiency ( $\eta_{dc}$ )	95%

#### A) BESS with No Additional Charging

In this section, the proposed Pre-EFR control algorithm implemented in the BESS model has been analysed with a 0.05 DB having no battery charge/discharge management as well as no battery SOC management in order to observe the BESS import/export SPM rates of each day of February (see Fig. 2.20), which is the most critical month in 2014. Analysing the proposed frequency response algorithm, the obtained simulation results of the BESS output power and SOC for 14th Feb and 19th Feb 2014, which are the worst and best day in Feb 2014, respectively in terms of under/lower frequency events, are shown in Fig. 2.21. It is clear from Fig. 2.20, having no control strategy in the algorithm, the BESS is able to deliver a continuous power to the grid, but provides quite low import/export SPM rates, causing a high amount of penalty to the availability payment. Table 2.8 shows that, despite the 100% import/export SPM rates of the best day (19th Feb 2014), in the worst day (14th Feb 2014), the battery is only 48% available for delivering frequency response to the grid, where the output battery SOC stays at the lowest operational limit of 20% at around 3am to 5am with no battery availability in 14th Feb (see Fig. 2.21 (e)); however the battery SOC stays at the lowest limit (20%) at only around 30 mins in the best day (see Fig. 2.21 (f)). The aim of this analysis is to observe the battery availability rates extracted from the Pre-EFR algorithm without having any control strategies;

and as a result of this develop suitable control strategies to be able to meet the NGET required battery import/export SPM of greater than 95%, providing 100% availability rate.

Table 2.8 Battery import/export SPM (%) of the worst (14th Feb) and best day (19th Feb) in 2014 for 0.05DB (no control strategy used)

Days	Import (%)	Export (%)
14 <sup>th</sup> Feb.	100	48
19 <sup>th</sup> Feb.	100	100

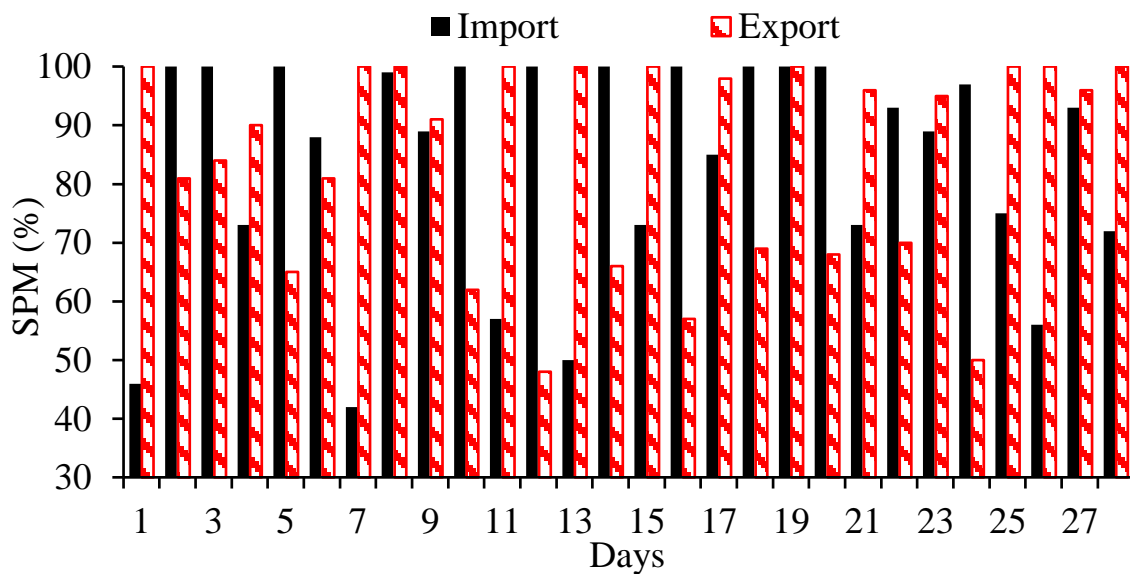
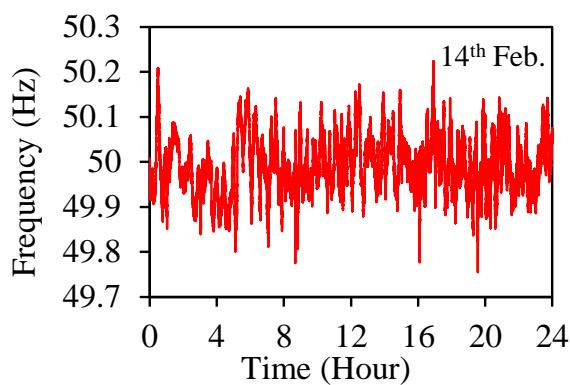
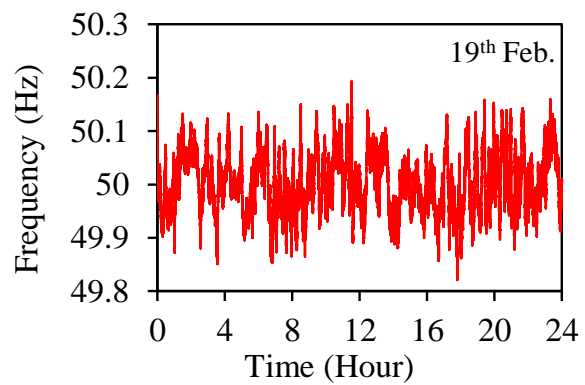


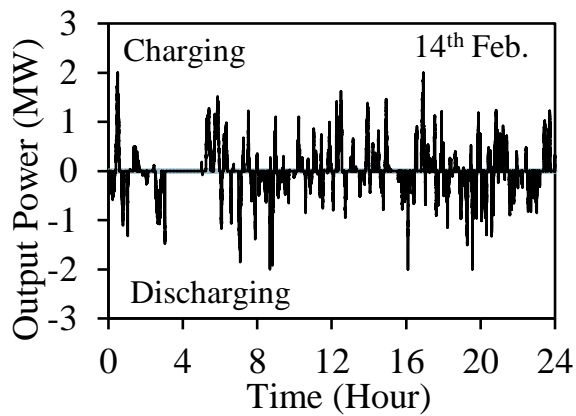
Fig. 2.20 Battery import/export SPM rate of each days of Feb 2014 for 0.05DB with no battery management.



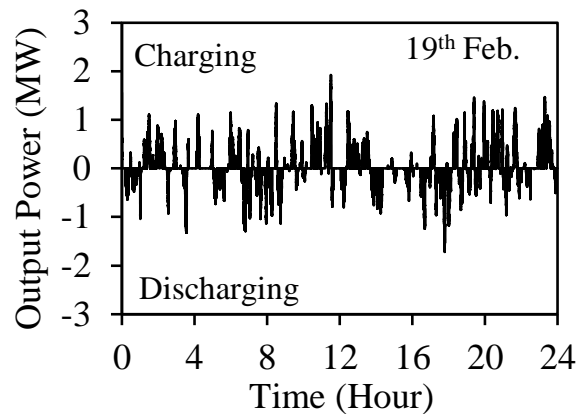
(a) Frequency of 14<sup>th</sup> Feb 2014



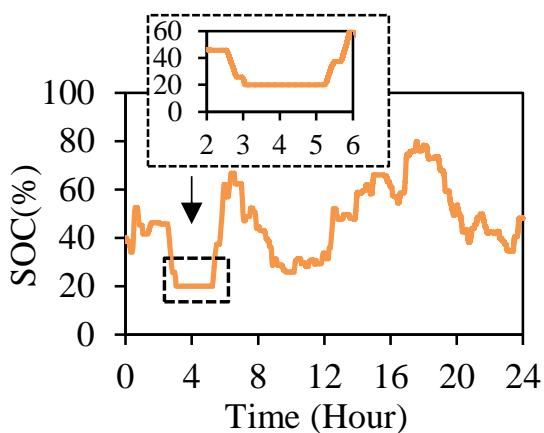
(b) Frequency of 19<sup>th</sup> Feb 2014



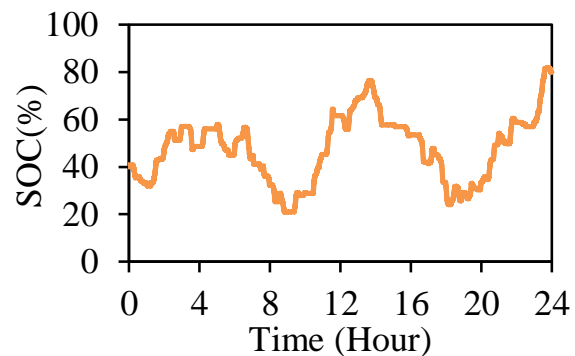
(c) Battery power of 14<sup>th</sup> Feb 2014



(d) Battery power of 19<sup>th</sup> Feb 2014



(e) Battery SOC of 14<sup>th</sup> Feb 2014



(f) Battery SOC of 19<sup>th</sup> Feb 2014

Fig. 2.21 Simulation results of the Pre-EFR algorithm with no battery management strategy for 0.05DB for 14th and 19th February 2014 frequency data.

*B) A Sensitivity analysis of Battery SOC Management and Battery Charge/Discharge Management*

After evaluating the SPM findings extracted in Part A, in order to increase the BESS availability, a sensitivity analysis of battery SOC management strategy (see Table 2.10) and a battery charge/discharge management method (see Table 2.9) based on SPM have been developed to implement in the proposed Pre-EFR algorithm for the NGET allowable DB ranges of 0.05Hz and 0.1Hz. The aim of the battery charge/discharge management is to achieve the battery optimum charge/discharge power amount for each considered DB in order to meet the NGET SPM requirement of higher than 95% (see Table 2.9).

Table 2.9 Battery import/export (I/E) SPM (%) of each month in 2014 for different DB ranges at their ideal battery charge/discharge power under 50-60% SOC band

2014	0.1 DB						0.05 DB					
	35kW		50kW		60kW		200kW		350kW		500kW	
	I	E	I	E	I	E	I	E	I	E	I	E
<b>Jan</b>	99	100	100	100	100	100	98	94	99	96	99	97
<b>Feb</b>	92	100	96	100	97	100	93	94	96	97	97	98
<b>Mar</b>	97	100	98	100	99	100	95	97	97	99	98	100
<b>Apr</b>	94	100	94	100	96	100	93	96	96	98	97	99
<b>May</b>	100	100	100	100	100	100	100	98	100	99	100	99
<b>Jun</b>	100	100	100	100	100	100	99	100	99	100	100	100
<b>Jul</b>	100	100	100	100	100	100	100	99	100	100	100	100
<b>Aug</b>	100	100	100	100	100	100	99	99	100	99	100	100
<b>Sep</b>	100	100	100	100	100	100	99	100	100	100	100	100
<b>Oct</b>	100	100	100	100	100	100	98	98	99	100	99	100
<b>Nov</b>	100	100	100	100	100	100	98	93	99	96	100	98
<b>Dec</b>	100	100	100	100	100	100	98	94	99	96	99	97

In the proposed sensitivity analysis of battery charge/discharge management strategy, for 0.1DB and 0.05DB, the battery charge/discharge power amount selected is 35kW, 50kW, 60kW and 200kW, 350kW, 500kW, respectively. From the analysis results in Table 2.9, the NGET required battery import/export SPM ranges (>95%) have been achieved at 60kW and 350kW charge/discharge power for 0.1DB and 0.05DB, respectively, setting the battery SOC band to 50-60%. Comparing the obtained SPM rates of each month of 2014 in Table 2.9, the optimal charge/discharge power amount forecasted is 60kW (orange-shaded box) for 0.1 DB and 350kW (yellow-shaded box) for 0.05 DB under the SOC band limit of 50-60%. It is observed that, the use of a tighter DB in the frequency response algorithm requires increased amount of battery charge/discharge power to be able to reach the expected battery SPM ranges. It is revealed that the higher the amount of battery charge/discharge power, the higher the BESS availability; however it should be noted that the primary aim of the local control strategy is to minimise the battery charge/discharge power to maximize the battery life time. Furthermore, it is understandable from an electricity grid balancing strategy that BESSs should be restricted in

power once they return to DB to maintain recovered stability. The proposed sensitivity analysis of battery SOC management strategy based on SPM is presented in Table 2.10, where the frequency response model is analysed for 0.05DB at its forecasted ideal battery charge/discharge power amount of 350kW (yellow box in Table 2.9), by varying the battery SOC target range as shown in Table 2.10. According to the SOC strategy, the battery import/export SPM findings of each month of 2014 are evaluated, revealing that SOC ranges of 55-65%, 60-70% and 65-75% are inferior due to their insufficient (<95%) battery import/export SPM ranges that are attained in April 2014. In addition to this, because of the inadequate SPM range obtained from the critical winter months of November, December and February in 2014, the SOC range of 40-50% and 45-55% are also undesirable.

Table 2.10 Battery import/export (I/E) SPM (%) of each month in 2014 for different SOC band for 0.05DB at its ideal power of 350kW

<b>Selected SOC Band (%) in the sensitivity analysis of SOC management strategy</b>													
<b>2014</b>	<b>40% - 50%</b>		<b>45% - 55%</b>		<b>50% - 60%</b>		<b>55%- 65%</b>		<b>60% - 70%</b>		<b>65%- 75%</b>		
	<b>I</b>	<b>E</b>	<b>I</b>	<b>E</b>	<b>I</b>	<b>E</b>	<b>I</b>	<b>E</b>	<b>I</b>	<b>E</b>	<b>I</b>	<b>E</b>	
<b>Jan</b>	100	93	99	95	99	96	98	97	97	98	95	98	
<b>Feb</b>	97	94	97	96	96	97	95	98	94	98	92	99	
<b>Mar</b>	99	97	98	98	97	99	97	99	96	100	93	100	
<b>Apr</b>	97	96	96	97	95	98	94	99	93	99	92	99	
<b>May</b>	100	97	100	98	100	99	100	99	99	99	98	100	
<b>Jun</b>	100	99	100	100	99	100	99	100	98	100	97	100	
<b>Jul</b>	100	98	100	99	100	100	100	100	99	100	98	100	
<b>Aug</b>	100	98	100	99	100	99	99	100	98	100	97	100	
<b>Sep</b>	100	99	100	100	100	100	99	100	99	100	98	100	
<b>Oct</b>	99	98	99	99	99	100	99	100	98	100	96	100	
<b>Nov</b>	100	93	100	94	99	96	99	97	98	98	96	99	
<b>Dec</b>	100	93	99	95	99	96	98	97	98	98	96	98	

Finally, the best SOC band limit forecasted is 50-60% as shown in the blue-shaded box in Table 2.10, which meets the NGET SPM requirement of greater than 95%, causing no availability

penalty to the BESS provider. It is also revealed that the initial battery SOC rate and the DB range set in the algorithm do not affect the forecasted SOC band limit.

Comparing a study in literature, *Lian et al.* [LIA17] investigated the potential use of LiFePO4 based BESSs to participate in the frequency response market of the UK NG. In the paper it was demonstrated that the optimal BESS SOC band is chosen as 50-60% for providing grid frequency response. Comparing that study, in this paper, by implementing the proposed sensitivity analysis of SOC management strategy in the BESS, the best SOC band is also chosen as 50-60% based on BESS availability on delivering grid frequency response service of Pre-EFR (see Table 2.10).

*C) BESS with Additional Charging and SOC band limit for 0.1DB and 0.05DB*

This section evaluates the performance of the developed battery charge/discharge management and the sensitivity analysis of SOC management strategy (Part B) implemented in the proposed frequency response algorithm for each considered NGET allowable DB of 0.1Hz and 0.05Hz.

Table 2.11 Battery import/export SPM (%) of the worst (14th Feb) and best day (19th Feb) in 2014 for 0.1DB (control strategy used)

<b>Days</b>	<b>Import (%)</b>	<b>Export (%)</b>
<b>14<sup>th</sup> Feb.</b>	100	92
<b>19<sup>th</sup> Feb.</b>	100	100

Analysing the simulation results, Fig. 2.22 and Fig. 2.24 show the battery availability ranges of each day of February 2014 for 0.1DB and 0.05DB obtained from the Pre-EFR algorithm limited to the previously selected charge and discharge powers of 60kW and 350kW, respectively, managing and setting the SOC band as 50-60%. It is clear that, despite analysing the critical winter month (February), the obtained battery SPM rates of each day of February 2014 are quite high due to the control strategy used in the algorithm. As seen from the simulation results of the BESS output power and SOC in Fig. 2.23 and Fig. 2.25, having the SOC control approach, the battery SOC is mostly maintained in the desired SOC band of 50-60% on the 14th and 19th February 2014, where the battery is not able to delivery power to the grid for only around one hour period in the worst day of 14th February as battery SOC remains at 0% at that time (Fig. 2.23 (c) and Fig. 2.25 (c)).

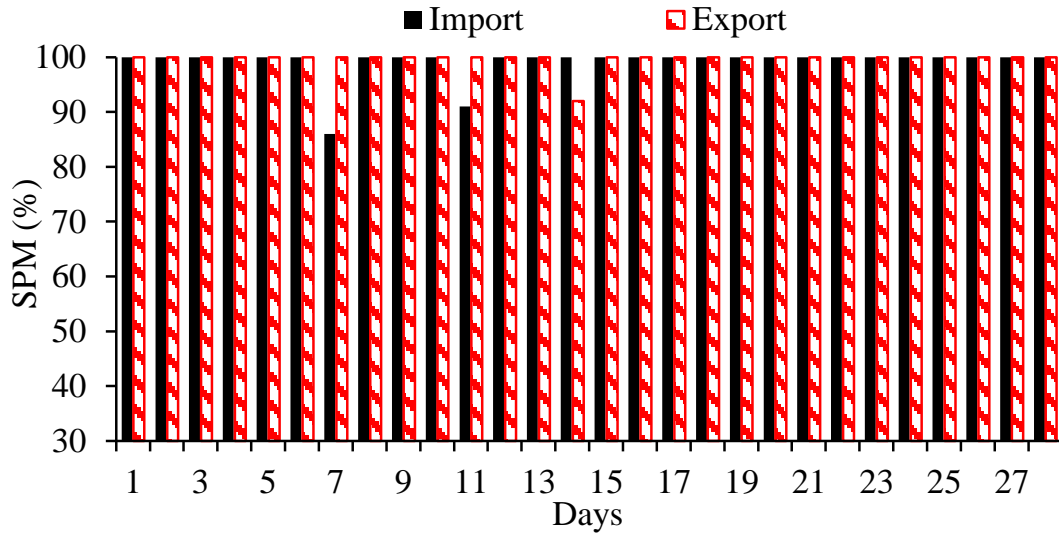
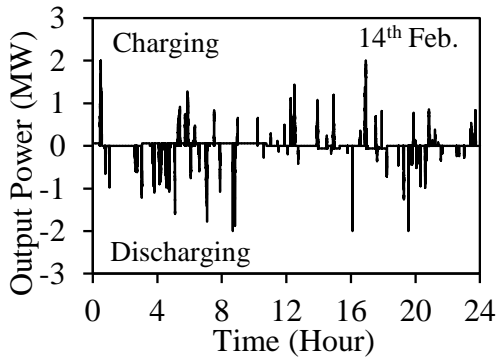
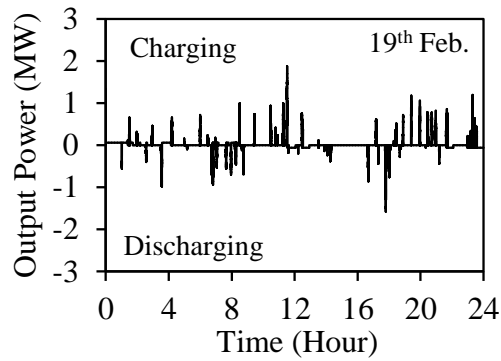


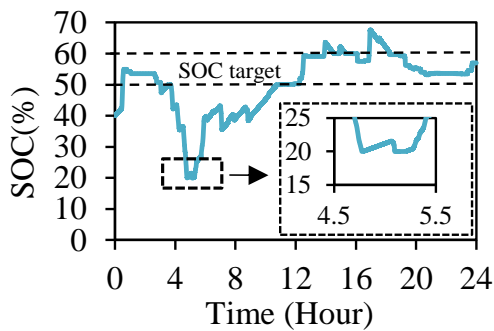
Fig. 2.22 Battery import/export SPM (%) of each days of Feb 2014 having the proposed control strategies in the frequency response algorithm for 0.1 DB.



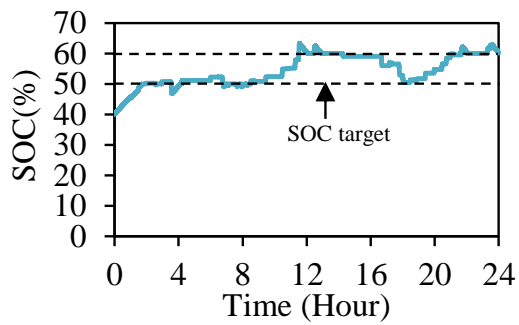
(a) Battery power of 14<sup>th</sup> Feb 2014



(b) Battery power of 19<sup>th</sup> Feb 2014



(c) Battery SOC of 14<sup>th</sup> Feb 2014



(d) Battery SOC of 19<sup>th</sup> Feb 2014

Fig. 2.23 Simulation results of the frequency response algorithm with the proposed control strategies for 0.1DB for 14th Feb (worst day) and 19th Feb (best day) in 2014.



Table 2.12 Battery import/export SPM (%) of the worst (14th Feb) and best day (19th Feb) in 2014 for 0.05DB (control strategy used)

Days	Import (%)	Export (%)
14 <sup>rd</sup> Feb.	100	80
19 <sup>th</sup> Feb.	100	100

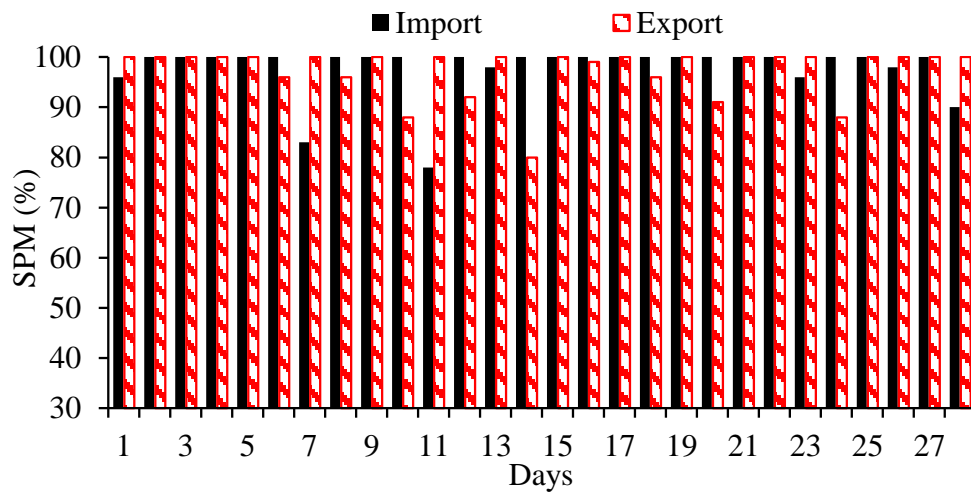
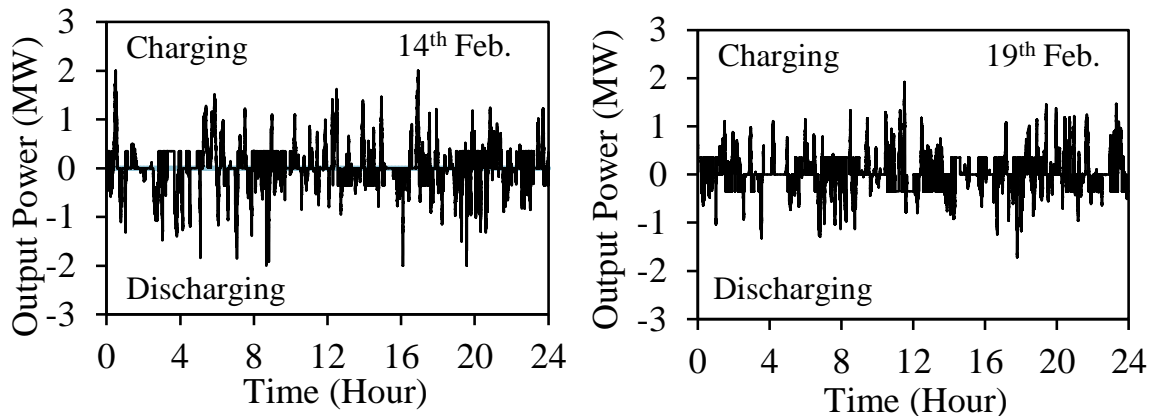


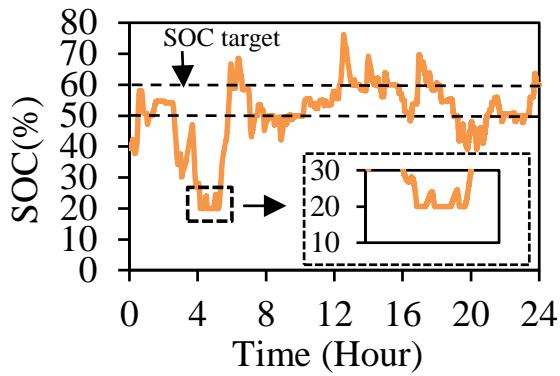
Fig. 2.24 Battery import/export SPM (%) of each days of Feb 2014 having the proposed control strategies in the frequency response algorithm for 0.05 DB.

Comparing the simulation findings obtained from the Pre-EFR algorithm with no control strategy in Part A, the battery import/export SPM rates of each day of February 2014 have been increased significantly in this part by implementing the ideal battery charge/discharge management method and the battery SOC management strategy into the developed frequency response algorithm.

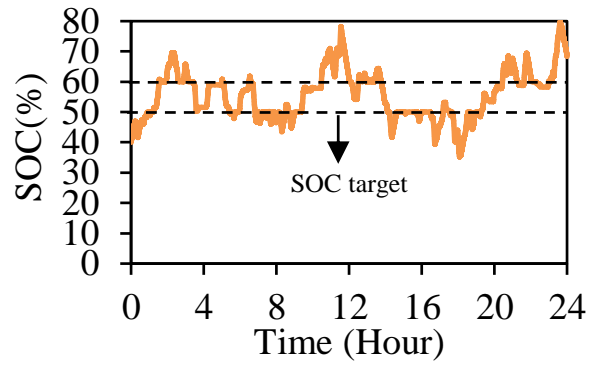


(a) Battery power of 14<sup>th</sup> Feb 2014

(b) Battery power of 19<sup>th</sup> Feb 2014



(c) Battery SOC of 14<sup>th</sup> Feb 2014



(d) Battery SOC of 19<sup>th</sup> Feb 2014

Fig. 2.25 Simulation results of the frequency response algorithm with the proposed control strategies for 0.05 DB for 14th Feb (worst day) and 19th Feb (best day) in 2014.

#### D) Analyses of the Simulation Results

In the proposed Pre-EFR algorithm it is possible to define two aims for power flow in and out of the battery; the first is defined as that of ideal charging/discharging battery i.e battery power is requested in either direction for the sole purpose of managing the battery SOC and not for the grid frequency response service; the second is import/export which represents when the BESS is performing a required response to a frequency event. Comparing the obtained battery SPM findings in Part A and Part C, it is revealed that by implementing the proposed battery SOC management approach and the battery charge/discharge management method into the frequency response algorithm, the battery SPM rates have been increased substantially day by day, particularly in the worst day (14th Feb), from 48% (Table 2.8) to 92% (Table 2.11) for 0.1DB, and also increased to 80% (

Table 2.12) for 0.05DB; causing a significant reduction in SPM penalty; and hence this results in a significant economic benefits to the energy storage providers.

## 2.4 BESS Control for Enhanced Frequency Response (EFR) Service

EFR is introduced as a new fast frequency response service for grid balancing that can deliver full-scale active power within one second of registering a grid frequency deviation. NGET prepared final EFR specification to facilitate a tender competition for 200 MW of support provision to be distributed amongst potential energy storage providers in 2016 [ONL16a].

### 2.4.1 NGET required EFR Service Specifications

The NGET required EFR service specifications used in the proposed EFR control algorithms are described in the following parts.

#### *A) Technical Requirements*

Energy storage providers must respond to deviations in nominal frequency (50 Hz) by decreasing or increasing their power output. Specifically, energy storage devices must provide power to the grid to respond to deviations in frequency outside of a DB. Within the DB, there is not a requirement to deliver power to the grid [ONL16a] but there is opportunity within power limits to charge/discharge the battery to achieve a desired SOC.

#### *B) Delivery Envelopes*

Providers must deliver continuous power to the grid as described in one of the two EFR service envelopes (Service-1, Service-2) in Fig. 2.26 and Table 2.13 [ONL16a]. As seen in Fig. 2.26, the power level must remain within the upper and lower envelopes at all times; power provided outside the envelope will decrease the SPM, and thus reduce the income revenue [ONL16a]. In DB, the reference power profile is at zero MW output and hence providers do not have to respond to changes in the grid frequency. The BESS can be freely operated to charge/discharge in DB, however, the maximum export/import power must not exceed 9% of the BESS's full-scale range [ONL16a].

#### *C) Ramp Rates*

Providers may operate anywhere within the upper and lower envelopes to deliver a continuous service to the power system, with respect to the specified limitations on ramp rates as given in Fig. 2.27, Table 2.14 and Table 2.15 [ONL16a]. For a BESS, this effectively provides some control over the SOC of the battery. For the zones A, C, D in Fig. 2.27, the ramp rate must obey the specified values in Table 2.14. Operation in zones C and D will result in payments at a lower SPM. Hence, in such cases, EFR power output has to return to the specified envelope with respect to the ramp-rate limits given in Table 2.14 [ONL16a].

Ramp-rate zone B is described as being the area between the upper and lower envelopes, excluding the DB, and extends to achieve the full power capability at  $\pm 0.5$  Hz [ONL16a]. The allowable ramp rates within zone B depend on the rate of change of frequency. For EFR Service-1 and Service-2, the ramp rate limitations for all frequencies in zone B are shown in

Table 2.15. With these ramp limits, output power changes proportionally to changes in grid frequency, whilst allowing the energy storage providers some flexibility [ONL16a] to manage the battery SOC.

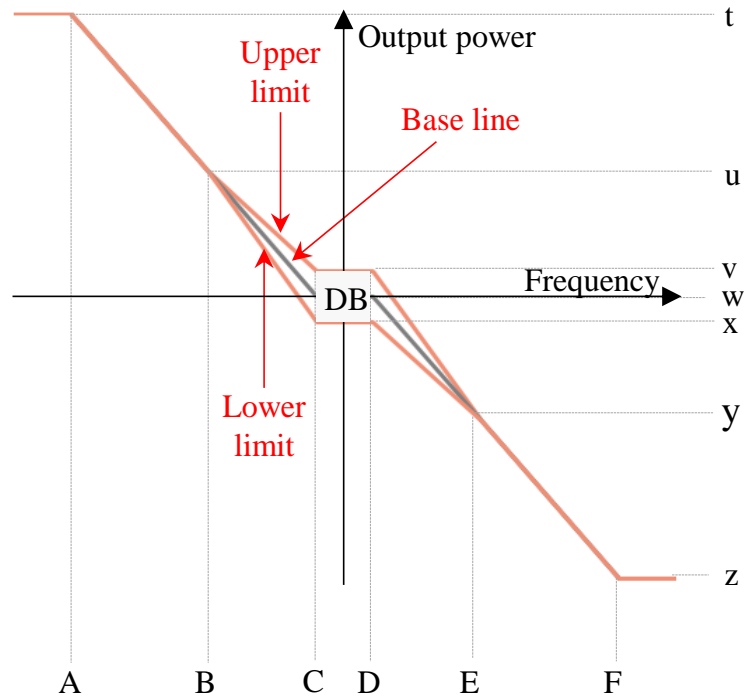


Fig. 2.26 NGET required EFR power versus frequency envelope [ONL16a].

Table 2.13 EFR envelope frequency and power boundaries [ONL16a].

Frequency (Hz)			Power (%)		
Ref. Point	Service-1	Service-2	Ref. Point	Service-1	Service-2
<i>A</i>	49.5	49.5	<i>t</i>	100	100
<i>B</i>	49.75	49.75	<i>u</i>	44.44444	48.4536
<i>C</i>	49.95	49.985	<i>v</i>	9	9
<i>D</i>	50.05	50.015	<i>w</i>	0	0
<i>E</i>	50.25	50.25	<i>x</i>	-9	-9
<i>F</i>	50.5	50.5	<i>y</i>	-44.44444	-48.4536
			<i>z</i>	-100	-100

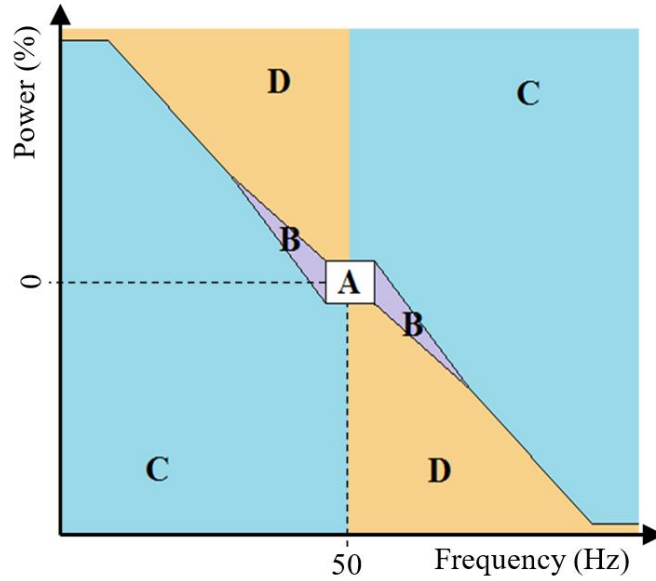


Fig. 2.27 NGET required EFR power zones [ONL16a].

Table 2.14 Ramp rate as a percentage of operational capacity for power zones A, C and D [ONL16a].

Area	Max Ramp Rate (%)	Min Ramp Rate (%)
A	1	0
C	200	0
D	10	0

Table 2.15 Ramp rate for zone B as a percentage of maximum power [ONL16a]

EFR Service	Max Ramp Rate (MW/s)	Min Ramp Rate (MW/s)
1 (wide)	$\left(-\frac{1}{0.45} \frac{df}{dt} + 0.01\right) \times 100$	$\left(-\frac{1}{0.45} \frac{df}{dt} - 0.01\right) \times 100$
2 (narrow)	$\left(-\frac{1}{0.485} \frac{df}{dt} + 0.01\right) \times 100$	$\left(-\frac{1}{0.485} \frac{df}{dt} - 0.01\right) \times 100$

#### 2.4.2 Standard EFR Control Algorithm (EFR-A1) Design

An EFR control algorithm with a 2MW/1MWh BESS, named EFR-A1, is developed in MATLAB/Simulink to deliver a grid frequency response service to the NGET specification.

The BESS model used is verified against experimental operation of the real WESS described in Chapter 2. Fig. 2.28 presents the EFR control scheme implemented in EFR-A1, where the inputs are real-time grid frequency ( $f$ ) and battery SOC, and the output is the required EFR power.

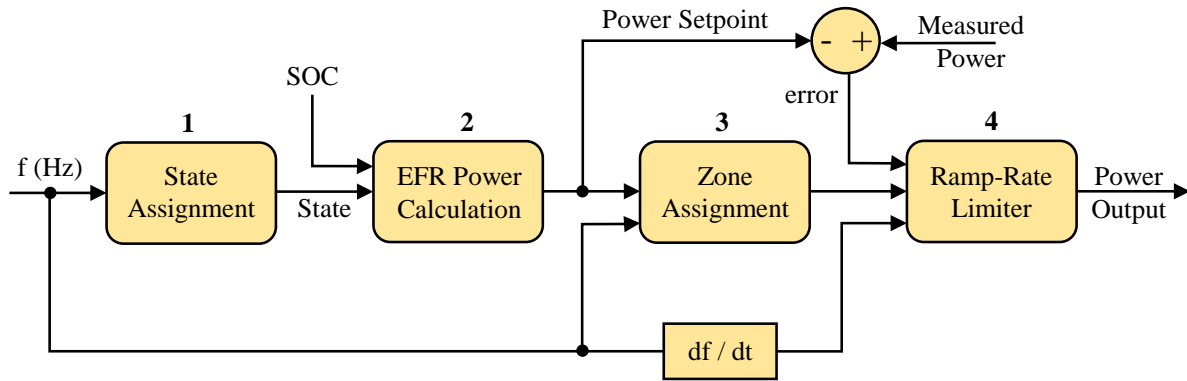


Fig. 2.28 EFR control scheme implemented in BESS model.

Table 2.16 State selection based on input frequency (Fig. 2.28, Block 1)

Condition	State
if ( $f \leq A$ )	0
if ( $A < f \leq B$ )	1
if ( $B < f \leq C$ )	2
if ( $C < f \leq D$ )	3
if ( $D < f \leq E$ )	4
if ( $E < f \leq F$ )	5
if ( $f > F$ )	6

The algorithm operates sequentially, where at each step time, a set of power decisions are taken. The algorithm starts by detecting the position of the measured grid frequency with respect to the zones bounded by vertical lines ‘A’ to ‘F’ in Fig. 2.26. This is achieved by the ‘State Assignment’ block (labelled ‘1’) in Fig. 2.28, where the state is re-configured according to the conditions set in Table 2.16. The next block in the sequence calculates the required EFR power (in terms of percentage capacity) as a function of available SOC and modifies the state of the machine. The power equations with their triggering conditions are presented in Table 2.17. Note that there are three sets of power equations for when the states equal ‘2’, ‘3’ and ‘4’. These equations refer to the upper, lower and central EFR reference lines, as seen Fig. 2.26,

and their selection is based on the available SOC at a given time. In the 2 MW BESS model, the frequency and power bounds are calculated as a function of the limits denoted in Fig. 2.26, with their values declared in Table 2.13. The power output is restricted to  $\pm 180$  kW (i.e. 9% of 2 MW) within the DB and both services include an upper, base and lower power line denoted U, Z and L, respectively. Block 2 in Fig. 2.28 selects the required power line with the decision being based on the measured SOC. For example, if the current SOC is below the desired SOC range, the demanded power is calculated using the equations derived for the upper line (U). This has the effect of either importing energy to charge the battery or minimising the exported energy to maintain a desired SOC range. In Block 2 in Fig. 2.28, an hysteresis SOC control is also implemented (Table 2.18) when the states equal ‘7’, ‘9’, ‘11’ for the control of SOC lower limit (SOC<sub>low</sub>) and ‘8’, ‘10’, ‘12’ for SOC upper limit control (SOC<sub>cup</sub>).

Table 2.17 EFR power calculation with battery SOC management (Fig. 2.28, Block 2)

Condition	EFR Power Setpoint $P_{set}$ (% Capacity)
if (State == 0)	$t$
if (State == 1)	$\left[ \left( \frac{B-f}{B-A} \right) x(t-u) \right] + u$
if (State == 2) && (SOC > SOC <sub>cup</sub> ) then: State = 7	$\left[ \left( \frac{C-f}{C-B} \right) x(u-v) \right] + v$
if (State == 2) && (SOC < SOC <sub>low</sub> ) then: State = 8	$\left[ \left( \frac{C-f}{C-B} \right) x(u-x) \right] + x$
if (State == 2) && (SOC <sub>low</sub> ≤ SOC ≤ SOC <sub>cup</sub> ) then: State = 13	$\left[ \left( \frac{C-f}{C-B} \right) x(u-w) \right] + w$
if (State == 3) && (SOC > SOC <sub>low</sub> ) then: State=11	$v$
if (State == 3) && (SOC < SOC <sub>cup</sub> ) then: State=12	$x$
if (State == 3) && (SOC <sub>low</sub> ≤ SOC ≤ SOC <sub>cup</sub> ) then: State=15	$w$
if (State == 4) && (SOC > SOC <sub>cup</sub> ) then: State = 9	$\left[ \left( \frac{f-D}{E-D} \right) x(y-v) \right] + v$
if (State == 4) && (SOC < SOC <sub>low</sub> ) then: State = 10	$\left[ \left( \frac{f-D}{E-D} \right) x(y-x) \right] + x$
if (State == 4) && (SOC <sub>low</sub> ≤ SOC ≤ SOC <sub>cup</sub> ) then: State = 14	$\left[ \left( \frac{f-D}{E-D} \right) x(y-w) \right] + w$
if (State == 5)	$\left[ \left( \frac{f-E}{F-E} \right) x(z-y) \right] + y$
if (State == 6)	$z$

Table 2.18 Hysteresis control of battery SOC upper and lower limit (Fig. 2.28, Block 2)

Condition	Hysteresis for SOC
if (State == 7) OR (State == 9) OR (State == 11)	SOC <sub>up</sub> = SOC <sub>up</sub> - 2
if (State == 8) OR (State == 10) OR (State == 12)	SOC <sub>low</sub> = SOC <sub>low</sub> + 2

Table 2.19 EFR power zone selection (Fig. 2.28, Block 3)

Condition	Zone
if (State == 15) OR ((State == 11) AND (error ≤ 0)) OR ((State == 12) AND (error ≥ 0))	A
if ((State == 7) AND (error ≤ 0)) OR ((State == 8) AND (error ≥ 0)) OR ((State == 9) AND (error ≤ 0)) OR ((State == 10) AND (error ≥ 0)) OR (State == 13) OR (State == 14) OR	B
if ((State == 0) AND (error ≤ 0)) OR ((State == 1) AND (error ≥ 0)) OR ((State == 5) AND (error ≥ 0)) OR ((State == 6) AND (error ≤ 0)) OR ((State == 8) AND (error < 0)) OR ((State == 9) AND (error > 0)) OR ((State == 11) AND (error > 0)) AND (f ≥ 50 Hz) OR ((State == 12) AND (error < 0)) AND (f ≤ 50 Hz)	C
if ((State == 0) AND (error > 0)) OR ((State == 1) AND (error > 0)) OR ((State == 5) AND (error < 0)) OR ((State == 6) AND (error < 0)) OR ((State == 7) AND (error > 0)) OR ((State == 10) AND (error < 0)) OR ((State == 11) AND (error > 0)) AND (f < 50 Hz) OR ((State == 12) AND (error < 0)) AND (f > 50 Hz)	D



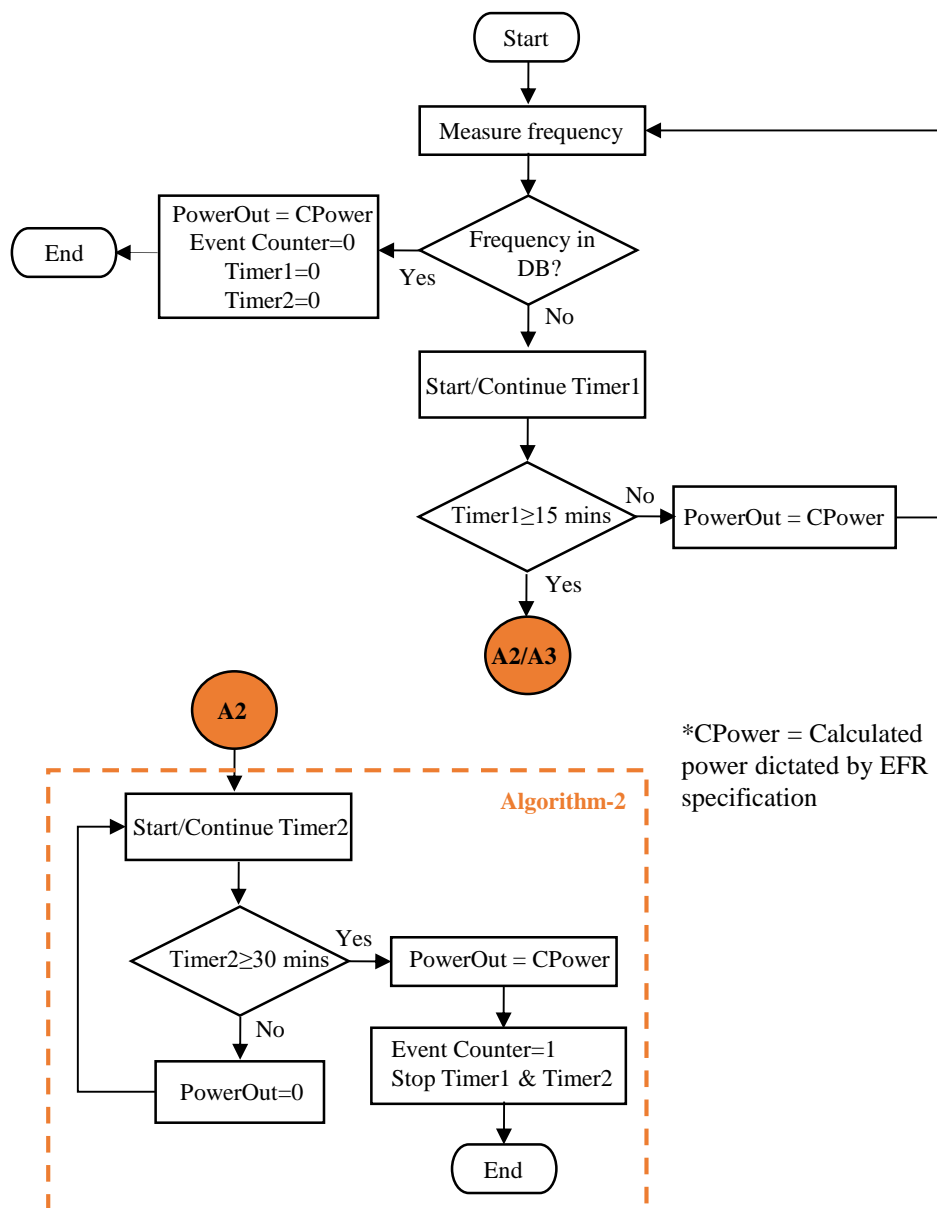
Table 2.20 Output power estimation with ramp rate up and low limiter (Fig. 2.28, Block 4)

Condition (Ramp Limiter)	Power Out (Pout) (kW)	Zone
If (Zone == A) AND (-error > 20) AND (Pset > 0)	$P_{out} = P_{meas} + 20$	A
If (Zone == A) AND (-error < -20) AND (Pset < 0)	$P_{out} = P_{meas} - 20$	
If (Zone == A) AND (-error <= 20) AND (-error >= -20)	$P_{out} = P_{set}$	
If (Zone == 2) AND (-error > RampU) AND (Pset >= 0)	$P_{out} = P_{meas} + RampU$	B
If (Zone == 2) AND (-error > RampU) AND (Pset <= 0)	$P_{out} = P_{meas} + RampU$	
If (Zone == 2) AND (-error < RampL) AND (Pset >= 0)	$P_{out} = P_{meas} + RampL$	
If (Zone == 2) AND (-error < RampL) AND (Pset <= 0)	$P_{out} = P_{meas} + RampL$	
If (Zone == 2) AND (-error <= RampU) AND (-error >= RampL)	$P_{out} = P_{set}$	
If (Zone == 3)	$P_{out} = P_{set}$	C
If (Zone == 4) AND (-error > 200) AND (Pset >= 0)	$P_{out} = P_{meas} + 200$	D
If (Zone == 4) AND (-error < -200) AND (Pset <= 0)	$P_{out} = P_{meas} - 200$	
If (Zone == 4) AND (-error <= 200) AND (-error >= -200)	$P_{out} = P_{set}$	
If (SOC >= 100 AND Pout < 0) OR (SOC <= 0 AND Pout > 0)	$P_{out} = 0$	

‘Zone Assignment’ (Block 3) in Fig. 2.28 is responsible for identifying the current operating zone (refer to Fig. 2.27) for the calculation of the power-output levels. The identified zones with their corresponding conditions are outlined in Table 2.19. Finally, in ‘Ramp-rate Limiter’ (Block 4) using the given ramp-rate limits in Table 2.14 and Table 2.15, the change in power output per time step (1 second) for each zone is determined as described in Table 2.20, where P is power setpoint, P<sub>meas</sub> is the process variable (called measured power here) and P<sub>out</sub> is output power.

### 2.4.3 Advanced EFR Control Algorithms (EFR-A2 and EFR-A3) Design

The EFR specification defines frequency outside DB for longer than 15 minutes as an extended event, whereby after the 15 minutes, it is optional to deliver power for up to 30 minutes post the grid frequency returning to DB. In order to increase the availability of the BESS with EFR-A1, by avoiding SOC limits, an extended 15-minute frequency event control algorithm is implemented in the advanced EFR control algorithms, called EFR-A2 and EFR-A3, as given in Fig. 2.29. EFR-A2 introduces a timed control block, which measures the length of time that the grid frequency is continuously outside of the DB.



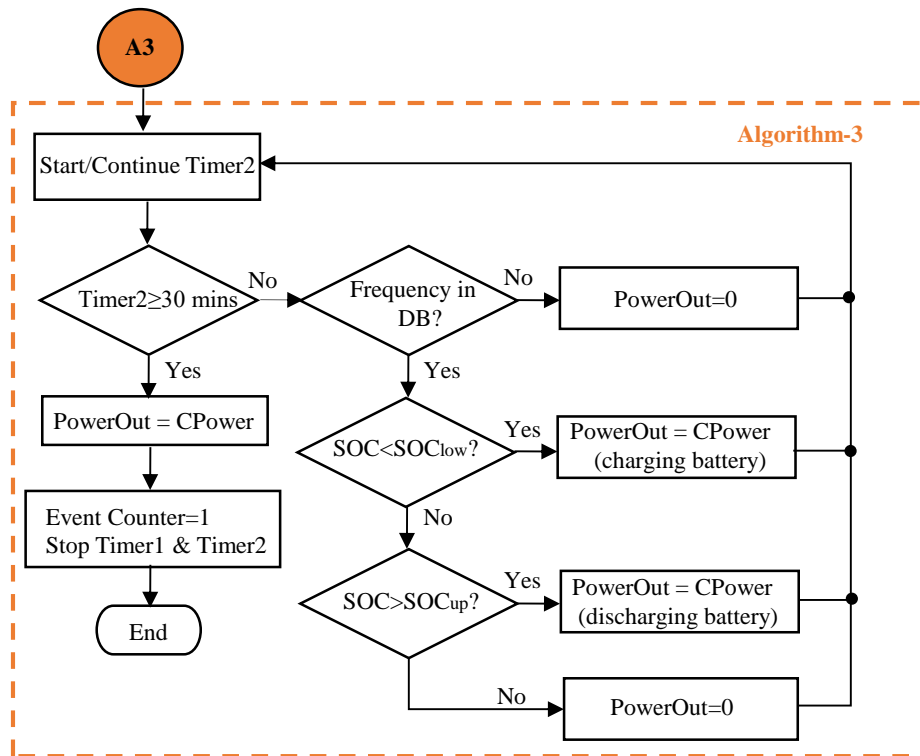
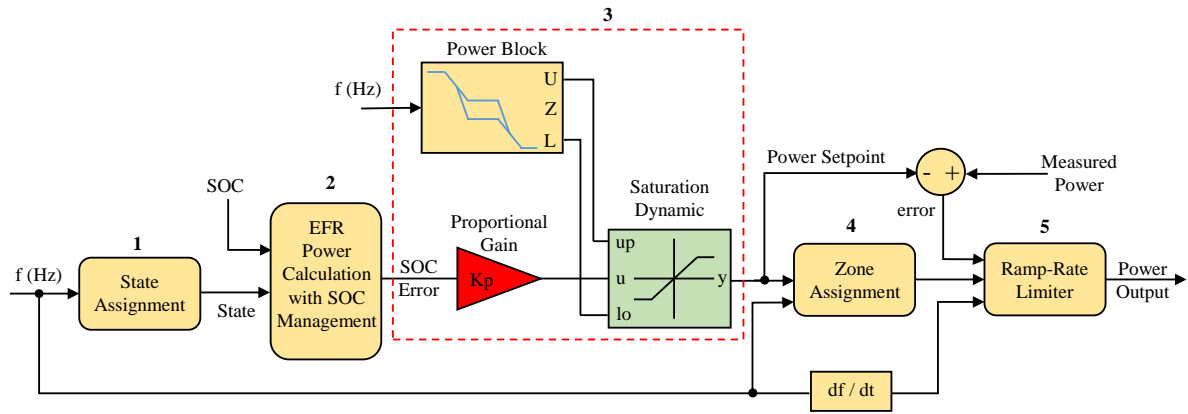


Fig. 2.29 Flow diagram of the advanced EFR control algorithm EFR-A2 and EFR-A3.

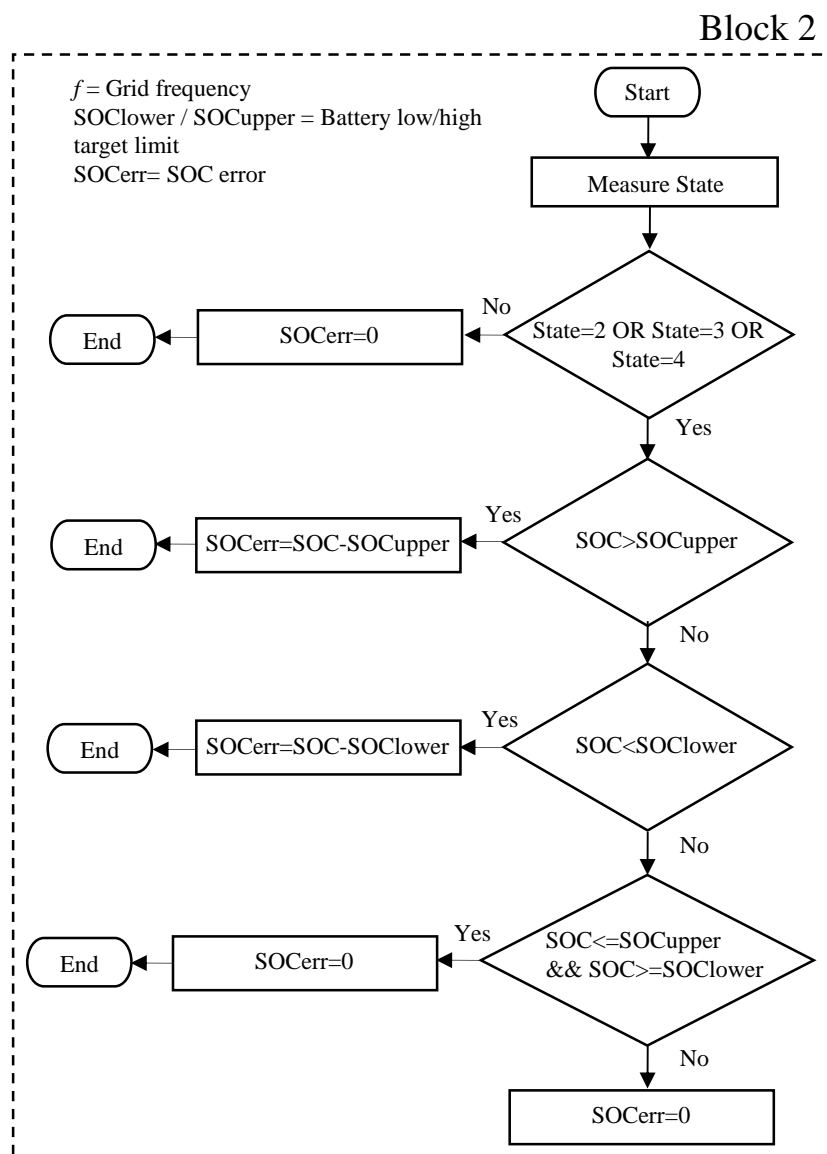
If this block measures a value higher than 15 minutes, then the BESS's output power is set to zero. The BESS remains in this state until the system frequency returns within DB, at which point a second timer starts timing for 30 minutes and the output power stays at zero until the timer expires, at which point, the EFR control is reset back to operating as EFR-A1. EFR-A3 allows the BESS to manage its SOC between its upper (SOC<sub>up</sub>) and lower limits (SOC<sub>low</sub>) during the 30-minute rest period by charging and discharging the battery within the  $\pm 9\%$  power limits.

#### 2.4.4 Standard EFR Algorithm with SOC-based Proportional Control (EFR-A4)

An EFR control algorithm having proportional control with a 2MW/1MWh BESS, named EFR-A4, is developed in MATLAB/Simulink to deliver a grid frequency response service to the NGET specification.



(a)



(b)

Fig. 2.30 Standard EFR control scheme with SOC-based proportional control (EFR-A4)

Fig. 2.30 presents the EFR control scheme implemented in EFR-A4, where the inputs are real-time grid frequency ( $f$ ) and battery SOC, and the output is the required EFR power.

The algorithm operates sequentially, where at each step time, a set of power decisions are taken. The algorithm starts by detecting the position of the measured grid frequency with respect to the zones bounded by vertical lines ‘A’ to ‘F’ in Fig. 2.26. This is achieved by the ‘State Assignment’ block (labelled ‘1’) in Fig. 2.30, where the state is re-configured according to the conditions set in Table 2.16. The next block in the sequence calculates the required EFR power (in terms of percentage capacity) as a function of available SOC and modifies the state of the machine. The power equations with their triggering conditions are presented in Table 2.17.

Note that when the states equal ‘2’, ‘3’ and ‘4’, the power output equals to SOC error (SOCerr), and its calculation is shown in Fig. 2.30. In the 2 MW BESS model, the frequency and power bounds are calculated as a function of the limits denoted in Fig. 2.26, with their values declared in Table 2.13. The power output is restricted to  $\pm 180$  kW (i.e. 9% of 2 MW) within the DB and both services include an upper, base and lower power line denoted U, Z and L, respectively. Block 2 in Fig. 2.30(a) calculates the SOC error with the decision being based on the SOC management shown in the given flow diagram in Fig. 2.30(b). For example, if the current SOC is below the desired SOC range, the SOC error is calculated extracting the lower SOC target band from the available SOC. This has the effect of either importing energy to charge the battery or minimising the exported energy to maintain a desired SOC range. In Block 2 in Fig. 2.30(a), an hysteresis SOC control is also implemented (Table 2.18) when the states equal ‘7’, ‘9’, ‘11’ for the control of SOC lower limit (SOC<sub>low</sub>) and ‘8’, ‘10’, ‘12’ for SOC upper limit control (SOC<sub>up</sub>).

Proportional control (Block 3 in Fig. 2.30(a)) is a type of linear feedback control system where a correction is applied to the controlled variable which is proportional to the difference between the desired value and the measured value [AST10]. In this section, a SOC-based proportional controller is applied to the Standard EFR control algorithm (EFR-A1) described in Section 2.4.2 in order to control the output EFR power as a proportional of battery SOC error in order to minimise the EFR power delivery without incurring a service penalty. In the proposed proportional control, the controller output is proportional to the error signal (SOC error), which is the difference between the desired value (available SOC) and the process variable (target SOC), as shown in Block 2 in Fig. 2.30(a). This means that the output of the proportional control is the multiplication product of the SOC error and the proportional gain ( $K_p$ ). The

algorithm then calculates the NGET required EFR response envelope in the Power Block, and sequentially the Saturation Dynamic Block limits the input signal to dynamic upper and lower saturation values, producing a power output signal that is the value of the input signal bounded to the saturation values from the input ports up (EFR power line U) and low (EFR power line L), as presented in Fig. 2.30. The aim of the use of the proportional controller in the basic EFR control scheme is to partially reduce the EFR power delivery and therefore battery C-rate without hitting a reduction in SPM in order to reduce the battery degradation rate; this will also help to prolong battery lifetime. The proportional control can also be implemented in the Advanced EFR control algorithms (EFR-A2 and EFR-A3). Simulation results of the EFR-A4 will be presented in Section 2.4.8 in detail.

‘Zone Assignment’ (Block 4) in Fig. 2.30(a) is responsible for identifying the current operating zone (refer to Fig. 2.27) for the calculation of the power-output levels. The identified zones with their corresponding conditions are outlined in Table 2.19. Finally, in ‘Ramp-rate Limiter’ (Block 5) using the given ramp-rate limits in Table 2.14 and Table 2.15, the change in power output per time step (1 second) for each zone is determined as described in Table 2.20, where  $P$  is power setpoint,  $P_{meas}$  is the process variable (called measured power here) and  $P_{out}$  is output power.

#### **2.4.5 Simulation Results of the Standard EFR Control Algorithm (EFR-A1)**

Using a real-time frequency data set obtained from NGET [ONL18k], the developed four EFR control algorithms are simulated in MATLAB/Simulink. The simulation results presented in this section are all based on the WESS model with Table 2.21 showing the parameters used. In order to show the performance of the reported EFR algorithm in Section 2.4.2, the real grid frequency data for the 21st of October of 2015 is employed herein, as this particular day is known to have a large period of under frequency. Fig. 2.31 and Fig. 2.33 show the simulation results of EFR-A1 for a ‘Service-1’ and ‘Service-2’ EFR with a target SOC band of 45-55%, respectively. On the frequency plot, the DB for Service-1 ( $\pm 0.05$ ) and Service-2 ( $\pm 0.015$  Hz) is shown by the green lines.

As seen from Fig. 2.31, however the standard EFR-A1 is simulated for an under frequency day (21<sup>st</sup> October 2015), the minimum battery SOC reaches to 33.08% (Fig. 2.31) comparing to 0% (Fig. 2.33) with EFR Service-2 due to the wide DB of  $\pm 0.05$ Hz used in Service-1 and the EFR

power stays within the NGET required EFR zones of ‘A’ and ‘B’ in Fig. 2.27. As shown in Fig. 2.31 and Fig. 2.32, since the SOC does not reach to 0% at any time in 21<sup>st</sup> Oct 2015, BESS is always available for delivering EFR power to the grid; hence this causes no penalty in the SPM in the EFR Service.

Table 2.21 System parameters used in EFR control algorithms [ONL16a]

<b>Parameter</b>	<b>Value</b>
Nominal frequency	50 Hz
Low/high DB	$\pm 0.015$ Hz (Service-2)
Max/min EFR power limit	$\pm 2$ MW
Battery rated power/capacity	2 MW/1 MWh
Battery initial SOC ( $SOC_{init}$ )	50%
SOC band ( $SOC_{low}$ - $SOC_{up}$ )	45-55%
Inverter efficiency ( $\eta_{inv}$ )	97%
Battery charge/discharge eff ( $\eta_C/\eta_D$ )	94%

Analysing the simulation results of the EFR-A1 with Service-2 (Fig. 2.33), it is clear that the SOC sharply drops, reaching 0% at 11:00, and stays there for ~30mins due to the grid frequency demands at that time. As the frequency stabilises, the EFR algorithm charges the battery when it is allowed and returns the SOC to within the specified band of 45-55%. The power response versus frequency plot of EFR-A1 with Service-2 for 21st October 2015 is shown in Fig. 2.34. The red lines represent the upper, reference and lower EFR power lines. It can be seen that the EFR power (blue circles) does not remain within the required zones of ‘A’ and ‘B’ (Fig. 2.34). As outlined in Fig. 2.33 and Fig. 2.34, this is because of the SOC reaching 0% and therefore there is no power available for delivery to the grid. This non-conformance would cause a penalty in the SPM and hence it is necessary to improve the EFR control algorithm to minimise such occurrences.

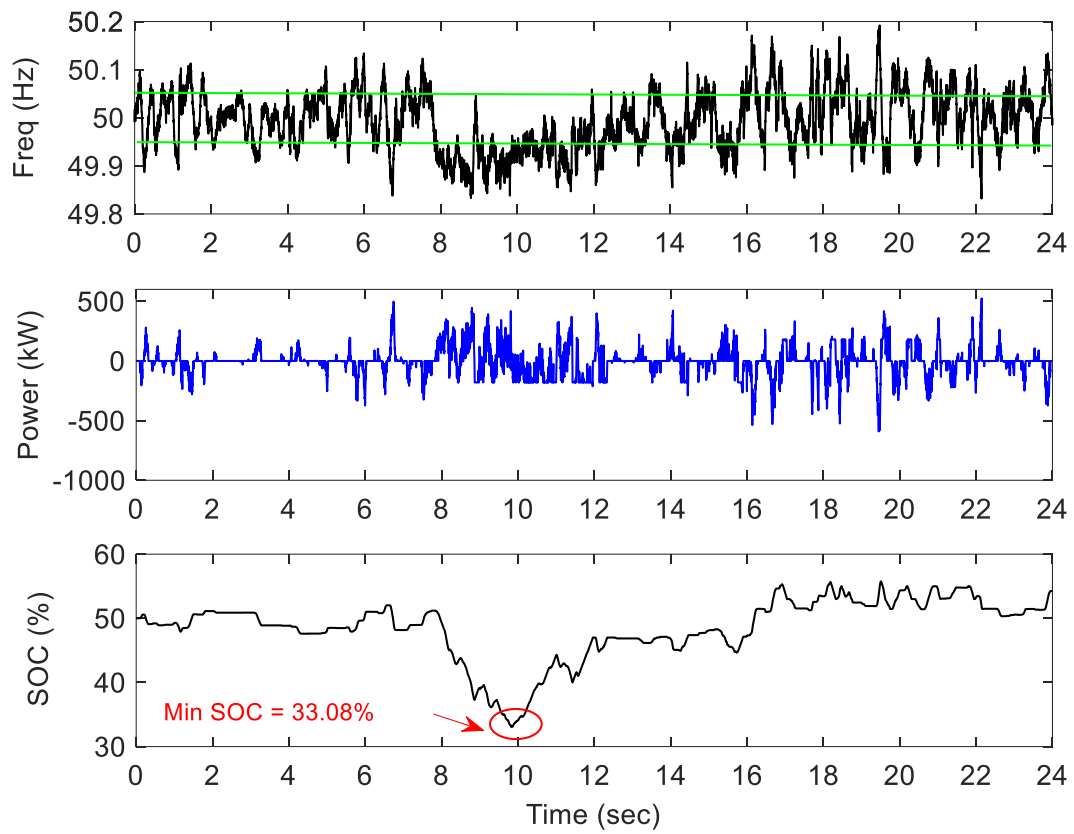


Fig. 2.31 Simulation results of EFR-A1 with Service-1 for 21st Oct 2015 frequency.

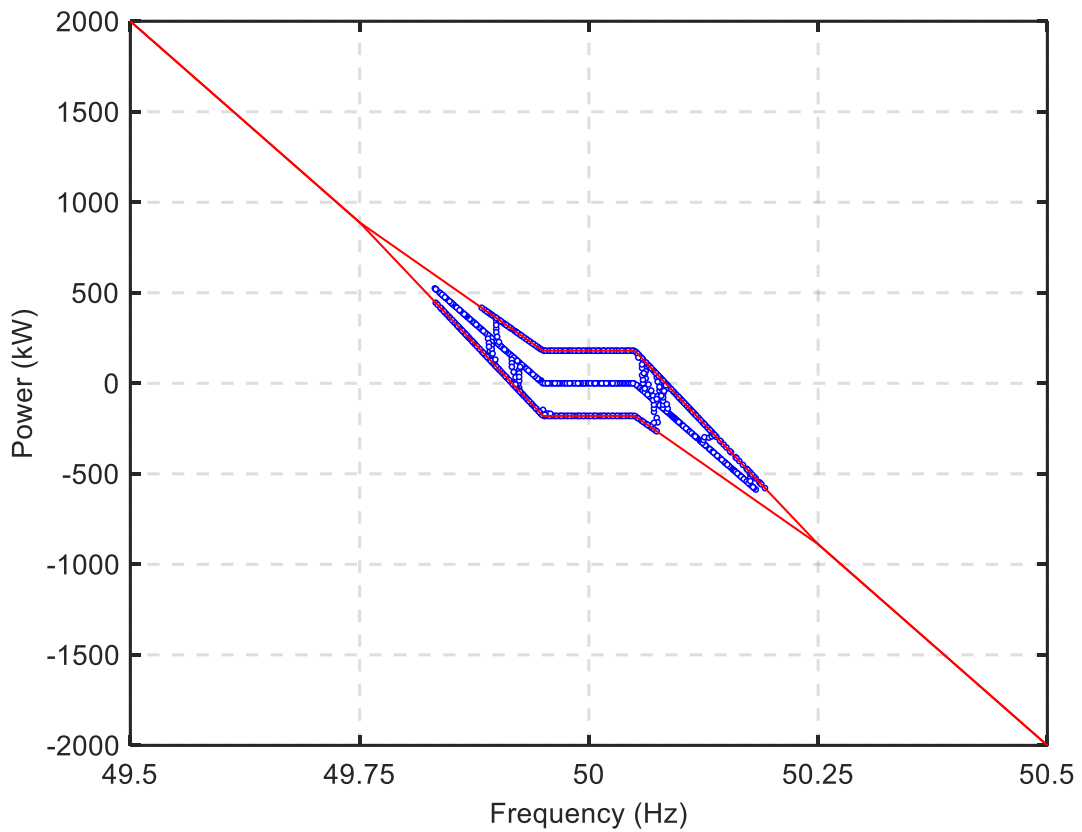


Fig. 2.32 EFR power vs frequency response of EFR-A1 (Service-1) for 21st Oct 2015.



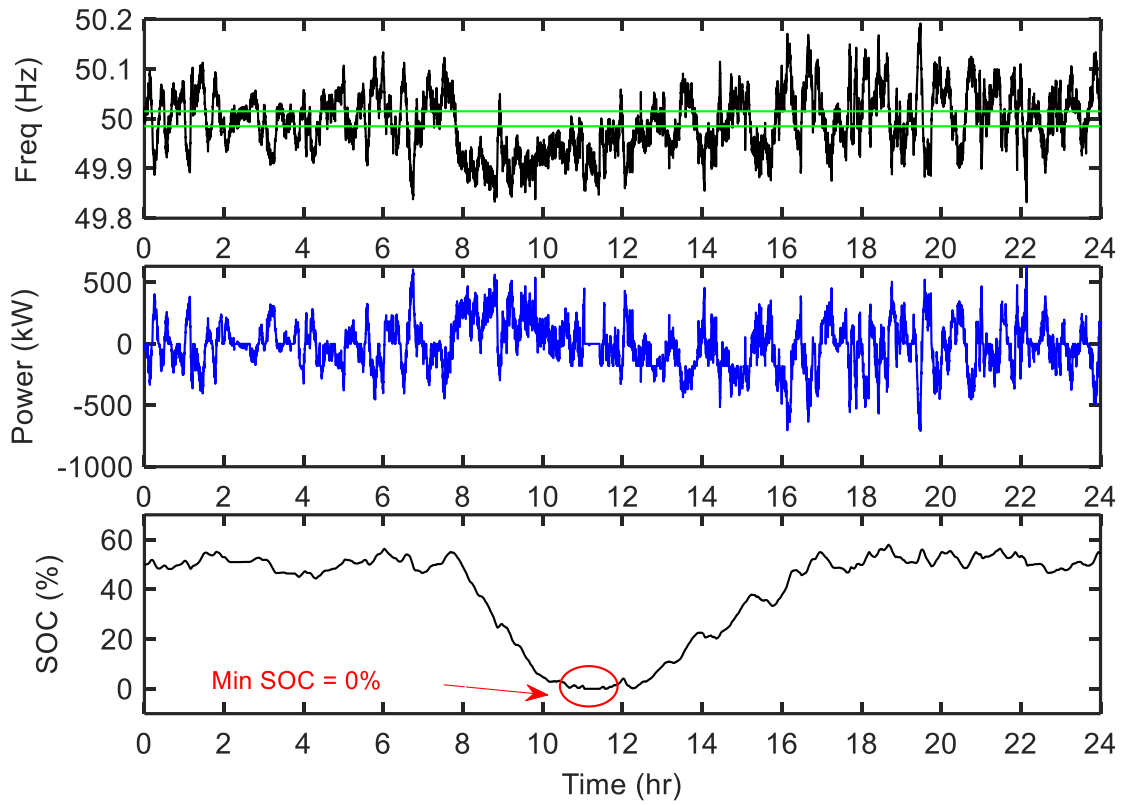


Fig. 2.33 Simulation results of EFR-A1 with Service-2 for 21st Oct 2015 frequency.

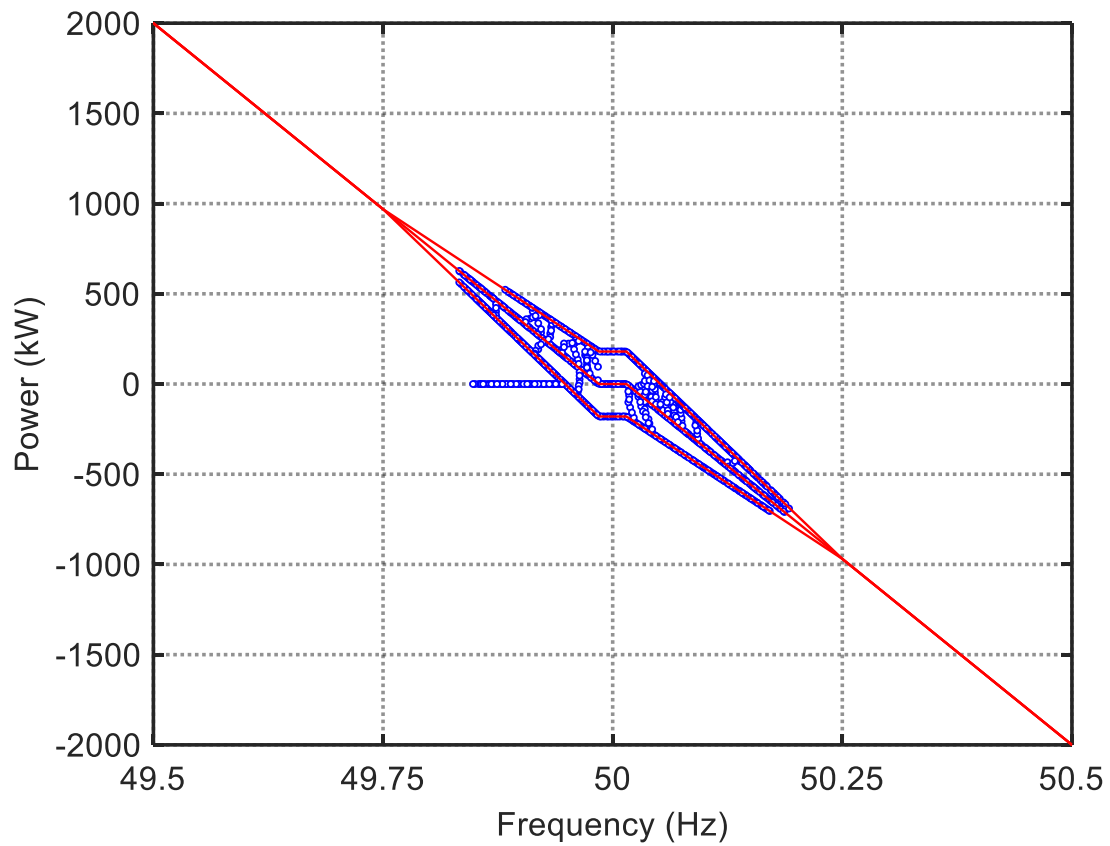


Fig. 2.34 EFR power vs frequency response of EFR-A1 (Service-2) for 21st Oct 2015.

#### 2.4.6 Simulation Results of the Advanced EFR Control Algorithm (EFR-A2)

The advanced EFR control algorithm (EFR-A2) described in Section 2.4.3 introduces the extended grid frequency event timer and cuts the EFR power output after 15 minutes (Fig. 2.29). Fig. 2.35 shows the simulation results of EFR-A2 for EFR Service-2 and the same frequency data (21<sup>st</sup> October 2015) is injected into the algorithm capturing 13 15-minute extended frequency events as given in the last plot of Fig. 2.35. The simulation results (Fig. 2.35) demonstrate that the minimum battery SOC reaches 30.7% compared to 0% (Fig. 2.33) in EFR-A1. Therefore, the BESS is 100% available for providing power according to the EFR specification as seen in Fig. 2.36.

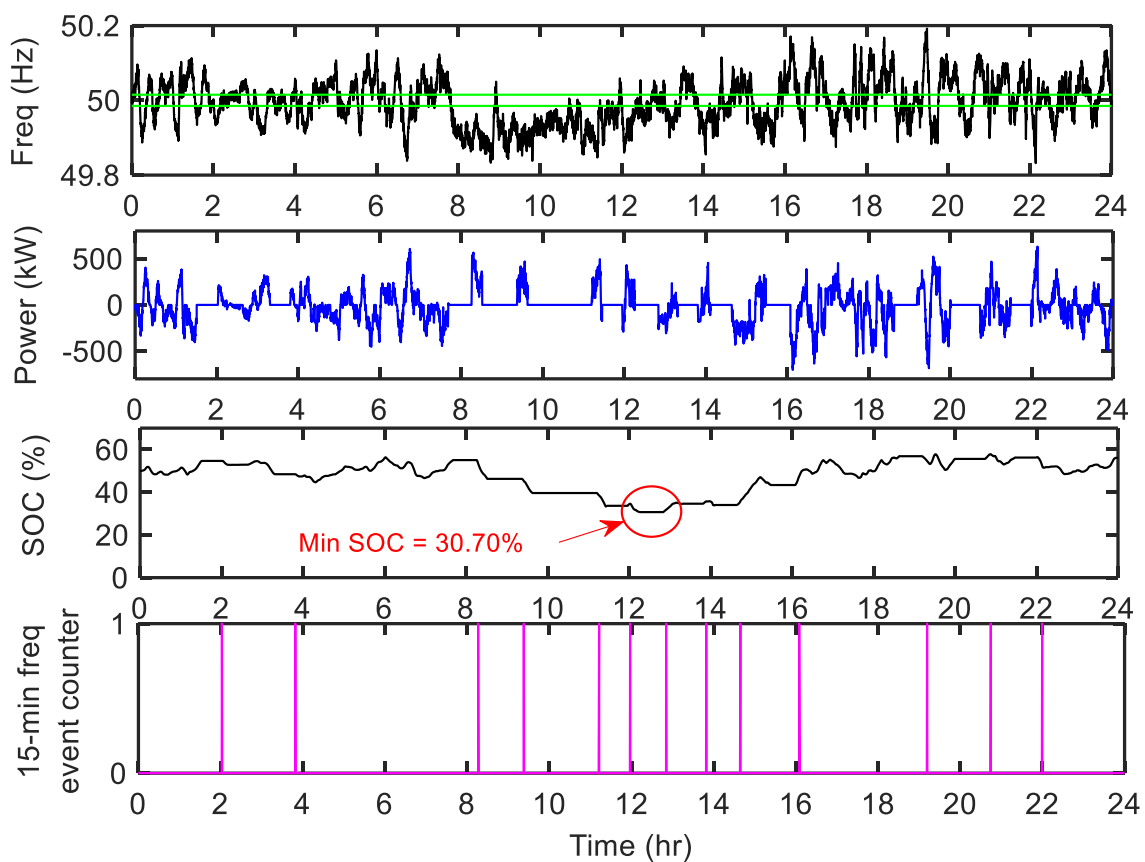


Fig. 2.35 Simulation results of EFR-A2 with Service-2 for 21st Oct 2015 frequency.

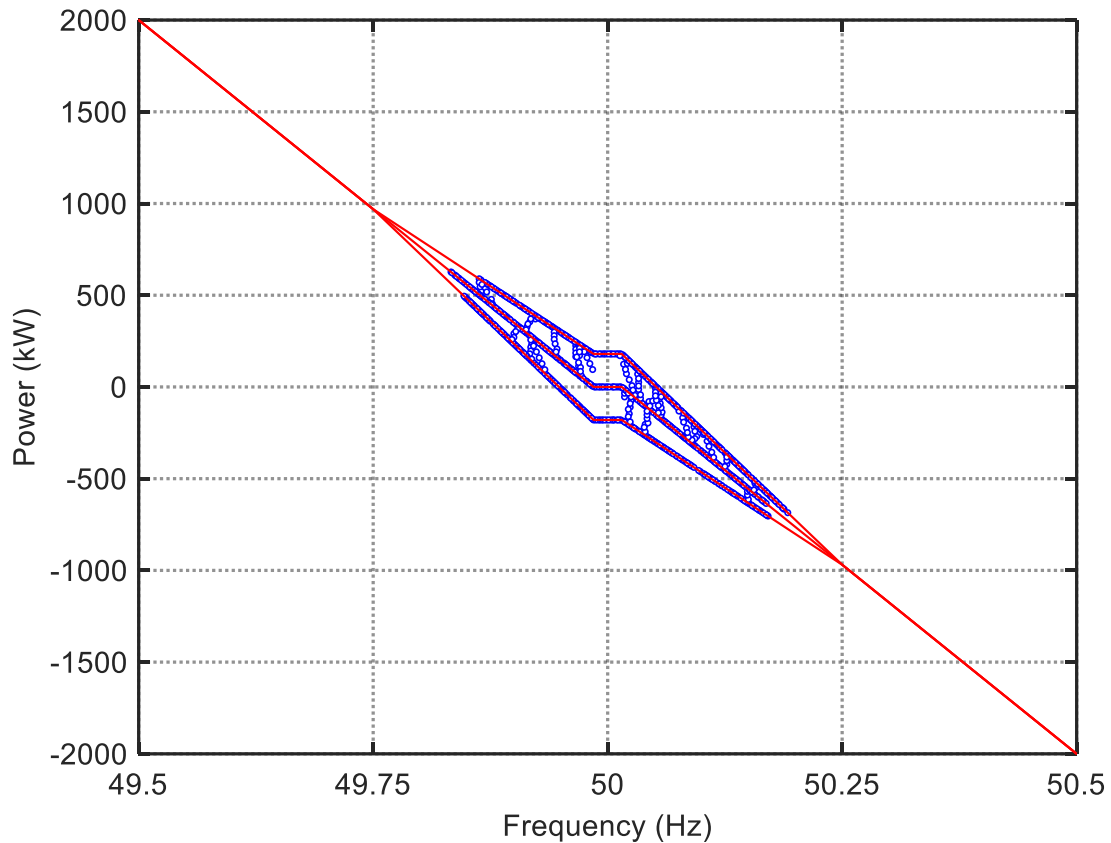


Fig. 2.36 EFR power vs frequency response of EFR-A2 (Service-2) for 21st Oct 2015.

#### 2.4.7 Simulation Results of the Advanced EFR Control Algorithm (EFR-A3)

The advanced EFR control algorithm (EFR-A3) described in Section 2.4.3 allows for the charge/discharge of the battery during the 30-minute rest period as seen in Fig. 2.29. The algorithm is simulated with the 21st October 2015 grid frequency data as shown in Fig. 2.37. The simulation results demonstrate that again, the BESS provides 100% availability as similar with EFR-A2 (see Fig. 2.36), however, the lowest SOC achieved with EFR-A3 is now 32.3% (see Fig. 2.37 and Fig. 2.38), compared to 30.7% (see Fig. 2.35 and Fig. 2.36) of EFR-A2. This is a substantial achievement in terms of maximising the utilisation of the BESS stored energy.

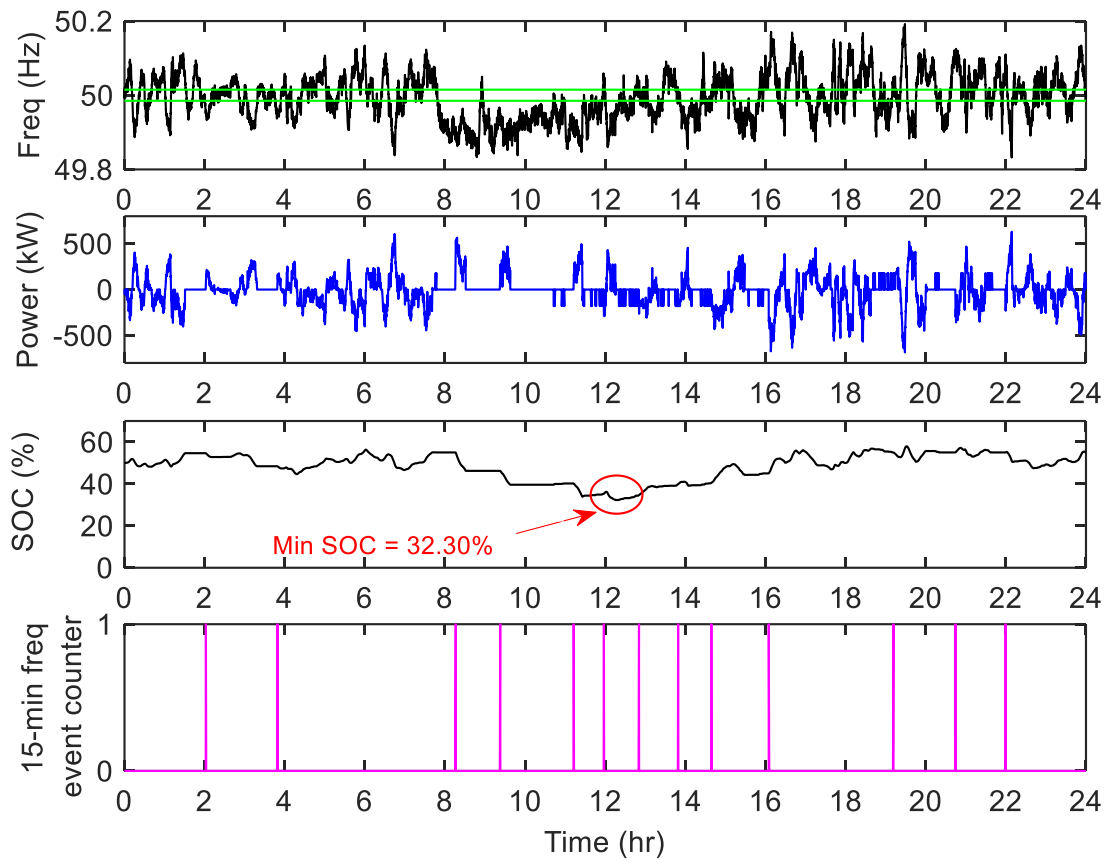


Fig. 2.37 Simulation results of EFR-A3 with Service-2 for 21st Oct 2015 frequency.

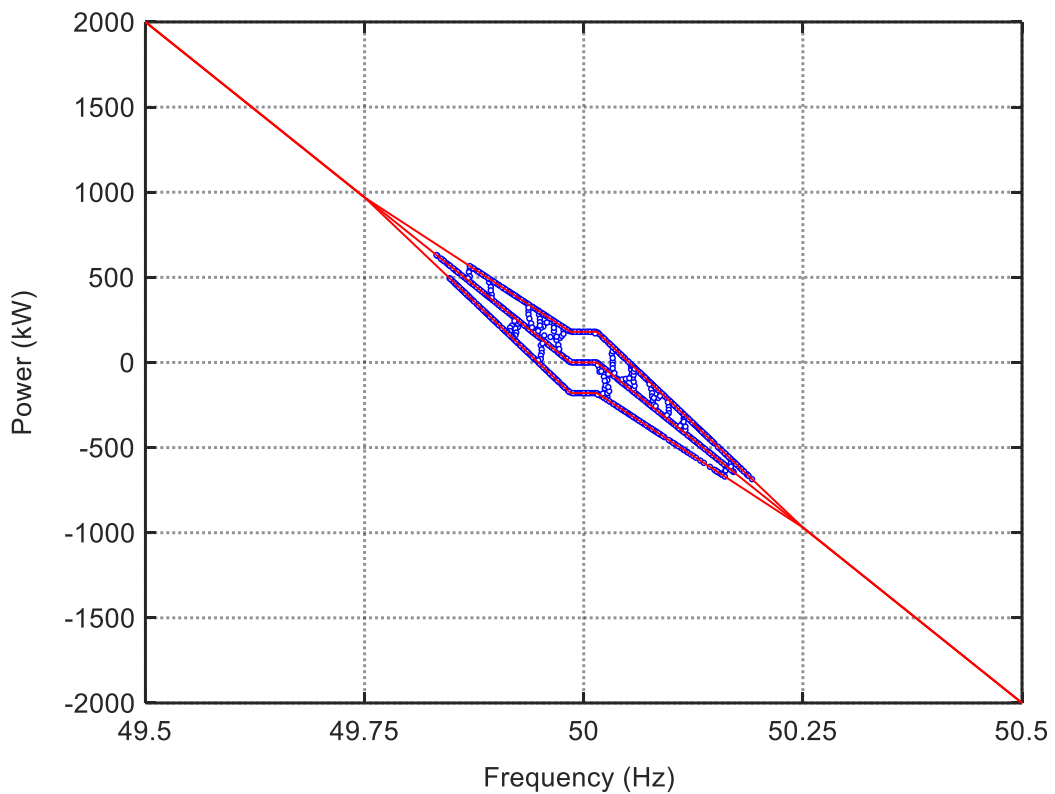


Fig. 2.38 EFR power vs frequency response of EFR-A3 (Service-2) for 21st Oct 2015.

#### 2.4.8 Simulation Results of the Standard EFR Control Algorithm with Proportional Control (EFR-A4)

The algorithm EFR-A4 includes a SOC based proportional control implemented in the standard EFR-A1 to reduce the amount of EFR power delivered to the grid without hitting a reduction in the SPM.

In order to compare the performance of the reported EFR-A1 described in Section 2.4.2 and the EFR-A4 described in Section 2.4.4, the real frequency data for the 1<sup>st</sup> January 2018 is used herein. Fig. 2.39 and Fig. 2.42 show the simulation results of the EFR-A1 and EFR-A4 for a ‘Service-2’ EFR with the  $K_p$  values of  $K_p = 1000000$  and  $K_p = 10000$  set in the proportional controller in EFR-A4, respectively. It is clear from the simulation results (Fig. 2.39 and Fig. 2.42), implementing proportional controller in the EFR-A4 the rate of EFR power delivery is relatively reduced based on the SOC error, without causing a BESS availability penalty in EFR service operation (Fig. 2.41 and Fig. 2.43), as similar in EFR-A1 (Fig. 2.40). The higher  $K_p$  value set in EFR-A4, the high EFR power delivery, as seen from the simulation results (Fig. 2.39 and Fig. 2.42). This is an effective way of reducing the peak C-rates because there is no requirement to have full power changes as seen in EFR-A1 (Fig. 2.39); additionally, a high speed of change to return to the SOC band (45-55%) is also not essential. Operating the BESS over long periods of time with lower C-rates will increase the life-time of the system and as shown, with no performance penalty on EFR service operation (Fig. 2.41 and Fig. 2.43). This will be discussed further in Chapter 5. As seen from Table 2.23 and Table 2.24 comparing the output energy findings of the EFR-A1 and EFR-A4 with setting the required  $K_p$  gain values, it can be seen that the amount of charge/discharge energy or import/export energy output can be reduced by implementing the proportional controller into the standard EFR-A1; however this may cause additional efficiency losses on the BESS system (Table 2.23 and Table 2.24).

Fig. 2.44, Fig. 2.46 and Fig. 2.48 show the simulation results of the EFR-A1 and EFR-A4 with the proportional gain set value of  $K_p = 10000$  and  $K_p = 1000000$  for the whole day of 1<sup>st</sup> January 2018, respectively. It is clear that the EFR-A4 having different proportional gain values set in the proportional controller does not cause a reduction in the BESS availability (Fig. 2.47 and Fig. 2.49) as similar as in EFR-A1 (Fig. 2.45); however it may cause energy losses on the system as shown in Table 2.24. It is observed that the lower  $K_p$  set in the proportional controller, the lower EFR output power (see Table 2.24).

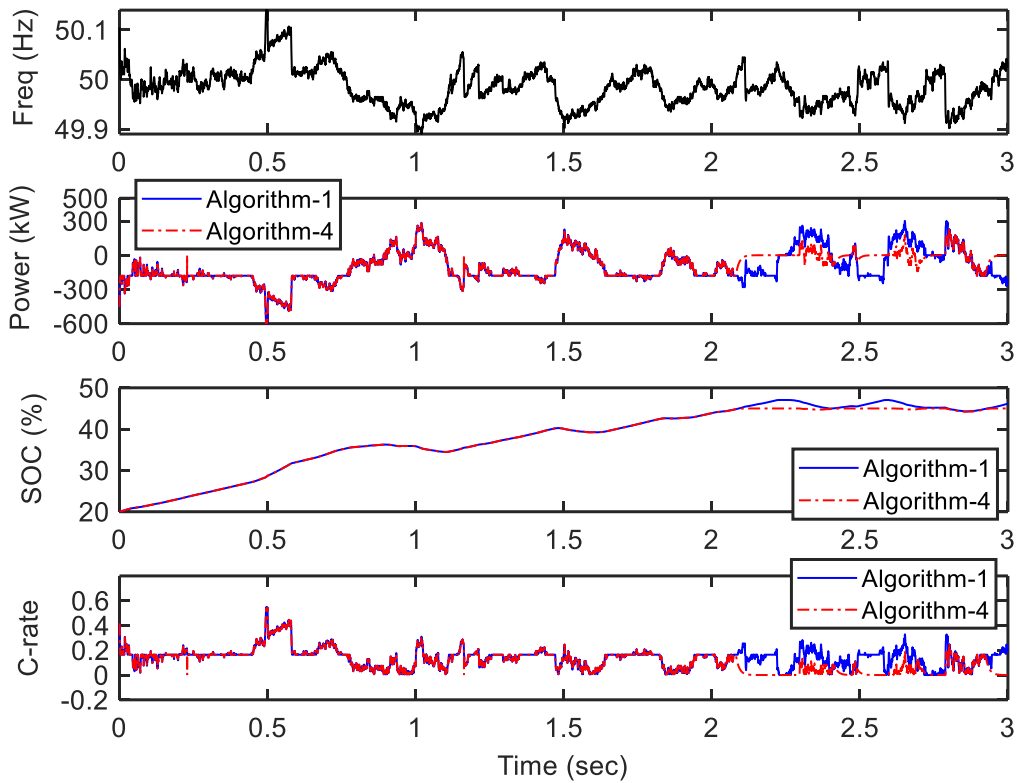


Fig. 2.39 Comparison of simulation results of EFR-A1 and EFR-A4 with  $K_p = 1000000$  for 1<sup>st</sup> January 2018 (first 3 hours) frequency data.

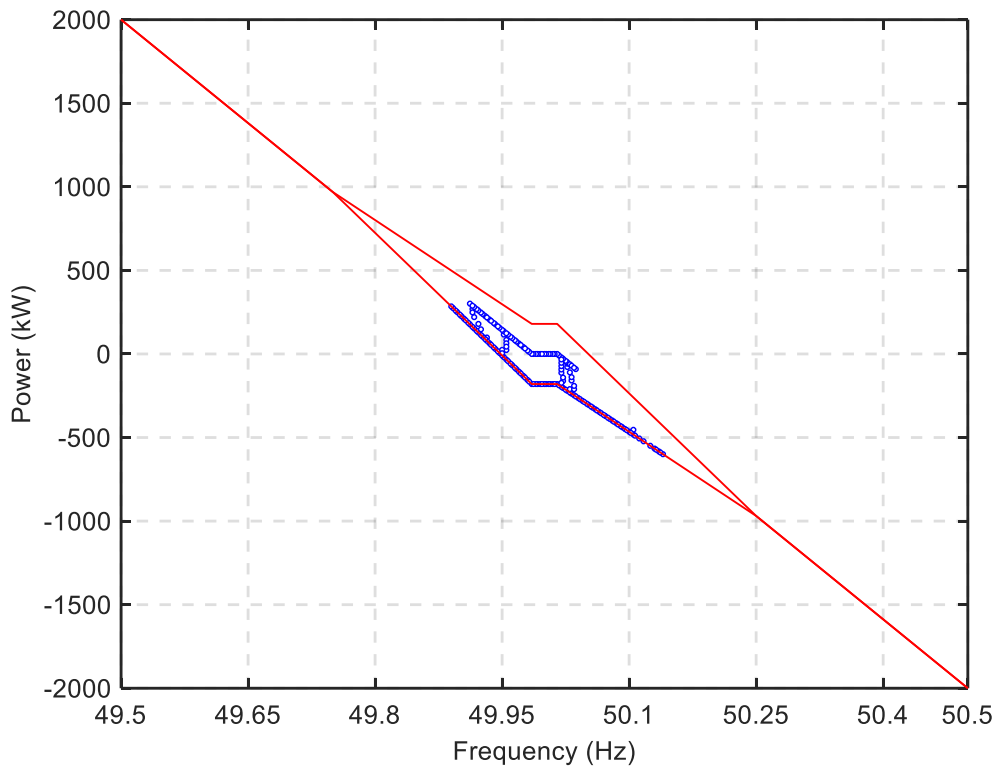


Fig. 2.40 EFR power versus frequency response of EFR-A1 for 1<sup>st</sup> January 2018 (first 3 hours) frequency data.

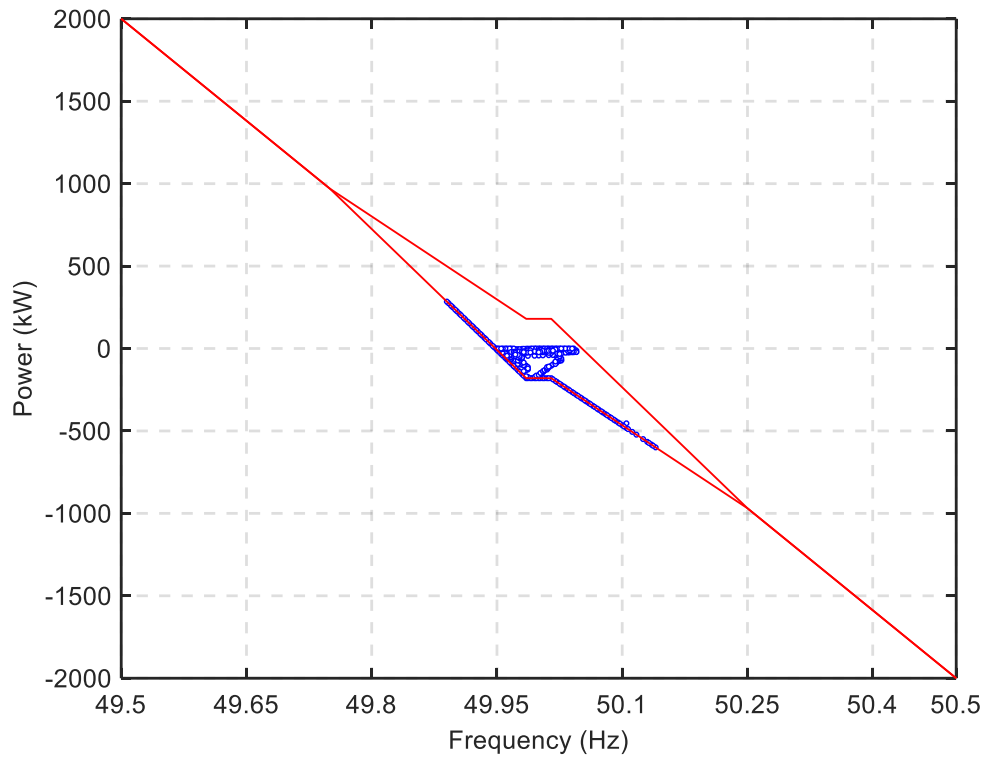


Fig. 2.41 EFR power versus frequency response of EFR-A4 with  $K_p = 1000000$  for 1<sup>st</sup> January 2018 (first 3 hours) frequency data.

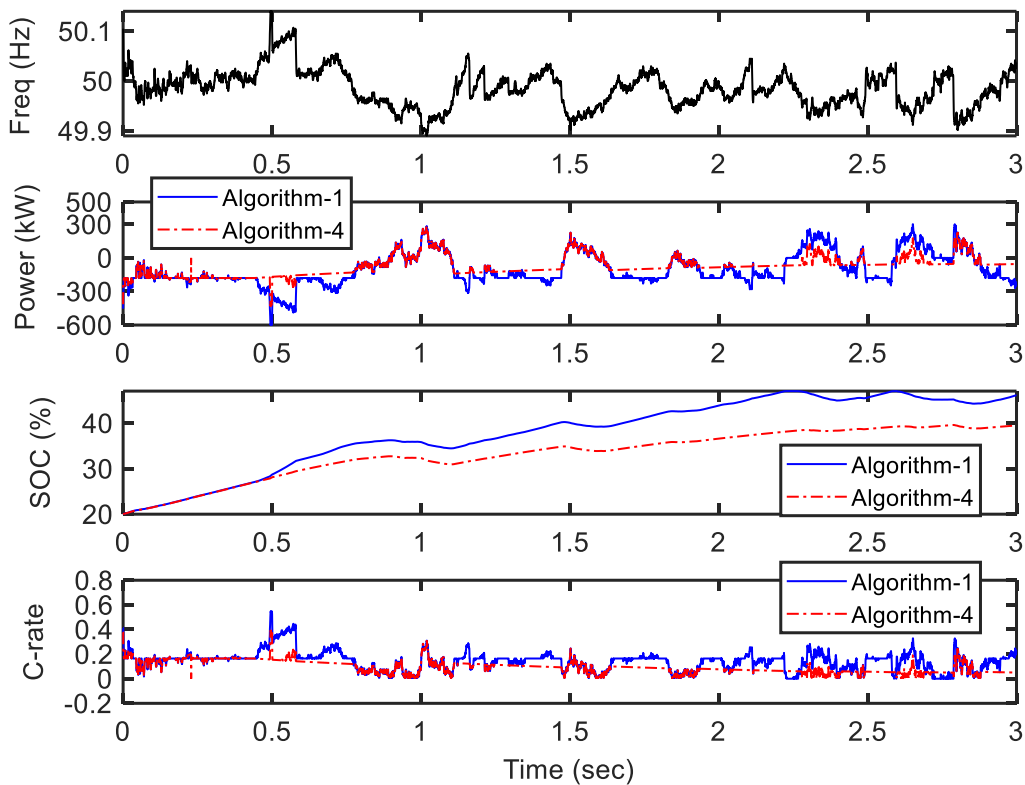


Fig. 2.42 Comparison of simulation results of EFR-A1 and EFR-A4 with  $K_p = 10000$  for 1<sup>st</sup> January 2018 (first 3 hours) frequency data.

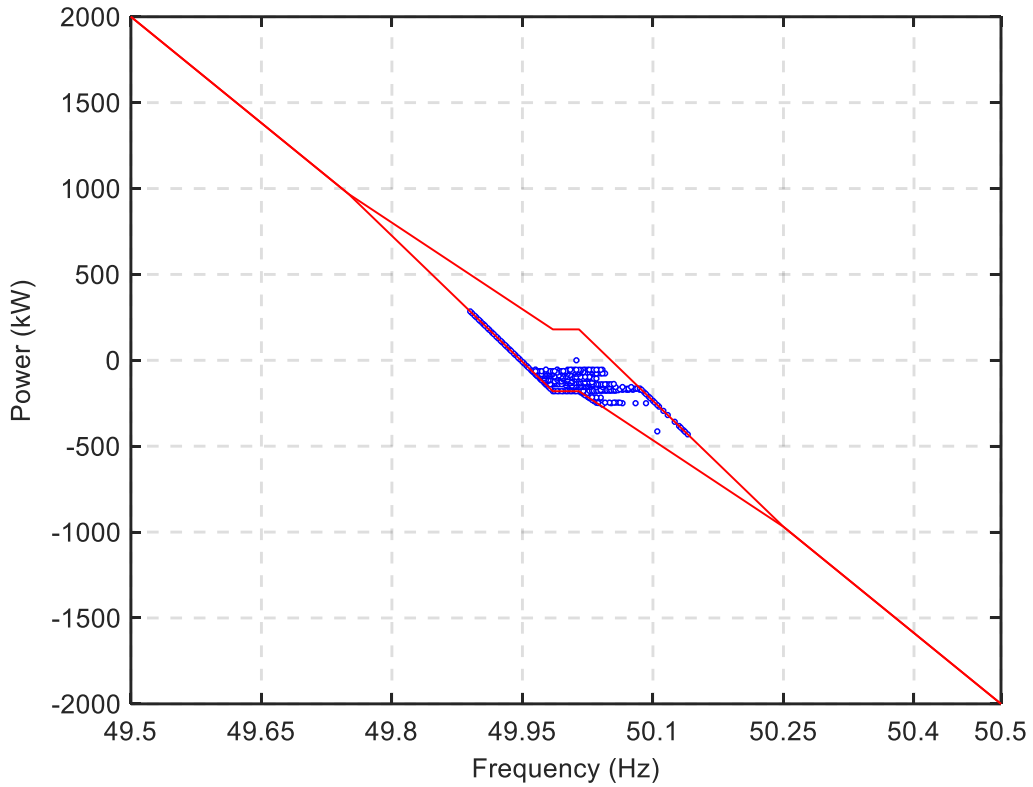


Fig. 2.43 EFR power versus frequency response of EFR-A4 with  $K_p = 10000$  for 1<sup>st</sup> January 2018 (first 3 hours) frequency data.

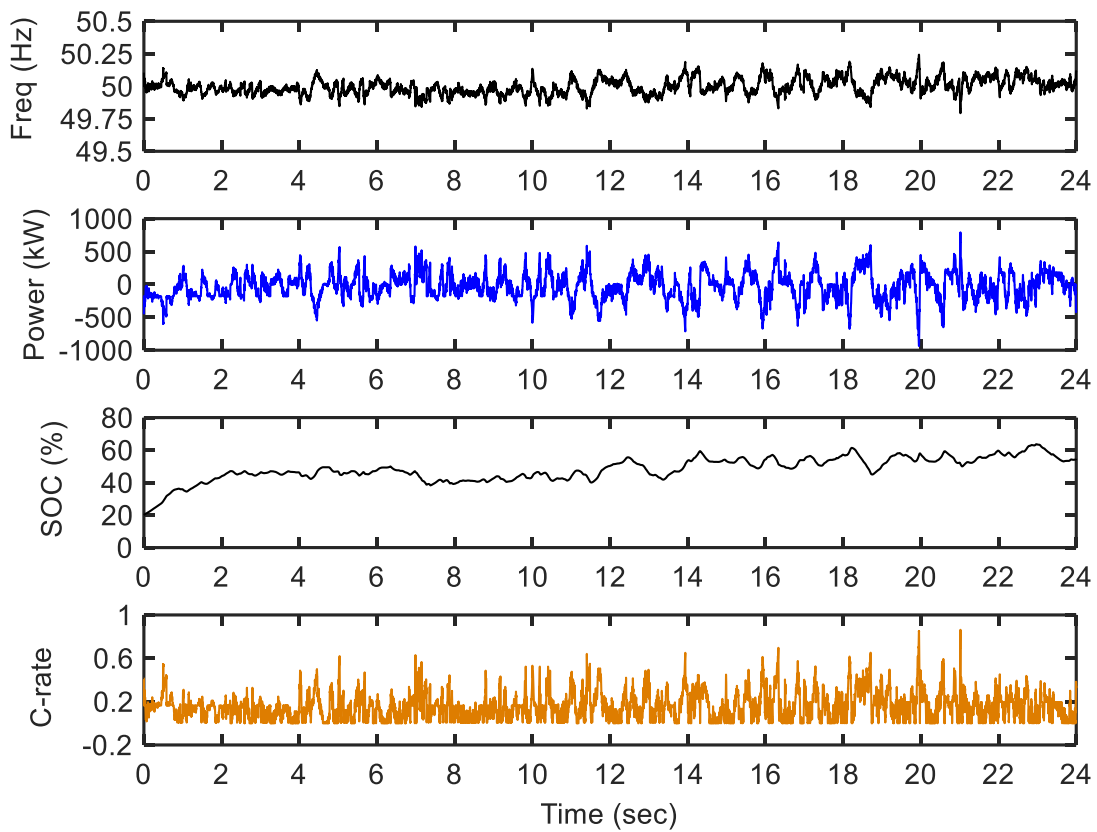


Fig. 2.44 Simulation results of EFR-A1 for 1<sup>st</sup> January 2018 frequency data.



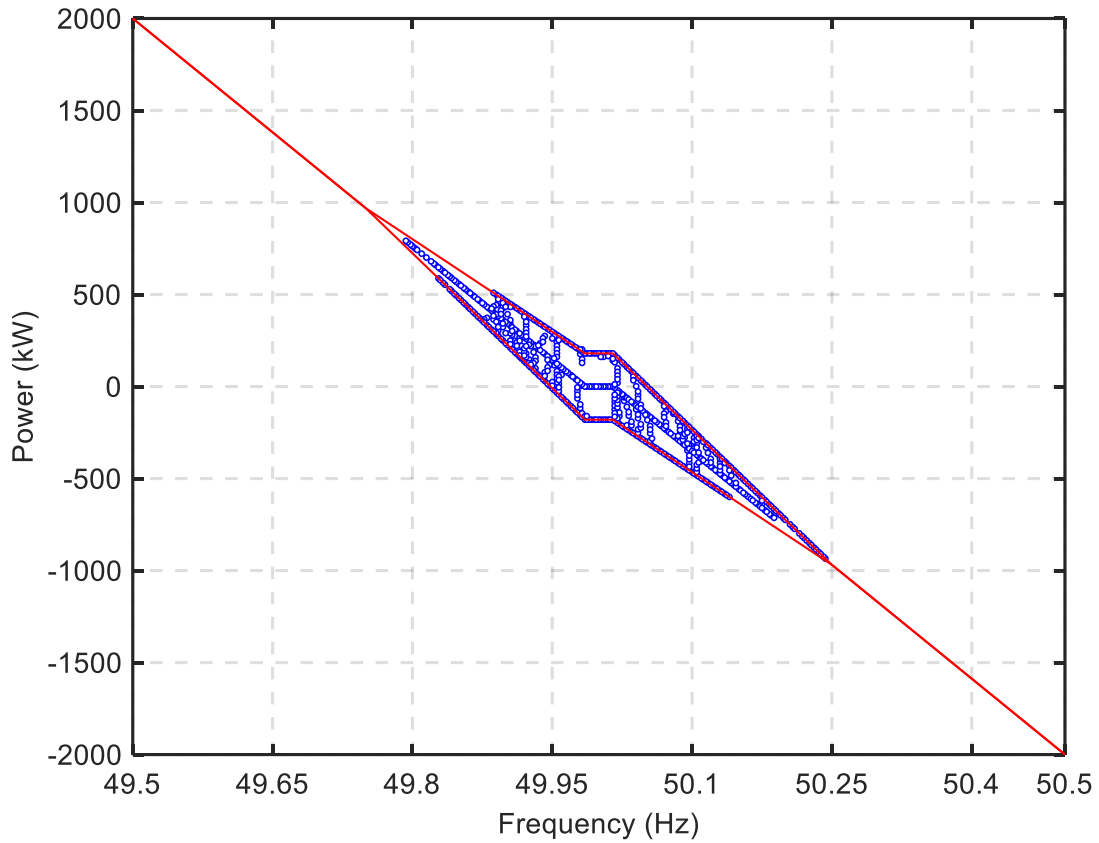


Fig. 2.45 EFR power versus frequency response of EFR-A1 for 1<sup>st</sup> January 2018.

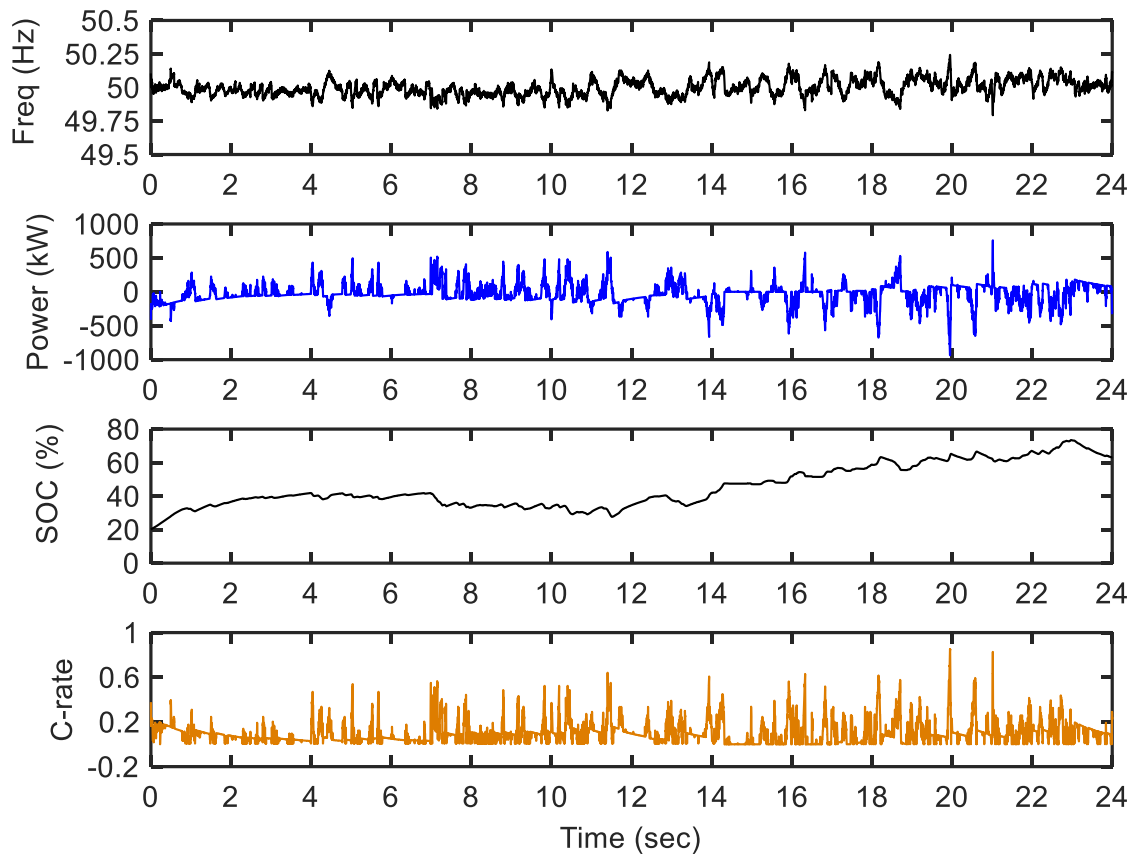


Fig. 2.46 Simulation results of EFR-A4 with  $K_p = 10000$  for 1<sup>st</sup> January 2018.

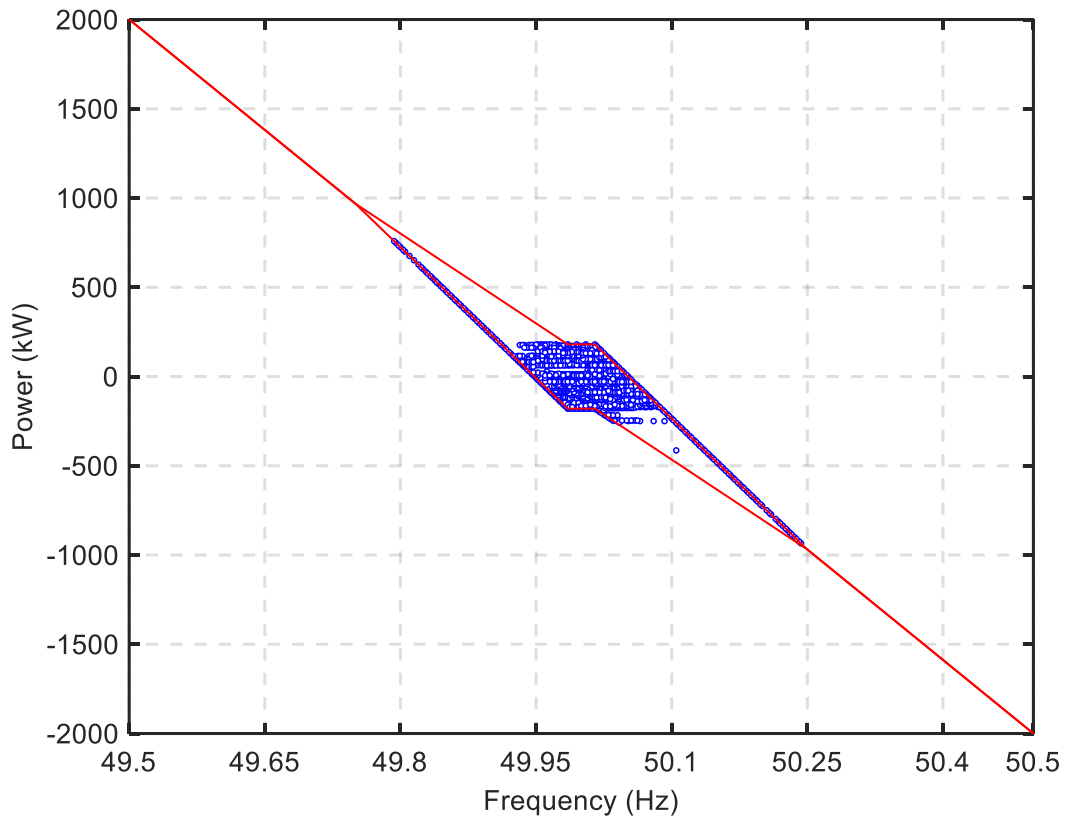


Fig. 2.47 EFR power versus frequency response of EFR-A4 with  $K_p = 10000$  for 1<sup>st</sup> January 2018 frequency data.

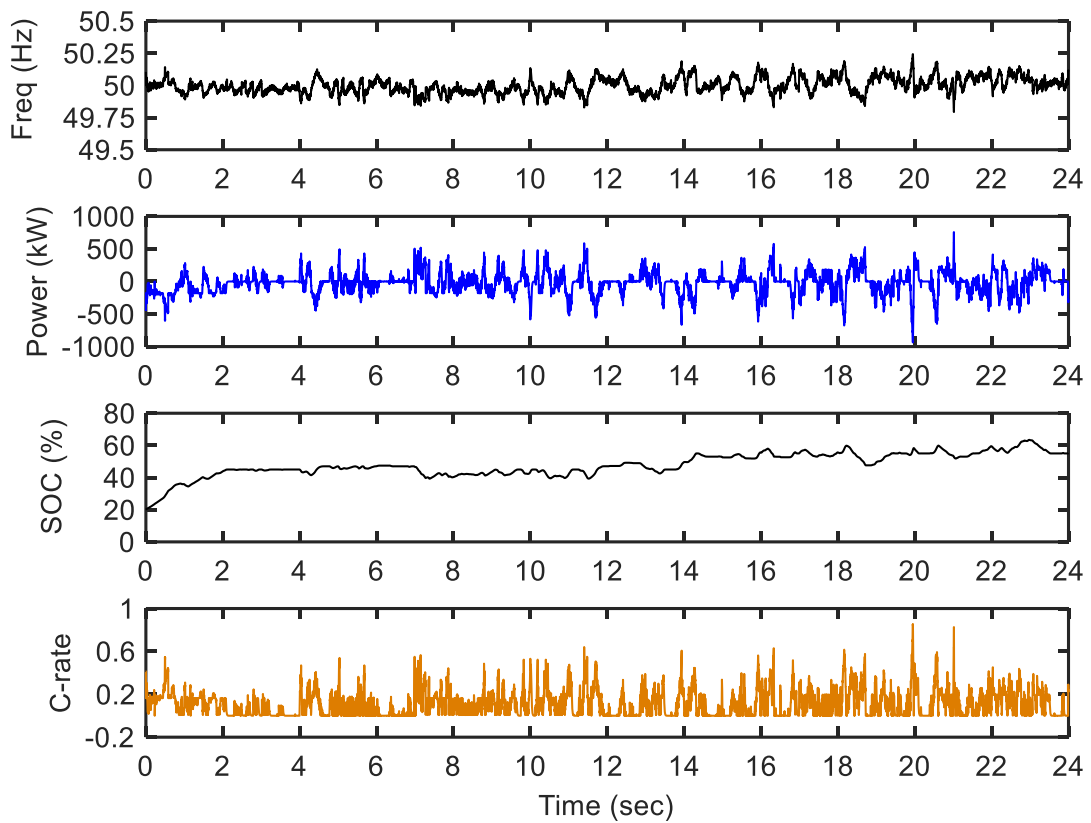


Fig. 2.48 Simulation results of EFR-A4 with  $K_p = 1000000$  for 1<sup>st</sup> January 2018.

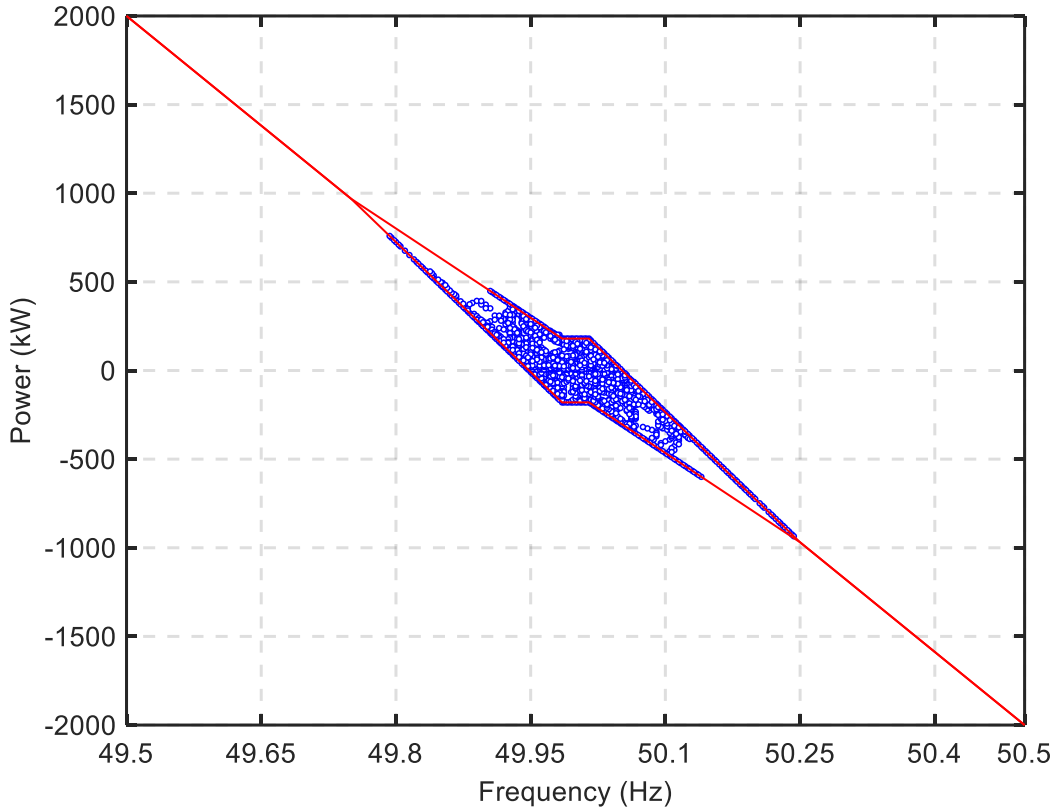


Fig. 2.49 EFR power versus frequency response of EFR-A4 with  $Kp = 1000000$  for 1<sup>st</sup> January 2018 frequency data.

#### 2.4.9 Analyses of Simulation Results of the all EFR Control Algorithms

In all EFR control algorithms (EFR-A1, EFR-A2, EFR-A3, EFR-A4) presented in this thesis, it is possible to define two aims for power flow in/out of the battery; the first is defined as charging and discharging the battery i.e. power is requested in either direction for the sole purpose of battery SOC management; the second is import and export which defines when the BESS is performing a mandatory response to a grid frequency event. The energy calculation of the BESS is given in (2.5) and (2.6) [CHO17].

$$\text{Discharge/Export: } P > 0 \rightarrow \frac{dE}{dt} = -\frac{P}{\eta_D} \quad (2.5)$$

$$\text{Charge/Import: } P < 0 \rightarrow \frac{dE}{dt} = -P \cdot \eta_C \quad (2.6)$$

where  $P$ ,  $E$ ,  $\eta_D$  and  $\eta_C$  represent the power exchanges by the BESS, present stored energy, and battery discharging and charging efficiencies, respectively.

The energy management findings of the standard (EFR-A1) and advanced control (EFR-A2 and EFR-A3) are summarised in Table 2.22. It is clear that, by implementing the extended 15-minute grid frequency event control in EFR-A2 and EFR-A3, the availability of the battery is increased from 98% to 100% (SPM). As desired, the battery's SOC has been shown in the simulation results to converge on the selected band of 45-55% in all of the EFR algorithms.

Table 2.22 Energy output findings of the three EFR control algorithms for 21<sup>st</sup> October 2015. Initial SOC=50%

<b>Algorithm</b>	<b>Min SOC (%)</b>	<b>Max SOC (%)</b>	<b>SPM</b>	<b>Battery Charging Energy (kWh)</b>	<b>Battery Discharging Energy (kWh)</b>	<b>Battery Import Energy (kWh)</b>	<b>Battery Export Energy (kWh)</b>	<b>Total Energy (kWh)</b>
<b>EFR-A1</b>	0	57.96	0.98	160.6	83.33	1744	1470	3458
<b>EFR-A2</b>	30.67	57.8	1	63.48	71.2	1225	950.5	2310
<b>EFR-A3</b>	32.3	57.93	1	136.2	102	1185	957	2381

Table 2.23 Energy output findings of EFR control algorithms for 1<sup>st</sup> January 2018 (first 3 hours) frequency data. Initial SOC=20%

<b>Control Algorithm</b>	<b>Kp</b>	<b>Charging (kWh)</b>	<b>Discharging (kWh)</b>	<b>Import (kWh)</b>	<b>Export (kWh)</b>	<b>Total Energy (kWh)</b>
<b>EFR-A1</b>	-	164.2	0	209.4	72.44	446.04
<b>EFR-A2</b>	-	144.9	0	191.9	35.8	372.6
<b>EFR-A3</b>	-	167.1	0	179.2	40.78	387.08
<b>EFR-A4</b>	2000	42.8	0	70.33	40.95	154.08
	5000	84.77	0	113.1	57.09	254.96
	10000	119.9	0	142.7	40.73	303.33
	50000	135.6	0	180.3	40.73	356.63
	100000	138.3	0	181.4	40.73	360.43
	1000000	139.7	0	183.2	40.73	363.63

In EFR-A3, the SOC converges faster towards the desired band and it is predicted that this will minimise SOC excursions towards the limits. However, compared to EFR-A2, this is at the expense of using more energy, solely for SOC management (charge/discharge) within the DB. This is important as energy used outside of the DB (import/export) can be classified as Applicable Balancing Services Volume (ABSVD) and it is possible for this to be excluded by the energy storage provider i.e. zero cost. It should be noted that the difference in import/export energy observed between EFR-A2 and EFR-A3 is because of the variation in SOC and so the BESS will not follow the same selection of EFR envelopes.

Table 2.24 Energy output findings of EFR-A1 and EFR-A4 for whole 1<sup>st</sup> January 2018 frequency data. Initial SOC=20%

Control Algorithm	Kp	Charging (kWh)	Discharging (kWh)	Import (kWh)	Export (kWh)	Total Energy (kWh)
<b>EFR-A1</b>	-	354.7	147.3	1902	1423	3827
<b>EFR-A2</b>	-	249.4	106.7	1373	944.7	2673.8
<b>EFR-A3</b>	-	387.1	128.3	1316	979.5	2810.9
<b>EFR-A4</b>	2000	166.4	11.19	1225	705.8	2108.39
	5000	229.9	54.82	1310	779.6	2374.32
	10000	268	96.45	1338	850	2552.45
	50000	300.8	139.9	1376	936.4	2753.1
	100000	297.6	133.4	1388	953	2772
	1000000	271	125.1	1417	964.1	2777.2

## 2.5 Conclusion

In this chapter, firstly, a dynamic (DFFR) and a static high (SFFR<sub>high</sub>) and low (SFFR<sub>low</sub>) firm frequency response control algorithm based on a model of a 1MW/1MWh BESS has been developed to meet the NGET published service requirements. When there is a grid frequency deviation, the BESS supplies a dynamic power according to a specified DFFR envelope. SFFR delivers a non-dynamic service where an agreed amount of power is delivered if the grid frequency reaches a certain trigger point of 49.7Hz (SFFR<sub>low</sub>) or 50.3Hz (SFFR<sub>high</sub>). Simulation results of the proposed FFR algorithms were carried out using NGET frequency data for 11 November 2015

(3-hour period), which contains both lower and under frequency events. The results based on an experimentally validated model by the WESS demonstrated that the proposed DFFR control algorithm provides 0.5% and 3% of MAPE SOC and power error for 12 Oct 2016, respectively.

Secondly, the NGET published a Pre-EFR specification in 2015 before finalising the EFR service requirements. Therefore, using the pre-published EFR specifications, a Pre-EFR frequency response control algorithm based on a model of a 2MW/1MWh BESS has been developed. When there is a frequency change on the power grid, the BESS provides a power response according to the specified Pre-EFR frequency response envelope. Simulations of the control algorithms were carried out using NGET real frequency data for February 2014, which is a critical winter month in terms of under/lower frequency events. It was shown that, the proposed model without any control strategy cannot meet the NGET required battery import/export SPM rate of greater than 95% for each allowable DB. In order to increase battery SPM, hence availability, a new battery SOC management strategy and a battery charge/discharge management method has been implemented in the developed frequency response control algorithm. According to the proposed strategies, the best SOC band target is 50-60% with 60kW and 350kW battery charge/discharge powers for a DB range of 0.1Hz and 0.05Hz, respectively. The simulation findings demonstrate that the proposed control algorithms implemented in the BESS model meet the UK's NGET frequency response specification and successfully manage the SOC by converging towards a defined target range of 50-60% and also achieve battery SPM requirement (>95), causing no penalties for the battery provider.

After the Pre-EFR specifications published in 2015, the NGET prepared a final EFR specification to facilitate a tender competition between potential energy storage providers in late 2016. Using the final NGET required EFR specifications, four EFR control algorithms, based on the model of a 2 MW/ 1 MWh BESS, have been developed to respond to changes in the grid's frequency with a proportionate active power output. Simulation results demonstrated that all four algorithms met the UK's NGET EFR requirements, whilst managing the battery's SOC by converging towards a desired band of 45-55%. It was shown that, for the historical dataset considered, the standard EFR algorithm, EFR-A1, would not be able to manage the extended 15-minute grid frequency events, thus, causing the battery's SOC to drop to 0%, which would incur a service performance penalty charge. The advanced control algorithm, EFR-A2, has demonstrated that in order to increase the availability of the BESS, it is necessary to stop any EFR activity after an extended 15-minute frequency event, as allowed by the EFR

specifications. The third control algorithm, EFR-A3, was shown to have a better performance in terms of SOC management by using the 30-minute rest periods in between frequency events as a window of opportunity to manage the SOC towards the desired band of 45-55%. However, there was a small increase in the net energy consumed. The results were validated experimentally on a 2MW / 1MWh BESS with some small variances accounted for. The last control algorithm, EFR-A4, extended by implementing a proportional controller into the standard EFR control design in order to reduce the output power delivery based on the proportion to the difference in battery SOC (SOC error) without hitting a reduction in BESS availability; this helps to reduce battery degradation rate through lower peak C-rates and hence extend its lifetime. The comparison of experimental and model findings indicates that the proposed EFR control algorithm (EFR-A1) provides <4.5% and ~0.3% of MAPE power and battery SOC for the 12-hour period in 21st Oct 2015.

### **3 BESS Control for Grid Scale Energy Storage Applications through Frequency Response Services**

This chapter investigates taking advantage of a combination of UK grid frequency response services, described in Chapter 3 of this thesis, with triad avoidance and energy arbitrage applications. This chapter first examines using the BESS in order to maximize triad avoidance benefit revenues by layering UK grid frequency response services. This chapter demonstrates that triad avoidance is always profitable at certain times of triad days during winter season. In the second section of this chapter, using historical UK electricity prices, a new balancing service scheduling approach has also been developed to maximize energy arbitrage revenue (AR) by layering different types of grid balancing services throughout the day. Simulation results show that the proposed algorithm delivers both dynamic and non-dynamic FFR services and also EFR service to NGET specifications whilst generating AR as well as service availability payments in the balancing market. A comparative study is also presented to compare the yearly AR obtained from the work presented in this chapter and a previous reference study.

#### **3.1 Introduction**

Global electricity demand is forecasted to increase by 3.1% annually from 2010 to 2050 [GUN17], [WAN16]. The UK electricity consumption in 2015 was 303 TWh [ONL18a]. BESSs can provide a wide spectrum of applications ranging from short term power quality support (e.g. frequency regulation, voltage support) to long term energy management (e.g. energy arbitrage, peak shaving, Triad Avoidance). The capital cost of battery storage technologies is continuing to fall, thus prompting a new study of its applications and economic benefits [MER09]. This chapter investigates a grid-tied BESS for grid scale applications; including Triad Avoidance (Section 3.2) and energy arbitrage (Section 3.3).

The Triad charging system is an effective way that large industrial electricity users can reduce their energy charges by reducing electricity consumption over peak periods. It also provides an environmentally-friendly solution for fulfilling peak power demands. Meeting peak demands, especially during the winter months, is one of the major challenges facing the NG as system operator [ONL18u]. A key method of managing power demand is the use of the Triad charging



system, a tool that has been used since the early 1990s and which is aimed especially at large industrial and commercial electricity users such as railways and steelworks. More detail about Triad Avoidance is given in the Section 3.2 of this chapter.

This thesis does not cover a Triad prediction method, but according to *Cesena et al.* [CES15], Triads can be predicted and these predictions, known as ‘Triad warnings’, are either provided on a commercial basis by specialists or made in-house by electricity retailers. The reference study [CES15] developed an algorithm to predict Triad days. In literature, there are some more studies on Triad Avoidance [MUL14], [KEL10], [DIX04], [TUR03], [DIX99], [MUL16], [CES15], [GRE16]. *Marmaras et al.* [MAR17] presented a predictive model which aims to assist the manager of a commercial building to reduce electricity bills by forecasting the Triad peak dates and the energy demand of the building on those dates. In the model, a stochastic model was developed to forecast the triad days and hours for the following year. A sensitivity analysis was also performed to estimate the weather impact on the electricity demand of a building. A predicting model was finally performed using Artificial Neural Networks (ANN) to predict the energy demand of the building at the most probable triad day and half-hour. The model was evaluated using real building energy consumption and weather data from commercial buildings at a science park. It was demonstrated that the developed model successfully forecasted the dates of the two out of three Triad peaks of 2014-2015. The times of all three Triad peak were also forecasted successfully. It was shown that the triad peaks tend to occur between 16:30 and 18:30. The building managers can use this predicted information and adjust their energy demand profiles to reduce their cost with the power demand of the building during a real Triad peak being forecasted with 97.6% accuracy. It was demonstrated that the weather information plays an essential role in the accuracy of the building demand forecast [MAR17].

*Mullen et al.* [MUL14] developed a model of the cost of distribution network use-of-service charges (DUoS), transmission charges (Triad) and energy charges for half-hourly metered (HHM) customers. The model is applied to a case study of a building at Newcastle University in which the use of standby generation for Triad avoidance is compared against the existing costs. Considering its diesel fuel consumption cost, the net profit of using standby generation for triad avoidance was also presented in the study.

The potential for electric vehicles (EVs) to generate income from energy provided to a commercial building together with revenue generated from additional ancillary services in the

UK such as triad avoidance was presented in [GOU17]. The paper evaluates the economic viability of electric vehicles used for vehicle-to-grid (V2G) service for triad demand reduction. Three V2G scenarios are evaluated using half-hourly electricity demand for a commercial building. The results demonstrated that great amount of income can be generated from triad avoidance; and the analysis demonstrates that net income generation is strongly dependent to battery degradation costs associated with V2G cycling [GOU17].

[PIM17] deals with the potential of ES to reduce the electricity bills of large enterprises, focusing on the University of Lancaster (UoL) as a case study. Through the analysis of the UoL recent generation and demand data (2013-14 and 2015-16), and present and future charges, it was demonstrated that in 2015 the UoL expected energy storage to provide annual savings of £27 per kWh of storage capacity by reducing network charges.

First part of this chapter (section 4.2) deals with take advantage of a combination of EFR and FFR service with triad avoidance. Therefore, a new effective triad strategy layering grid frequency response service is developed to increase battery storage availability in order to maximize triad revenues. In this chapter, a Triad Avoidance approach through EFR service is developed using the advanced EFR control algorithms, EFR-A2 and EFR-A3, described in Chapter 3. It was clearly explained in Chapter 3 that, the EFR-A2 addresses the EFR service design with an extended 15-minute frequency event control, in order to optimise the use of the available stored energy; and the EFR-A3 also extends the EFR control algorithm to include a dynamic SOC target to maximise the energy stored on real/predicted triad days. This chapter introduces a strategy to generate additional revenues from ancillary services such as triad avoidance only available during the winter season. The performance of the EFR service delivery through Triad Avoidance Benefit (TAB) is quantified. All in all, this chapter considers layering the new advanced UK grid frequency balancing service, EFR, with triad avoidance in order to maximise the system's availability and profitability. The chapter 3 presented the EFR control methodologies with their simulation results; and this chapter extends to show how this can be used to maximise profits from other services such as triad avoidance.

The other part of this chapter (Section 3.3) investigates a grid-tied BESS operating in energy arbitrage application through the grid frequency response services. The electricity price tends to follow a daily pattern of a low price during off-peak night time hours and a high price during on-peak day-time hours. If the BESS stores energy at off-peak times with the lower price and then resells at on-peak times at a higher price, it can make profit from the price difference, this

is referred to as arbitrage [GUN17]. The emergence of wholesale electricity markets in the UK, together with significant increases in prices, and price volatility of electricity have raised the interest in potential economic opportunities for electrical energy storage [SIO09]. One of the main profit streams for ES is temporal arbitrage opportunity obtained by price volatility in the wholesale market. Energy arbitrage refers to the participation of ES in the day-ahead energy market; and it involves utilizing ES to benefit from electricity price fluctuations by charging during low-price periods, discharging during high-price periods, and profiting from the price differential [TEN17], [DUR14]. ES can also generate revenue through the delivery of ancillary services such as grid frequency regulation [XIN17].

In literature, there are many papers relating to the energy arbitrage application [AMP17], [BAR12], [GIL13], [KHA15], [DUN16a], [DUN16b]. *Sioshansi et al.* [SIO09] presented one of the leading studies on energy arbitrage that analyses four key aspects of the economic value of electricity storage in the Pennsylvania-New Jersey-Maryland (PJM) markets: -The basic relationship among storage energy capacity, storage efficiency and the arbitrage value of ES; - The accuracy of theoretical ES dispatch and the value of arbitrage using perfect foresight of future electricity prices; -The temporal and regional variation in the value of energy arbitrage, investigating natural gas price variations, transmission constraints and fuel mixes on energy storage economics. The impact of larger storage devices, investigating how the use of ES can decrease on-peak hourly prices and increase off-peak hourly prices diminishing the value of arbitrage, while producing welfare effects for generators and consumers.

In [ANW16], a Building-to-Grid (B2G) model was developed to evaluate energy arbitrage value of smart thermal ESS devices in residential buildings across Ireland. The paper [ORT14] presents an energy arbitrage scheduling algorithm for EVs under a real time pricing scheme with uncertainty and evaluates also the battery degradation. The authors in [ADE16] investigate arbitrage operation of an ES facility in Alberta electricity market.

The reference study [WAN17] deals with the optimal scheduling of ES in a distribution network with a substantial PV penetration. The method used considers simultaneously the provision of regulation service, energy arbitrage, peak shaving and the minimisation of deviations from the forecast. Because part of the ES capacity is allocated for grid regulation services on the day ahead, only the remaining capacity can be used for peak shaving and other uses.

*Ampatzis et al.* [AMP17] investigate the application of robust optimisation for two functions of ES devices, including energy arbitrage and provision of flexibility. Both functions are examined against future income streams for batteries with their implementation being essential to their integration in the smart grid. The authors also explore the effectiveness of the robust optimisation model in summer and winter seasons, corresponding to different dynamic electricity retail price characteristics. In [BAR12], a generic heuristic optimisation of ESS was developed for provision of energy arbitrage on a spot market, this took the form of an ESS schedule based on a price signal and the characteristics of the ESS device. [GIL13] examines the optimal use of an ESS tied to wind farms in a curtailment scheme. The ESS is able to access two revenue streams, including reduction of generation curtailment and arbitrage on a spot market. The study extends the method developed in [BAR12] in order to achieve the optimal combination of these two modes and hence maximise the revenue to an ESS unit. The authors in [LUN09], [KHA15] provided different optimisation methods and the importance of electricity price forecast accuracy, however similarly, were based on historic market prices. [DUN16a] stated that more acute and more frequent price differentials would generate additional opportunities for arbitrage that could become a more profitable revenue stream in the future. *Grunewald et al.* [GRU11] presented an important analysis of this phenomenon for future UK systems, providing that 32 GW of wind capacity would enable the gross value of storage to include its capital costs and investment could be commercially viable through price arbitrage alone. [DUN16b] investigates the sensitivity of arbitrage revenue to changes in carbon price, gas price, capacity margin and wind power capacity in the UK market and the impact of these variables on the preferred ES device characteristics. [DEN09] presents a basic financial performance metric for the energy arbitrage-only scenario; however it does not cover the determination of the optimal storage value that would require co-optimization with grid ancillary services and other potential values. [ORT14] presents a scheduling algorithm for EVs under a real time electricity pricing scheme with uncertainty. The study considers the battery degradation cost not only when used to deliver services to the system but also in terms of the EV utilisation for mobility. It was demonstrated that the scheduling of the V2G services is sensitive to the price uncertainty and to the degradation costs derived from energy arbitrage.

In comparison with those previous studies, the focus of this chapter is related to not only energy arbitrage, but also the scheduling of grid balancing services such as frequency response for additional benefit. Chapter 3 of this thesis presented a DFFR control algorithm that enables BESSs to deliver dynamic power in response to deviation in the grid frequency. A SFFR<sub>high</sub>

and  $SFFR_{low}$  static frequency response control algorithm is demonstrated to deliver a non-dynamic power if the grid frequency reaches a certain high and low grid frequency. In this chapter, by using the historical electricity price profiles, a new grid balancing service scheduling method is developed to achieve maximum energy AR that can be generated from the grid balancing services by layering EFR, DFFR,  $SFFR_{high}$  and  $SFFR_{low}$  throughout the day. The proposed approach is not only providing AR but also generating further income through balancing service availability payments (SAPs); this maximizes the system's profitability and availability. In this chapter, the UK daily electricity price pattern has been forecasted by observing the real electricity price of several week/weekend days and also their grid frequency profiles, and then considering this pattern the service scheduling method has been improved with 18 different energy arbitrage scenarios by analysing various week/weekend days of each season of a year; this provides a robust and reliable sensitivity analysis of service layering technique for maximizing energy AR. This chapter also demonstrates that arbitrage strategies can be forecasted that do not incur losses whilst maximising profits in favourable seasons.

### **3.2 Triad Avoidance**

In the UK, the "Triad" refers to the three half-hours settlement periods with the highest system demand between the months of November and February, separated by at least ten clear days. The timing of these peaks is typically between 16:00 to 18:00. These three periods are not known in advance and therefore are determined from the measured data analysed in March of every year. HHM electricity customers in the UK pay charges proportional to their consumption during the Triad; this is called the Transmission Network Use of Service (TNUoS). The HHM customers can minimise their TNUoS charges by reducing their demand during Triad periods. Many commercial customers have an ES device or back-up generators to ensure the maintenance of critical supplies in case of a failure that can also be engaged to decrease Triad demand; this is known as 'Triad avoidance' [ONL181], [MUL14], [GOU17]. It is also possible for generating assets such as BESSs to export power to the grid during the Triad, this results in a payment from the electricity supplier known as the TAB. It is a complex task to predict the Triad periods in advance, however, many electricity suppliers offer Triad prediction services based on insufficient system margin (NISM) provided by NG and other factors such as the weather forecast. The NG does not predict the Triads and they are not known

in advance. Therefore, in order to avoid charges, HHM customers should avoid all potential peaks; this smooths the demand across the winter [ONL18u].

Triad is not a commercial service, however it does represent a benefit for substantial revenues from ESS. The mean energy demand within the three half-hours provide an important proportion of the annual network use charges imposed by the NG. By delivering energy during the Triad periods, ESS can make revenue by either absorbing the inverse of the charge directly or, if metered by an energy supply company, by decreasing the cost to the energy supply company and gaining an agreed proportion of the saving [GRE15].

The Triad peaks for each year are calculated after the end of February, utilizing system demand data for the half-hour settlement periods between November and February. The Triad calculation method provided by the NG [ONL18s] is described as following (see Fig. 3.1) using the 2014-2015 demand diagram:

Step 1: Calculate the half hourly system demand between November and February.

Step 2: From the data attained in Step 1, take the highest half hourly system demand. This settlement period is one of the three triad periods.

Step 3: Set aside 10 clear days on both sides of the settlement period attained in Step 2.

Step 4: From the rest of half hourly system demand data, take the highest half hourly system demand. This settlement period is one of the three triad periods.

Step 5: Set aside 10 clear days on both sides of the settlement period attained in Step 4.

Step 6: From the rest of half hourly system demand data, take the highest half hourly system demand. This settlement period is one of the three triad periods.

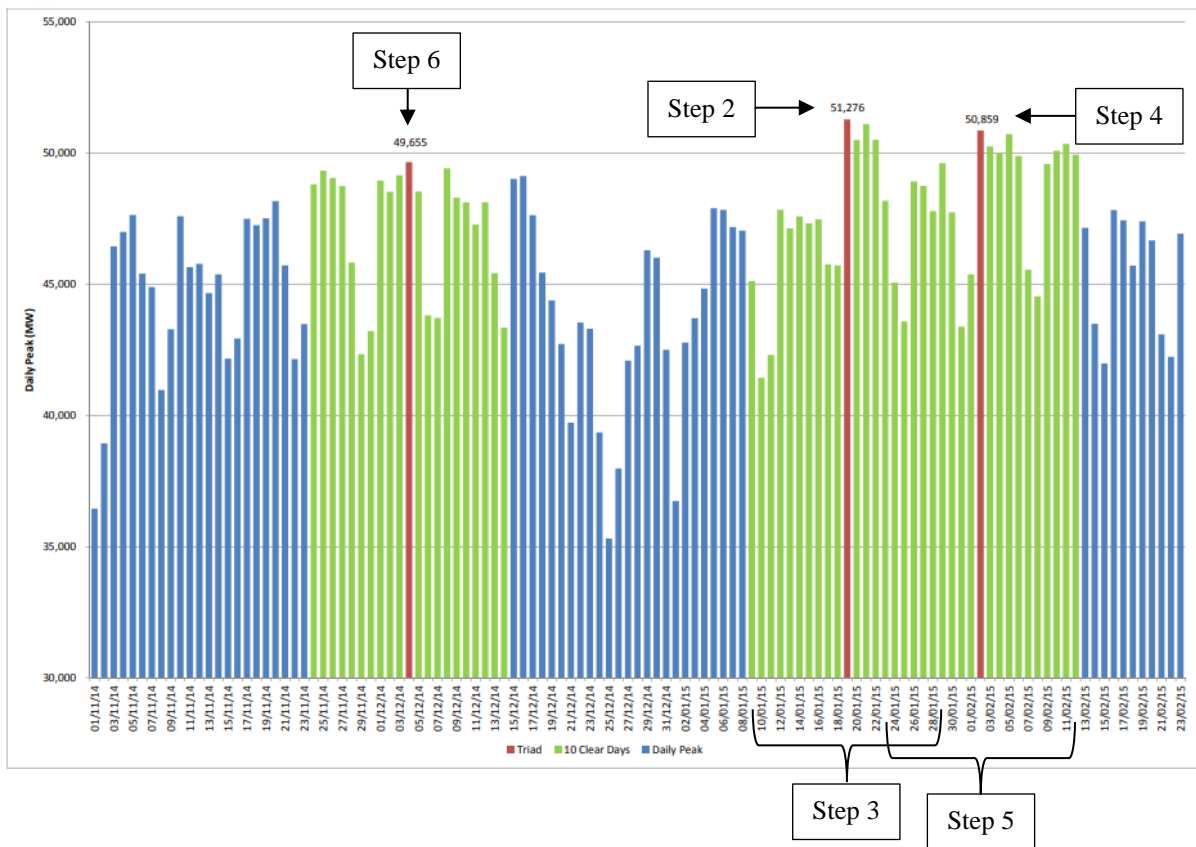


Fig. 3.1 Calculating of the Triads using 2014-2015 system demand data [ONL18s].

The triads only affect the consumers who have HHM which measure their demand on a half-hourly basis (normally medium/large commercial and industrial customers). If these customers do not consume electricity in the three Triad half-hours, they do not pay TNUoS charges for the whole financial year [ONL18s].

The triads are not known in advance, however, NG issues notice of inadequate system margin when the system is likely to be under stress owing to high energy demand and low generation. Furthermore, the suppliers may provide a Triad warning service to alert when there is likely to be a Triad period.

Triad management is a complex business. It does not only rely on having access to accurate prediction, but also on having a useful strategy to either reduce electricity consumption or switch to ES or on-site generation. This chapter considers scheduling a frequency support service (i.e EFR service in the UK) with Triad Avoidance in order to maximise the system's availability and profitability.

### 3.2.1 Triad Avoidance Strategy through EFR service

In this section, a new Triad Avoidance strategy through EFR service is developed in order to increase the BESS availability for maximizing Triad Avoidance benefit revenue. According to the proposed Triad Avoidance strategy, the EFR service control algorithm (EFR-A2 and EFR-A3), described in Chapter 3, is delivered from midnight, whilst managing the SOC of the battery to within a typical range of 45-55%. The control algorithm then switches (referring as SW in Table 3.1) the SOC target range to 90-95% on receiving Triad warnings to maximize the available energy for delivery. Between 16:00 and 19:00 real power is exported using a weighted profile based on the statistical likelihood that a Triad would occur in each half-hourly period, as shown in Table 3.1. It should be noted that if the BESS discharges to the grid by delivering constant power (Table 3.1) during the Triad period, the SOC of the battery may decrease sharply and hit to 0%; hence this may reduce the service performance or cause an unavailability of the BESS system. Therefore, in the proposed Triad Avoidance scheme, the real power (Table 3.1) is discharged as a proportion of the available battery SOC at the Triad period in order to avoid the unavailability of the BESS.

Table 3.1 Power profile used for Triad Avoidance

<b>Time (hr)</b>	<b>Service used for Triad</b>	<b>SOC band (%)</b>	<b>Power Delivery (kW)</b>
00:00 – SW	EFR	45-55	EFR
SW – 16:00	EFR	90-95	EFR
16:00 – 16:30	Discharge	-	200
16:30 – 17:30	Discharge	-	500
17:30 – 18:00	Discharge	-	300
18:00 – 18:30	Discharge	-	200
18:30 – 19:00	Discharge	-	100
19:00 – 00:00	EFR	45-55	EFR



### 3.2.2 Simulation Results of the Triad Avoidance Strategy

It is known that the real Triad days of 2014-2015 are the 4th December 2014, 19th January 2015, 2nd February 2015. In this section, both EFR-A2 and EFR-A3 are compared for TAB using the real-time frequency dataset for the 4th December 2014, 19th January 2015, 2nd February 2015 [ONL18d], [ONL18l], [ONL18r] and 20th December 2015 [ONL18l], [ONL18r], these represent the 2014-2015 year actual Triad days, and a high under-frequency day in 2015, respectively. This chapter considers that all the triad periods in 2014-15 were between 17:30 to 18:00. For the windows that would coincide with a Triad the earliest window time for 2014-2015 is 16:00.

Table 3.2 Starting battery SOC (%) for Triad period at 16:00

Real/ predicted Triad days in 2015	EFR Models used for Triad	Switch (SW) Mode to Triad Preparation at			
		10am	11am	12pm	1pm
4 <sup>th</sup> Dec 2014	EFR-A2	91.42	91.5	90.65	78.27
	EFR-A3	91.48	91.98	91.48	79.13
	<b>Recovery</b>	0.06	0.48	0.83	0.86
19 <sup>th</sup> Jan 2015	EFR-A2	90	84.84	72.06	64.54
	EFR-A3	92.43	86.48	73.61	66.07
	<b>Recovery</b>	<b>2.43</b>	<b>1.64</b>	<b>1.55</b>	<b>1.53</b>
2 <sup>nd</sup> Feb 2015	EFR-A2	99.83	99.83	99.7	98.55
	EFR-A3	99.26	99.26	99.24	97.89
	Recovery	0.57	0.57	0.46	0.66
20 <sup>th</sup> Dec 2015	EFR-A2	70.08	70.08	63.99	56.57
	EFR-A3	87.17	87.08	70.39	60.56
	<b>Recovery</b>	<b>17.09</b>	<b>17</b>	<b>6.4</b>	<b>3.99</b>

The analysis in this section considers varying the time that when the system mode is changed to prepare for triad, meaning that the SOC target is set to 90-95%, between 10:00 and 13:00. The simulation results show the SOC achieved by 16:00, with a higher SOC giving a maximum potential revenue through TAB. From Table 3.2 it can be seen that on 20th Dec 2015, preparing for Triad later than 12:00 is sub-optimal as seen in Fig. 3.4 and Fig. 3.5; a lower SOC is achieved at 1pm compared to earlier times as seen in Table 3.2, providing the SOC of 56.57% in EFR-A2 and 60.56% in EFR-A3. This is because it is a particular day which has a large period of under-frequency events, as seen in Fig. 3.4 and Fig. 3.5. Preparing for Triad at 10:00, there is a considerable improvement, and it can be seen that there are further gains to be made using EFR-A3 (87.17%) over EFR-A2 (70.08%), as shown in Fig. 3.2 and Fig. 3.3. It is revealed from the simulation results, preparing for Triad at 10am is optimal for 20<sup>th</sup> Dec 2015.

Table 3.2 shows that for the real triad day (4<sup>th</sup> Dec 2015), preparing Triad at 10am, 11am and 12pm is ideal and at these times the significantly high SOC is achieved (>90%) compared to the latest time of 1pm, providing the SOC of 78.27% in EFR-A2 and 79.13% in EFR-A2 at 10am, as seen in Fig. 3.6 and Fig. 3.7.

As seen from Table 3.2, for the real Triad day (19<sup>th</sup> Jan 2015), preparing for Triad at 13 pm is sub-optimal and the lowest SOC is achieved at 1pm providing the SOC of 64.54% in EFR-A2 and 66.07% in EFR-A3, compared to earlier times of 10 am, 11pm and 12pm. However, preparing for Triad at 10am, there is a significant recovery in the battery SOC, and it is revealed that there are further profits to be generate using EFR-A3 (92.43%) over EFR-A2 (90%), as shown in Fig. 3.8 and Fig. 3.9.

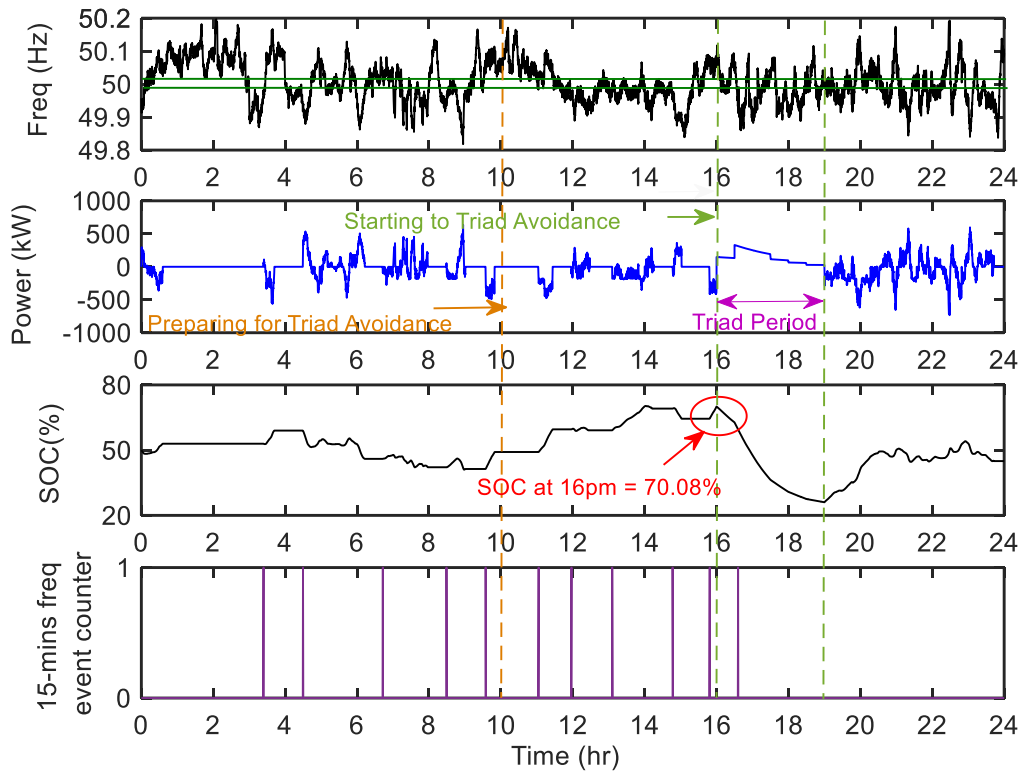


Fig. 3.2 Simulation results of Triad Avoidance strategy through EFR-A2 for 20<sup>th</sup> Dec 2015, switching mode to triad preparation at 10am.

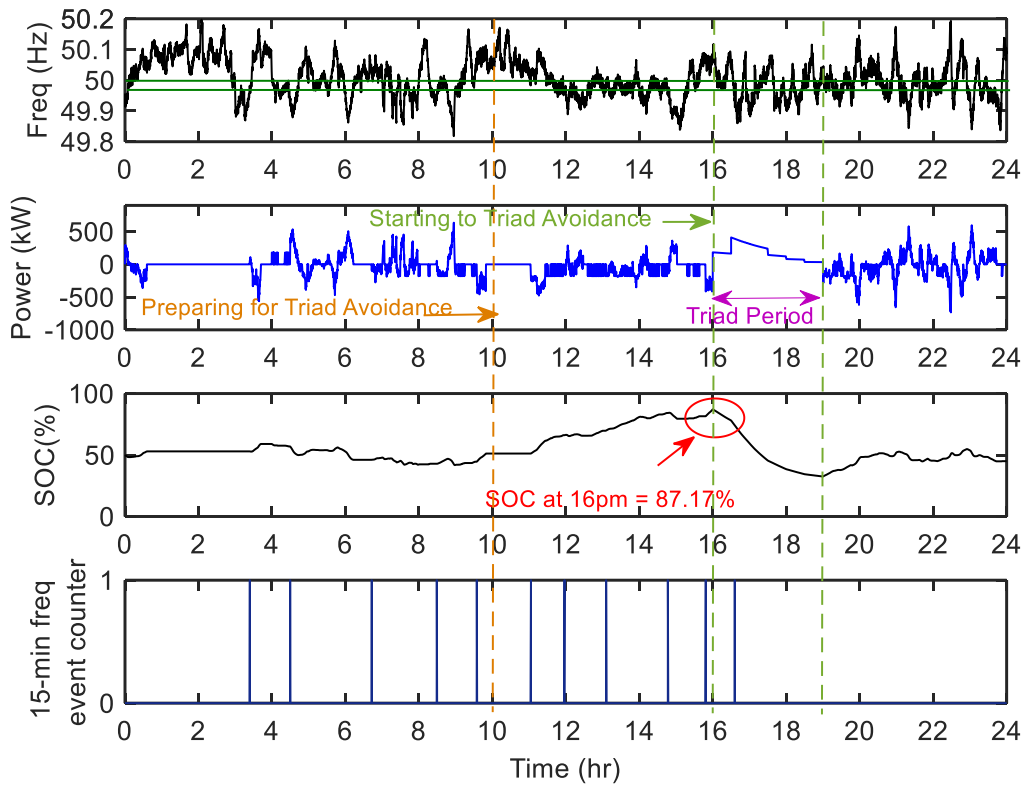


Fig. 3.3 Simulation results of Triad Avoidance strategy through EFR-A3 for 20<sup>th</sup> Dec 2015, switching mode to triad preparation at 10am.

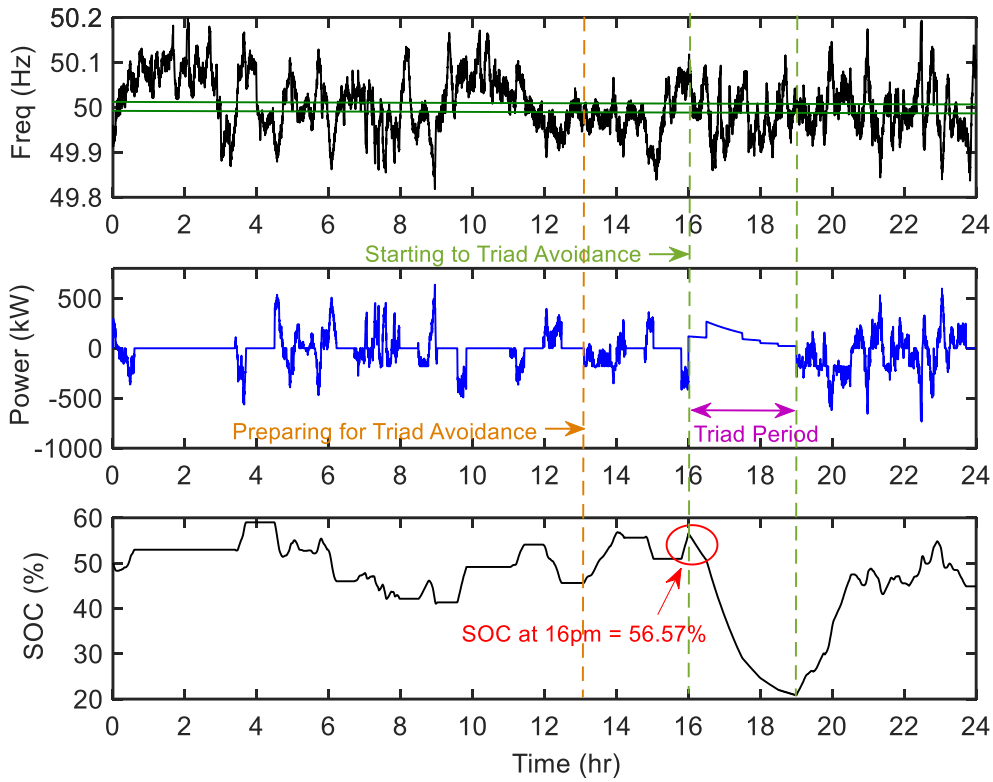


Fig. 3.4 Simulation results of Triad Avoidance strategy through EFR-A2 for 20<sup>th</sup> Dec 2015, switching mode to triad preparation at 1pm.

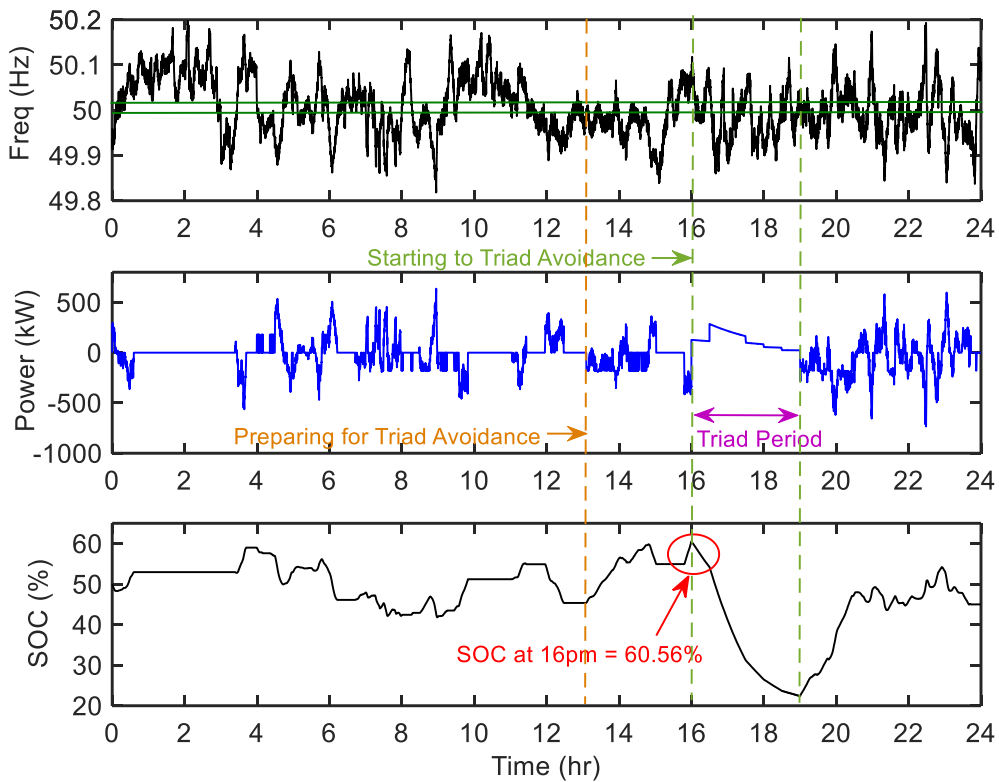


Fig. 3.5 Simulation results of Triad Avoidance strategy through EFR-A3 for 20<sup>th</sup> Dec 2015, switching mode to triad preparation at 1pm.

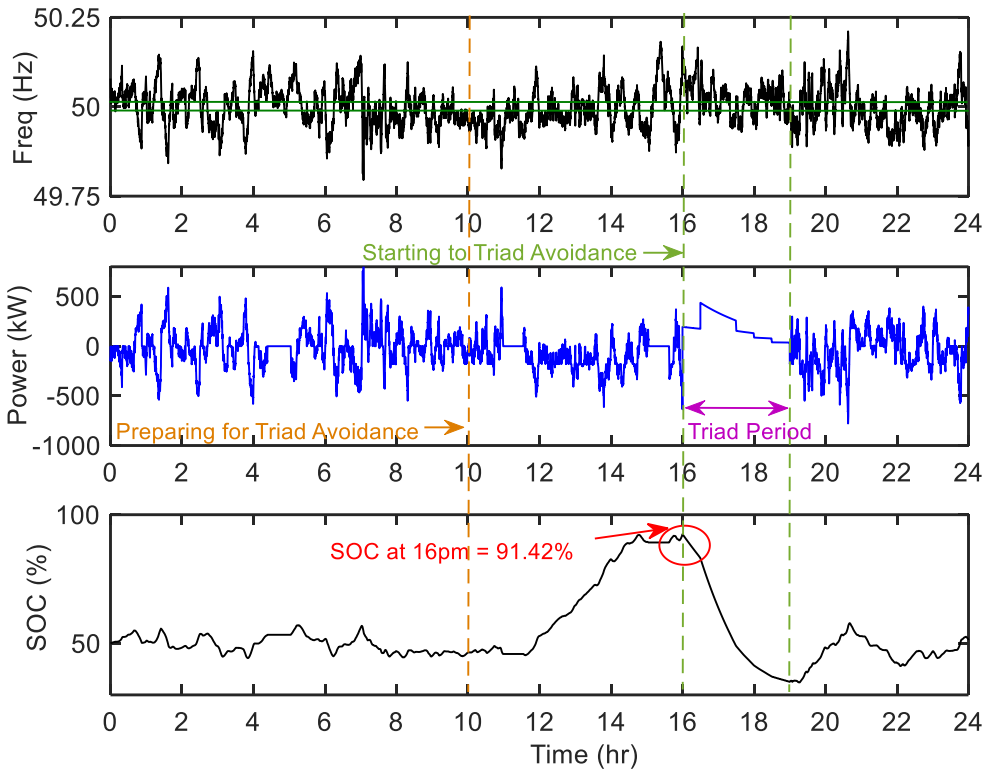


Fig. 3.6 Simulation results of Triad Avoidance strategy through EFR-A2 for 4<sup>th</sup> Dec 2015, switching mode to triad preparation at 10am.

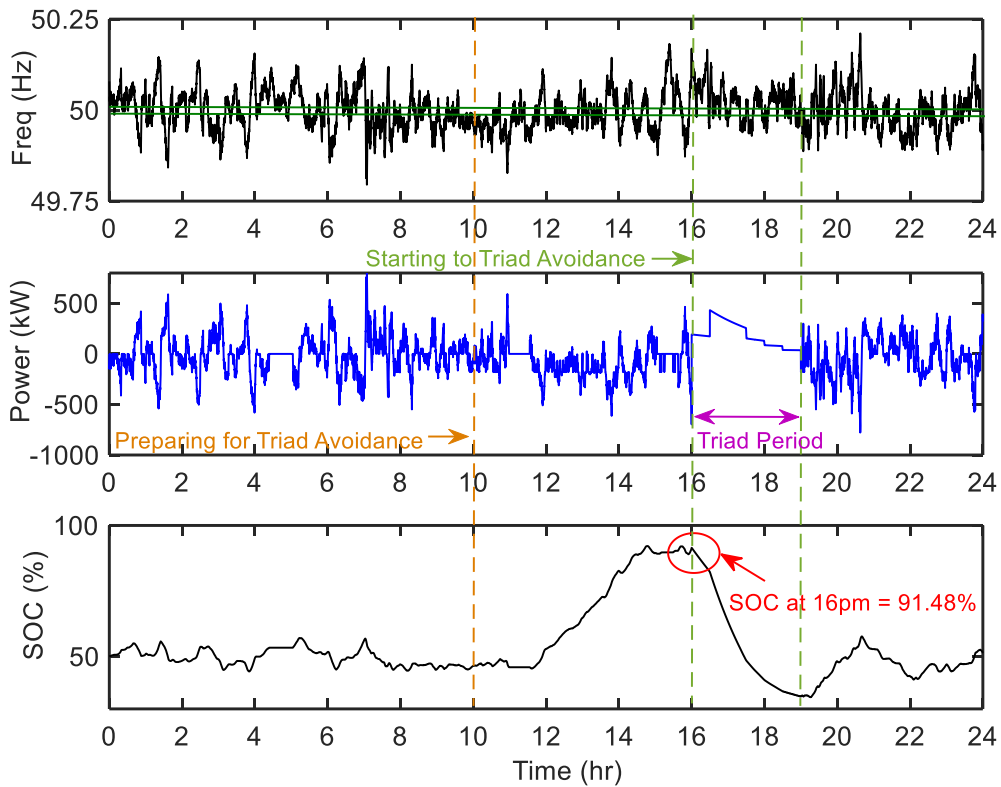


Fig. 3.7 Simulation results of Triad Avoidance strategy through EFR-A3 for 4<sup>th</sup> Dec 2015, switching mode to triad preparation at 10am.

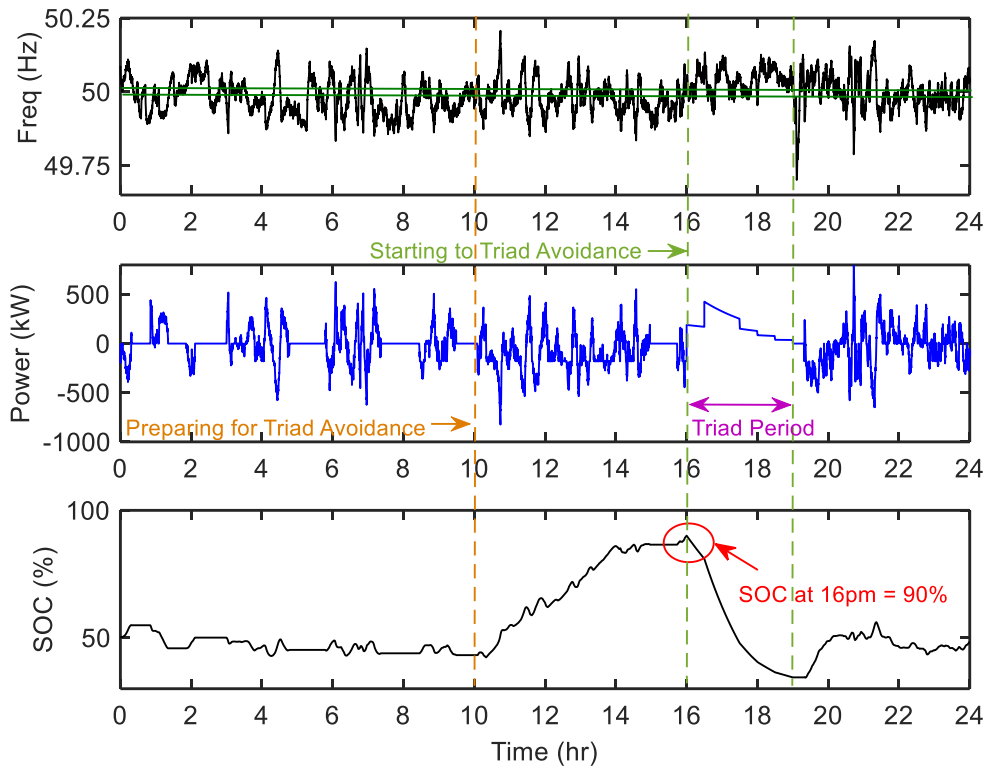


Fig. 3.8 Simulation results of Triad Avoidance strategy through EFR-A2 for 19<sup>th</sup> Jan 2015, switching mode to triad preparation at 10am.

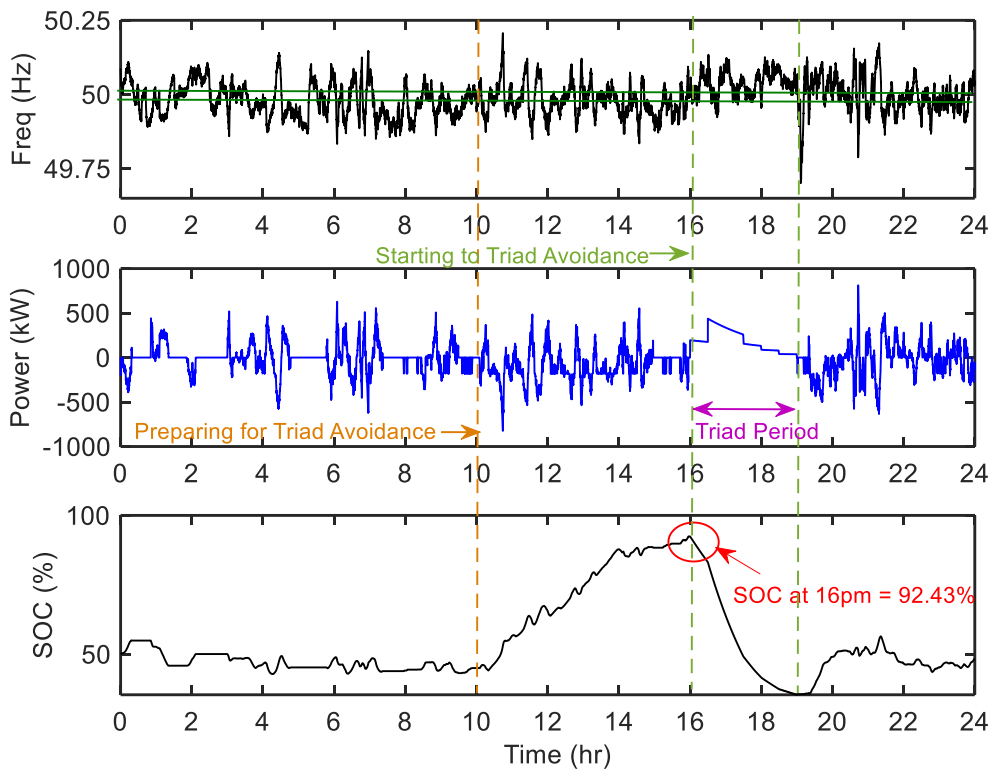


Fig. 3.9 Simulation results of Triad Avoidance strategy through EFR-A3 for 19<sup>th</sup> Jan 2015, switching mode to triad preparation at 10am.

Table 3.3 Power and SOC (%) obtained from the starting of Triad time at 17:30

		Switch (SW) Mode to Triad Preparation at							
		10am		11am		12pm		1pm	
Triad days	EFR Alg.	Power (kW)	SOC (%)	Power (kW)	SOC (%)	Power (kW)	SOC (%)	Power (kW)	SOC (%)
4 <sup>th</sup> Dec 2014	EFR-A2	153	48.54	153	48.56	153	48.55	131.8	41.84
	<b>EFR-A3</b>	<b>154.6</b>	<b>49.9</b>	<b>153.8</b>	<b>48.68</b>	<b>151.5</b>	<b>48.09</b>	<b>130.4</b>	<b>41.36</b>
19 <sup>th</sup> Jan 2015	EFR-A2	151.1	47.94	141.9	45.03	120.3	38.2	107.6	34.15
	<b>EFR-A3</b>	<b>155.1</b>	<b>49.21</b>	<b>144.8</b>	<b>45.93</b>	<b>123</b>	<b>39.02</b>	<b>110.2</b>	<b>34.97</b>
2 <sup>nd</sup> Feb 2015	EFR-A2	165.9	52.66	165.9	52.66	165.8	52.54	163.6	51.93
	<b>EFR-A3</b>	<b>166.8</b>	<b>52.95</b>	<b>166.8</b>	<b>52.97</b>	<b>166.6</b>	<b>52.87</b>	<b>164.7</b>	<b>52.25</b>
20 <sup>th</sup> Dec 2015	EFR-A2	114.8	36.42	114.8	36.44	104.6	33.16	91.71	29.11
	<b>EFR-A3</b>	<b>143.5</b>	<b>45.51</b>	<b>143.5</b>	<b>45.56</b>	<b>115.3</b>	<b>36.61</b>	<b>98.55</b>	<b>31.28</b>

For 2014-2015 the triads occurred at 17:30pm-18:00pm. The TAB payment used in this thesis is also £45 / kWh [ONL18l], [ONL18m]. Considering these information, total triad revenues can be calculated using the equation (3.1).

$$Total\ Triad\ Revenue\ (\pounds) = \frac{Power\ (kW)\ at\ 17:30pm}{BESS\ Power/Capacity} \times TAB\ payment\ (\pounds) \quad (3.1)$$

Using the equation (3.1) and the power values at 17:30 shown in Table 3.3, the total triad profits obtained from EFR-A2 and EFR-A3 for 2014-2015 are calculated as given in Table 3.4.

On 20th Dec2015 which is an under-frequency event day, total triad revenues of £3229 (143.5 kW / 2 x £45) and £2583 (114.8 kW / 2 x £45) are obtained for EFR-A2 and EFR-A3 respectively (Table 3.4). This means that in EFR-A3, the SOC converges faster (17.09%) causing the highest triad revenue (£646) as shown in Table 3.4 since the battery has an opportunity for charging/discharging during the 30-min rest periods in the EFR-A3, as shown by the many 15-minutes events in Fig. 4.3. In comparison, there is no significant SOC recovery (<2.5%) between EFR-A2 and EFR-A3 at 10:00 on the real Triad days of the year of 2014-

2015 because of the low amount of extended under frequency events. This causes less amount of Triad profit improvement between EFR-A2 and EFR-A3 at 10am on the Triad days of 4th Dec 2014 (£36), 19th Jan 2015 (£90) and 2nd Feb 2015 (£20).

Table 3.4 Total Triad profit (£) obtained at 17:30-18:00 predicted Triad times

Real/ predicted Triad days in 2015	EFR Alg. used for Triad	Switch (SW) Mode to Triad Preparation at			
		10am	11am	12pm	1pm
4 <sup>th</sup> Dec 2014	EFR-A2	3442	3442	3409	2934
	EFR-A3	3478	3460	3442	2965
	<b>Recovery</b>	36	18	33	31
19 <sup>th</sup> Jan 2015	EFR-A2	3400	3193	2707	2421
	EFR-A3	3490	3258	2767	2479
	<b>Recovery</b>	<b>90</b>	<b>65</b>	<b>60</b>	<b>58</b>
2 <sup>nd</sup> Feb 2015	EFR-A2	3733	3733	3730	3681
	EFR-A3	3753	3753	3748	3706
	Recovery	20	20	18	25
20 <sup>th</sup> Dec 2015	EFR-A2	2583	2583	2353	2063
	EFR-A3	3229	3223	2594	2217
	<b>Recovery</b>	<b>646</b>	<b>640</b>	<b>241</b>	<b>154</b>

As seen from the Triad profit findings in Table 3.4, switching to Triad preparation after 10am causes reduced amount of Triad revenues with both EFR-A2 and EFR-A3 for the all considered Triad days of 2014-2015.

It can be seen from Table 3.2, analysing the Triad approach through EFR-A2 and EFR-A3 for the real/predicted Triad days of 2014-2015, the BESS provides 100% availability for delivering Triad service, however the highest battery SOC is achieved with EFR-A3 at the considered Triad preparation starting time of 10am, 11am, 12pm and 1pm.



Table 3.5 Energy output (kWh) findings of the EFR-A2 and EFR-A3 with Triad Avoidance for the real/predicted triad days of 2014-2015

Real/pre dicted Triad days in 2015	Switch Mode to Triad Preparation at	EFR Service Algorithm used for Triad	Charge (kWh)	Discharge (kWh)	Import (kWh)	Export (kWh)
4 <sup>th</sup> Dec 2014	10am	EFR-A2	282.5	65.67	1522	1014
		<b>EFR-A3</b>	<b>286.2</b>	<b>63.98</b>	<b>1522</b>	<b>1025</b>
	11am	EFR-A2	285.9	64.52	1524	1023
		<b>EFR-A3</b>	<b>315.1</b>	<b>63.98</b>	<b>1521</b>	<b>1048</b>
	12pm	EFR-A2	282.8	63.69	1519	1026
		<b>EFR-A3</b>	<b>320.2</b>	<b>63.97</b>	<b>1500</b>	<b>1035</b>
	1pm	EFR-A2	262.8	56.01	1477	1058
		<b>EFR-A3</b>	<b>300.4</b>	<b>56.32</b>	<b>1459</b>	<b>1068</b>
19 <sup>th</sup> Jan 2015	10am	EFR-A2	270	36.02	1331	876.7
		<b>EFR-A3</b>	<b>302</b>	<b>36.41</b>	<b>1317</b>	<b>876.5</b>
	11am	EFR-A2	261	57.21	1316	887.1
		<b>EFR-A3</b>	<b>296.2</b>	<b>53.44</b>	<b>1297</b>	<b>890.5</b>
	12pm	EFR-A2	263.4	48.33	1289	944.8
		<b>EFR-A3</b>	<b>300.4</b>	<b>49.38</b>	<b>1266</b>	<b>948.5</b>
	1pm	EFR-A2	246.2	43.26	1272	964.4
		<b>EFR-A3</b>	<b>276.8</b>	<b>44.3</b>	<b>1254</b>	<b>963.7</b>
2 <sup>nd</sup> Feb 2015	10am	EFR-A2	199.7	44.33	1394	842.6
		<b>EFR-A3</b>	<b>212</b>	<b>61.96</b>	<b>1391</b>	<b>835.7</b>
	11am	EFR-A2	199.7	44.33	1394	842.6
		<b>EFR-A3</b>	<b>212</b>	<b>61.96</b>	<b>1391</b>	<b>835.7</b>
	12pm	EFR-A2	202.1	44.3	1387	839.5
		<b>EFR-A3</b>	<b>226.6</b>	<b>61.96</b>	<b>1372</b>	<b>832.7</b>
	1pm	EFR-A2	204.5	43.99	1376	839.6
		<b>EFR-A3</b>	<b>223.1</b>	<b>67.19</b>	<b>1371</b>	<b>831.9</b>
20 <sup>th</sup> Dec 2015	10am	EFR-A2	228.2	51.81	962.1	793.6
		<b>EFR-A3</b>	<b>401.3</b>	<b>76.67</b>	<b>923.8</b>	<b>804.5</b>
	11am	EFR-A2	228.2	51.81	962.1	793.6
		<b>EFR-A3</b>	<b>401.3</b>	<b>76.67</b>	<b>923.8</b>	<b>804.5</b>
	12pm	EFR-A2	222.1	51.85	926.2	782.9
		<b>EFR-A3</b>	<b>323.8</b>	<b>67.61</b>	<b>885.8</b>	<b>792.5</b>
	1pm	EFR-A2	228.3	69.06	931	821.8
		<b>EFR-A3</b>	<b>304.2</b>	<b>77.03</b>	<b>901.2</b>	<b>828.3</b>

This is because with EFR-A3, the battery SOC converges faster towards the desired band of 45-55% and this minimises SOC excursions towards the limits. Energy output findings of the proposed Triad avoidance strategy through EFR service (EFR-A2 and EFR-A3) for the real and predicted triad days of 2014-2015 are summarised in Table 3.5. The difference in charge/discharge and import/export energy observed between EFR-A2 and EFR-A3 is because of the variation in battery SOC and hence the BESS will not follow the same selection of EFR envelopes. It is revealed that using the EFR-A3 for Triad Avoidance provides a substantial achievement in terms of maximizing the utilisation of the BESS stored energy; however, compared to EFR-A2 this is at the expense of using more energy, solely for battery SOC management (charge/discharge) within DB.

### **3.3 Energy Arbitrage**

A BESS is capable of charging at off-peak night time hours when there is a low electricity price and then discharging at on-peak day time hours when there is a high price in order to make arbitrage profit from the price difference. In this chapter, a new service scheduling approach is proposed to achieve maximum arbitrage profits whilst layering EFR and FFR services throughout the day to maximise revenue. The proposed service scheduling method is developed based on the typical daily electricity price pattern, the time of day, grid frequency profile and is based on foresight.

#### **3.3.1 Investigation of the General UK Electricity Price Pattern**

To examine the general pattern of daily (week/weekend) electricity price, the historical UK system pricing for the 7th Monday, 7th Thursday and 9th Sunday of each season across 2014-2015 were extracted as sample electricity price profiles Fig. 3.10 [ONL17]. It is clear from the samples of the selected days shown in Fig. 3.10 [ONL17], that daily UK system prices show a significant volatility at off-peak and on-peak hours during weekdays and weekend days. It is observed that the system price is significantly higher in April, October, January and February due to the cold weather conditions causing a high amount of energy demand on the power grid. The system price sharply decreases in summer season, especially in July, due to better weather conditions and increasingly higher generation from embedded solar sources. It is clear from Fig. 3.10, on the 7th Monday of each season of 2014-2015, the system price is low during night time hours between 11pm-7am and relatively high during day time hours; where the price peaks

between 4pm-11pm. The price shows a similar pattern on the 7th Thursday of each season of 2014-2015, however the peak price is shifted between 8am-12pm for the 17 July 2014. It is observed that in the non-working weekend days, the electricity price deviates from its general pattern as seen in Fig. 3.10. On 27 April 2014, the price is generally low during night hours and relatively high during daytime hours, where the price reaches its peak between 10am-3pm (Fig. 3.10). The price follows the general pattern on 27 July 2014 and on 1 Feb 2015; however on 2 Nov 2014, due to the extreme weather the price is relatively high during night time as well as day time, but the peak price is observed between 4pm-11pm, again following previous patterns. In conclusion, despite some exceptions the UK system electricity buy/sell price follows a common pattern that the price is lower during the night time period (11pm-7am) and higher during the daytime period, where the price typically peaks between 4pm-11pm with this shifting during summer months to 8pm-11pm.

### **3.3.2 Scheduling Approach of Grid Tied BESS Participating in Frequency Response for Energy Arbitrage**

The aim of the above information is to understand the UK electricity price trends to use in the proposed method. The daily electricity pattern is now determined using the selected historical UK electricity price profiles Fig. 3.10 [ONL17]. To supplement the potential arbitrage profits, the grid services under consideration in this thesis are EFR, DFFR, SFFR<sub>low</sub> and SFFR<sub>high</sub> services. An existing fast EFR control algorithm, EFR-A3, has been developed in Chapter 3 and is used in this chapter for EFR service delivery. It is shown in Chapter 3 that the EFR service can be delivered whilst generating arbitrage profits, this is achieved by manipulating the battery SOC target in the proposed frequency response control algorithms; decreasing the SOC target band when electricity prices are high, and increasing the SOC band when the prices are low; effectively shaping the BESS energy delivery profile to export at high prices and import at low prices. Using UK historical electricity pricing data [ONL17], the proposed SOC management strategy selects the appropriate battery SOC profile to maximise the arbitrage revenue whilst delivering the EFR service. Detailed analysis of the EFR service design control algorithm and the NGET service requirements can be found in Chapter 3 in this thesis. For the DFFR and SFFR services, considering the electricity price discrepancy during the day, the proposed arbitrage control algorithm selects the appropriate frequency balancing services considering the grid frequency conditions of the day and the time to maximize arbitrage. SFFR<sub>high</sub> and SFFR<sub>low</sub> services are commonly preferred at night time (off-peak) period with

cost-effective electricity; however DFFR can be utilised during on-peak as well as off-peak time periods due to the dynamic power delivery to the power grid. This thesis does not cover any optimisation strategy for maximizing or calculating energy AR. The major aim of this chapter is to understand the benefits that can be gained from layering different balancing services throughout a day with different off-peak and on-peak service prices. Therefore, any existing energy arbitrage optimisation methods or any arbitrage calculation methods in literature can be implemented in the proposed balancing service scheduling approach in order to generate profits from energy arbitrage as well as frequency response service delivery. The arbitrage calculation method used in the proposed approach is described as follows. Stored energy in the BESS is expressed in (3.2), (3.3) [GUN18b], [GUN17].

$$\text{Discharging: } P_t > 0 \quad E_t = \int_0^t \frac{P_t}{\eta_D} \cdot dt \quad (3.2)$$

$$\text{Charging: } P_t < 0 \quad E_t = \int_0^t P_t \cdot \eta_C \cdot dt \quad (3.3)$$

where  $\eta_D$  is the battery discharging efficiency,  $\eta_C$  is the battery charging efficiency,  $E_t$  is the energy stored in the BESS at hour t, if  $P_t > 0$  BESS exports power at hour t, if  $P_t < 0$  BESS imports power at hour t. The cost of the BESS charge/discharge and the total AR can be simply calculated using the following equation in (3.4), (3.5) [GUN18b].

$$C_C = \sum_{t=1}^{24} E_t \cdot A_{t\_sell} \quad \text{if } P_t < 0 \quad (3.4)$$

$$C_{DC} = \sum_{t=1}^{24} E_t \cdot A_{t\_buy} \quad \text{if } P_t > 0 \quad (3.5)$$

where  $C_{DC}$  is cost of BESS discharging,  $C_C$  is cost of BESS charging,  $A_{t\_sell}$  is system electricity sell price in £/MWh at hour t and  $A_{t\_buy}$  is system electricity buy price in £/MWh at hour t.

$$APR_d = C_{DC} - C_C \quad (3.6)$$

$$APR_y = \frac{SDT \cdot SP}{PD} \cdot 365 \quad (3.7)$$

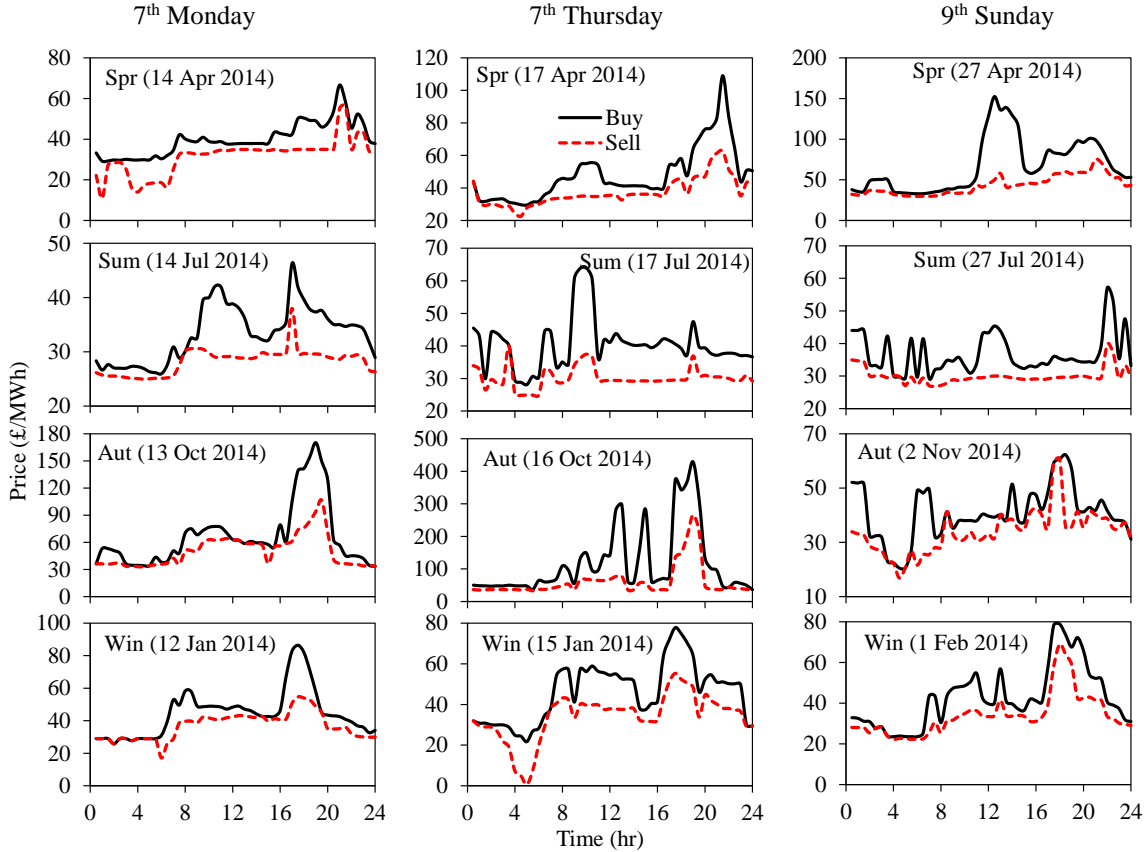


Fig. 3.10 Real UK Electricity system price of 7th Monday, 7th Thursday and 9th Sunday of each season of 2014-2015.

The charge/discharge energy output of BESS can be calculated for charging cost and discharging cost as expressed in (3.4) and (3.5), respectively. In addition, the total arbitrage revenue  $APR_d$  can be calculated by using (3.4) and (3.5) as given in (3.6) [GUN18b]. As seen from the Table 3.7, Table 3.8, Table 3.9,  $APR_y$  is calculated in a year basis (£/kWh.yr) as given in (3.7), where  $SDT$  is the selected balancing service delivery time in hours (hr),  $SP$  is selected service price in £/hr,  $PD$  is the amount of delivered power by the selected service in kW. It should be noted that  $PD$  is 2000kW for the EFR service [GUN18a] and 1000kW for DFFR and SFFR services in this study.

### 3.3.3 Simulation Results of the Scheduling Approach

The proposed balancing service scheduling control method is developed in MATLAB/Simulink and the simulation results are all based on the experimentally validated 1MWh capacity of BESS delivering 2MW EFR power [GUN18a] and 1MW FFR power [GUN18b] to the system. The frequency data of 7th Monday, 7th Thursday and 9th Sunday of each season of 2014-2015, containing high/medium/low frequency events, are simulated here to compare their ARs. Based on recorded UK system sell/buy electricity price [ONL17], the proposed grid balancing service scheduling method has been analysed for 18 different scenarios (S) in Table 3.6. The findings of the proposed control algorithm of the 7th Monday, 7th Thursday and 9th Sunday of each season over the 2014-2015 are shown in Table 3.7, Table 3.8, Table 3.9, respectively. The arbitrage price revenue ( $APR_d$ ) for the day period was summed over the year to attain annual values ( $APR_y$ ) on a £/kWhr.yr basis. Considering the daily electricity price pattern extracted in Section 3.3.1, the sensitivity analysis of service scheduling approach with 18 different scenarios for maximizing energy arbitrage is described in Table 3.6; and their arbitrage findings and import/export energy outputs for above selected days are given in Table 3.7, Table 3.8, Table 3.9.

According to scenario 2 (S2), the first service selected is the fast EFR service with a SOC band of 90-95% to charge the battery until 4am during off-peak period with relatively low electricity price. Then, SFFR<sub>high</sub> service is selected until 6am in order to absorb a maximum constant active power (-1MW) from the grid at a specified high trigger frequency of 50.3Hz in order to respond to this high grid frequency event on the system. The third service selected is again EFR with a high SOC band of 90-95% to charge the battery until 8pm during low system costs and then its SOC band is decreased to a low band of 15-20% in order to deliver power to the grid at on-peak time where the electricity price is high. Comparing the  $APR$  findings of the scenario S1, S2, S3, S4 given in Table 3.7, Table 3.8, Table 3.9, these scenarios do not seem beneficial for maximizing arbitrage profit because they mostly make arbitrage losses rather than profit in a number of considered days (14 July 2014, 17 July 2014, 2 Nov 2014 and 12 Jan 2015). But, if there is high frequency event (>50.3Hz) on power grid in the considered day (e.g 14 April 2014), SFFR<sub>high</sub> was successful in charging the battery which benefitted the AR, by storing energy from the grid with cheap electricity in order to sell it at on-peak period with expensive price; this helps to increase arbitrage gain. For instance, it can be seen from Fig. 3.12, 14 April 2014 has a high frequency event (>50.3Hz) during the night time because of

surplus power on the grid. At this day,  $SFFR_{high}$  was successful in charging the battery which benefitted the AR. The stored low cost energy is then sold to the grid during on-peak hours by delivering EFR service by lowering the target SOC of the control algorithm. It is revealed that S1, S2, S3, S4 can be favourable in the spring season in terms of grid balancing as well as arbitrage benefit. However, these scenarios, covering  $SFFR_{high}$  service, are rare as they difficult to achieve without foresight.

Comparing S5 with S1, S2, S3, S4, despite using exactly the same services ( $SFFR_{high}$  and EFR) during the day, when delivering EFR service at on-peak time period, battery SOC will always be managed as the control algorithm does this. It is revealed that battery SOC management on delivering EFR plays an essential role in making arbitrage profit as well as grid frequency support. As seen from Table 3.6, scenario S6, S7, S8, S9 have the same balancing service (only EFR) throughout the day; the *APR* obtained from each scenario is different because of the effect of the selected different SOC target profiles in the SOC management control during the EFR service delivery. For those scenarios, not only is SOC management essential for the AR, but also the electricity price profile of the considered days needs to be favourable to increase the amount of AR. For instance, comparing the ARs generated from S7 in the considered days, on the 7th Thursday of autumn (16 Oct 2014), S7 provides a significant amount of arbitrage profit (£25.02) due to its high electricity price profile, however the *APR* is less than £1 on the 7th Monday (14 July 2014), 7th Thursday (17 July 2014) and 9th Sunday (27 July 2014) of the summer of 2014-2015. It can be also seen that S6, S7, S8 do not make arbitrage losses in any day of the seasons and actually return a profit.

In scenario 10 (S10), the only selected service is DFFR with the DB of  $\pm 0.015\text{Hz}$  to deliver only dynamic active power throughout the day. With S10, which is a common choice for maximizing arbitrage profit, the battery can make arbitrage profit or service benefit from only DFFR service by importing/exporting power from the grid without having a battery SOC management control. This chapter does not consider reducing the DFFR tendered power to reserve power for SOC management. According to the scenario 12 (S12) shown in Table 3.6 the first service selected is DFFR with the DB of  $\pm 0.015\text{Hz}$  to deliver dynamic active power until 4 am with a relatively low electricity price and then  $SFFR_{high}$  service is selected until 7am in order to draw a maximum constant power (-1 MW) from the grid at a high trigger frequency of 50.3Hz. The third service selected is EFR with a SOC band of 90-95% to charge the battery until 4pm during low costs and then its SOC band is decreased to 15-20% in order

to supply power to the grid at peak time with high electricity price. Comparing S10, S11 and S12, S10 and S12 do not suffer any arbitrage losses in any considered days, S11 has a ~£5 loss in 14 April 2014 as there is a high frequency event ( $>50.3$ ) in that day; the battery stores energy by absorbing 1MW power from the grid with cheap electricity at 4am-7am, but cannot adequately resell the power with expensive electricity at 7am-12pm due to the absence of battery SOC management in DFFR service. But here S12 makes ~£1 *APR* comparing the ~£4.8 loss generated by S11. It can be seen that providing a service where the battery SOC can be managed is beneficial when there is a frequency excursion.

According to scenario 17 (S17), the first frequency response service selected is EFR with a high SOC band (90-95%) to charge the battery until 4am at off-peak time with low electricity price. Then SFFR<sub>low</sub> service is selected until 7am to send a constant 1MW active power to the grid at the specified low trigger frequency of 49.7Hz in order to respond to this low grid frequency event in the power system. The third service is then selected as EFR with the high SOC band of 90-95% to charge the battery until 4pm with low-cost electricity and then its SOC band is decreased to 15-20% in order to export power to the grid selling at a high price (Fig. 3.11). The scenarios S13, S14, S15, S16, S17, and S18 use SFFR<sub>low</sub> service during off-peak time periods at varying times however, there is no low frequency event ( $<49.7$ Hz) during night time for all the considered days. Therefore, those scenarios cannot generate arbitrage profit from SFFR<sub>low</sub> service, but as seen from the Table 3.10 the service availability payment is generated during the service delivery time with SFFR off-peak price of £4/hr. Comparing the *APR* obtained from those scenarios, S13, S14, S16, S18 make a loss at least one time in the considered days. But, S15 and S17 do not make any arbitrage losses in any days, hence these scenarios are suitable for making arbitrage profit, especially in high electricity price days (e.g *APR* in S15=£29.66, S17=£22.94 in 16 Oct 2014). All in all, considering the general UK daily electricity pricing pattern, the proposed balancing service method can make the AR as shown in Table 3.7, Table 3.8, Table 3.9. It is also revealed that S10 makes the highest arbitrage profit through service delivery with no power required for SOC management. In this thesis, the *APR* findings from the proposed service scheduling approach are compared with the optimized yearly arbitrage profit attained from the 6MW/10MWh Leighton Buzzard battery system in [NEW16]. Comparing both *APR* values in year base (/kWh.yr), the potential AR earned from the experimental battery in [NEW16] is higher (£5.91/kWh.yr) than the *APR* generated from many scenarios in this proposed method for several different days Table 3.7, Table 3.8, Table 3.9; because in the reference study only arbitrage is considered, no other balancing services are



delivered simultaneously. Using frequency response service payments (for EFR=£10/hr, DFFR=£11/hr and SFFR off peak=£4 and on-peak=£6/hr) [ONL18a], the daily and yearly frequency response service availability payment (*SAP*) generated from each scenario in Table 3.6 are shown in Table 3.10. It can be seen from Table 3.10, scenario 10 (S10), which delivers only DFFR throughout the day, makes the highest *SAP* (£96.36/kWh.yr) due to the highest availability price of DFFR service (£11/day.hr) in the balancing service. It should be noted in the previous study [GUN18b], in the calculation of yearly based *APR*, the delivered service power (*PD*) was set to 2 MW for all the services considering the 2MW EFR power as a reference *PD* power for all the balancing service, roughly. But the author's method used in [GUN18b] is improved in this thesis as the *APR* is independently calculated for each delivered service by using their own *PD* power (*PD* in EFR=2MW and FFR=1MW). Considering this, S1 is selected as the best scenario in the previous study [ONL18b], with £2.315/kWh.yr AR. This chapter almost doubles the AR (£4.292/kWh.yr) with scenario 10 (S10), by delivering only DFFR service throughout the day; and also around 20% higher revenue with S8, delivering only EFR service that has effective SOC management.

Table 3.6 Proposed service scheduling method for energy arbitrage with 18 scenarios

Scenario (S)	Time (hr)	Service	SOC band (%)	Scenario (S)	Time (hr)	Service	SOC band (%)
S1	12am-2am	EFR	90-95	S9	12am-4pm	EFR	90-95
	2am-6am	SFFRhigh	-		4pm-11pm	EFR	15-20
	6am-8pm	EFR	90-95		11pm-12am	EFR	45-55
	8pm-12am	EFR	15-20	S10	12am-12am	DFFR	-
S2	12am-4am	EFR	90-95	S11	12am-4am	DFFR	-
	4am-6am	SFFRhigh	-		4am-7am	SFFRhigh	-
	6am-8pm	EFR	90-95		7am-12pm	DFFR	-
	8pm-12am	EFR	15-20	12am-4am	DFFR	-	
S3	12am-4am	EFR	90-95	S12	4am-7am	SFFRhigh	-
	4am-7am	SFFRhigh	-		7am-4pm	EFR	90-95
	7am-8pm	EFR	90-95		4pm-12am	EFR	15-20
	8pm-12am	EFR	15-20		12am-7am	SFFRlow	-
S4	12am-7am	SFFRhigh	-	S13	7am-8pm	EFR	90-95
	7am-8pm	EFR	90-95		8pm-12am	EFR	15-20
	8pm-12am	EFR	15-20		12am-7am	SFFRlow	-
S5	12am-4am	EFR	90-95	S14	7am-4pm	EFR	90-95
	4am-7am	SFFRhigh	-		4pm-12am	EFR	15-20
	7am-4pm	EFR	45-55	S15	12am-7am	SFFRlow	-
	4pm-12am	EFR	15-20		7am-12am	DFFR	-
S6	12am-7am	EFR	90-95	S16	12am-4am	DFFR	-
	7am-4pm	EFR	45-55		4am-7am	SFFRlow	-
	4pm-12am	EFR	15-20		7am-12am	DFFR	-
S7	12am-7am	EFR	90-95	S17	12am-4am	EFR	90-95
	7am-4pm	EFR	70-75		4am-7am	SFFRlow	-
	4pm-12am	EFR	15-20		7am-4pm	EFR	90-95
S8	12am-4pm	EFR	90-95		4pm-12am	EFR	15-20
	4pm-12am	EFR	15-20	S18	12am-4am	EFR	90-95
			4am-7am		SFFRlow	-	
			7am-12am		DFFR	-	
			11pm-12am		EFR	45-55	

Table 3.7 APR findings and energy output of 7th Monday of each season of 2014/2015

7 <sup>TH</sup> MONDAY OF EACH SEASON OF 2014/2015												
Scen. (S)	SPRING (14 April 2014)			SUMMER (14 July 2014)			AUTUMN (13 Oct 2014)			WINTER (12 Jan 2015)		
	Energy Output (kWh/day)		APR (£/kWh)	Energy Output (kWh/day)		APR (£/kWh)	Energy Output (kWh/day)		APR (£/kWh)	Energy Output (kWh/day)		APR (£/kWh)
	Imp.	Exp.		Imp.	Exp.		Imp.	Exp.		Imp.	Exp.	
S1	1528	1287	<b>2.315</b>	1397	1071	<b>-0.414</b>	1529	1299	<b>0.008</b>	1348	845.1	<b>-2.841</b>
S2	1614	1359	<b>2.455</b>	1434	1102	<b>-0.267</b>	1650	1400	<b>1.594</b>	1382	873.1	<b>-2.555</b>
S3	1524	1284	<b>2.439</b>	1397	1070	<b>-0.364</b>	1597	1355	<b>1.129</b>	1352	848.2	<b>-2.754</b>
S4	1355	1142	<b>1.7</b>	1297	986.8	<b>-0.73</b>	1385	1178	<b>-1.462</b>	1199	720.1	<b>-3.429</b>
S5	1513	1269	<b>0.779</b>	1129	976.1	<b>0.733</b>	1520	1303	<b>5.024</b>	1006	900.7	<b>1.97</b>
S6	1363	1143	<b>1.606</b>	1482	1272	<b>0.913</b>	1762	1504	<b>6.165</b>	1093	973.6	<b>2.044</b>
S7	1392	1170	<b>2.146</b>	1525	1307	<b>0.986</b>	1772	1513	<b>7.716</b>	1147	1025	<b>1.723</b>
S8	1512	1267	<b>2.82</b>	1522	1305	<b>1.149</b>	1757	1500	<b>6.888</b>	1317	1077	<b>0.604</b>
S9	1546	1267	<b>2.608</b>	1566	1260	<b>0.676</b>	1788	1497	<b>6.682</b>	1350	915.8	<b>-0.558</b>
S10	901.8	958.2	<b>4.292</b>	830.9	775.7	<b>0.912</b>	1010	1197	<b>15</b>	1016	1476	<b>13.64</b>
S11	1636	873.5	<b>-4.791</b>	735.9	662.1	<b>0.666</b>	957.5	978	<b>12.46</b>	988.4	1466	<b>13.62</b>
S12	1619	1270	<b>0.872</b>	1458	1230	<b>0.266</b>	1320	1507	<b>9.158</b>	1312	971.6	<b>1.402</b>
S13	1237	1044	<b>1.954</b>	1297	986.8	<b>0.73</b>	1385	1178	<b>-1.462</b>	1199	720.1	<b>-3.429</b>
S14	1232	1033	<b>1.562</b>	1255	1082	<b>0.501</b>	1384	1189	<b>3.721</b>	1077	875.1	<b>-0.16</b>
S15	698.1	714.7	<b>2.298</b>	607.2	508.3	<b>0.27</b>	790.5	736.1	<b>11.13</b>	772.5	1344	<b>14.61</b>
S16	830.9	873.5	<b>3.295</b>	735.9	662.1	<b>0.666</b>	957.5	978	<b>-12.46</b>	988.4	1466	<b>13.62</b>
S17	1338	1122	<b>2.335</b>	1355	1165	<b>0.867</b>	1606	1374	<b>5.969</b>	1229	1003	<b>0.5308</b>
S18	1305	737.4	<b>2.917</b>	1224	518.1	<b>-3.754</b>	1538	746.7	<b>4.839</b>	1158	1384	<b>12.84</b>

Table 3.8 APR findings and energy output of 7th Thursday of each season of 2014/2015

7 <sup>TH</sup> THURSDAY OF EACH SEASON OF 2014/2015												
Scen. (S)	SPRING (17 April 2014)			SUMMER (17 July 2014)			AUTUMN (16 Oct 2014)			WINTER (15 Jan 2015)		
	Energy Output (kWh/day)		APR (£/kWh)	Energy Output (kWh/day)		APR (£/kWh)	Energy Output (kWh/day)		APR (£/kWh)	Energy Output (kWh/day)		APR (£/kWh)
	Imp.	Exp.		Imp.	Exp.		Imp.	Exp.		Imp.	Exp.	
S1	1343	1156	<b>5.052</b>	1520	907.1	<b>-2.277</b>	1630	1315	11.6	1546	1124	<b>-0.447</b>
S2	1464	1257	<b>5.344</b>	1581	958.1	<b>-1.823</b>	1703	1377	12.93	1661	1220	<b>0.583</b>
S3	1378	1186	<b>5.259</b>	1552	933.2	<b>-2.027</b>	1663	1335	12.78	1593	1163	<b>0.402</b>
S4	1183	1022	<b>4.574</b>	1408	813.2	<b>-2.334</b>	1441	1158	7.604	1409	1009	<b>-1.118</b>
S5	1206	1042	<b>2.488</b>	1183	956.1	<b>0.454</b>	1464	1246	23.13	1453	1203	<b>3.567</b>
S6	1501	1289	<b>3.056</b>	1472	1198	<b>0.737</b>	1731	1470	24.29	1700	1410	<b>4.775</b>
S7	1495	1284	<b>4.808</b>	1520	1238	<b>0.929</b>	1782	1512	25.02	1718	1424	<b>5.161</b>
S8	1554	1333	<b>5.751</b>	1563	1274	<b>1.134</b>	1790	1518	24.3	1724	1430	<b>5.024</b>
S9	1624	1282	<b>4.73</b>	1647	1248	<b>0.493</b>	1967	1464	22.69	1874	1409	<b>4.113</b>
S10	1066	1057	<b>2.586</b>	746.5	918.5	<b>5.0</b>	1016	1082	31.99	962.7	1017	<b>3.865</b>
S11	968.2	939.4	<b>2.081</b>	690.8	851.8	<b>4.569</b>	880.8	921.1	30.71	873	913.2	<b>3.0</b>
S12	1003	1462	<b>11.16</b>	1482	1200	<b>0.2</b>	1559	1266	17.42	1400	1412	<b>4.777</b>
S13	1183	1022	<b>4.574</b>	1408	813.2	<b>-2.334</b>	1441	1158	7.604	1409	1009	<b>-1.118</b>
S14	993.3	863.8	<b>2.905</b>	1333	1081	<b>0.31</b>	1399	1191	17.76	1352	1119	<b>2.188</b>
S15	650.5	559.6	<b>1.316</b>	562.6	716.2	<b>4.37</b>	786.7	808.7	29.66	666.9	663.8	<b>2.562</b>
S16	968.2	939.4	<b>2.081</b>	690.8	851.8	<b>4.569</b>	880.8	921.1	30.71	873	913.2	<b>2.998</b>
S17	1357	1168	<b>5.405</b>	1476	1201	<b>0.615</b>	1601	1360	22.94	1537	1273	<b>3.707</b>
S18	1503	600.4	<b>-6.028</b>	988.7	738.4	<b>2.309</b>	1406	840.7	25.63	1390	668.5	<b>-1.716</b>

Table 3.9 APR findings and energy output of 9th Sunday of each season of 2014/2015

9 <sup>TH</sup> SUNDAY OF EACH SEASON OF 2014/2015												
Scen. (S)	SPRING (27 April 2014)			SUMMER (27 July 2014)			AUTUMN (2 Nov 2014)			WINTER (1 Feb 2015)		
	Energy Output (kWh/day)		APR (£/kWh)	Energy Output (kWh/day)		APR (£/kWh)	Energy Output (kWh/day)		APR (£/kWh)	Energy Output (kWh/day)		APR (£/kWh)
	Imp.	Exp.		Imp.	Exp.		Imp.	Exp.		Imp.	Exp.	
S1	1397	1156	<b>4.56</b>	1385	1147	<b>0.3204</b>	1382	1039	<b>-0.47</b>	1417	1195	<b>0.801</b>
S2	1456	1205	<b>5.347</b>	1440	1194	<b>0.192</b>	1480	1121	<b>-0.004</b>	1554	1310	<b>1.1</b>
S3	1414	1170	<b>4.621</b>	1417	1174	<b>0.207</b>	1439	1086	<b>-0.19</b>	1523	1284	<b>1.126</b>
S4	1269	1048	<b>3.62</b>	1209	1000	<b>0.49</b>	1238	918.3	<b>-1.034</b>	1259	1063	<b>0.6</b>
S5	1160	988.5	<b>3.586</b>	1252	1087	<b>0.043</b>	1283	1076	<b>1.115</b>	1340	1141	<b>1.864</b>
S6	1411	1199	<b>3.636</b>	1422	1229	<b>0.007</b>	1506	1262	<b>1.635</b>	1544	1312	<b>2.294</b>
S7	1461	1241	<b>5.599</b>	1433	1238	<b>0.042</b>	1520	1274	<b>1.958</b>	1579	1342	<b>3.038</b>
S8	1565	1328	<b>7.126</b>	1462	1263	<b>0.062</b>	1510	1266	<b>2.38</b>	1641	1393	<b>3.293</b>
S9	1667	1299	<b>6.045</b>	1492	1250	<b>-0.18</b>	1623	1246	<b>1.592</b>	1724	1371	<b>2.723</b>
S10	545.6	494.3	<b>5.572</b>	773.7	705.6	<b>1.148</b>	814.1	907.4	<b>4.401</b>	866.9	824.1	<b>3.273</b>
S11	521	464.9	<b>5.491</b>	670	581.6	<b>0.752</b>	766	850	<b>3.597</b>	815.6	762.7	<b>2.889</b>
S12	1620	1120	<b>1.456</b>	1201	1169	<b>1.906</b>	1140	1291	<b>5.181</b>	1561	1197	<b>1.247</b>
S13	1269	1048	<b>3.62</b>	1209	1000	<b>0.49</b>	1238	918.3	<b>-1.034</b>	1259	1063	<b>0.597</b>
S14	1297	1104	<b>4.8</b>	1166	1016	<b>0.394</b>	1170	981.8	<b>1.054</b>	1258	1073	<b>2.374</b>
S15	455.1	386.1	<b>5.189</b>	568.2	459.9	<b>0.08</b>	563.3	607.6	<b>2.513</b>	695.5	619.1	<b>2.247</b>
S16	521	464.9	<b>5.491</b>	670	581.6	<b>0.752</b>	766	850	<b>3.597</b>	815.6	762.7	<b>2.889</b>
S17	1442	1225	<b>5.794</b>	1374	1189	<b>0.111</b>	1392	1167	<b>1.879</b>	1522	1294	<b>2.904</b>
S18	1144	457	<b>1.803</b>	1465	461.3	<b>-6.327</b>	1439	613	<b>-4.3</b>	1461	745.5	<b>-2.043</b>

Table 3.10 SAP obtained from each scenario of the service scheduling approach in Table 3.6

Scenario (S)	DFFR			SFFR			EFR			SAP (£/day)	SAP (£/kW h.yr)
	SDT (hr/day)	SP (£/hr)	SAP (£/kWh.yr)	SDT (hr/day)	SP (£/hr)	SAP (£/kWh.yr)	SDT (hr/day)	SP (£/hr)	SAP (£/kWh.yr)		
S1	-	-	-	4	£4	£5.84	20	£10	£36.50	£216	<b>£42.34</b>
S2	-	-	-	2	£4	£2.92	22	£10	£40.15	£228	<b>£43.42</b>
S3	-	-	-	3	£4	£4.38	21	£10	£38.32	£222	<b>£42.7</b>
S4	-	-	-	7	£4	£10.22	17	£10	£31.02	£198	<b>£41.24</b>
S5	-	-	-	3	£4	£4.38	21	£10	£38.32	£222	<b>£42.7</b>
S6	-	-	-	-	-	-	24	£10	£43.8	£240	<b>£43.8</b>
S7	-	-	-	-	-	-	24	£10	£43.8	£240	<b>£43.8</b>
S8	-	-	-	-	-	-	24	£10	£43.8	£240	<b>£43.8</b>
S9	-	-	-	-	-	-	24	£10	£43.8	£240	<b>£43.8</b>
S10	24	£11	£96.36	-	-	-	-	-	-	£264	<b>£96.36</b>
S11	21	£11	£84.31	3	£4	£4.38	-	-	-	£243	<b>£88.69</b>
S12	4	£11	£16.06	3	£4	£4.38	17	£10	£31.02	£226	<b>£51.46</b>
S13	-	-	-	7	£4	£10.22	17	£10	£31.02	£198	<b>£41.24</b>
S14	-	-	-	7	£4	£10.22	17	£10	£31.02	£198	<b>£41.24</b>
S15	17	£11	£68.25	7	£4	£10.22	-	-	-	£215	<b>£78.47</b>
S16	21	£11	£84.31	3	£4	£4.38	-	-	-	£243	<b>£88.69</b>
S17	-	-	-	3	£4	£4.38	21	£10	£38.32	£222	<b>£42.7</b>
S18	17	£11	£68.25	3	£4	£4.38	4	£10	£7.3	£239	<b>£79.93</b>

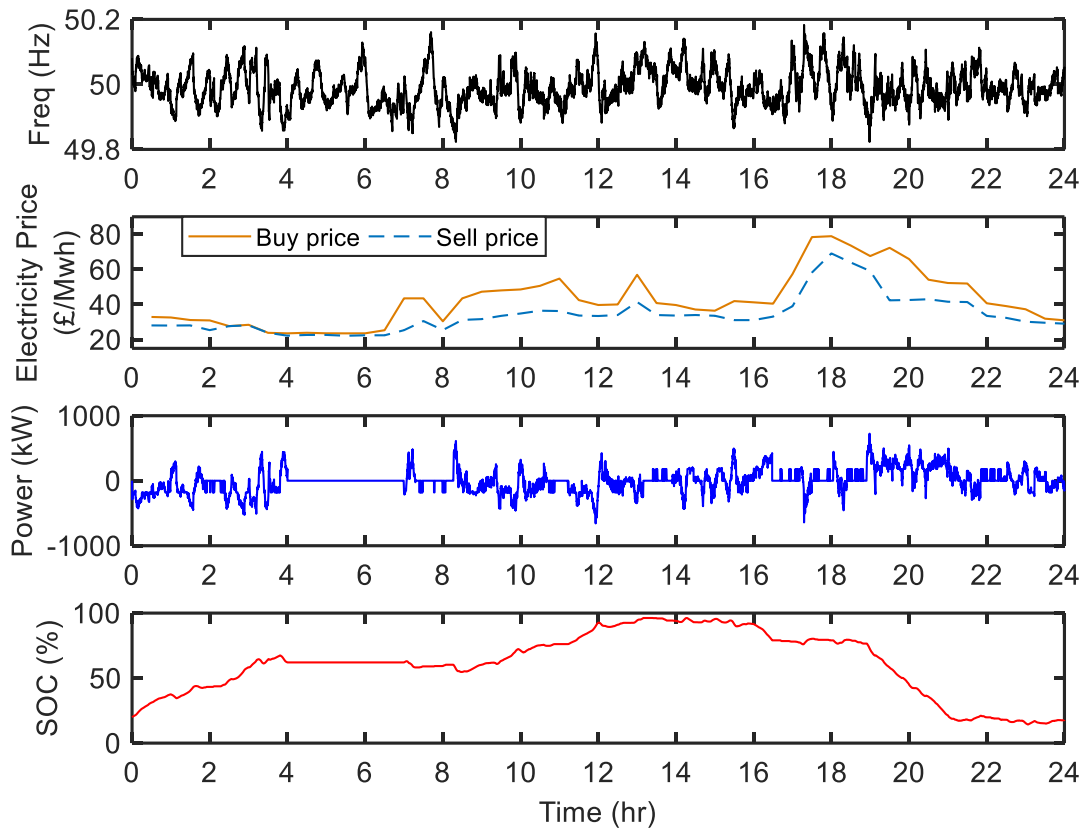


Fig. 3.11 Simulation results of the service scheduling algorithm for 1st Feb 2015 for S17.

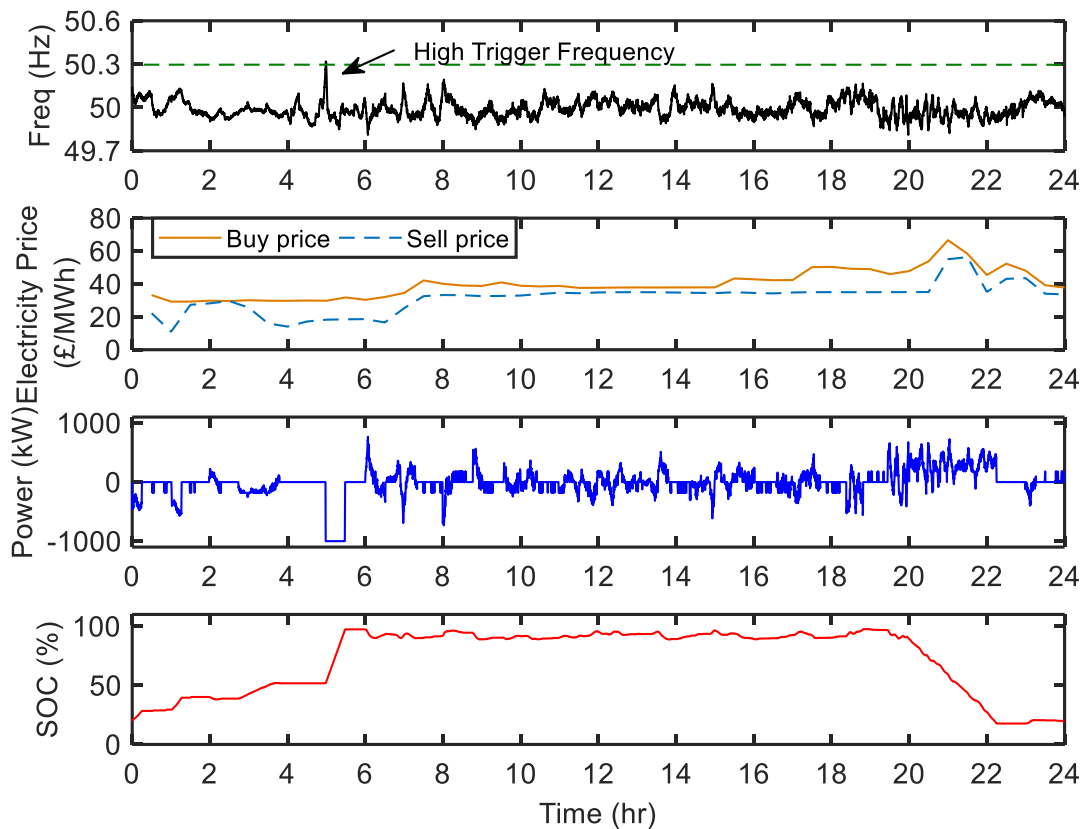


Fig. 3.12 Simulation results of the service scheduling algorithm for 14th April 2014 for S2.

### 3.4 Conclusion

In the energy arbitrage section of this chapter, a DFFR, a SFFR<sub>high</sub> and SFFR<sub>low</sub> frequency response control algorithm based on a model of a 1MW/1MWh BESS has been developed to meet the NGET published service requirements. When there is a grid frequency deviation on the grid, the BESS supplies a dynamic power according to a specified DFFR envelope. SFFR delivers a non-dynamic service where an agreed amount of power is delivered if the grid frequency reaches a certain trigger point of 49.7Hz (SFFR<sub>low</sub>) or 50.3Hz (SFFR<sub>high</sub>). Therefore, a new balancing service scheduling method for maximizing energy arbitrage has been presented that uses layering of grid balancing services (DFFR, SFFR<sub>high</sub>, SFFR<sub>low</sub> and EFR) throughout the day with market pricing foresight. The advantage of this scheduling method is that it generates arbitrage profit and combines balancing service availability payment revenue through service layering and new SOC management techniques. The EFR control algorithm, described in Chapter 3, has been used in the proposed approach; where the battery SOC target band is periodically moved according to the electricity pricing profile for the day in order to generate arbitrage revenue. Setting the SOC band low has the effect of exporting energy setting the SOC band high imports energy. Simulation results of the proposed service scheduling approach were carried out using NGET frequency data for 7th Monday, 7th Thursday, 9th Sunday of each season of 2014/2015, which contains a mix of frequency profile days. The simulations are based on experimentally validated model of the WESS demonstrating that arbitrage profits can be made by layering different balancing services throughout the day with foresight. The revenue generated by a BESS can be maximized using a suitable scheduling scenario that will vary depending on the day/month/season of the year.

In the triad avoidance section of this chapter, it is revealed from the simulation results with proper management of the battery's SOC during EFR delivery the BESS could be prepared in order to maximise the available energy to export for TAB.

Based on the 2016 TAB payment of £45.83 / kWh, it is revealed that in 20th Dec 2015 which is an under-frequency event day, total triad revenues of £3229 and £2583 are obtained for EFR-A2 and EFR-A3 respectively. This means that in EFR-A3, the SOC converges faster (17.09%) causing the highest triad revenue (£646), since the battery has an opportunity for charging/discharging during the 30-min rest periods in the EFR-A3, due to the many 15-minutes events in 20<sup>th</sup> Dec 2015. In comparison, there is no significant SOC recovery (<2.5%)

between EFR-A2 and EFR-A3 at 10:00 on the real Triad days of the year of 2014-2015 because of the low amount of extended under frequency events. This causes less amount of Triad profit improvement between EFR-A2 and EFR-A3 at 10am on the real Triad days of 4th Dec 2014 (£36), 19th Jan 2015 (£90) and 2nd Feb 2015 (£20).

The results show that the amount of energy available to export would depend greatly on the frequency conditions of the day and the time that a decision is made to commit to preparing for TAB.

#### 4 Willenhall Energy Storage System

The UK’s first largest grid-tied Lithium-titanate (LTO) based 968kWh/2MW BESS, named Willenhall Energy Storage System (WESS), was commissioned in 2015 by the University of Sheffield (UoS). The WESS facility comprises a 968kWh, 2MW Toshiba LTO battery, interfaced to the power grid through 11kV feed at the Willenhall Primary Substation (WPD) in the UK. Network connection of proposed and deployed storage in the UK is shown in Fig. 4.1.

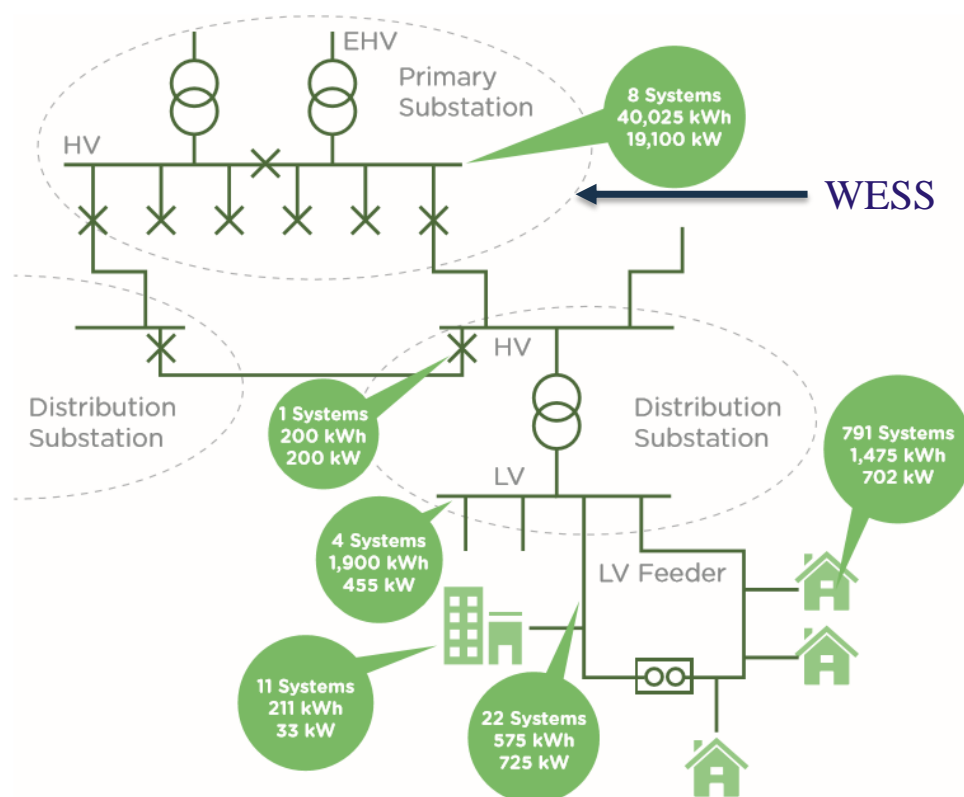


Fig. 4.1 Network connection of proposed and deployed storage in the UK. (DNO projects as of 1 December 2014).

In addition, the WESS site also houses a 120kW ABB inverter, interfaced through bespoke DC/DC converters to a rack containing second life batteries. Moreover, there is a 1MWh DC Lead-Acid battery system connected through a 800kVA GE Inverter as part of the storage facility. The three systems operate independently with their own G59 control relay. The operation of each system being designed so as not to adversely affect the other systems. A single line diagram of the site is supplied in Fig. 4.2 [ROY17].

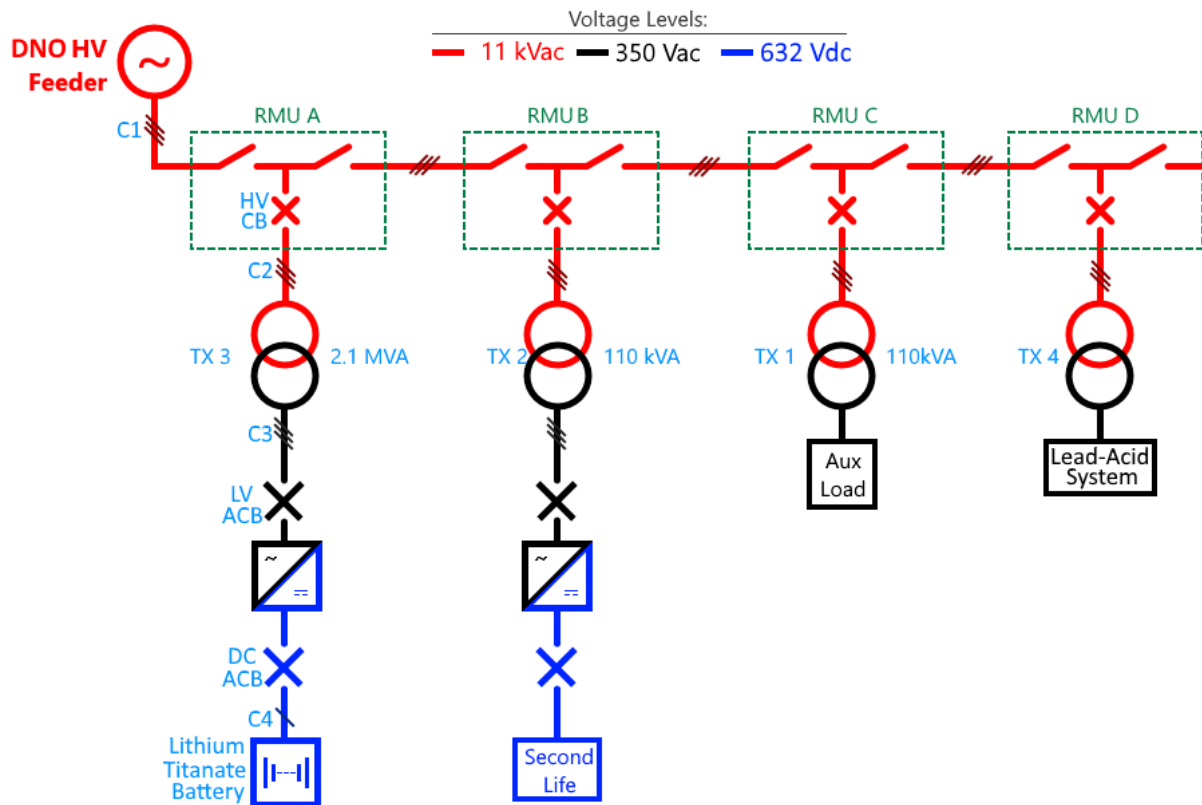


Fig. 4.2 Single line representation of Willenhall Energy Storage System [ROY17].

This was an Engineering and Physical Sciences Research Council (EPSRC) capital funded project with follow on projects from varying sources examining the characteristics of the LTO battery, how various battery chemistries can work together for grid scale energy storage applications and the coordination of large storage with second life EV batteries. The WESS facility is being managed by the UoS for carrying out research works on LTO cell degradation and integrating battery characteristics. Southampton and Aston Universities are also involved in the WESS project investigating the optimum use of second life EV batteries and vehicle-to-grid (V2G) applications. It aims to investigate the characteristics of a LTO type battery, as well as different battery chemistries, for delivering grid support functions at scale [ONL18g], [ONL18h]. A LTO battery was selected for used in WESS as a new technology offering

increased performance in terms of a relatively long cycle life, safety and rapid recharging capability. The battery storage is made up of 40 parallel-connected racks, each consisting of 22 series-connected battery modules, and each module consists of 24 battery cells in a 2P12S formation. There are 21,120 cells in the DC battery unit with a total capacity of approximately 1MWh. The basic structure of the WESS consist of a 968kWh battery (DC storage), PCS100 ESS Converter (2MW) which allows active/reactive power control based on the system requirement, and a transformer (2.1MVA) which connect the power converter to the 11kV AC grid [FEE16]. The communication and control between the storage and converter in system is implemented using a bespoke control system built by the UoS. An overview schematic of the system is illustrated in Fig. 4.3 [FEE16]. In the figure, the control interface between converter and BMS is achieved through a ModBus TCP/IP protocol; the outer system control loop rate is 100ms with the converter capable of a full power response (-2MW to +2MW) in 2 cycles of mains supply (40ms).

In addition to the BESS, a flexible DC/DC and 100kVA inverter based system is installed for interfacing ‘second life’ EV batteries to the utility supply for grid support applications. The systems are grid tied to the 11kV utility supply at the WPD Willenhall substation in the West Midlands. To facilitate operation, the whole system can be controlled remotely over a dedicated VPN connection, over ‘fibre’ or a 3G network. Data from the system is available via a local SQL database, updated on a 100ms timescale or via a publicly accessible InfluxDB at 1 second intervals. The bespoke nature of the system enables flexible control and rapid response from the hardware [FEE16].

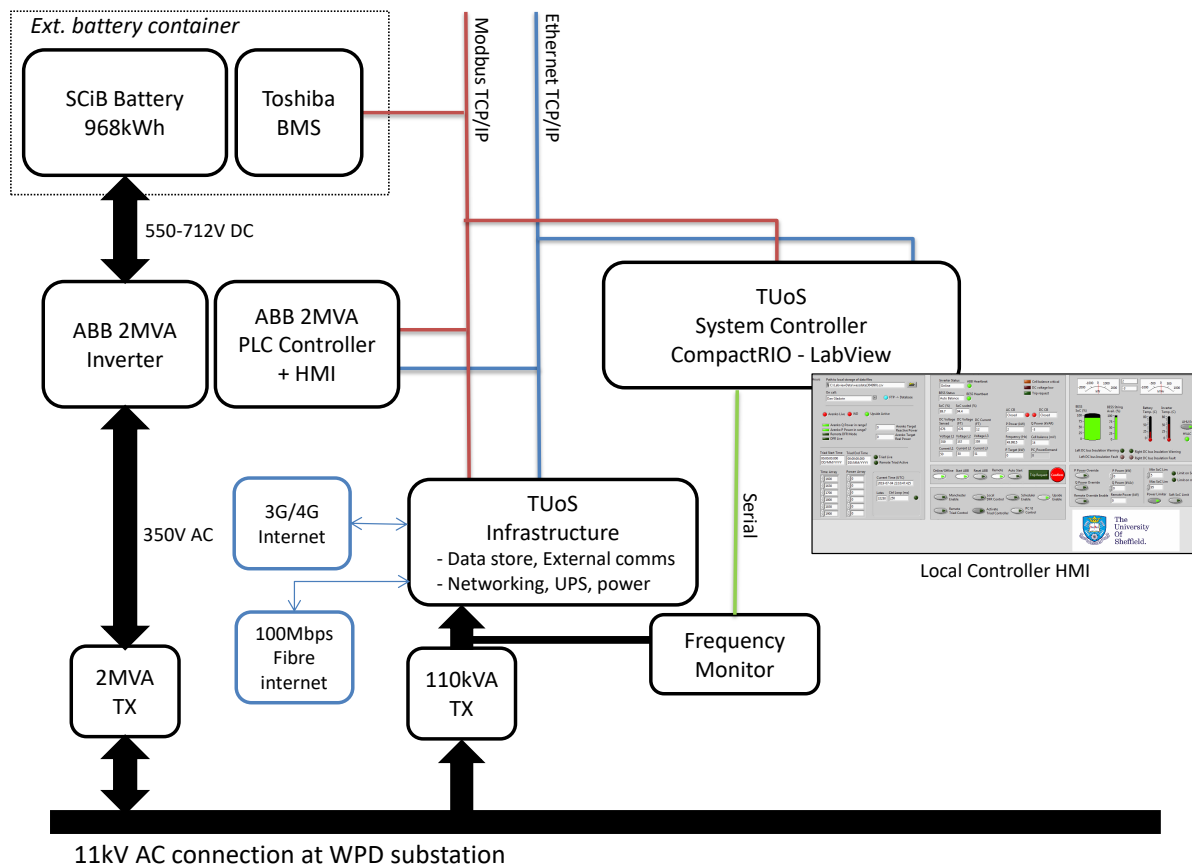
#### **4.1 WESS Control**

To facilitate WESS operation, the whole system can be controlled remotely using a dedicated VPN connection, over ‘fibre’ or a 3G or 4G network Fig 4.3(a). Data from the system is available via a local SQL database, updated on a 100ms timescale or via a publicly accessible InfluxDB at 1 second intervals. The bespoke nature of the system enables flexible control and rapid response from the hardware. In the WESS, the communication and control between the storage and converter is implemented using a bespoke control system built by the UoS. An overview schematic of the system is illustrated in Fig. 4.3. In the figure, the control interface between converter and BMS is achieved through the ModBus TCP/IP protocol; the outer system control loop rate is 100ms with the converter capable of a full power response (-2MW

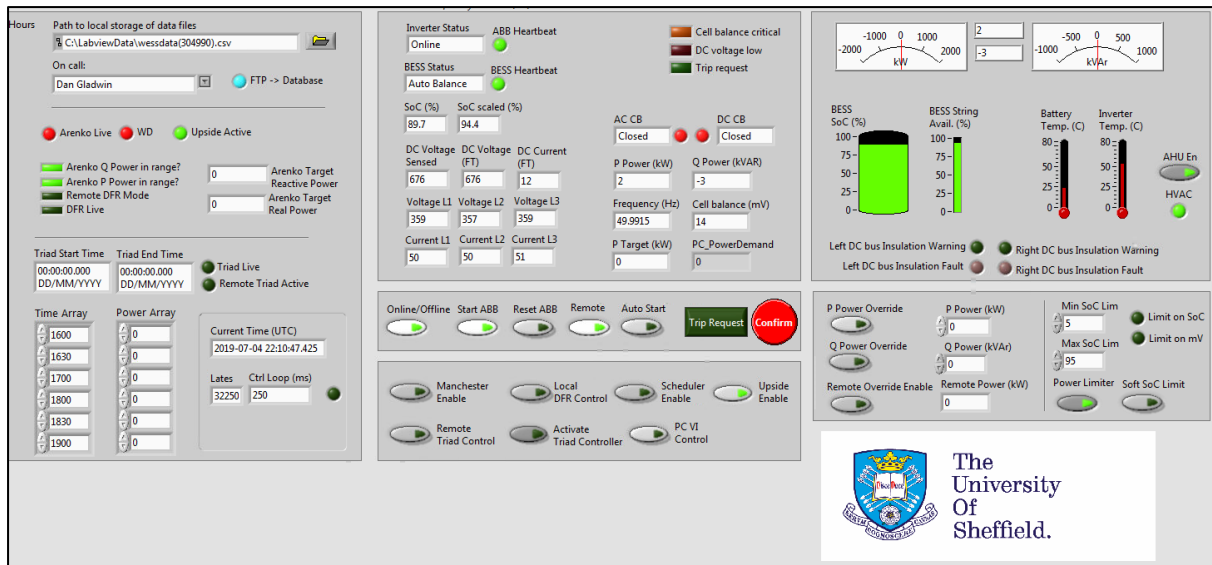


to +2MW) in 2 cycles of mains supply (40ms). The CompactRIO sends the power commands using ModBus TCP/IP to the ABB PLC that then signals the converter modules over CAN bus. The BMS and the converter are monitored by the UoS controller for any fault condition.

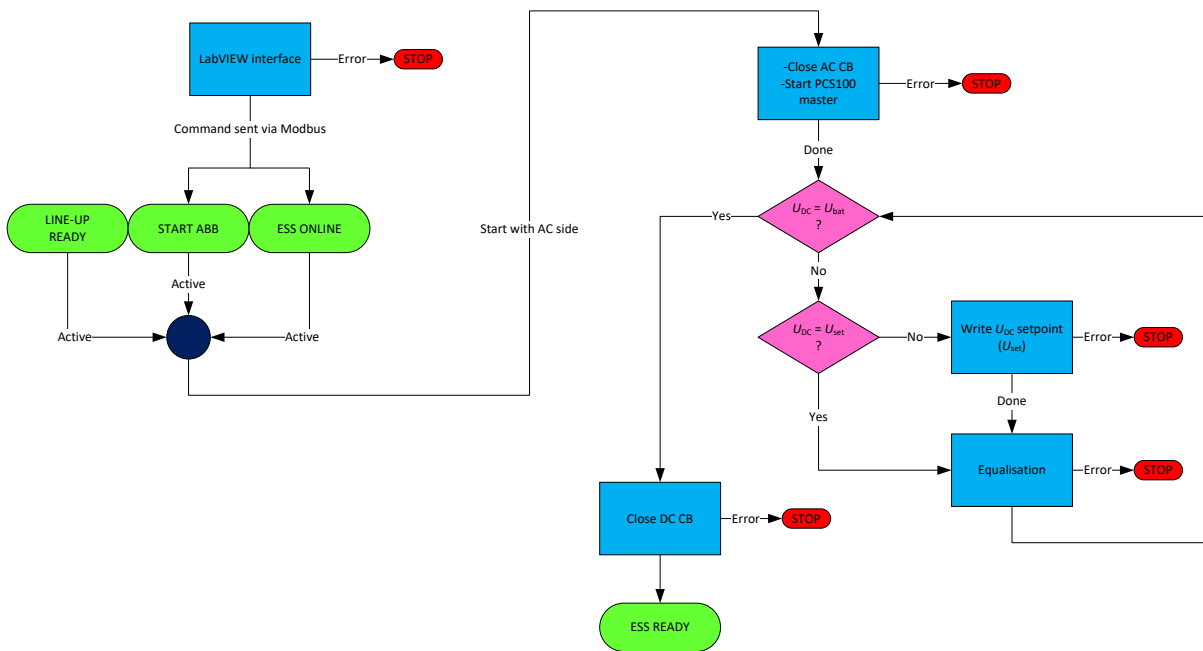
In order to achieve experimental results of EFR-A1 with WESS, the MATLAB coding of EFR-A1 has been converted to the LabVIEW code as provided in Fig C.1 to Fig C.18 in Appendix C. Figure 4.3(c) shows WESS start up procedure by running LabVIEW on host PC.



(a)



(b)

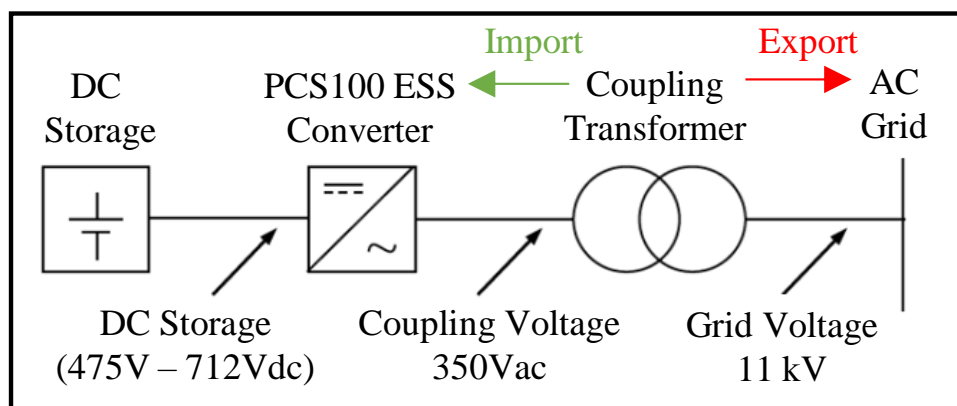


(c)

Fig. 4.3 Control scheme of the 2MW/968kWh Willenhall Energy Storage System (a); Photo of local controller HMI in the Willenhall control system (b); WESS start up procedure used in the local controller (c).

## 4.2 WESS Design

The BESS design in the Willenhall Project will be explained in this section. Batteries are connected to a power conversion system (PCS) which converts a variable battery DC voltage to three phase AC voltage of the grid (Fig. 4.4.a). The PCS100 ESS is an energy storage system converter product from ABB, it allows active (P) and reactive (Q) power set point control over Modbus TCP/IP. The PCS100 ESS converters used in the BESS employ IGBT's and integral sinusoidal filters, as seen in Fig. 4.7. The  $\Delta/\Delta$  coupling transformer (350V/11kV) is used to connect the power converter to the grid (Fig. 4.4.b).



(a)





(b)

Fig. 4.4 Block diagram (a) and photo (b) of the 968kWh//2MW WESS plant.

### 4.2.1 Battery Pack Information

The SCiB Lithium-Titanate rechargeable batteries provided by Toshiba offer superior performance in terms of reliability, relatively long cycle life and rapid recharging capability compared to other Li-ion technologies at the time of writing. The specifications of a SCiB battery cell and a module used in the project is given in Table 4.1. The Battery section consists of 40 parallel connected battery racks, each rack is composed of 22 battery modules series connected in order to form a string, each battery module is consisted of 24 cells in a 2P12S (2 cells in parallel and 12 series strings). Therefore, there are total of 21120 cells (40racks x (22modules x 24 cells)) in the battery unit (see Fig. 4.5). The total capacity of BESS is ~968kWh (40 racks x (22modules x 1.1kWh)).

Table 4.1 The description of Toshiba SCiB cell and module used in the BESS project

SCiB™ Cell		
	Nominal Voltage	2.3V (Range: 1.5V-2.7V)
	Nominal Capacity	20Ah
	Energy Density	176Wh/L
	Dimension	115(W)x22(D)x103H
	Weight	515g
SCiB™ Module		
	Nominal Voltage:	27.6V (Range: 18V-32.4V)
	Nominal Capacity	40Ah/1.1kWh
	Dimension	359(W)x187(D)x124(H)
	Weight	14kg
	SCiB Cell 2P12S	
	CMU (with CAN I/F)	

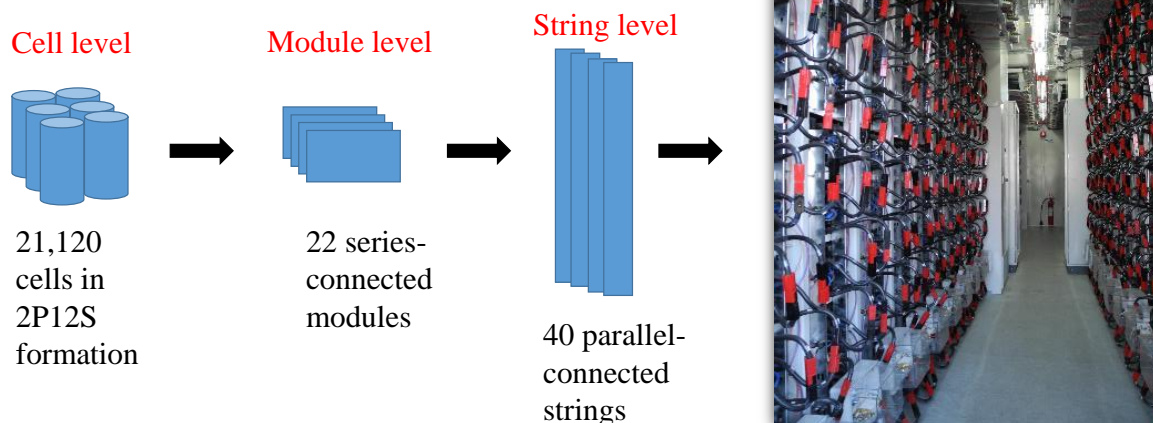


Fig. 4.5 Battery pack design in WESS.

Each battery rack consists of 22 battery modules (nominal 1.1kWh/module), for a total of 24.2kWh/rack, where the nominal DC voltage is 607.2V with its available DC voltage range from 475V to 712V. According to the Toshiba battery tender specification provided for UoS, the required minimum DC voltage is 550V, this is due to a restriction on the minimum voltage of the ABB converter. Hence, the batteries are used from the 550V to 712V, which lies in the SOC range from 30% to 100%. Since the SOC range has a marginal allowance of around 30%, therefore a relatively longer battery life time can be expected.

#### 4.2.2 Power Converter Control

In the WESS project, there are total 24 ABB PCS100 converters with 2MW power capability, as seen in Fig. 4.6. Physical and schematic diagram of the power converters used are shown in Fig. 4.7. BESS operates in Current Source Inverter (CSI) mode and the operational inverter control system with 2MW charge is shown in Fig. 4.8.



Fig. 4.6 Photos of 24 x ABB PCS100 converter in WESS.

The CSI control mode provides benefits to large grids, whereby only positive sequence current is injected into the grid resulting in minimal ripple current in the DC storage. Being a current source, faster response is achieved as opposed to the virtual generator Voltage Sourced Inverter (VSI) mode. CSI operates in bi-directional P/Q power flow control (P/Q setpoint-fixed power) (see Fig. 4.8) and provides fast sub-cycling current response to a change in P or Q command. Demanded power level will be generated or absorbed from the grid with respect to actual batteries SOC and batteries power limits.

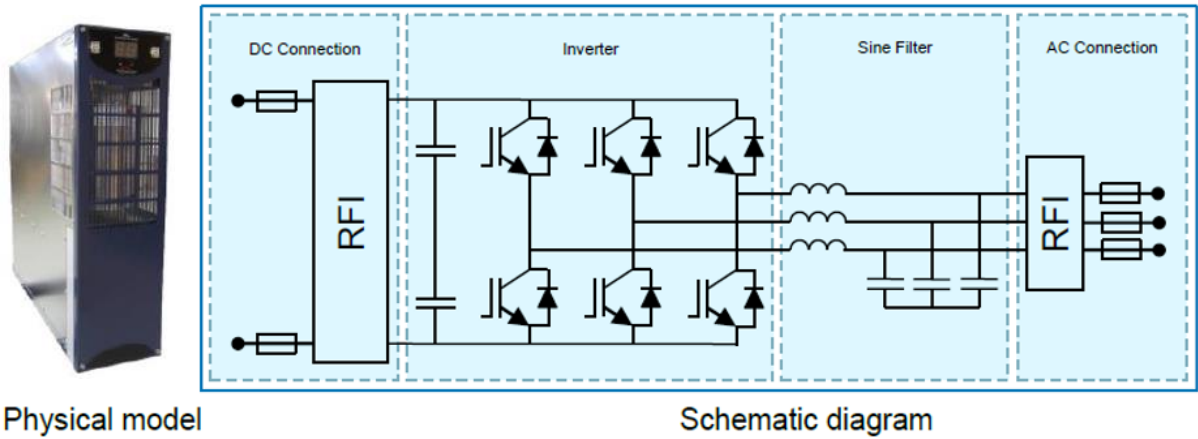


Fig. 4.7 Diagram of power converter used in WESS.

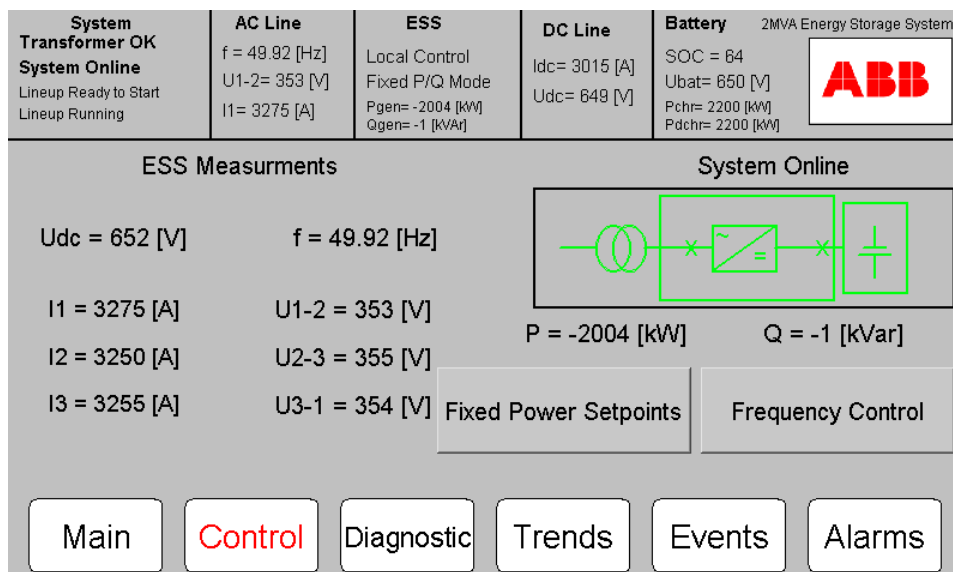


Fig. 4.8 WESS- 2kW charge in converter.

### 4.2.3 Transformer

In the WESS, a 2.1MVA isolated transformer is used to connect the 2MW ABB PCS100 power converters (Fig. 4.6) with 350kVac voltage output to the 11kV AC grid [FEE16], as shown in Fig. 4.4.a. The picture of 2.1MVA transformer used in WESS is illustrated in Fig. 4.9.



Fig. 4.9 A 2.1 MVA transformer used in WESS.

### **4.3 WESS Grid Scale Applications**

The WESS facility aims to examine the effects of energy storage on the grid, allowing experiments into response times for fast frequency response and other grid support functions. WESS provides grid frequency regulation services to the NG, such as SFR and DFR frequency response services. Such services help balance the grid and will become increasingly valuable as more intermittent renewable generation comes on to the system. WESS facility allows research to be conducted at a power levels commensurate with industrial installations thus allowing the UK's power sector to observe the viability of energy storage for peak power buffering and grid stability and reinforcement provision at realistic levels and to assess both economic and technical potential of such systems [ONL19c]. Possible future grid scale applications providing by the WESS can be frequency [GUN17b], [GUN18a], [GUN18b], and voltage control [FEE16], energy arbitrage [GUN17b], [GUN19], peak shaving [FEE16], Triad Avoidance [GUN18b], and trading in the balancing energy market.

## 4.4 WESS Experimental Results

In this section, in order to experimentally validate the performance of the proposed EFR and DFFR control algorithm implemented in 1MW/1MWh BESS model, the WESS utilized as a test bed, described in this chapter.

### 4.4.1 Experimental Verification with WESS for EFR-A1 Control Algorithm

In order to experimentally validate the performance of the standard EFR control algorithm implemented in BESS model, WESS was utilised as a test bed. Fig. 4.10 and Fig. 4.11 show a comparison of the results obtained from the developed EFR-A1 and the real WESS, responding to grid frequency deviations through the EFR service for a 12-hour operation period for 21st Oct 2015. The figures show that the model is representative of the real system with a RMSE of 0.19% and a MAPE of 0.31% for SOC. The slight variances in power are explained by a small difference in SOC at the boundaries of the SOC target band, meaning that each system will chose a different EFR envelope line to use.

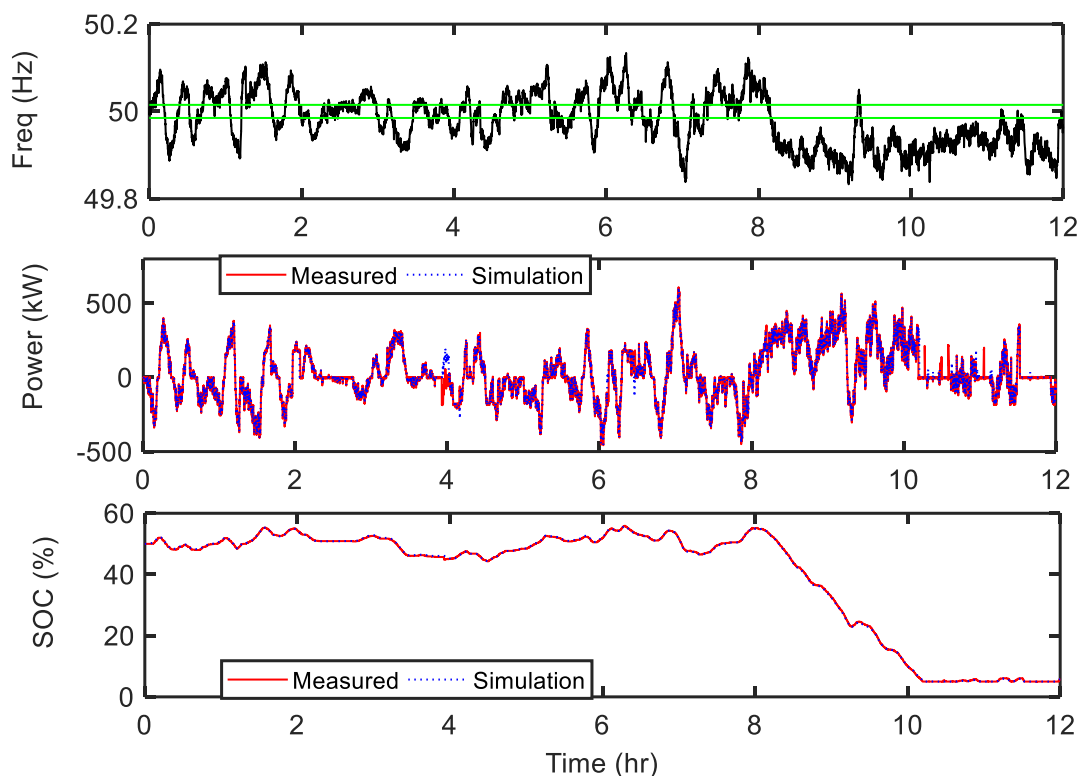
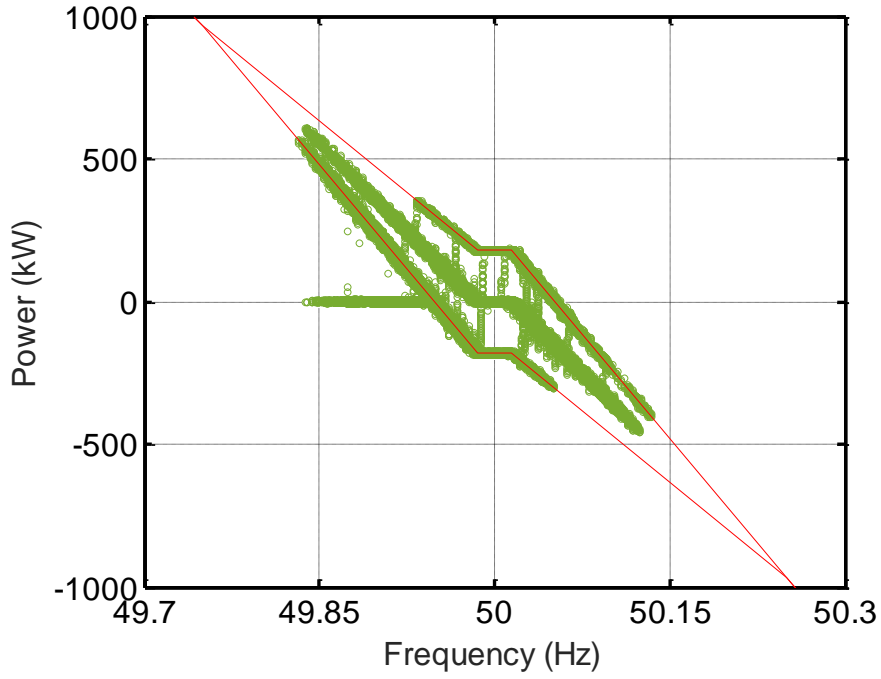
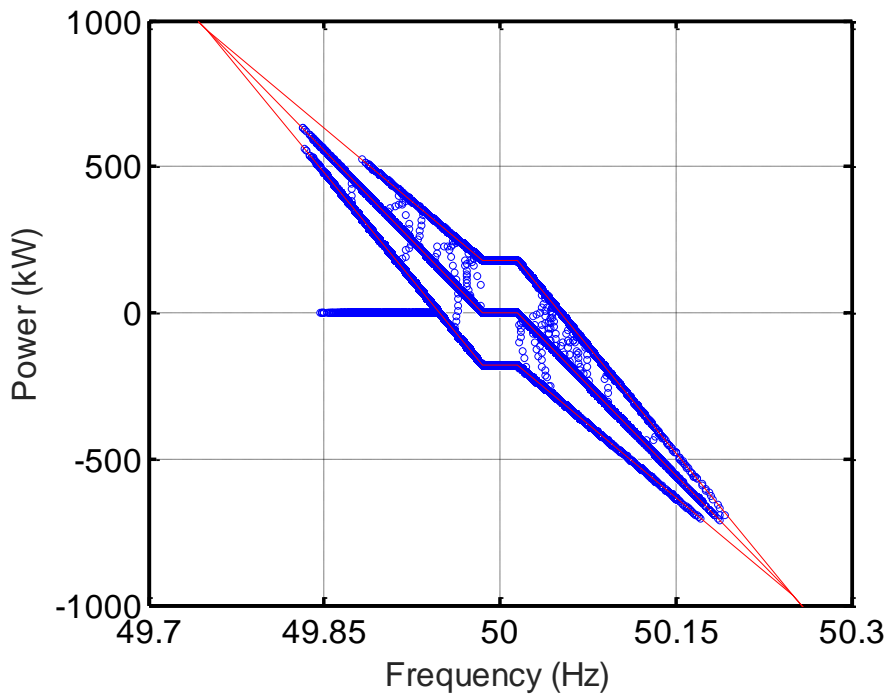


Fig. 4.10 Comparison of the experimental and simulation results obtained on EFR-A1 for 21<sup>st</sup> Oct 2015 (first 12 hours) frequency data.





(a)



(b)

Fig. 4.11 EFR power versus frequency plot for (a) measured and (b) simulation using EFR-A1 for 21<sup>st</sup> Oct 2015 (first 12 hours) frequency data.

Small deviations can be accounted from the increased losses in the experimental system when compared to the model operating at very low power (<100kW). This is due to the operational efficiencies of the inverter being outside of its optimised operating range. It should also be

noted that WESS is configured with an operational SOC band of 5-95%. Fig. 4.11 presents the delivery envelope of the proposed control algorithm for both simulation and experimental using EFR-A1. The comparison of experimental and model findings indicates that the proposed EFR control algorithm shows a good performance with <4.5% and ~0.3% of MAPE power and battery SOC for the 12-hour period in 21st Oct.

Table 3.23 Energy output findings of EFR-A1 (simulation) and experimental WESS (measured) for 21<sup>st</sup> Oct 2015 (first 12 hours data)

	<b>Import/Charge (kWh)</b>	<b>Export/Discharge (kWh)</b>
<b>Measured</b>	569.5	741.3
<b>Simulation</b>	558.5	758

#### 4.4.2 Experimental Verification with WESS for DFFR Control Algorithm

Fig. 4.12 compares the results attained from the 1MW/1MWh BESS model developed in MATLAB/Simulink and the real WESS, responding to grid frequency deviations through the DFFR service for 12 Oct 2016 frequency data. The figure shows that the DFFR control algorithm is representative of the real system with a RMSE of 0.71% and MAPE of 0.5% for battery SOC and a RMSE of 29.5kW and MAPE of 3% for power.

However, the sampling time set is 25ms in the both real WESS and simulated BESS model, it can be observed from Fig. 4.12 there is a slight shifts between the measured and simulated grid frequency due to the sampling time error in the grid frequency (RMSE frequency error= 0.0136Hz). As a result this unmatched frequency causes a significant error in battery SOC and especially in power output. In addition, small deviations can be accounted from the increased losses in the WESS experimental system when compared to the BESS MATLAB model operating at very low power (<100kW), as especially seen from the night time period of the power and SOC plots in Fig. 4.12. This is because of the inverter operation efficiencies being outside of its optimised power range. It is also observed that the inverter efficiency of the real battery system shows variations in different power ranges during the operation. The inverter achieves >97% efficiency when operating above 70% rated power, however this efficiency falls with lower power. The comparison of experimental and simulation findings indicates that

the proposed DFFR control algorithm shows a good performance with 0.71% and 29.5kW of RMSE SOC and power error for 12 Oct 2016 frequency data, respectively.

The power versus frequency plot of the experimental WESS and simulated BESS model for 12 Oct 2016 is shown in Fig. 4.13 and Fig. 4.14, respectively. The red line represents the NGET required DFFR power line. It can be seen that the FFR power does remain within the envelope and hence this does not cause a penalty in SPM.

As shown in the energy output findings of the DFFR algorithm having no SOC management and experimental WESS, there is only a small difference between the measured and simulated energy (see Table 4.2); hence the results are like suggest that the model and simulation method is appropriate.

Table 4.2 Energy output findings of DFFR Algorithm with no SOC management (simulation) and experimental WESS (measured) for 12 Oct 2016

	<b>Import/Charge (kWh)</b>	<b>Export/Discharge (kWh)</b>
<b>Measured</b>	1052	792.5
<b>Simulation</b>	1048	779

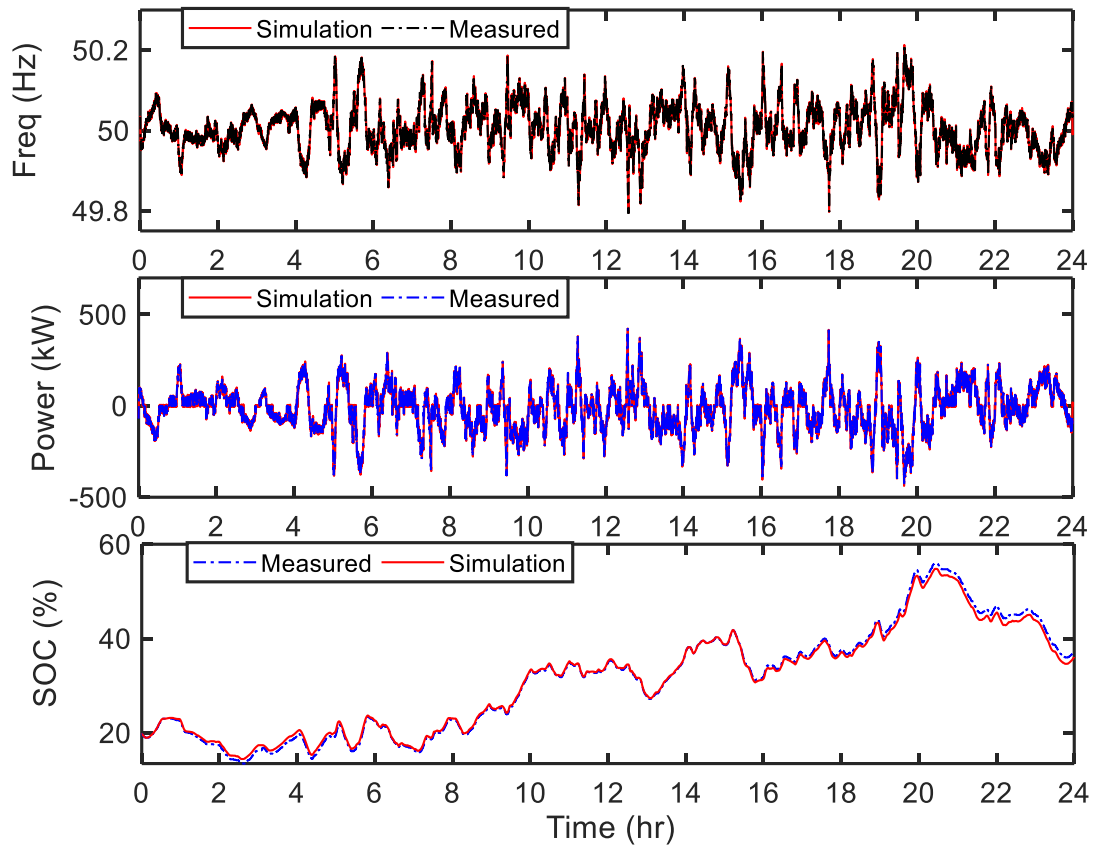


Fig. 4.12 Comparison of the experimental and simulation results of DFFR control algorithm for 12 Oct 2016 frequency data.

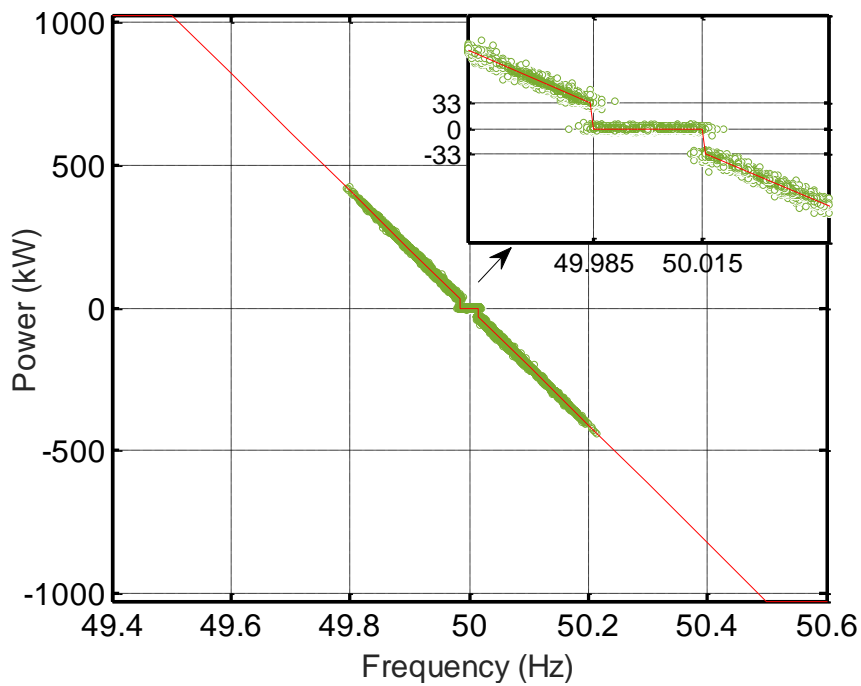


Fig. 4.13 Power versus frequency plot of measured DFFR algorithm with no SOC management for 12 Oct 2016 frequency data.

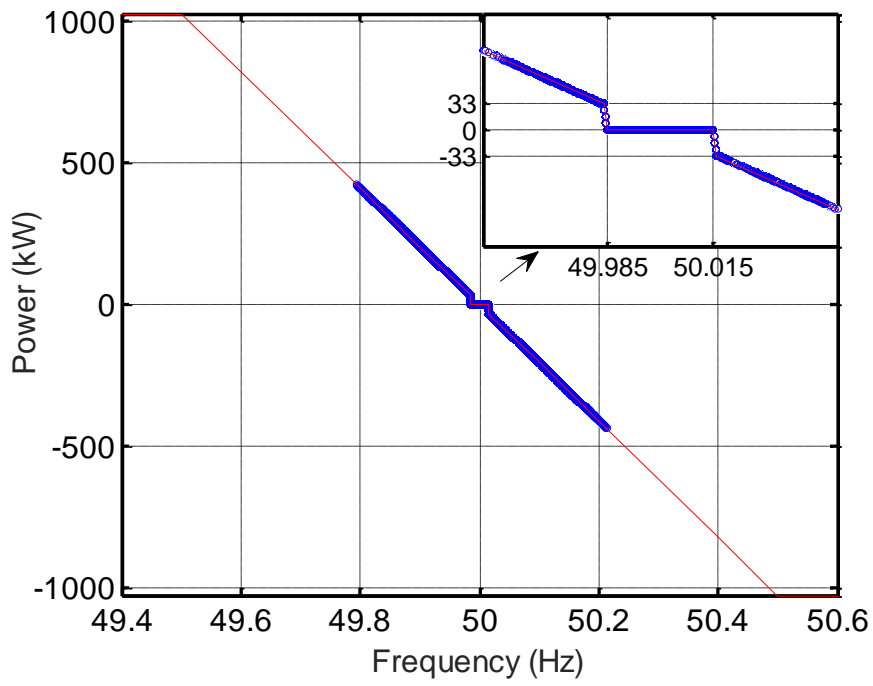


Fig. 4.14 Power versus frequency plot of simulated DFFR algorithm for 12 Oct 2016.

## 5 Lifetime Analyses of BESS Operating in Grid Frequency Regulation

In this chapter, a new fast battery cycle counting method (CCM) for grid-tied BESS operating in frequency regulation is presented. The methodology provides an approximation for the number of battery full charge-discharge cycles based on historical microcycling SOC data typical of BESS frequency regulation operation. The proposed basic fast CCM is then improved by modifying it to group cycles by current C-rate, SOC and DOD. Using the existing Miner Rule's degradation analysis method, a lifetime analysis using the CCM is carried out to provide a comparison between LTO and NMC batteries for grid scale batteries. The FFR and EFR control algorithms, developed in Chapter 3 in this thesis, are used for the analysis. Finally, it is proposed how the CCM grouped metrics (C-rate & SOC) could be used with experimental data to provide a more accurate prediction of SOH.

### 5.1 Introduction

Battery degradation is inevitable during usage and is a significant issue for applications requiring long life. Battery ageing leads to a deterioration in battery performance, electrically this is observed as an increase in resistance and decrease in capacity. As these are important features in any application it is necessary to understand how these change with lifetime of the battery. Furthermore, it is essential to identify how a battery management strategy can be implemented to minimize battery degradation under varying usage conditions.

There are several factors affecting battery aging, such as C-rate, temperature, accumulated ampere-hour throughput, SOC range and DOD range. To extend battery lifetime by optimising its operating conditions, it is important to understand the impacts of these factors on battery aging [GAO18].

Numerous studies have been carried out for the degradation behaviours of li-ion batteries under different conditions. The research studies [GAO17], [MON15] examine the long-term effects of C-rate and charging cut-off voltage on battery degradation. The reference studies [OUY15], [SOM16] demonstrate that charging at a high C-rate or low temperature induces lithium plating, which will cause the rapid deterioration of battery capacity. With respect to the impact of SOC, the average SOC and the changes of SOC ( $\Delta$ SOC) or DOD are the two important aspects [SAX16]. Most of the studies agree that the battery aging rate rises with the increasing of DOD

[WAT14], [ECK14], [WAN14]. The reference studies [SAX16], [HOK13] demonstrated that the capacity degradation range is faster when the battery is cycled around a high mean SOC. Research in [GAO18] is beneficial to the optimal usage of SOC range to increase battery lifetime, also gives to understanding the degradation inconsistency of batteries in a pack caused by the SOC inconsistency.

Battery lifetime degradation caused by charge/discharge cycles, calendar life, operating temperature and DOD is still relatively unknown for different types of power applications [EIC13], [NEJ15], [NEJ16]. Similar to other storage applications, BESS cells have a rated life that is typically determined by the total number of deep battery charge-discharge cycles before reaching 80% of the initial capacity [ALA16]. This percentage of current capacity against initial capacity is referred to as the SOH and an estimation of SOH plot against full charge-discharge cycles is often given by manufacturers (an example given in Fig. 5.11). The difficulty in cycle counting for BESS operation in frequency regulation is the presence of irregular charge-discharge cycles of varying SOC. These microcycles (small cycles of <5% within a main charge-discharge time history) that exist in a SOC profile for a given period of time need to be interpreted to estimate the total battery cycle information, which then can be used to approximate the associated degradation of the BESS and provide a battery lifetime analysis [ALA16], [LUT15], [CER05]. It should be noted that other factors such as charge-discharge rate and temperature should also be considered to give an accurate estimation of SOH. This chapter only focuses on the cycle count approximation based on battery SOC, C-rate and DOD. In literature, an approximation technique, called “Rainflow Cycle Counting Method” (RCCM) has been applied to battery cycle counting, it can also be used for fatigue analysis [MAT68], lifetime assessment of power semiconductor switches [RED15], BESS life degradation analysis for frequency regulation [CHA10] and BESS sizing [TAN13]. A comparison of the proposed fast counting method and the conventional RCCM [AMZ94] is presented as following;

- 1) The RCCM [AMZ94] can only be applied to extreme points (peak and valleys), and hence the load data is transformed to a dataset with only peak and valley information, furthermore, it cannot be applied to real time data [MUS12]. However, this chapter introduces a fast cycle counting method (CCM) that approximates the number of full cycles a battery has endured for frequency response delivery. The change in the SOC is measured for each sample point, one second in the case of the data presented in this chapter. The CCM algorithm then considers

each positive and negative value as up (charge) and down (discharge) indexes, independently. The sum of all up and down indexes forms the charging data set and the discharging data set respectively. The proposed cycle estimation method processes all of the stored data and can be applied to real time data logged from a BESS.

2) In the RCCM, half-cycles are counted only at the end of data. Therefore, it is difficult to calculate remaining useful life in between the load points [MUS12]. In the proposed CCM method, as the data is processed, if either the battery charging data set or discharging data set reach 100%, the half charge or half discharge cycle counts are incremented, independently. A full equivalent cycle is determined as the average of the battery charge and discharge cycles for the given period of time. This means that, the number of full equivalent cycles are estimated during the analyses rather than at the end of the data set. Therefore, it is simple to approximate remaining useful life in between the load points.

3) In the RCCM, the calculation of mean temperature is independent of the time period [GOP15], however this is out of scope for this thesis.

According to *Xu et al.* [XU18] electrochemical batteries have limited cycle life due to the fading of active materials caused by the battery charging and discharging cycles. This cycle aging is mainly caused by the growth of the cracks in the active materials that is a similar process with fatigue in materials subjected to cyclic mechanical loading. Heuristic battery lifetime models [XU18] assume that battery degradation is caused by various stress factors, each of which can be represented by a stress model acquired from experimental data. The effect of these stress factors change with the battery degradation type. It is convenient to divide those stress factors into two groups based on whether or not they are directly affected by the way a grid-tied battery is operated [XU18]:

- 1) Operational Factors: Over charge, over discharge, C-rate, cycle depth and SOC.
- 2) Non-operational Factors: Ambient temperature, calendar time, battery state of health.

Cycle Depth: Cycle depth is a key factor in a battery's degradation, and is the most important component in the battery energy storage dispatch market. For instance, a 7Wh NMC battery has been demonstrated to perform more than 50,000 cycles at 10% cycle depth, producing a lifetime energy throughput (i.e the total amount of energy charged and discharged from the cell) of 35kWh. If the same battery cell is cycled at 100% cycle depth, it has only been demonstrated



to perform 500 cycles, producing a lifetime energy throughput of only 3.5kWh [ECK14], [XU18].

Over Charge and Over Discharge: In addition to battery cycle depth effect, extreme battery SOC levels significantly decrease battery life. However, overcharging and over discharging can be avoided by applying lower and upper limits on the SOC either in the dispatch or by the BESS management control [XU18].

Current Rate (C-rate): C-rate defines how fast a battery is charged or discharged. Charging at high C-rate induces lithium plating, which will result in the rapid deterioration of battery capacity [GAO18].

Average State of Charge: Evaluating the degradation of a battery cycled under various SOC ranges is important for the optimal control of operational SOC range. The battery aging rate increases with greater changes of SOC ( $\Delta$ SOC) [GAO18].

Temperature: Temperature is a major aspect in battery performance, shelf life, charging and voltage control. The rated capacity of a battery is based on an ambient temperature of 25°C (77°F); any variation from this operating temperature could alter the performance of the battery and shorten its expected lifetime. In this thesis, it is assumed that the battery is always being operated at an ambient temperature of 25°C as a BESS maintains the temperature of the cells in a controlled environment.

According to *Swierczynski et al.* [SWI13a] li-ion based BESS are attractive for stationary energy storage applications and in this paper the business case is investigated. In [SWI13a] the lifetime of an LFP based BESS, desirable owing to long calendar and cycle lifetime and intrinsic safety, was analysed when utilised for PFR service on the Danish electricity market. A semi-empirical lifetime model of the LFP battery cells was developed based on the findings of laboratory accelerated lifetime testing. The economic viability of the PFR service is studied showing it to be profitable with a great Net Present Value (NPV). However, it is shown that a significant impact on the NPV of the investment is the BESS lifetime. It is possible to improve the BESS lifetime through management of idling SOC and hence increase the NPV, but this needs a detailed lifetime model and knowledge about the Li-ion aging behaviour.

*Stroe et al.* [STR17] investigated from the Li-ion based BESS lifetime point the sustainability of five methods for providing the PFR service and re-establishing the SOC of the BESS. It was

demonstrated that the proposed approach has a significant impact on a system's lifetime; for the proposed PFR delivery and system's SOC re-establishing approaches, the expected lifetime of the Li-ion BESS varied between 8.5 and 13.5 years. From the analysis, it was concluded that Strategy-A (i.e. symmetrical participation in both down- and up-regulation markets and system's SOC re-establish immediately after each grid frequency event passed) is a less appropriate method for PFR service delivery. In addition, by analysing the impact of the cycle depth and temperature on the expected lifetime of the BESS, the authors concluded that it is the temperature and not the cycle depth which shows a greater impact on batteries lifetime diminish when delivering the PFR service.

In [SWI14], a methodology for the selection of the most appropriate ESS technology for integration with Wind Power Plants (WPPs) was presented. The methodology relied on the selection of ESS technology candidates with the lowest annual accumulated cycle cost for a specific ancillary service. PFR was studied in the paper for the presentation of methodology and it was revealed that li-ion batteries have the lowest annual accumulated cycle cost. In addition, they are advantageous due to their characteristics such as relatively long calendar lifetime, low self-discharge rate and decreasing cost. It is known that the Li-ion battery family is broad, however, the main focus of the paper is on LTO and NMC battery cells because they are suitable choices for grid integration, with both technologies providing high charge/discharge rates, relatively long lifetime, and high safety, which are important for renewable energy storage applications. In order to investigate the Virtual Power Plant (VPP) for different operating conditions, it is important to have accurate information about battery cell behaviour at all operating points. Therefore, in the paper, electrochemical impedance spectroscopy (EIS) based performance models of the LTO and LFP battery cells were also developed. The models are able to forecast the electrical characteristics of battery cells at different temperatures, SOC and SOH. Furthermore, it was revealed that the same configuration of the equivalent electrical circuit can be used for LTO and LFP cells, producing accurate results.

[STR16] dealt with the degradation behaviour of LFP battery cells when such batteries are used to deliver PFR in the Danish energy market. For achieving a reliable analysis, a lifetime model was developed for the considered battery cells and a field measured mission profile characteristics to the PFR application was examined. By implementing the PFR mission profile to the considered LFP battery cell lifetime model, it was revealed that the capacity is the

performance parameter that limited the considered LFP battery cells' lifetime and not the power capability. The major contribution to the estimated capacity fade caused from the calendar dimension; the calendar capacity fade was accelerated by the operation conditions that involve idling the LFP cell at a high SOC range. Therefore, the lifetime of the considered battery cell might be increased by reducing the idling SOC range to values lower than 90%; though this reduction in idling SOC range would decrease the revenues generated from the up-regulation service, because less power would be bid into the market. However, for the proposed field-measured PFR mission profile and with the existing PFR energy management method, the LFP cell would be able to meet the up-regulation service for a period of about 10 years before the EOL criterion would be reached.

In [THO13], three control methods of the Li-ion based BESS for delivering PFR were analysed and compared. All three methods were linked to high economic benefits, and they were exposed to the same scenario, regarding frequency profile and market data. The BESS's SOC profile is revealed to have a significant influence on the outcome. An example was demonstrated in [THO13], the first control method in the paper had the highest profits in the first year, however the NPV for his method was the lowest. This is because the nature of this method; i.e larger degradation owing to more substantial DODs. Accordingly, the estimated NPV for the second and third method in the paper were greater and associated with lower DOD characteristics. The price for PFR up-regulation service are greater than the down-regulation. This shows that higher revenue for the PFR service can be generated, by bidding for more PFR up-regulation than down-regulation generation; causing the SOC set-point to be increased (originally 50% in the paper). The disadvantage by doing so is a shorter battery lifetime, because higher SOC intervals accelerate the batteries degradation. Findings from prior study [SWI13b] were used to determine the relation between cycles and cell capacity degradation at various SOC ranges for the LFP batteries. It was revealed that the benefits were not increased by higher SOC ranges, as suggested, conversely, the benefits did increase by decreasing the SOC set-point. A lower price value for batteries, and different price relation between up-regulation and down-regulation, could affect these outcomes. Therefore, SOC management should be influenced more from a lifetime point of view than increasing income revenues.

Aiming to attain a serviceable and economical BESS, a battery sizing strategy was developed in [VEN09], focusing on peak demand shaving in a residential power distribution feeder with a PV system. However, in the study the lifetime analyses of BESS is considered and estimated

in the sizing procedure. *Yang et al.* [YAN14] presented a novel method to solve the above issues. The BESS usage, lifetime and system performance in terms of battery sizing were analysed on the developed distribution power system under different PV penetration levels.

According to *Gee et al.* [GEE13], combining two or more ESSs provides the beneficial attributes from each device to be used. The aim of the study is to utilize the high cycle life of supercapacitors in a supercapacitor/battery hybrid ESS to improve battery lifetime. The work demonstrated that the active hybridization of supercapacitors and batteries can yield an improvement in the overall ESS power handling. It is revealed in [GEE13] that a supercapacitor-battery hybrid has higher overall system efficiency, lower battery costs and a general increase in battery life. The work also presents a new approach to quantify the potential increase in battery cycle lifetime owing to the addition of supercapacitor ES, and presents a means of system implementation and analysis.

This chapter introduces a fast CCM for a grid-tied BESS, operational in grid frequency regulation, subjected to microcycles. The proposed CCM is then improved by considering only C-rate, then considering both C-rate and SOC and after that considering the DOD effect on the battery lifetime. In this chapter, all frequency response control algorithms developed in Chapter 3 are simulated to produce battery SOC data for a given time period using historical frequency data, these are then used to demonstrate the battery cycle counting estimation algorithm. Finally, this chapter quantifies the microcycling in terms of full cycles to aid in the approximation of the degradation of a battery and the battery lifetime analysis using the Miner's Rule method.

## **5.2 Review on CCMs and Battery Degradation Methodologies**

This section investigates the type of cycle counting methods and the battery degradation methodology, called Miners' Rule Method, used in this thesis. For better understanding, battery terminologies and characteristics have been introduced in 1.4.1.

### **5.2.1 CCMs**

The lifetime of the battery is strongly affected by the number of charge/discharge cycles [TAN13]. The method in this thesis for estimating the battery lifetime is shown in Fig. 5.1. The BESS power is characterised by various microcycles with different magnitudes during the operation of grid support services such as ancillary services. Some microcycles are not

completed full cycles; as discussed in the introduction they can be considered as half cycles by using an appropriate method, i.e the RCCM.

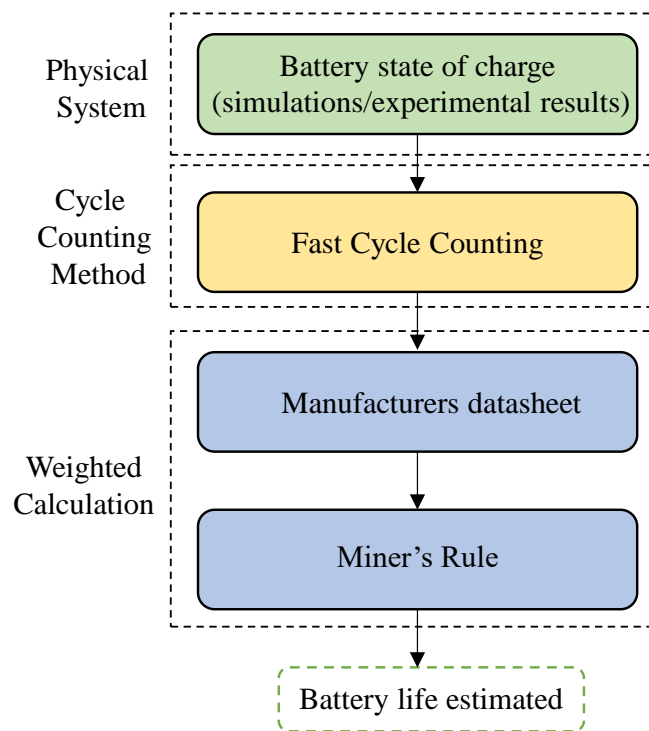


Fig. 5.1 Proposed battery lifetime estimation process.

To estimate the life of a component subjected to a variable amplitude load history, cycle counting techniques are applied to reduce the complex load history into a number of events. The well-known cycle counting methods are 1) Peak counting, 2) Hayes method, 3) Level counting, 4) Simple range counting and 5) Racetrack method. The most common cycle counting technique, The RCCM, has gained much interest as it provides the average value and has minimal relative error [MAI11]. The conventional RCCM first developed by Matsuishi and Endo [MAT68] is derived from the rain flowing (dripping) off the pagoda roofs [GOP15].

A BESS operating in grid support applications such as grid frequency regulation, energy arbitrage, triad avoidance etc. experiences a SOC evaluation which does not typically have a regular cycling pattern. Therefore, a cycle counting algorithm has been used in this chapter to identify the equivalent number cycles experienced by the battery for every possible DOD under such operational conditions. RCCM is traditionally used in mechanical engineering for the fatigue analyses of components under cyclic stress [AMZ94]. The RCCM can also be used for battery lifetime estimation [SCH09], [BEL12]. The reference study [BEL16] implemented the

RCCM algorithm in Matlab to determine the number of cycles experienced by the batteries operating as an ESS in the PV power plant.

According to *Nuhic et al* [NUH13], the RCCM is also used in the work for SOC cycle counting, to count e.g how often the battery SOC jumps from one value to another and vice versa. If the time axis in Fig. 5.2 is rotated by 90° in a clockwise direction, then the dotted lines on the left side of the curve arise at its maximum (horizontal curve's view), flow to its next minimum ( $\overline{AB}$ ) and drop down. Rainflows from a higher maximum source interrupt rainflows from a lower maximums ( $\overline{CB'}$ ). In addition, a rainflow is stopped when it meets a maximum or minimum (horizontal view) that is beneath the starting rainflow source ( $\overline{BC}$ , because the minimum at D is beneath the starting minimum). A half cycle is counted between a maximum and minimum of one line,  $\overline{EF}$  in Fig. 5.2. This has to be done also for the right of the curve, only that now sources are the minimums (horizontal curve's view). The resulting cycle is a combination of two half cycles from the left and right side of the curve, with the same maximum and minimum values. In Fig. 5.2, these are A-D-G, E-F-E' and B-C-B', and the counter will be increased only for the correspondent classes 1-7, 2-5 and 4-6.

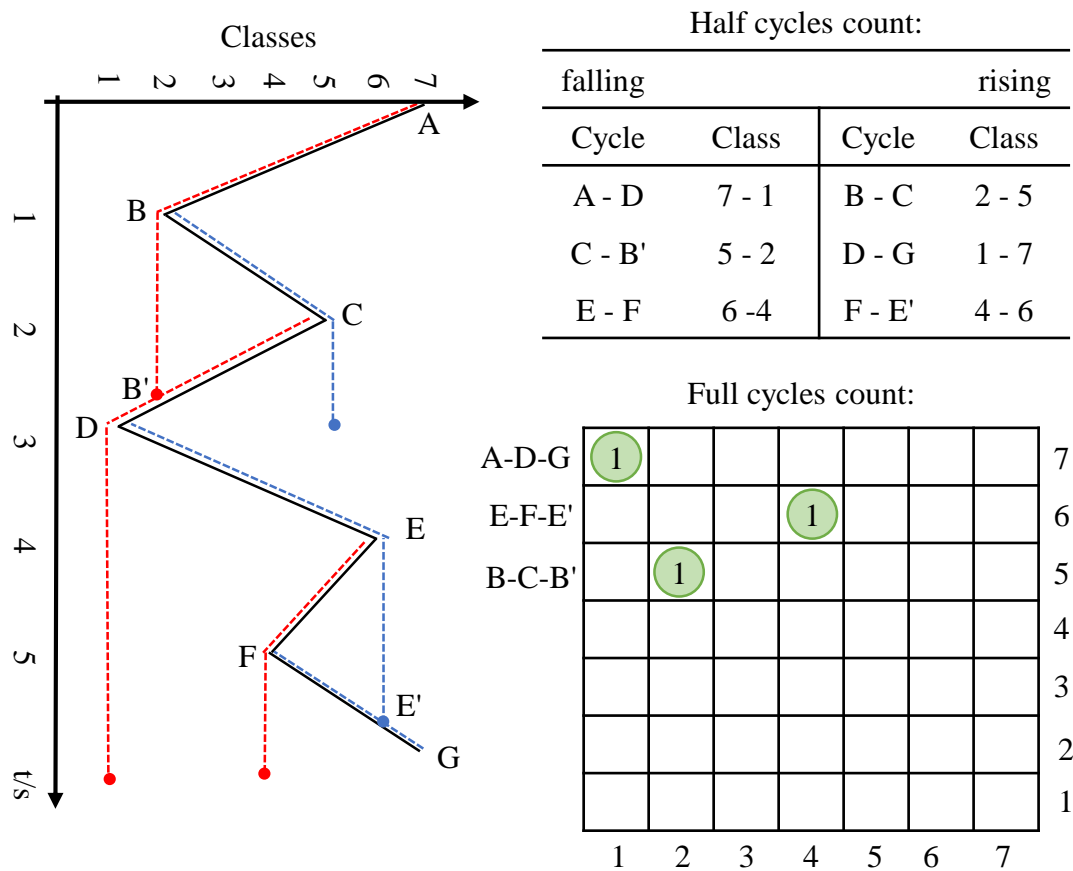


Fig. 5.2 Demonstration of Rainflow cycle counting in [NUH13].

According to *Chawla et al.* [CHA10], every charge-discharge cycle causes degradation, qualitatively. Fig. 5.11 shows an example plot of the number of cycles as a part of the sub-cycle DOD amplitude for the LTO battery. For instance, if a battery typically generates 600-700 cycles at 100% DOD, it will generate many more cycles at a lower DOD. It can be said that a battery which has a life of X with 100% DOD cycles and proportionally larger life with smaller depth cycles, would generate more than 2X number of cycles of 50% DOD [CHA10].

A BESS response for grid frequency regulation contains random microcycling of varying C-rate and DOD making them complex. Therefore, RCCM is used in [CHA10] to transform these complex cycles into simple sub-cycles, where two fundamental assumptions were made:

- 1) A complex cycle can be decomposed into a set of equivalent, simple sub-cycles of different DOD and amplitude;
- 2) The aging from the combination of sub-cycles is cumulative and can be summed up from the individual sub-cycle effects.

One cycle is described as a complete charge-discharge from/to the same point, either SOC or DOD can be used for this analysis. In [CHA10], both SOC and DOD were used interchangeably. More detail about the demonstration of the RCCM algorithm used can be found in [CHA10]. Each sub-cycle introduces a certain degradation in the LTO battery, based on the partial DOD cycle data in Fig. 5.11 [ONL18y]. Degradations due to the different DOD sub-cycles are added and this provides the total degradation of the battery over the considered profile.

## 5.2.2 Battery Degradation Analyses Methodology

As discussed in the introduction, research has been carried out on the degradation analysis of the different types of batteries. The contributing factors mostly investigated are: the number of cycles experienced, the charge and discharge rates, the operational temperature, the DOD of the cycles, the available SOC of the battery, the total processed energy and the end of charge voltage. In this chapter, three degradation factors, the number of cycles experienced during operation and their DOD, SOC and C-rate, are considered.

Once the number of cycles is determined using the RCCM, it is compared with the cycling capacity curves of the various batteries, for a LTO battery (see Fig. 5.11). These curves obtained from the battery manufactures show the number of cycles that a battery can support

(before reaching EOL) for different DODs. The ageing experienced by the various batteries throughout the simulated year and the ratio of the battery lifetime that has been consumed can be estimated according to the Palmgren-Miner's rule with the equation (5.1).

$$Battery\ Degradation = \sum_{DOD=1}^{DOD=100} \frac{N_{cyc}(DOD)}{N_{max}(DOD)} \quad (5.1)$$

Where  $N_{max}$  is the number of cycles that the battery can withstand for each specific DOD, according to capacity evolution curves of the various batteries such as PbA and LTO (Fig. 5.11); and  $N_{cyc}$  is the number of cycles returned by the RCCM algorithm and experienced for each amplitude (defined by the DOD variable).

In practice, since the batteries are considered to be EOL when the ‘‘Battery Degradation’’ parameter given in equation (5.1) reaches a value equal to 1, the battery expected lifetime can be estimated, taking into account that the simulated period is equal to one month, as in (5.2):

$$Battery\ Lifetime = \frac{Length\ of\ simulated\ period}{Battery\ Degradation} \quad (5.2)$$

Therefore, this calculation can also be performed for the various types of batteries and for the different energy capacities considered.

### 5.3 A New Fast CCM Considering Various Effects on Battery Lifetime

A new fast CCM considering various effects, including C-rate, SOC and DOD, on battery lifetime for grid-tied BESS operating in grid frequency regulation is presented in this section. Firstly, the proposed CCM is described and demonstrated to count generic cycles. Then, the proposed CCM is improved by considering only C-rate effect and then considering both C-rate and SOC conditions on battery lifetime. Finally, the fast CCM considering DOD in partial charge and discharge cycles is developed in the last section. After that, the recovery discharge capacity versus number of cycles plot of the Toshiba SCiB LTO battery as shown in Fig. 5.11, Fig. 5.12 and the NMC battery (Fig. 5.13) will be used for lifetime analysis.



### 5.3.1 A Basic Fast CCM

The proposed fast CCM is demonstrated for a BESS delivering frequency response services (e.g EFR and FFR) to the grid. This service demands from the BESS irregular charge-discharge cycles of varying power caused by the real grid frequency variability as discussed in Chapter 3.

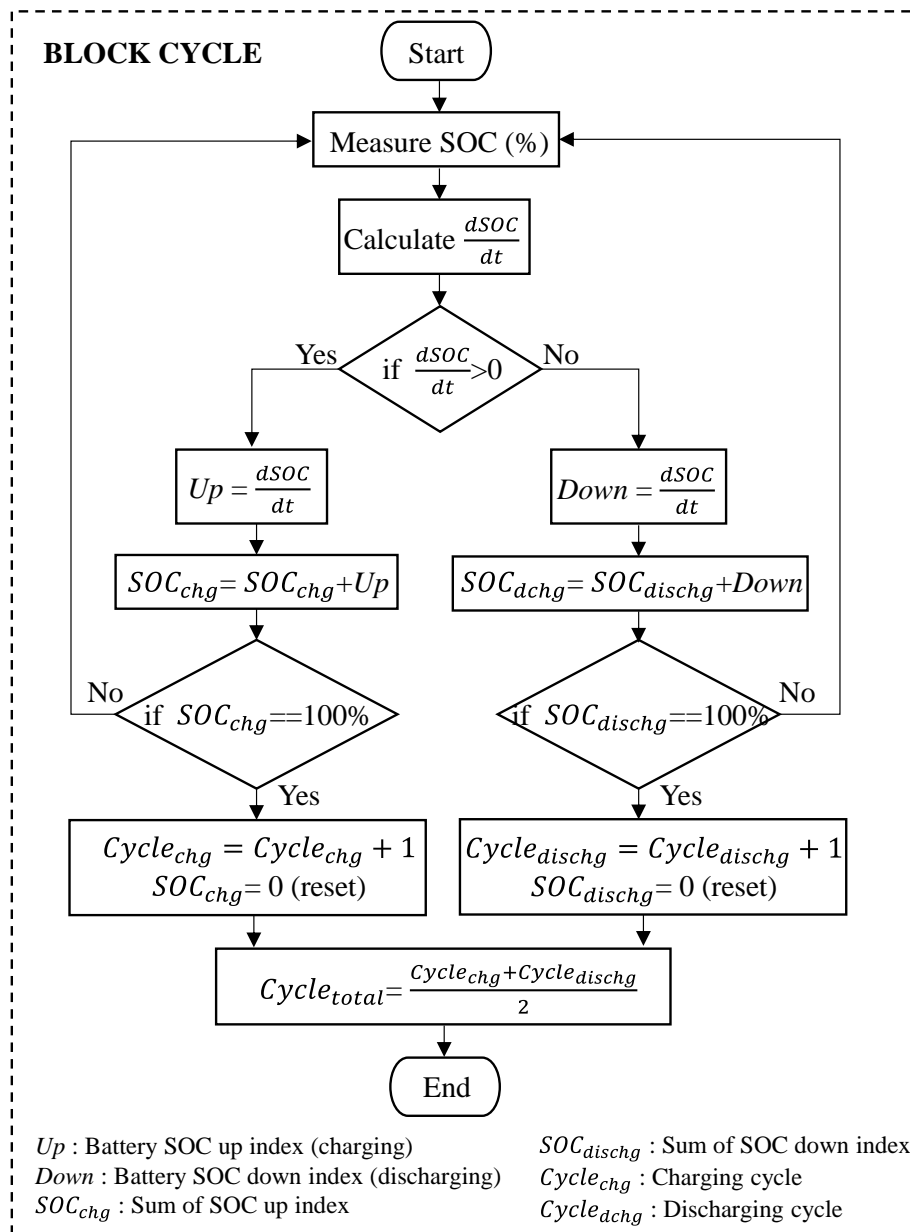


Fig. 5.3 Flow chart of the basic CCM for a grid-tied BESS subjected to microcycles.

The proposed basic fast CCM shown in Fig. 5.3 is used to approximate the number of full cycles a battery has endured using historical battery SOC data for EFR delivery. The method is described as following:

- The algorithm loops through the historical SOC data that has been previously obtained by simulating the EFR control algorithm over a period of time. In the first step, the change in battery SOC ( $dSOC/dt$ ) is extracted for each second by second. If  $dSOC/dt$  is greater than zero, the battery is charging; if it is less than zero, the battery is discharging; or if it is equal to zero, the battery is resting.
- The algorithm considers each positive and negative value of  $dSOC/dt$  as “Up” and “Down” indexes, respectively. In the second step (Fig. 5.3), the sum of all up indexes forms the battery SOC charging data set  $SOC_{chg}$  and the sum of all down indexes forms the battery SOC discharging data set  $SOC_{dischg}$ .
- In the third, during the simulation when each  $SOC_{chg}$  and  $SOC_{dischg}$  equals to 100%, the battery charge  $Cycle_{chg}$  and discharge cycle  $Cycle_{dischg}$  are incremented, independently. A full battery cycle  $Cycle_{total}$  is calculated as the average of battery charge and discharge cycles for the given period of time.
- The algorithm processes the SOC data recursively providing a total cycle count at the end.

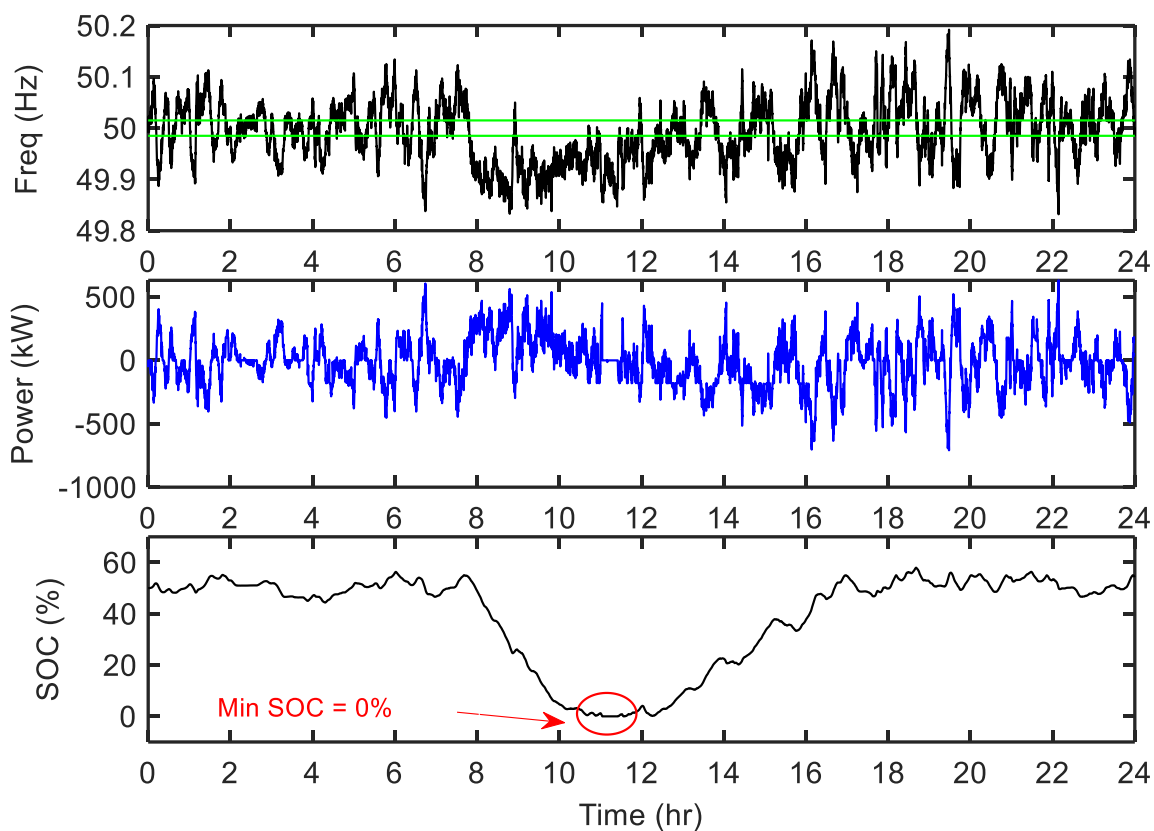


Fig. 5.4 Simulation results of EFR-A1 with Service-2 for 21st Oct 2015 frequency.

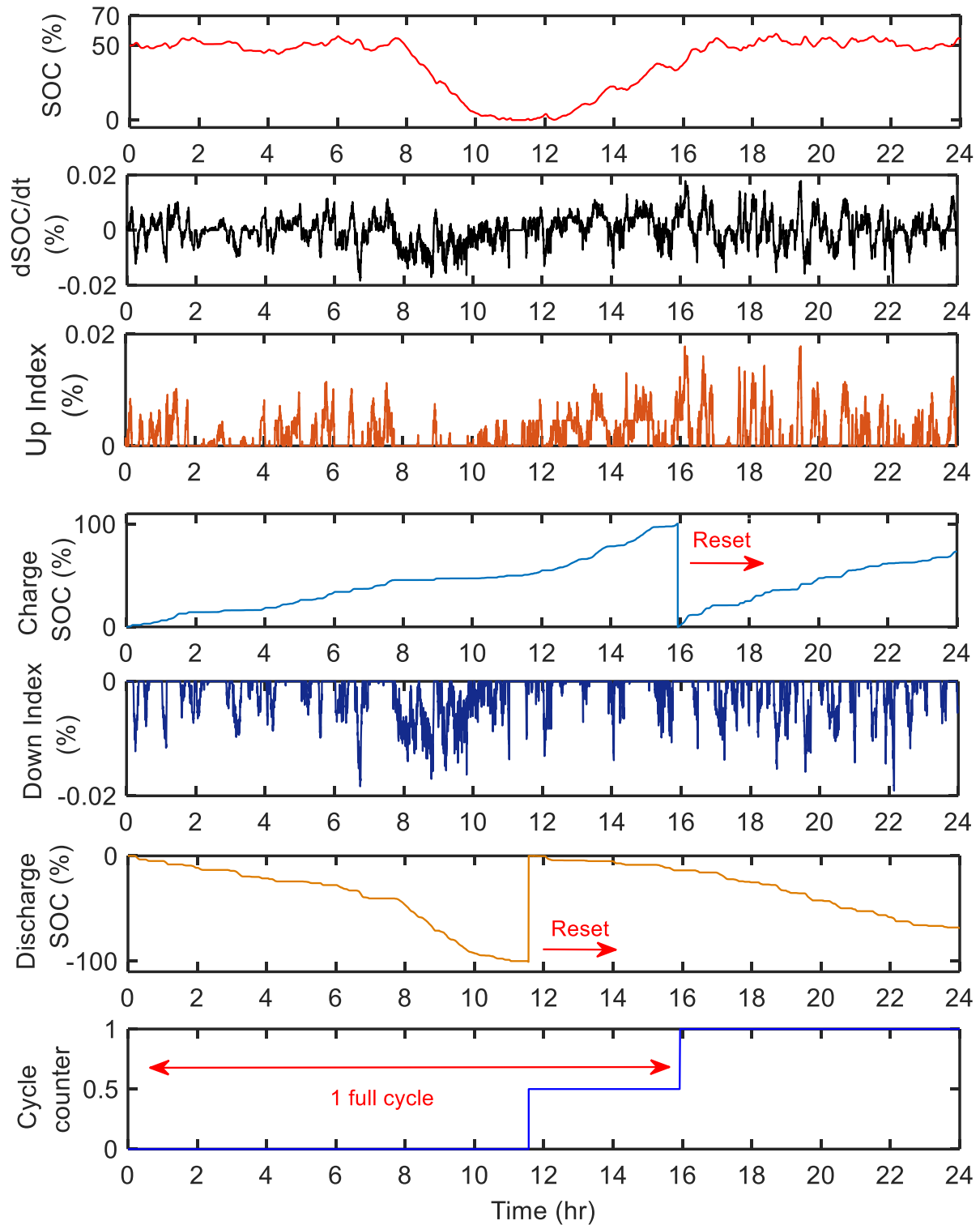


Fig. 5.5 Demonstration of the proposed fast basic CCM on a 24-hour profile of a battery SOC data set obtained by simulating the EFR-A1 for 21st Oct 2015 frequency data.

The operational principle of the proposed basic CCM is demonstrated on the 24-hour profile of a battery SOC obtained by simulating the EFR-A1 with Service-2 for the 21st October 2015 (Fig. 5.4). Using the proposed method in Fig. 5.3, it can be seen that one charging and one

discharging half-cycle is counted, hence in total one full battery cycle is obtained from 21st October 2015 as shown in Fig. 5.5.

### 5.3.2 Simulation Results of the Basic Fast CCM

In this section the considered frequency response control algorithms from Chapter 3 have been simulated in MATLAB/Simulink to achieve the output battery SOC data for use in analysing the proposed CCM algorithm. In order to demonstrate the performance of the proposed frequency response control algorithm, the real grid frequency data for the October 2015 [ONL18v] is used herein, which is a particular month that is known to have a large period of under frequency.

#### *A. Simulation Results of the EFR-A1, EFR-A2, EFR-A3, EFR-A4 and DFFR Algorithms*

The simulation results of the EFR–A1 and the DFFR control algorithm are shown in Fig. 5.6 and Fig. 5.8, respectively. The simulation results of the EFR–A2, EFR–A3 and EFR–A4 with different proportional gain values ( $K_p = 2000, 10000, 100000$ ) are shown in Appendix Fig. B.1, Fig. B.3, Fig. B.5, Fig. B.7 and Fig. B.9 in Appendix B.

According to Fig. 5.6, the EFR–A1 delivers to the EFR specification, whilst managing the battery SOC to the specified band of 45-55%. In the EFR algorithm it is possible to define two purposes for power flow in and out of the battery; the first is defined as that of charging/discharging the battery i.e power is requested in either direction for the sole purpose of managing the battery SOC and not for EFR; the second is import/export which defines when the BESS is performing a mandatory response to a grid frequency event.

According to the EFR–A2 simulation findings in Fig. B.1 in Appendix B, the algorithm covering the extended grid frequency event controller cuts the EFR power output after 15 minutes; as a result the BESS is 100% available for delivering power according to the EFR specification. According to the EFR–A3 simulation findings in Fig. B.3 in Appendix B, the algorithm covering the extended grid frequency event controller allows for the charge/discharge of the battery during the 30-minute rest period. The simulation results demonstrated that again, the BESS delivers 100% availability as similar with EFR–A2, however, the lowest SOC achieved with EFR–A3 (Fig. B.3 in Appendix B) is higher than that of EFR–A2 (Fig. B.1 in Appendix B). This is a significant achievement in terms of maximising the utilisation of the BESS stored energy.

Fig. B.5, Fig. B.7, Fig. B.9 in Appendix B show the simulation results of the EFR–A4 covering proportional controller with the proportional gain of ( $K_p = 2000, 10000, 100000$ ) set, respectively. It is clear from the simulation results, applying proportional controller in EFR–A4, the amount of EFR power delivered is relatively reduced without causing a BESS availability penalty in EFR service. Since there is no requirement to have full power changes as performed in EFR–A1 (Fig. 5.6), implementing proportional controller into the algorithm reduces the battery C-rate; hence this will increase the battery lifetime.

According to the DFFR simulation findings in Fig. 5.8, the algorithm delivers to the DFFR specification with the DB of  $\pm 15$  mHz. The DFFR algorithm with no SOC management only imports (buy) or only exports (sell) power from/to grid, responding to the grid frequency event. This means the DFFR algorithm does not allow the battery managing its SOC in the DB.

#### *B. Simulation Results of the Basic Fast CCM Algorithm for EFR and DFFR Service Delivery*

In this section, data analysis is carried out using the basic CCM algorithm described in Section 5.3.1 for a 1MWh capacity of grid-tied BESS in order to quantify the microcycling to the equivalent number of full charge-discharge cycles. Using the battery SOC data obtained by simulating the EFR–A1 and the DFFR control algorithm for the whole of October 2015, the proposed basic CCM algorithm is processed in MATLAB/Simulink with the results shown in Fig. 5.7 and Fig. 5.9, respectively. Using the battery SOC data obtained by simulating the EFR–A2, EFR–A3, and EFR–A4 with different proportional gain values ( $K_p = 2000, 10000, 100000$ ) for the whole of October 2015, the basic CCM algorithm is processed with the results shown in Fig. B.2, Fig. B.4, Fig. B.6, Fig. B.8, Fig. B.10 in Appendix B, respectively.

The basic CCM algorithm (Fig. 5.3) approximates the total number of equivalent full charge-discharge cycles experienced by the grid-tied BESS for EFR delivery in October 2015. As can be seen from the simulation results in Fig. 5.7, the average  $dSOC/dt$  is  $\leq 0.2\%$ , causing many microcycles due to the variability in the real grid frequency. The proposed fast basic CCM identifies and measures all microcycles for October 2015 as shown in Fig. 5.7. Following the next steps in the algorithm, if the changes in SOC are positive ( $dSOC/dt > 0$ ), the battery is charging or if those changes are negative ( $dSOC/dt < 0$ ), the battery is discharging. Therefore, by summing the charging ( $Up$ ) and discharging ( $Down$ ) indexes detected from the considered SOC data, 49 battery charging and discharging half-cycles are obtained independently,

approximating to a total of 49 battery full cycles. It can be seen from the analysis that this algorithm can be applied to larger SOC data sets or even applied in real-time. Comparing this, a total of 34 and 35 cycle is obtained by analysing the proposed cycle counting algorithm for October 2015; it can be said that based on cycling alone, EFR-A1 (Fig. 5.7) will tend to degrade the battery at a higher rate than EFR-A2 (Fig. B.2 in Appendix B) and EFR-A3 (Fig. B.4 in Appendix B). It can be seen from Fig. B.6, Fig. B.8, Fig. B.10 in Appendix B, a total of 21, 24 and 26 cycles are counted from analysing EFR-A4 by setting different gain values of  $K_p = 2000, 10000, 100000$  respectively. It is revealed that the higher  $K_p$  value set in the proportional controller in EFR-A4, the higher degradation rate in the battery because of the higher EFR power delivered to the grid responding to the grid frequency events. In addition, one year of data analysis is carried out using the basic fast CCM for all the considered frequency response control algorithms. Using the battery SOC data obtained by simulating the EFR-A1, EFR-A2, EFR-A3 and EFR-A4 with the proportional gain of  $K_p = 10000$ , and the DFFR control algorithm for the whole year of 2015, the basic CCM algorithm is processed for LTO and NMC batteries with the results shown in Table 5.1.

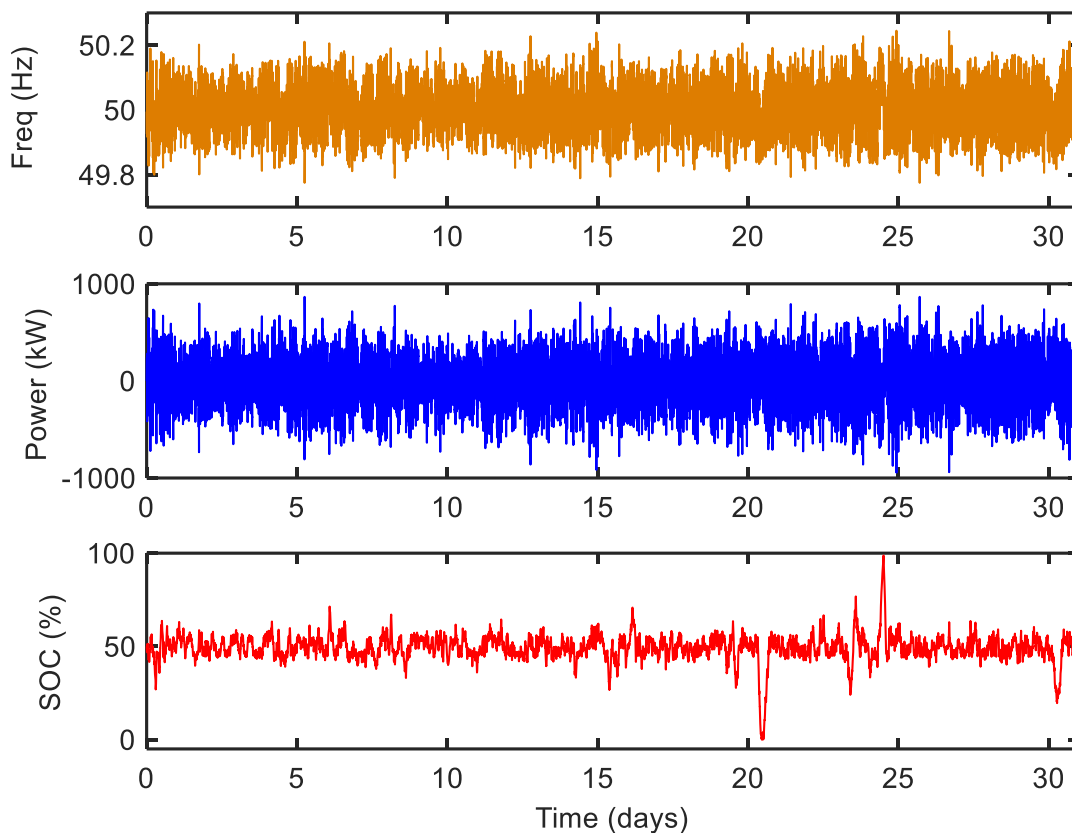


Fig. 5.6 Simulation results of the EFR-A1 with Service-2 for October 2015.

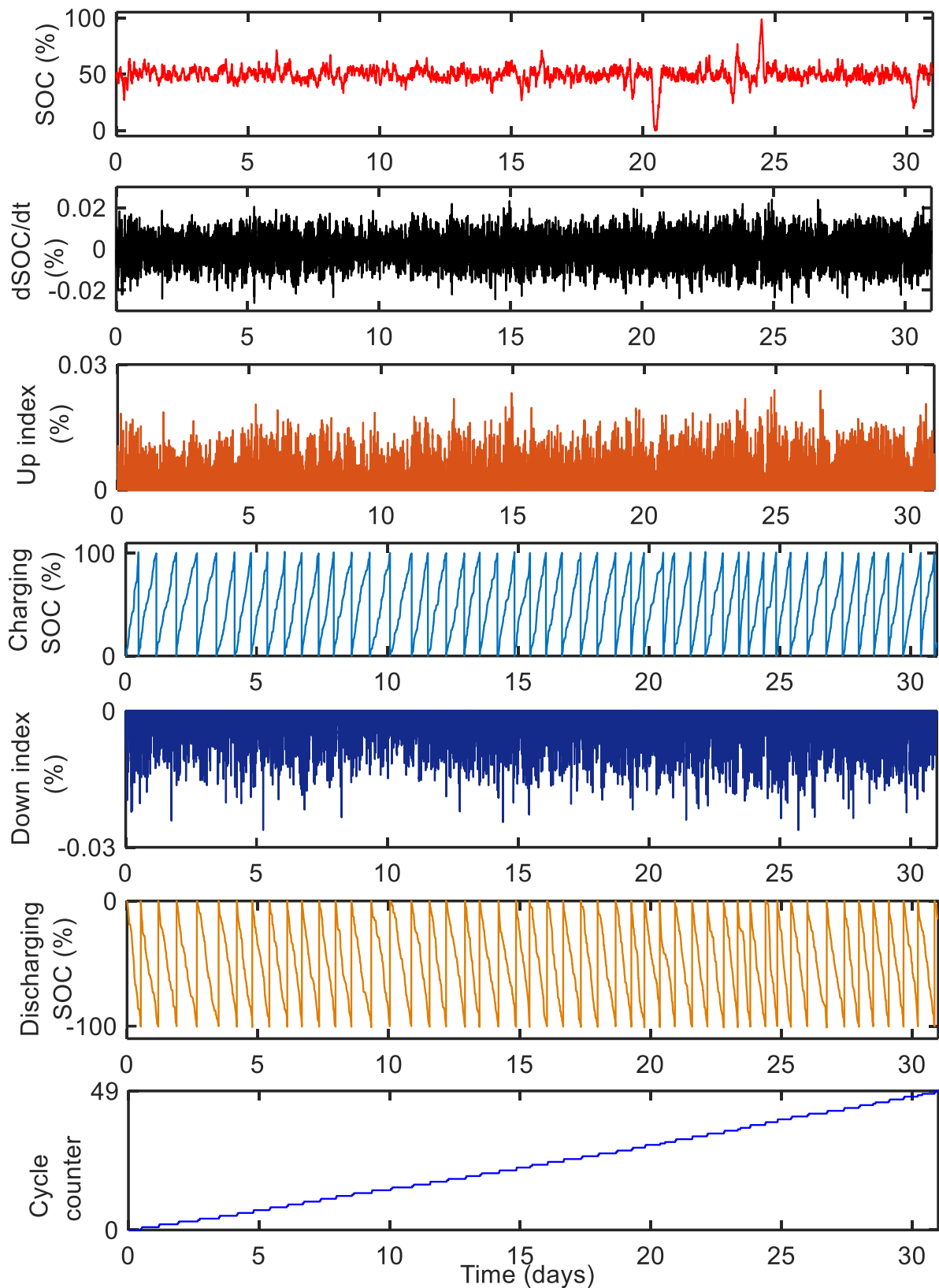


Fig. 5.7 Demonstration of the basic CCM on 1-month profile of a battery SOC data set obtained by simulating the EFR-A1 for whole October 2015 frequency data.

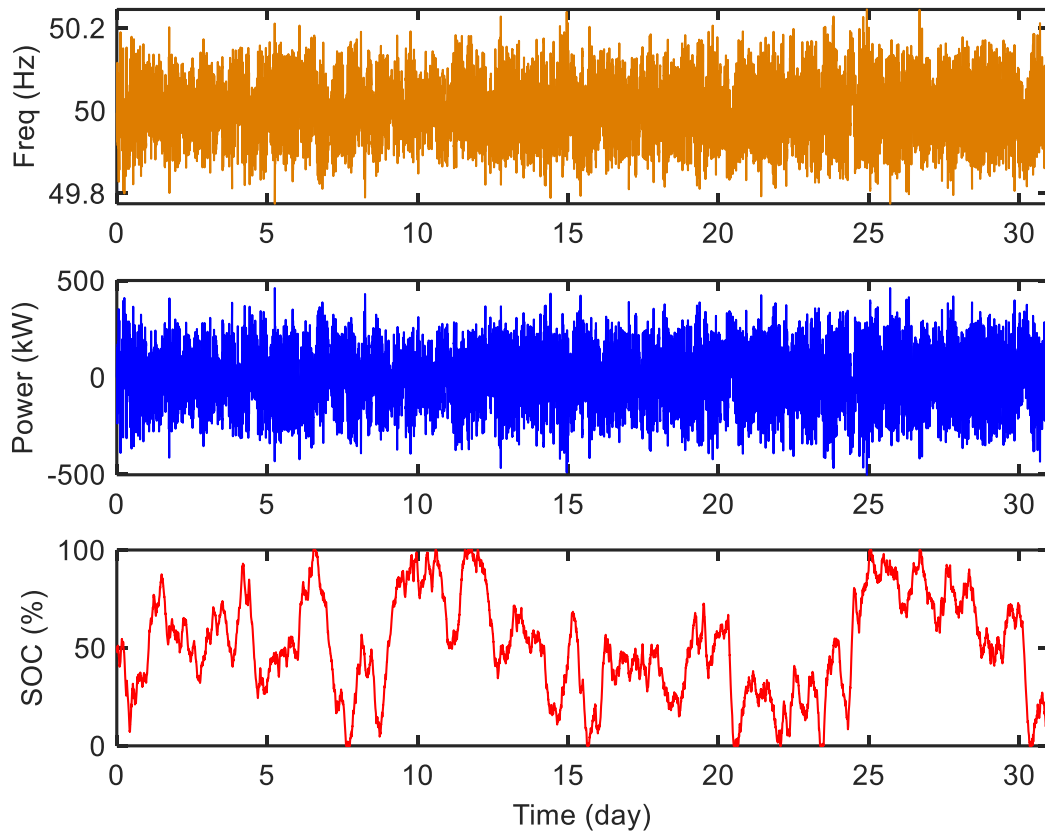


Fig. 5.8 Simulation results of the DFFR Algorithm for October 2015.

In this thesis, utilising the manufacturer cycling (12,000 cycles for LTO and 8,000 cycles for NMC battery) and the extracted number of cycles, the Miner Rule's method, described in 5.2.2 with the equations (5.1) and (5.2), is used for determining the degradation rate in the batteries. As seen from the cycle and degradation findings in Table 5.1, EFR-A1 degrades the LTO and NMC battery ~4.6% and ~6.9% in a year on EFR service operation, respectively. EFR -A4 setting  $K_p = 10000$  deteriorates the batteries much lower than EFR-A1, without getting a system availability penalty on delivering EFR service; this reduces the C-rate and hence increases the life time of the batteries. As seen from Table 5.1 and Table 5.2, the EFR-A2 and EFR-A3 degrade the LTO and NMC batteries at almost the same rate, but lower than that of EFR-A1.

Comparing with the EFR control algorithms, the DFFR algorithm delivers only half the amount (1MW) of dynamic power by the same capacity of battery (1MWh), however it degrades the batteries quite fast in a year under dynamic frequency response operation; because the algorithm cannot manage the batteries SOC in order to extend the battery lifetime.



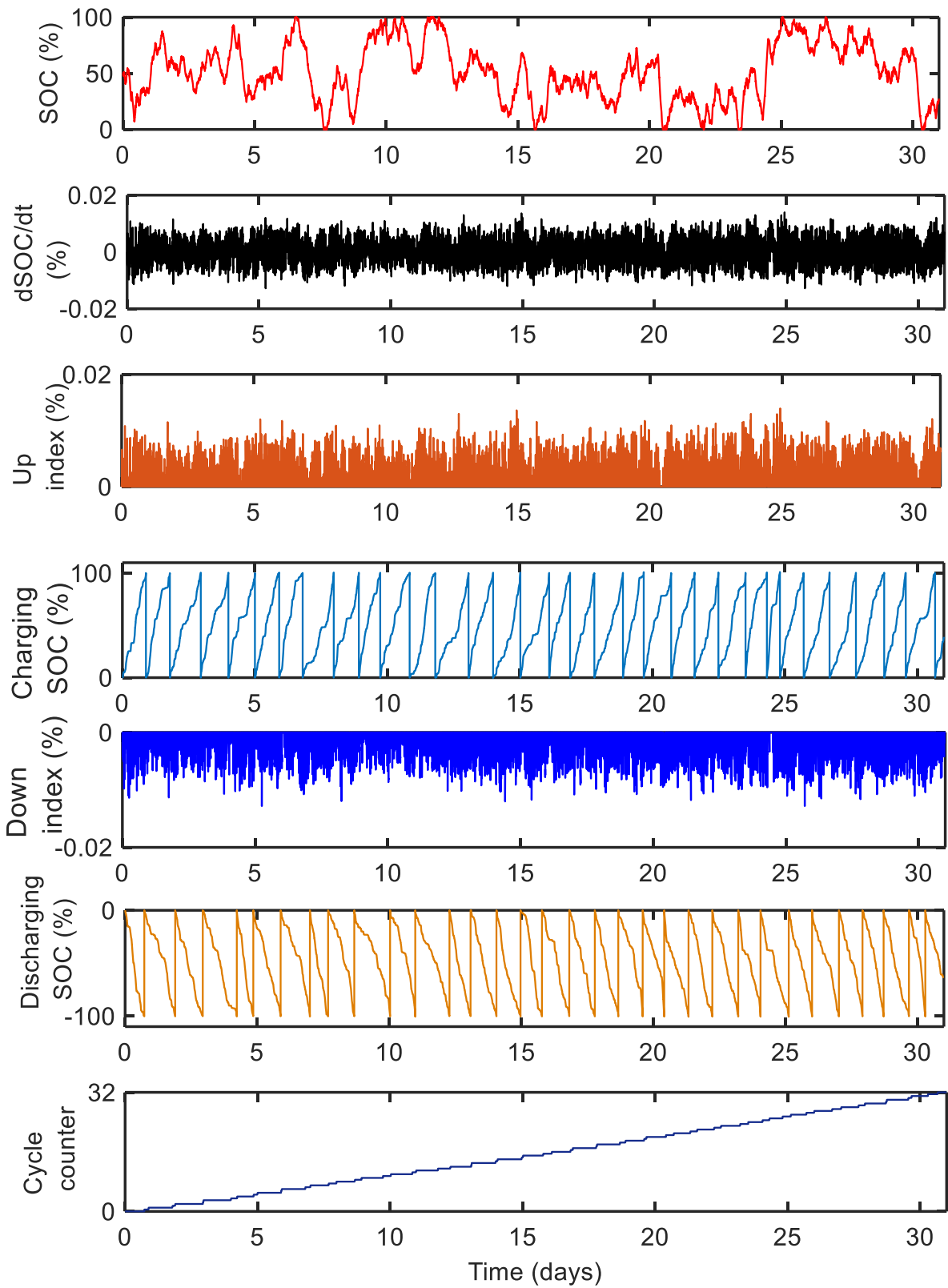


Fig. 5.9 Demonstration of the basic CCM on 1-month profile of a battery SOC data set obtained by simulating the DFFR algorithm for whole October 2015 frequency data.

Table 5.1 Cycling findings from the basic CCM and degradation rate findings from the Miner Rule's Method for LTO (manufacturer cycling=12,000 cycles) and NMC (manufacturer cycling=8,000 cycles) battery with all the considered frequency response algorithms for October 2015 (1 month data)

Frequency response algorithm	Total no of cycles (cycle)	LTO battery degradation (%)	NMC battery degradation (%)
EFR-A1	49	0.4083	0.6125
EFR-A2	34	0.2833	0.425
EFR-A3	35	0.2916	0.4375
EFR-A4 ( $K_p = 10,000$ )	24	0.2	0.3
DFFR	32	0.2666	0.4

Table 5.2 Cycling findings from the basic CCM and degradation rate findings from the Miner Rule's Method for LTO (manufacturer cycling=12,000 cycles) and NMC (manufacturer cycling=8,000 cycles) battery with all the considered frequency response algorithms for the whole year of 2015 (1 year data)

Frequency response algorithm	Total no of cycles (cycle)	LTO battery degradation (%)	NMC battery degradation (%)
EFR-A1	553	4.6083	6.9125
EFR-A2	375.5	3.1292	4.6937
EFR-A3	383.5	3.1958	4.7937
EFR-A4 ( $K_p = 10,000$ )	256	2.1333	3.2
DFFR	364	3.0333	4.55

### 5.3.3 Fast CCM considering only C-rate Effect on Battery Lifetime

In this section, the basic CCM described in 5.3.1 is improved by considering the effect of C-rate on battery lifetime analysis.

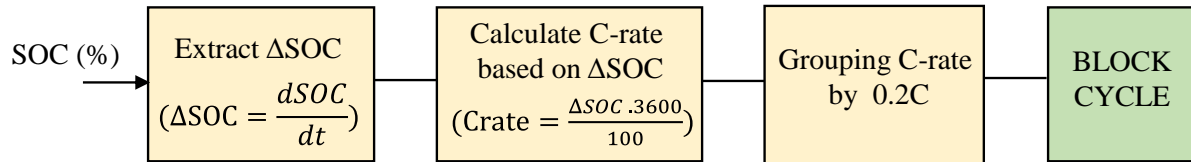


Fig. 5.10 Scheme of the fast cycle counting method considering C-rate effect.

The proposed method in this section as shown in Fig. 5.10 determines the number of charge and discharge cycles a battery subjected under different C-rate values grouped by 0.1C, 0.2C, 0.4C, 0.6C, 0.8C and 1C. The proposed CCM considering C-rate effect on battery lifetime is described as following:

- The algorithm loops through the historical battery SOC data attained by simulating the frequency response control algorithm over a period of time. In the first step, the change in battery SOC ( $dSOC/dt$ ) is extracted for each second by second.
- In second step, battery C-rate is calculated based on  $dSOC/dt$  ( $\Delta SOC$ ) as formulized in equation from (5.3) to (5.8). At this step, it is possible to calculate C-rate based on the amount of battery power, however it is revealed that using  $\Delta SOC$  for extracting C-rate provides more accurate results. At the end of this step, the battery C-rate profile is extracted for each second by second. In this chapter, the calculation of C-rate based on  $\Delta SOC$  is extracted from the following equations:

$$SOC(t) = SOC(t - 1) + \frac{1}{3600 \cdot Q} \int_{t-1}^t P \cdot dt \quad (5.3)$$

$$\frac{dSOC}{dt} (\%) = SOC(t) - SOC(t - 1) \quad (5.4)$$

$$\frac{dSOC}{dt} (\%) = \frac{1}{3600 \cdot Q} \int_{t-1}^t P \cdot dt \quad (5.5)$$

$$\Delta SOC(\%) = \frac{1}{3600 \cdot Q} \cdot P \cdot \Delta t \quad (5.6)$$

$$Crate = \frac{P}{Q} \quad (5.7)$$

$$Crate = \frac{\Delta SOC(\%) \cdot 3600}{100} \quad (5.8)$$

- In third step, the obtained C-rate data is grouped by 0.1C, 0.2C, 0.4C, 0.6C, 0.8C or 1C in order to determine the number of cycles at that point of C-rate. It should be noted that the C-rate data can be grouped by different scales as desired.
- In the last step, the algorithm approximates the number of cycles the battery subjected at each C-rate value over the period of time. This step has already described in Section 5.3.1 and its flow diagram (Fig. 5.3) is named as “Block Cycle” in the proposed cycle counting method considering C-rate effect in Fig. 5.10 (green block).

#### 5.3.4 Simulation Results of the Fast CCM considering C-rate Effect

In this section, data analysis is carried out using the fast CCM algorithm, described in Section 5.3.3 (Fig. 5.10), for a 1MWh capacity of grid-tied BESS in order to quantify the microcycling to the equivalent number of full charge-discharge cycles under different C-rate values. Using the battery SOC data obtained by simulating the frequency response algorithms (EFR and DFFR) for the whole of October 2015, the proposed fast CCM algorithm (Fig. 5.10) is processed in MATLAB/Simulink with the results shown in this section.

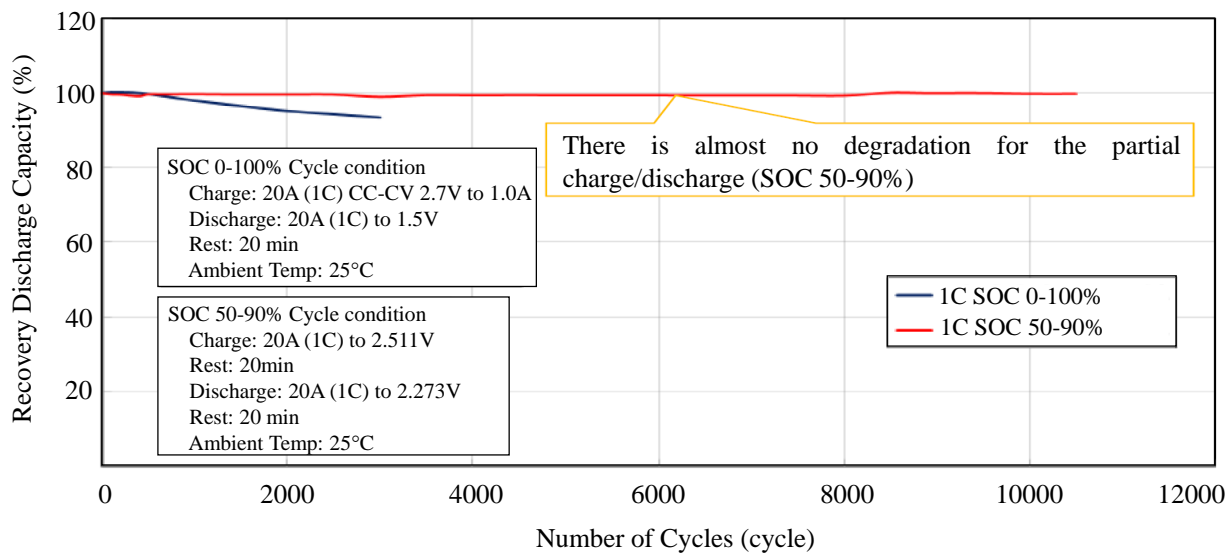


Fig. 5.11 Cycle characteristics of Toshiba SCiB LTO battery cell [ONL18y].

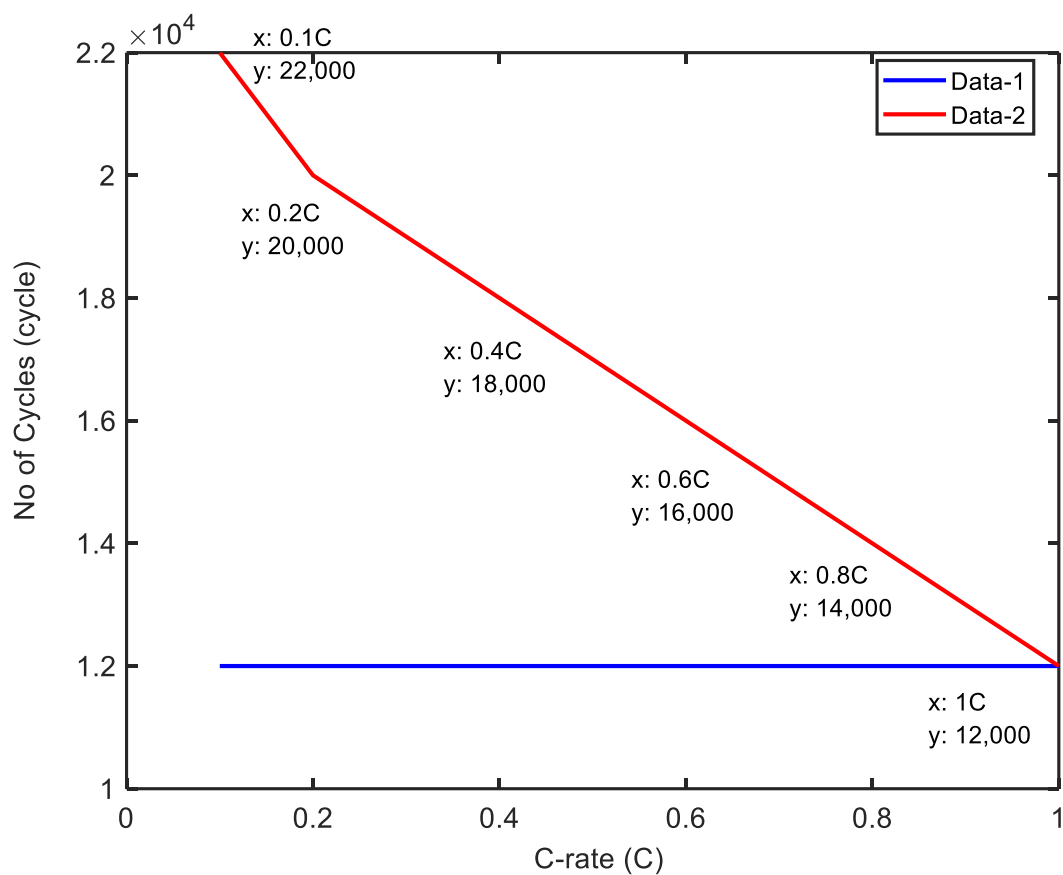


Fig. 5.12 LTO battery cycle characteristic assumed in this thesis.

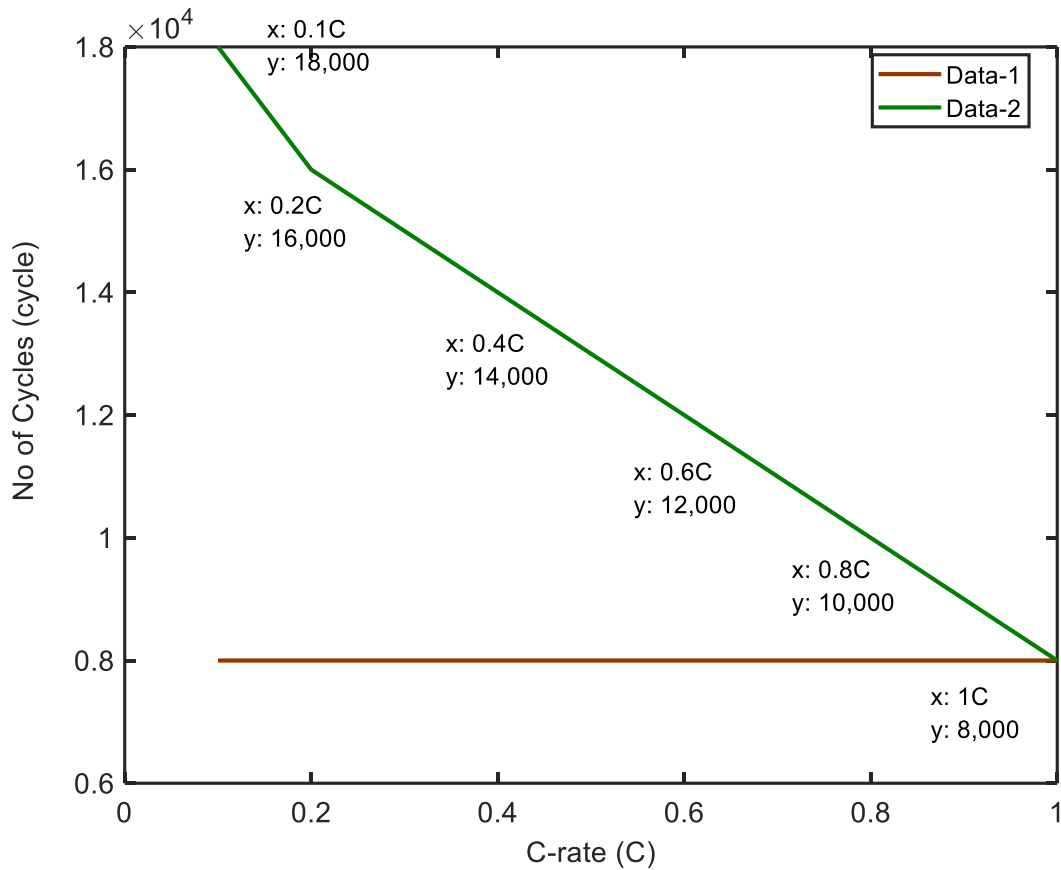


Fig. 5.13 NMC battery cycle characteristic assumed in this thesis.

In this section, using the battery SOC data attained by simulating the EFR-A1 for a ‘Service-2’ EFR for the whole of October 2015, the proposed CCM algorithm is simulated in MATLAB/Simulink in this section with the results in Table 5.3 and Table 5.4. The proposed algorithm determines the number of charge-discharge cycles experienced by the BESS operating in EFR service at each C-rate levels grouped by 0.1%, 0.2%, 0.4%, 0.6%, 0.8%, and 1% in October 2015. As previously mentioned in Section 5.3.2 (Fig. 5.7 and Table 5.1), the battery is subjected to 49 full charge-discharge cycles on delivering EFR service with the EFR-A1 in October 2015. Comparing this, in this section as seen from Table 5.3, the highest number of charge-discharge cycle occurs at the C-rate value of 0.2C to 0.4C with 20.23 cycles, and the second great number of cycle is obtained at 0.1-0.2C with 17.42 cycles. Therefore, it can be said that the battery spends most of its time in this operating region, therefore one could consider degradation rates associated with 0.1C-0.4C range (Table 5.3 and Table 5.4). The table shows that the number of cycle at higher than 0.8C is almost zero; this means that the battery rarely operates at higher C-rate (>0.8C) in October 2015; causing close to zero percent degradation in the battery during EFR service operation.

This chapter has two assumptions on the LTO and NMC battery manufacturer cycling data: in Data-1 it is assumed that the battery lifetime is 12,000 and 8,000 cycles for LTO and NMC battery for all the C-rate values; however in Data-2 it is assumed that the LTO and NMC battery lifetimes show variations for each grouped C-rate value, as shown in Fig. 5.12 and Fig. 5.13, respectively. The higher C-rate level, the lower battery cycling. Therefore, using the battery manufacturer's data and the extracted number of cycle at each C-rate grouped, the total battery degradation rate caused by BESS cycling under different C-rate values can be formulized as in equations (5.9) and (5.10) utilizing the Miner's Rule aging analysis method described in Section 5.2.2.

$$\text{Battery Degradation at each } C \text{ (\%)} = \frac{\text{No of Cycles at each } C}{\text{Maximum No of Cycles}} \quad (5.9)$$

$$\text{Total Degradation (\%)} = \text{Sum of Battery Degradation at each } C \text{ (\%)} \quad (5.10)$$

Table 5.3 Degradation findings obtained from the fast cycle counting method under different C-rate values for LTO and NMC battery with EFR -A1 for October 2015 frequency

<b>C-rate (C)</b>	<b>No of Cycles (cycle)</b>	<b>LTO degradation at each C-rate (%)</b>	<b>NMC degradation at each C-rate (%)</b>
C≤0.1	6.03	0.05	0.0754
0.1C < C-rate ≤0.2C	17.42	0.1452	0.2177
0.2C < C-rate ≤0.4C	20.23	0.1686	0.2529
0.4C < C-rate ≤0.6C	5.266	0.0439	0.0658
0.6C < C-rate ≤0.8	0.432	0.0036	0.0054
0.8C < C-rate ≤1C	0.02511	0.0002	0.0003
		Total LTO battery degradation (%): 0.4115	
		Total NMC battery degradation (%): 0.6175	

Table 5.4 Degradation findings obtained from the fast cycle counting method under different C-rate values for LTO and NMC battery with EFR -A1 for October 2015 frequency

C-rate (C)	No of Cycles (cycle)	LTO degradation at each C-rate (%)	NMC degradation at each C-rate (%)
$C \leq 0.1$	6.03	0.0274	0.0335
$0.1C < C\text{-rate} \leq 0.2C$	17.42	0.0871	0.1089
$0.2C < C\text{-rate} \leq 0.4C$	20.23	0.1124	0.1445
$0.4C < C\text{-rate} \leq 0.6C$	5.266	0.0329	0.0439
$0.6C < C\text{-rate} \leq 0.8$	0.432	0.0031	0.0043
$0.8C < C\text{-rate} \leq 1C$	0.02511	0.0002	0.0003
		Total LTO battery degradation (%): 0.2631	
		Total NMC battery degradation (%): 0.3354	

Using the constant battery cycling Data-1 for LTO (Fig. 5.12) and NMC (Fig. 5.13) battery, Table 5.3 shows that the total degradation rate caused by BESS cycling is determined as around 0.41% for LTO battery and 0.62% for NMC battery per month (October 2015). On the other hand, using battery cycling Data-2 which considers the cycling variable for each group C-rate level as seen from Fig. 5.12 and Fig. 5.13, the total degradation rate caused by BESS cycling is calculated as 0.26% for LTO battery and 0.34% for NMC battery per month. Comparing the results, there is a significant difference on the total degradation findings of the LTO and NMC battery in Table 5.3 and Table 5.4, this shows that the effect of C-rate on battery lifetime analysis should be considered for more accurate and sensitive lifetime analysis. Table 5.4 shows that the BESS participating in EFR service delivery is mostly operated at 0.2-0.4C with 20.23 cycles, causing 0.17% and 0.25% degradation in LTO and NMC battery respectively.

### 5.3.5 Fast CCM considering both C-rate and SOC Effect on Battery Lifetime

In this section, the CCM described in Section 5.3.3 is improved by considering the effect of C-rate and SOC on battery lifetime. The proposed CCM in this section approximates the number of complete battery charge-discharge cycles experienced by the grid-tied BESS under different



C-rate values grouped by 0.1C, 0.2C, 0.4C, 0.6C, 0.8C, 1C for each SOC range grouped by 10%, as shown in Fig. 5.14 .

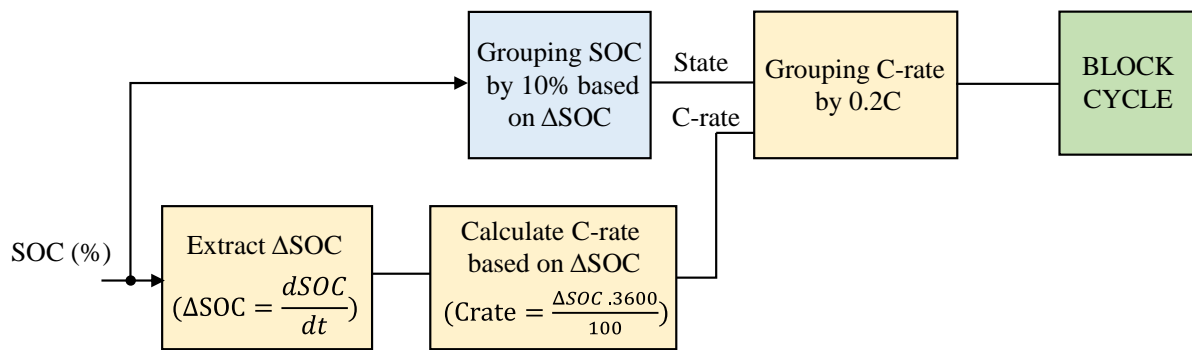


Fig. 5.14 Scheme of the fast CCM considering both C-rate and SOC effect on battery lifetime.

In this section, the proposed fast CCM considering C-rate and SOC effect on battery lifetime is described as following:

- The algorithm loops through the historical battery SOC data attained by simulating the frequency response control algorithm over a period of time. In the first step, the change in battery SOC ( $dSOC/dt$ ) is extracted for each second by second.
- In second step, battery C-rate is extracted for each second. In this section, the C-rate is calculated using  $\Delta SOC$ , as derived from the equations from (5.3) to (5.8). At this step, it is possible to calculate C-rate based on the amount of battery power, however it is revealed that using  $\Delta SOC$  for extracting C-rate provides more accurate results.
- In third step, the battery SOC is grouped by 10% to create a state for extracting the C-rate values at that point of the SOC; this step is shown in the blue block in Fig. 5.14.
- In the fourth step, the obtained C-rate data is grouped into groupings of 0.1C, 0.2C, 0.4C, 0.6C, 0.8C or 1C in order to determine the number of cycles at that point of C-rate.
- In the last step, the basic CCM algorithm, presented in Fig. 5.5 in Section 5.3.1, approximates the number of cycles the battery is subjected to at each C-rate value for each SOC range grouped by 10%. This basic cycle counting step is shown in the green 'BLOCK CYCLE' in Fig. 5.14.

### 5.3.6 Simulation Results of the Fast CCM considering both C-rate and SOC effect

For the battery lifetime analysis, it is assumed in this section that the LTO and NMC battery cycling data for each C-rate for each grouped SOC range is given in Table 5.5 and Table 5.6, respectively. Therefore, using the battery’s manufacturer cycling data and the extracted number of cycle at each C-rate for each SOC grouped, the total battery degradation rate caused by BESS cycling can be calculated as in (5.11) and (5.12) utilizing the Miner Rule’s aging analyses method described in 5.2.2.

*Battery Degradation at each C for each SOC (%)*

$$= \frac{\text{No of Cycles at each C for each SOC}}{\text{Maximum No of Cycles}} \quad (5.11)$$

*Total Degradation (%)*

$$= \text{Sum of Battery Degradation at each C for each SOC (%)} \quad (5.12)$$

Table 5.5 Cycling data assumed for LTO battery for each C-rate for each SOC range grouped.  
(for LTO battery)

		C-rate					
		0.1	0.2	0.4	0.6	0.8	1
SOC (%)	10	26,500	24,500	22,500	20,500	18,500	16,500
	20	26,000	24,000	22,000	20,000	18,000	16,000
	30	25,500	23,500	21,500	19,500	17,500	15,500
	40	25,000	23,000	21,000	19,000	17,000	15,000
	50	24,500	22,500	20,500	18,500	16,500	14,500
	60	24,000	22,000	20,000	18,000	16,000	14,000
	70	23,500	21,500	19,500	17,500	15,500	13,500
	80	23,000	21,000	19,000	17,000	15,000	13,000
	90	22,500	20,500	18,500	16,500	14,500	12,500
	100	22,000	20,000	18,000	16,000	14,000	12,000

Table 5.6 Cycling data assumed for NMC battery for each C-rate for each SOC range grouped.  
(for NMC battery)

		C-rate					
		0.1	0.2	0.4	0.6	0.8	1
SOC (%)	10	22,500	20,500	18,500	16,500	14,500	12,500
	20	22,000	20,000	18,000	16,000	14,000	12,000
	30	21,500	19,500	17,500	15,500	13,500	11,500
	40	21,000	19,000	17,000	15,000	13,000	11,000
	50	20,500	18,500	16,500	14,500	12,500	10,500
	60	20,000	18,000	16,000	14,000	12,000	10,000
	70	19,500	17,500	15,500	13,500	11,500	9,500
	80	19,000	17,000	15,000	13,000	11,000	9,000
	90	18,500	16,500	14,500	12,500	10,500	8,500
	100	18,000	16,000	14,000	12,000	10,000	8,000

Table 5.7 Number of cycles obtained from the fast cycle counting method considering SOC and C-rate effect for EFR-A1 for October 2015 frequency data. (for LTO and NMC battery)

		C-rate					
		0.1	0.2	0.4	0.6	0.8	1
SOC (%)	10	0.03176	0.08897	0.05415	0.003499	0	0
	20	0.009354	0.02281	0.0738	0.00559	0	0
	30	0.07636	0.2257	0.2241	0.06883	0.00216	0
	40	0.1782	0.6087	0.723	0.2022	0.01163	0.0005625
	50	3.186	8.626	9.047	2.23	0.1693	0.003902
	60	2.409	7.226	9.249	2.508	0.2179	0.01754
	70	0.1026	0.4928	0.665	0.2053	0.02576	0.003105
	80	0.01563	0.04898	0.1061	0.02974	0	0
	90	0.009212	0.04938	0.03559	0.01201	0.005155	0
	100	0.0114	0.02604	0.0555	0	0	0

Table 5.8 Degradation analysis using the fast cycle counting method considering SOC and C-rate effect for EFR-A1 for October 2015 frequency data. (for LTO battery)

		C-rate					
		0.1	0.2	0.4	0.6	0.8	1
SOC (%)	10	0.00011985	0.000363	0.000241	0.0000171	0	0
	20	0.0000359	0.000095	0.000335	0.000028	0	0
	30	0.00029945	0.00096	0.001042	0.000353	0.000012	0
	40	0.0007128	0.002647	0.003443	0.001064	0.000068	0.000004
	50	0.01300408	0.038338	0.044132	0.012054	0.001026	0.000027
	60	0.0100375	0.032845	0.046245	0.013933	0.001362	0.000125
	70	0.0004366	0.002292	0.00341	0.001173	0.000166	0.000023
	80	0.0000679	0.000233	0.000558	0.000175	0	0
	90	0.00004094	0.000241	0.000192	0.0000728	0.000035	0
	100	0.00005181	0.00013	0.000308	0	0	0

Total LTO battery degradation (%): 0.2346

Table 5.9 Degradation analysis using the fast cycle counting method considering SOC and C-rate effect for EFR-A1 for October 2015 frequency data. (for NMC battery)

		C-rate					
		0.1	0.2	0.4	0.6	0.8	1
SOC (%)	10	0.000141	0.000434	0.000293	0.000021	0	0
	20	0.000042	0.000114	0.00041	0.000035	0	0
	30	0.000355	0.001157	0.001281	0.000444	0.000016	0
	40	0.000849	0.003204	0.004253	0.001348	0.000089	0.0000051
	50	0.015541	0.046627	0.05483	0.015379	0.001354	0.0000372
	60	0.012045	0.040144	0.057806	0.017914	0.001816	0.000175
	70	0.000526	0.002816	0.00429	0.001521	0.000224	0.0000327
	80	0.000082	0.000288	0.000707	0.000229	0	0
	90	0.00005	0.000299	0.000245	0.000096	0.000049	0
	100	0.000063	0.000163	0.000396	0	0	0

Total LTO battery degradation (%): 0.2902

Using the number of cycles obtained from the fast CCM algorithm considering SOC and C-rate effect for EFR-A1 (Table 5.7) and also using the LTO and NMC battery cycling data assumed as in Table 5.5 and Table 5.6, the total degradation rate caused by BESS cycling is calculated as 0.23% for LTO battery and 0.29% for NMC battery per month (October 2015). Comparing the results, there is a significant difference on the total degradation findings of the LTO and NMC battery in Table 5.3 and Table 5.8; as well as Table 5.4 and Table 5.9. This shows that considering the effect of both C-rate and SOC on battery lifetime analysis provides more accurate degradation results than that of considering only C-rate; because higher C-rate level and SOC range cause a higher degradation rate in the battery.

*A. Simulation Results of the Fast CCM Considering SOC and C-rate Effect on Battery Lifetime for EFR –A1, EFR –A2, EFR –A3 for October 2015*

Using the battery SOC data attained by simulating the EFR –A1 for the whole of October 2015 (Fig. 5.6), the proposed CCM algorithm is processed with the results in Fig. 5.15. The algorithm determines the number of full charge-discharge cycles experienced by the BESS at each C-rate value grouped by 0.2C for each SOC range grouped by 10% during EFR service operation for October 2015.

As seen from Fig. 5.15, the CCM algorithm counts to ~9.2 cycles at 0.2-0.4C for 60% SOC, and to ~9 cycles at the same C-rate but for 50% SOC. It is revealed that greater number of full charge-discharge cycles are obtained at 0.2-0.4C for 50% to 60% SOC level, because the battery SOC is managed at 45-55% in all EFR algorithms thanks to the existing SOC control management.

As seen from Fig. 5.15, the third and fourth highest number of cycles are obtained at 0.1-0.2C for 50% SOC with ~8.6 cycles, and at 0.1-0.2C for 60% SOC with ~7.2 cycles. Therefore, it can be said that the BESS participating in EFR service operation with the EFR-A1 is mostly operated between 0.1C to 0.4C for 50-60% SOC level; the battery spends most of its time in this operating region, therefore one could consider degradation rates associated with the 0.1-0.4C range. Fig. 5.15 shows that the battery cycling at higher than 0.8C and at higher than 80% SOC or at lower than 40% SOC is almost zero; this means that the battery rarely operates at higher C-rate and at higher and lower SOC range on delivering EFR service with EFR-A1 in October 2015, due to the existing SOC management.

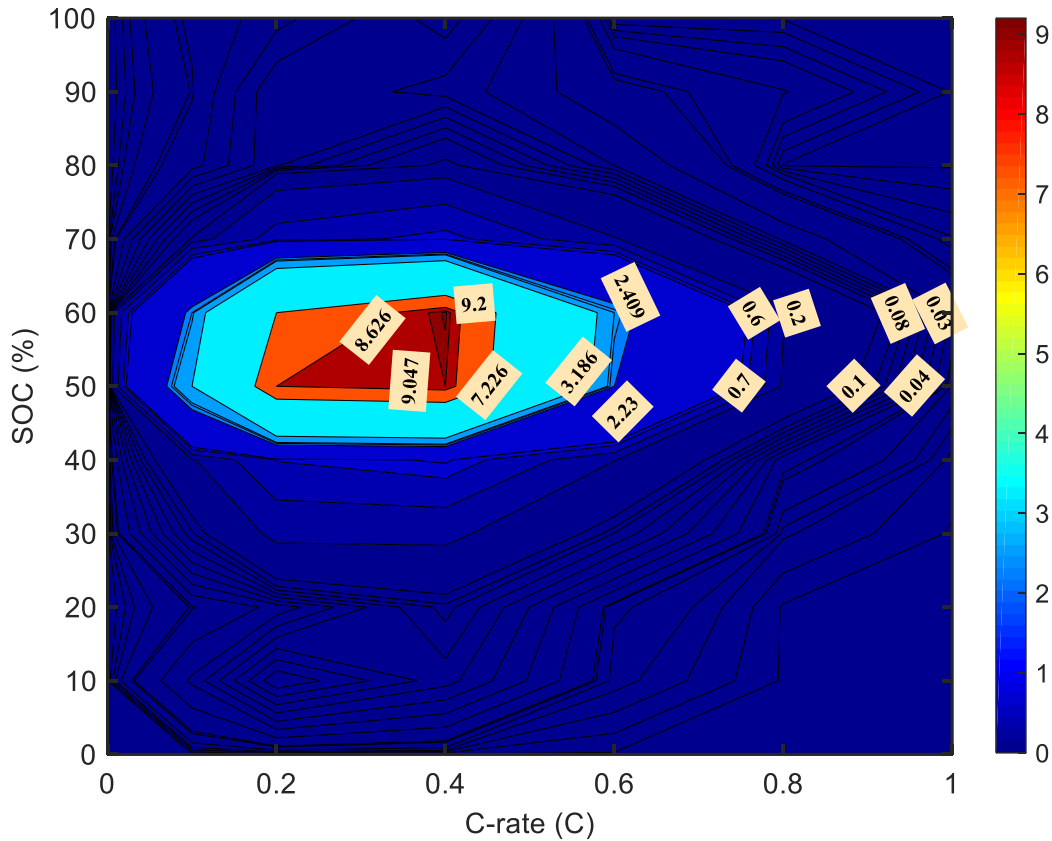


Fig. 5.15 Simulation results of the fast CCM under different C-rate for each grouped SOC for EFR-A1 for October 2015. (Maximum scale is 9.2 cycles).

As seen from Fig. 5.16, the BESS operating in EFR service with EFR-A2 having 15-min frequency event controller is mostly operated at 0.2-0.4C for 50-60% SOC level with the highest number of battery cycling in October 2015. The battery is subjected to ~7 full cycles at 0.2-0.4C for 50% SOC range, and to ~6.9 full cycles at 0.2-0.4C for 60% SOC, and also to ~6.4 full cycles at 0.1-0.2C for 50% SOC. The battery spends most of its time in this operating region, therefore one could consider degradation rates associated with the 0.1-0.4C range for 50-60%.

As seen from Fig. 5.17, the BESS operating EFR service with EFR-A3 having 15-min frequency event controller is mostly operated at less than 0.4C for 50% to 60% SOC level in October 2015. The battery is subjected to 7.149 cycles at 0.4C for 50% SOC, and to ~7 cycles at 0.2C for 50% SOC. It is demonstrated that the battery spends most of its time in this operating region, therefore one could consider degradation rates associated with  $\leq 0.4C$  range for 50-60% SOC level per month (October 2015), due to the SOC management in EFR-A3 (Fig. 5.17), as similar in EFR-A1 (Fig. 5.15) and EFR-A2 (Fig. 5.16).

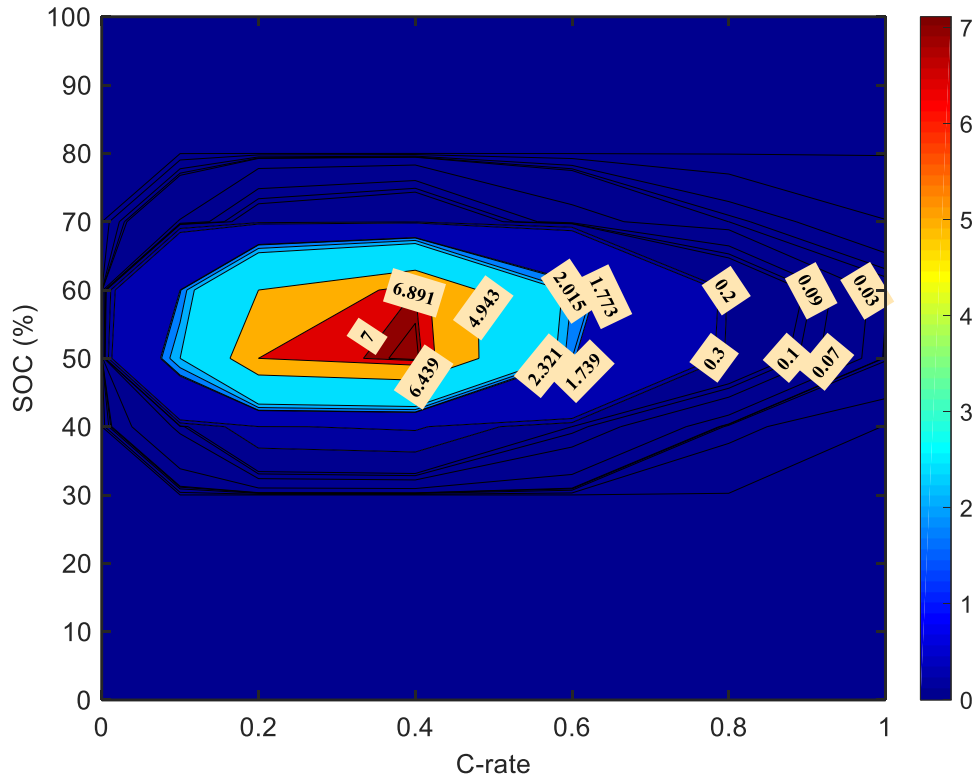


Fig. 5.16 Simulation results of the fast CCM under different C-rate for each grouped SOC for EFR-A2 for October 2015. (Maximum scale is 7 cycles).

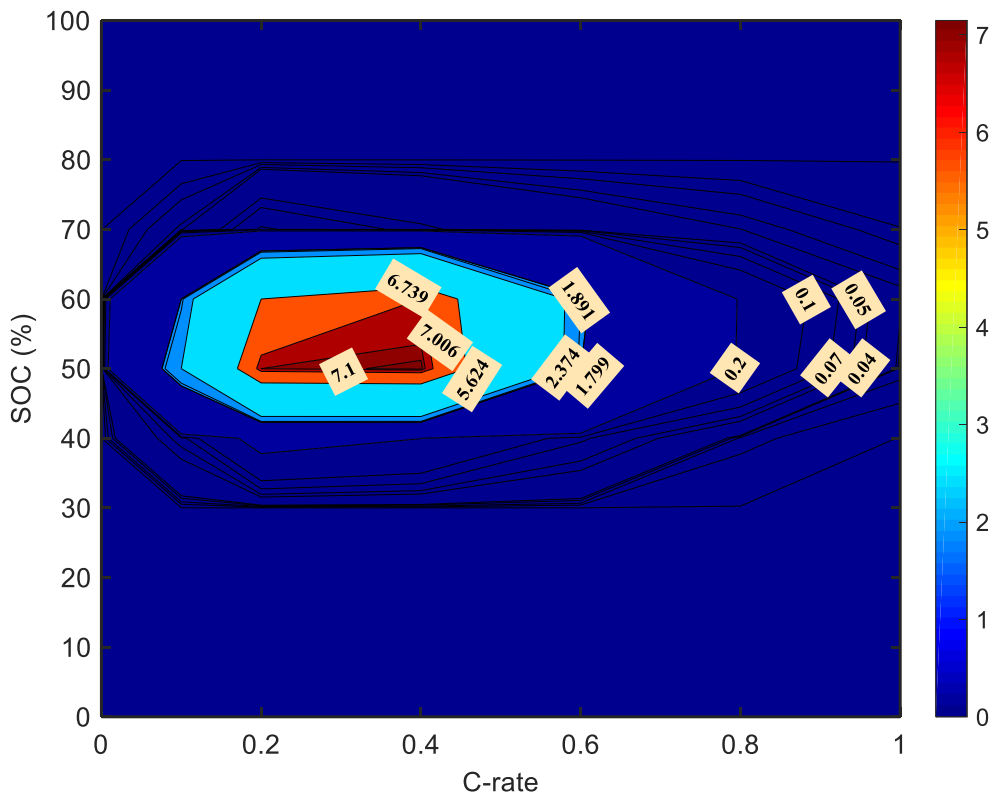


Fig. 5.17 Simulation results of the fast CCM under different C-rate for each grouped SOC for EFR-A3 for October 2015. (Maximum scale is 7.1 cycles).

Comparing the number of battery full charge-discharge cycles obtained from analyzing EFR-A1 (Fig. 5.15), EFR-A2 (Fig. 5.16) and EFR-A3 (Fig. 5.17), the proposed CCM algorithm determines the highest number of cycle at each considered C-rate for each grouped SOC level, with the EFR-A1. The EFR-A1 causes the greatest amount of degradation in the battery per month, comparing to those in EFR-A2 and EFR-A3. This also can be seen from Table B.1, Table B.2, Table B.3 in Appendix B.1.

*B. Simulation Results of the Fast CCM considering SOC and C-rate Effect on Battery Lifetime for EFR Algorithm-4 for October 2015*

As discussed in Chapter 3, the aim of the proportional controller in the EFR-A4 is to reduce battery C-rate, and hence reduce the battery degradation rate in order to increase battery lifetime. Therefore, comparing the cycle findings in Fig. 5.15 with Fig. 5.18, it can be seen that EFR-A1 degrades the battery higher than EFR-A4 due to the higher cycles occurred at that point of C-rate for each grouped SOC range per month during EFR service delivery. Because, applying a proportional controller in the EFR-A4, the number of cycles the BESS endured is reduced without getting a reduction in the BESS availability; hence battery lifetime will be increased.

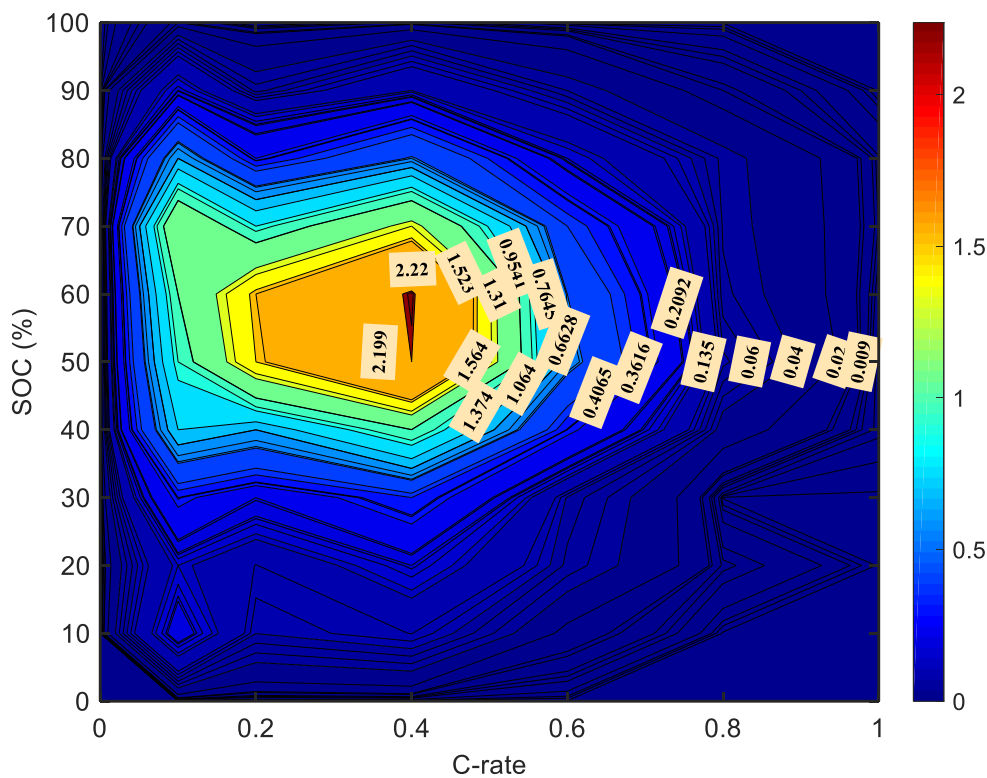


Fig. 5.18 Simulation results of the fast CCM under different C-rate for each grouped SOC for EFR-A4 ( $K_p = 2000$ ) for October 2015. (Maximum scale is 2.22 cycles).



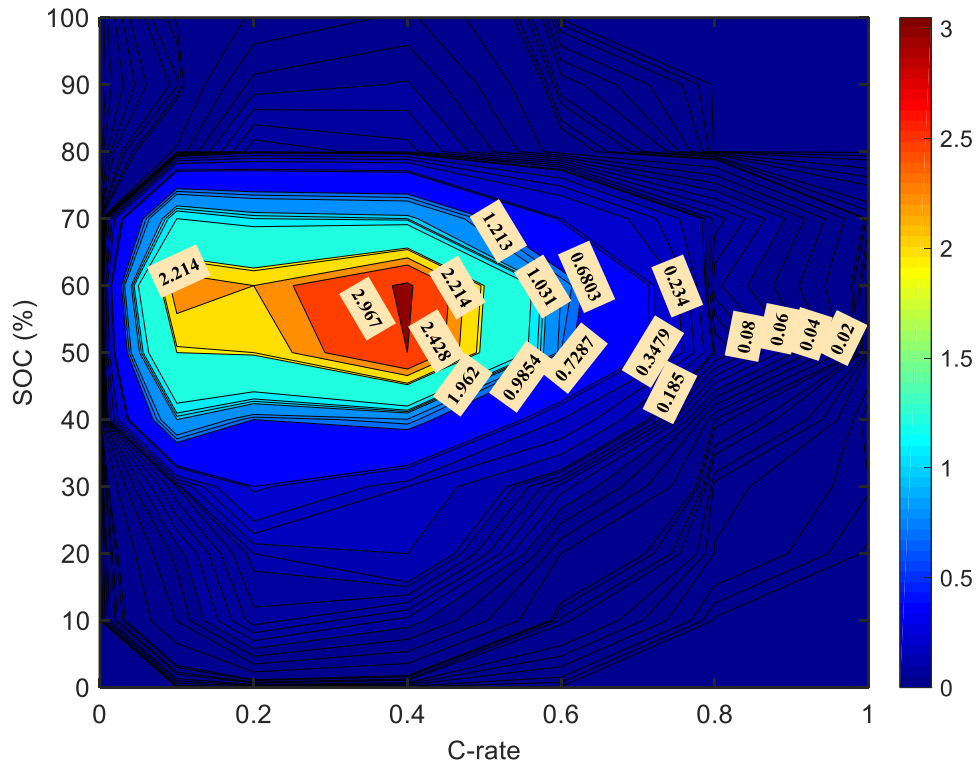


Fig. 5.19 Simulation results of the fast CCM under different C-rate for each grouped SOC for EFR-A4 ( $K_p = 10,000$ ) for October 2015. (Maximum scale is 3 cycles).

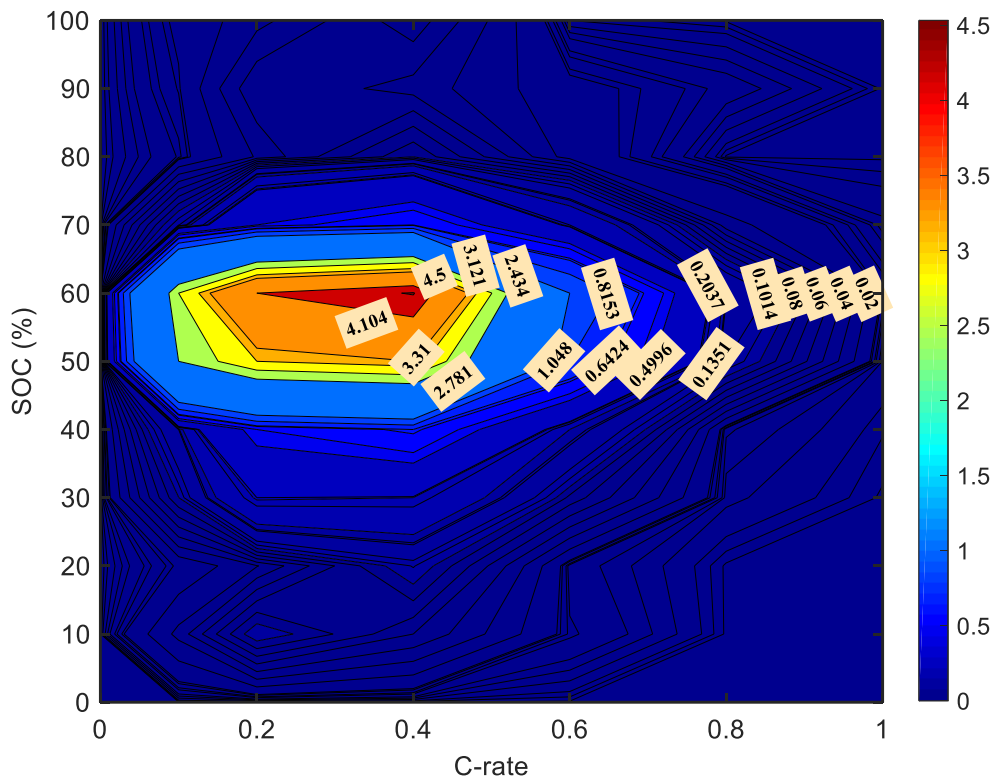


Fig. 5.20 Simulation results of the fast CCM under different C-rate for each grouped SOC for EFR-A4 ( $K_p = 100,000$ ) for October 2015. (Maximum scale is 4.5 cycles).

It is also revealed that, increasing the gain value ( $Kp$ ) set in the proportional controller in EFR-A4, the number of battery charge-discharge cycles experienced by the BESS at each C-rate for each SOC range grouped increases relatively (Fig. 5.18, Fig. 5.19, Fig. 5.20); this causes increasing amount of degradation in the battery. This also can be seen from Table B.4, Table B.5 and Table B.6 in Appendix B.1.

*C. Simulation Results of the Fast CCM with SOC and C-rate Effect on Battery Lifetime for DFFR Algorithm October 2015*

As seen from Fig. 5.21 and Table B.7 in Appendix B.1, the battery is subjected to highest number of cycles (~2.5 cycles) at 0.1C to 0.2C for 50% SOC range; and to second highest number of cycles (~2.38 cycles) at 0.1C to 0.2C for 60% SOC on delivering dynamic frequency response service. Therefore, it is revealed that the battery spends most of its time in this operating region, therefore one could consider degradation rates associated with 0.1-0.2C.

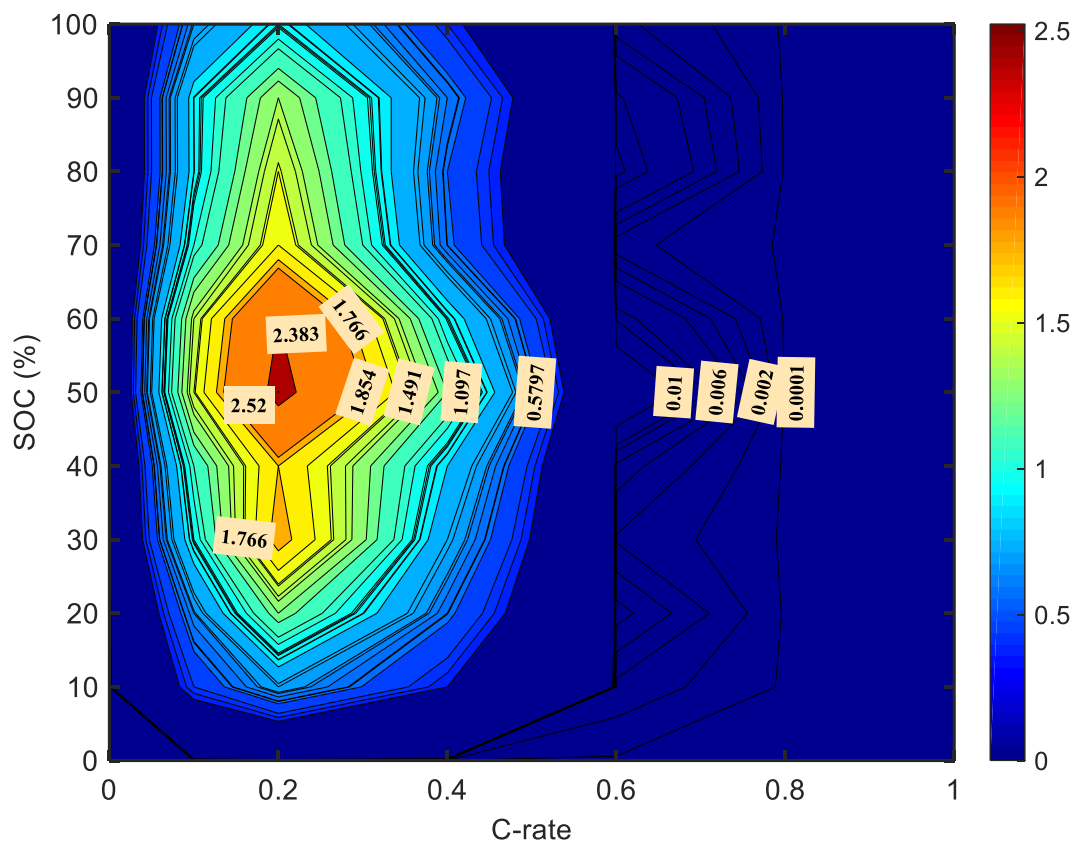


Fig. 5.21 Simulation results of the fast CCM under different C-rate for each grouped SOC for DFFR control algorithm for October 2015. (Maximum scale is 2.52 cycles).

Fig. 5.21 and Table B.7 show that the battery cycling at higher than 0.4C for each SOC range grouped is almost zero; this means that the battery mostly does not operate at  $\geq 0.4C$  for each grouped SOC range, because the 1MWh capacity of BESS delivers only 1MW power to the grid under DFFR service operation; hence this reduces the battery C-rate. It is clear from Fig. 5.21 the number of cycles the battery is subjected to are generally less than 0.4C for each SOC ranges grouped by 10% with less than 2 cycles. On the other hand, implementing a proper SOC management into the DFFR algorithm, the lifetime of the BESS can be significantly increased by decreasing the number of cycles the BESS endured at different C-rate for each SOC value under DFFR service operation.

### 5.3.7 Fast CCM considering Effect of DOD in Partial Charge/Discharge Cycling

The proposed CCM method in this section approximates the number of partial charge and discharge cycles a battery subjected under different DOD ranges. The operational principle of the proposed technique considering effect of DOD in battery partial charge and discharge cycling is demonstrated on the 23-second profile of a battery SOC given in Fig. 5.22 and Table 5.10. The proposed method is described as following:

- The algorithm loops through the considered battery SOC data over a period of time, as an example in Fig. 5.22. In the first step, the change in battery SOC ( $dSOC/dt$ ) is extracted for each second, as seen from the second column in Table 5.10.
- In second step, adding up  $dSOC/dt$  values until change in sign, the depth of charge (+) and discharge (-) ranges are extracted and listed over the period of time. Counting DOD ranges in the method performs like a hill climbing, adding up  $dSOC/dt$  rates until change in sign, as shown on the red line in Fig. 5.22. This step is shown in the third column in Table 5.10.
- In third step, the algorithm extracts each partial charge (+) and discharge (-) cycle at each DOD range independently over the list of DOD extracted, as seen from the forth column in Table 5.10.
- In the last step, total number of partial charge-discharge cycles at each DOD range is obtained by summing up each partial charge and discharge cycle at same DOD range, as given in the last column in Table 5.10.

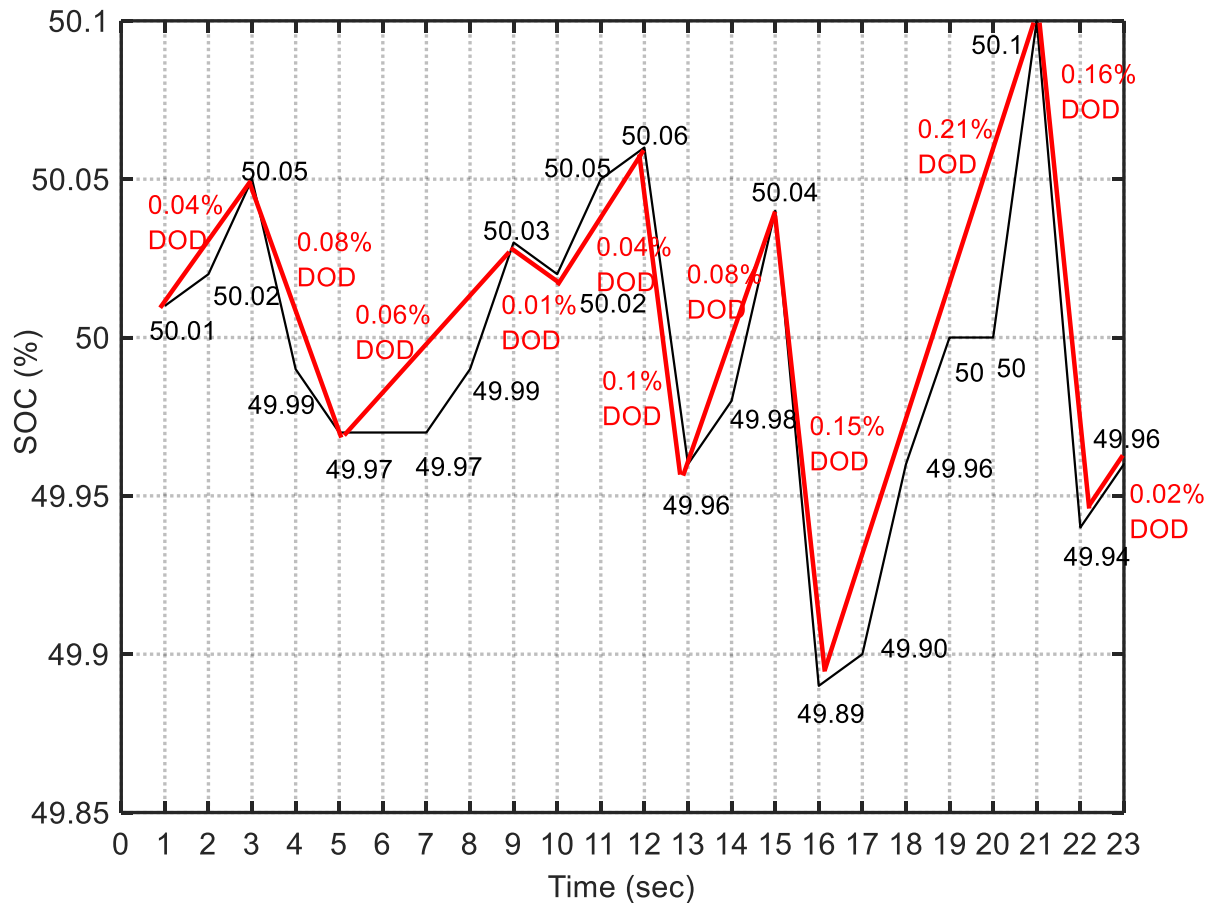


Fig. 5.22 Demonstration of the performance of the new fast CCM considering effect of DOD in battery charge-discharge cycling over the 23-second period of battery SOC.

Using the proposed method, it can be seen from Table 5.10 and Fig. 5.23, at each DOD range of 0.01%, 0.02%, 0.06%, 0.1%, 0.15%, 0.16% and 0.21%, a total of 1 partial cycle is counted individually; and at each DOD range of 0.04% and 0.08%, 2 partial cycles are also counted individually. The partial cycles at each DOD ranges counted in the CCM algorithm affect the degradation rate in a battery and thus its battery lifetime, as described in the battery aging analysis methodology in Section 5.2.2. Therefore, the effects of DOD in battery cycling should be examined in the battery lifetime analysis.

Table 5.10 Demonstration of the operational principle of the fast CCM considering effect of DOD in battery partial charge and discharge cycling over the 23-second period of battery SOC

SOC (%)	dSOC/dt (%)	List of DOD	Partial charge/discharge cycles	Total no of partial charge discharge cycles at each DOD	
				DOD	Cycle
50.01	0	0		<b>0.01%</b>	<b>1 cycle</b>
50.02	0.01	+0.04	1 partial charge cycle @ 0.04% DOD	<b>0.02%</b>	<b>1 cycle</b>
50.05	0.03			<b>0.03%</b>	-
49.99	-0.06	-0.08	1 partial discharge cycle @ 0.08% DOD	<b>0.04%</b>	<b>2 cycle</b>
49.97	-0.02			<b>0.05%</b>	-
49.97	0	0		<b>0.06%</b>	<b>1 cycle</b>
49.97	0			<b>0.07%</b>	-
49.99	0.02	+0.06	1 partial charge cycle @ 0.06% DOD	<b>0.08%</b>	<b>2 cycle</b>
50.03	0.04			<b>0.09%</b>	-
50.02	-0.01	-0.01	1 partial discharge cycle @ 0.01% DOD	<b>0.10%</b>	<b>1 cycle</b>
50.05	0.03	+0.04	1 partial charge cycle @ 0.04% DOD	<b>0.11%</b>	-
50.06	0.01			<b>0.12%</b>	-
49.96	-0.1	-0.10	1 partial discharge cycle @ 0.1% DOD	<b>0.13%</b>	-
49.98	0.02	+0.08	1 partial charge cycle @ 0.08% DOD	<b>0.14%</b>	-
50.04	0.06			<b>0.15%</b>	<b>1 cycle</b>
49.89	-0.15	-0.15	1 partial discharge cycle @ 0.15% DOD	<b>0.16%</b>	<b>1 cycle</b>
49.90	0.01	+0.21	1 partial charge cycle @ 0.21% DOD	<b>0.17%</b>	-
49.96	0.06			<b>0.18%</b>	-
50	0.04			<b>0.19%</b>	-
50	0			<b>0.20%</b>	-
50.1	0.1			<b>0.21%</b>	<b>1 cycle</b>
49.94	-0.16	-0.16	1 partial discharge cycle @ 0.16% DOD	<b>0.22%</b>	-
49.96	0.02	+0.02	1 partial charge cycle @ 0.02% DOD	<b>0.23%</b>	-

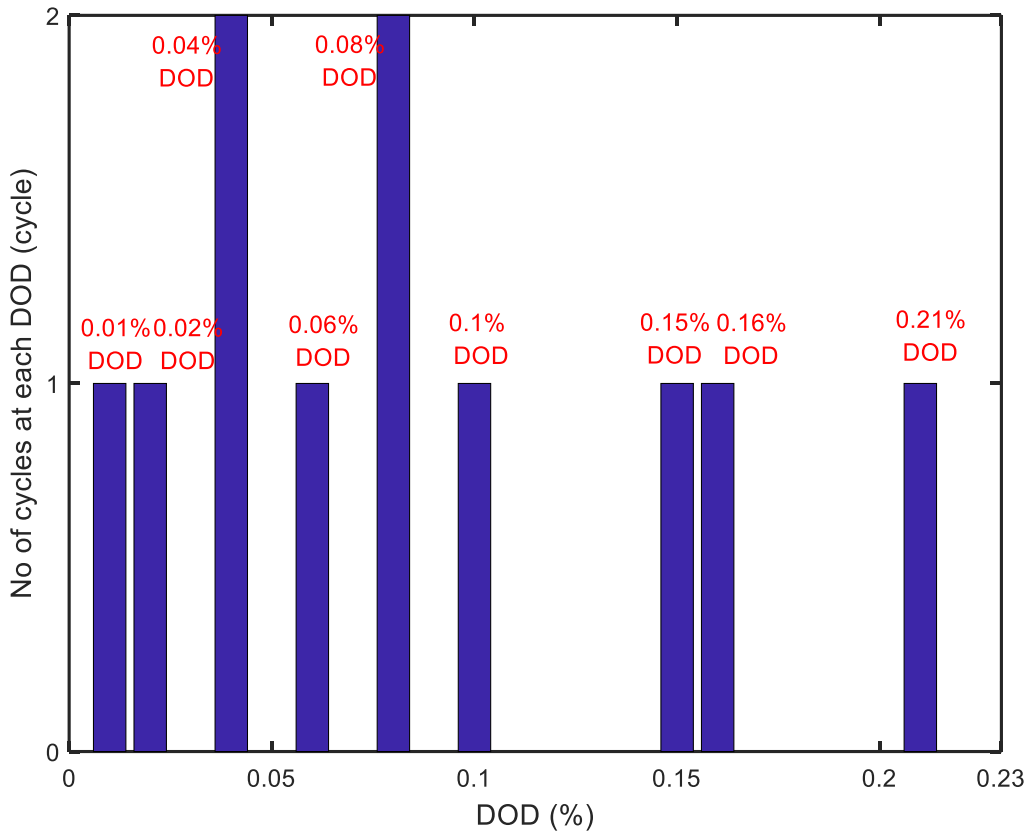


Fig. 5.23 Number of partial charge and discharge cycles at each DOD obtained from analysing the CCM in Table 5.10 over the 23-second period of SOC.

*A. Simulation Results of the Fast CCM considering the effect of DOD in Battery Partial Charge and Discharge Cycling for EFR-A1*

Using the battery SOC data attained by simulating EFR-A1 (Fig. 5.6), the proposed CCM algorithm considering DOD effect on battery SOH (Section 5.3.7) is processed with the results in Fig. 5.24. The algorithm approximates the number of partial charge-discharge cycles experienced by the BESS at each DOD range.

As seen from the simulation results, the changes in battery SOC are mostly less than 0.1%, therefore, the proposed CCM algorithm identifies and detects all microcycles; and following the steps in the algorithm; if the changes in SOC are positive ( $dSOC/dt > 0$ ), the battery is charging or if those change is negative ( $dSOC/dt < 0$ ), the battery is discharging. Therefore, adding up  $dSOC/dt$  values until a change in sign (positive to negative or negative to positive), partial charge discharge cycles at different DOD ranges are obtained, independently, approximating to a total of partial cycles at each different DOD value.

As seen from the Fig. 5.24, the BESS is subjected to 1978 partial cycles at 0.001% DOD; to 1195 partial cycles at 0.002% DOD; to 891 partial cycles at 0.003% DOD; to 621 partial cycles at 0.005% DOD, respectively for the whole of the October 2015.

Analysing the proposed CCM algorithm using the EFR-A1 for October 2015, it is revealed that, the number of partial charge discharge cycles experienced by the BESS at each DOD range decreases at each increasing DOD ranges. Total partial cycles at  $\geq 2\%$  DOD obtained is mostly less than 5 cycles for the whole Oct 2015 (Fig. 5.24). It can be seen from the analysis that this algorithm can be applied to larger SOC data sets; causing increasing number of partial charge-discharge cycles at different DOD ranges; hence the increase of DOD effect in the battery cycling will increase the rate of battery degradation in the battery.

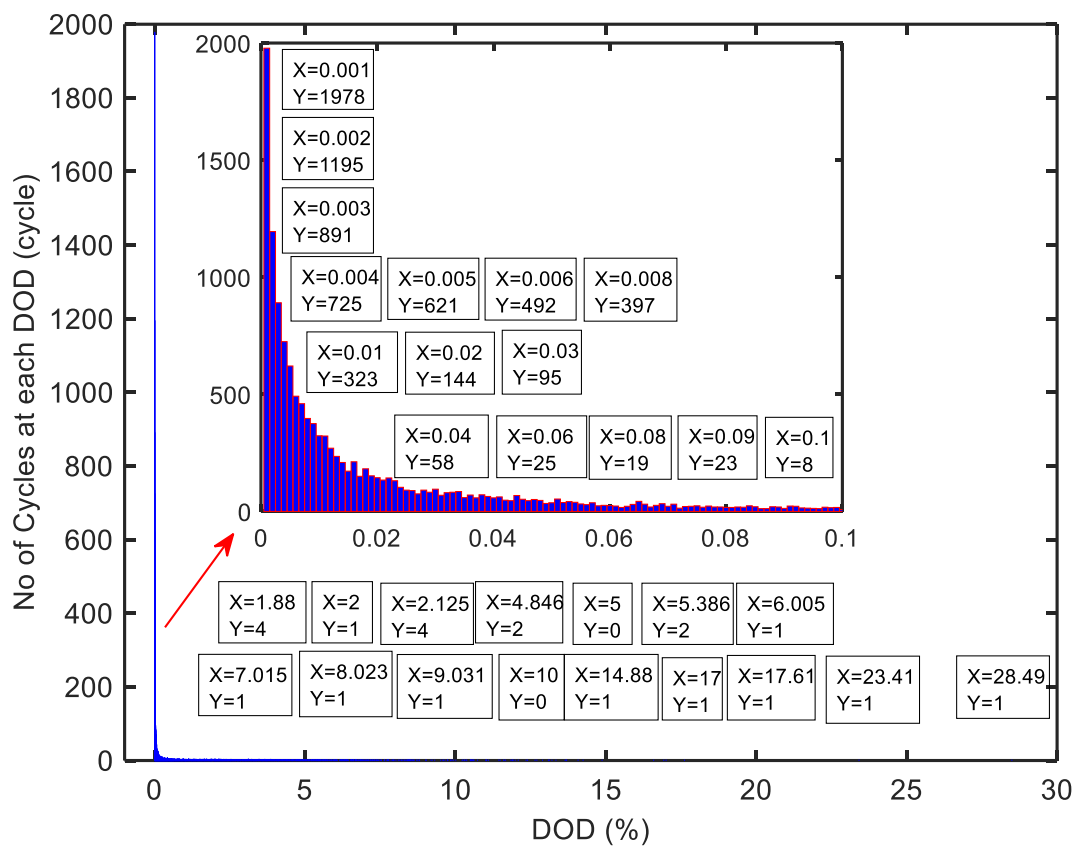


Fig. 5.24 Total number of partial charge discharge cycles at each DOD range extracted from the fast cycle CCM considering effect of DOD in battery cycling for EFR-A1 for October 2015

*B. Simulation Results of the Fast CCM considering the effect of DOD in Battery Partial Charge and Discharge Cycling for EFR-A2 and EFR-A3*

Using the battery SOC data attained by simulating EFR-A2 and EFR-A3 for the whole of October 2015 as shown in Fig. B.1 and Fig. B.3 in Appendix B, respectively, the proposed CCM algorithm considering DOD effect on battery SOH (Section 5.3.7) is processed with the results in Fig. 5.25 and Fig. 5.26.

As seen from the Fig. 5.25, the BESS are subjected to 1247 partial cycles at 0.001% DOD; to 791 partial cycles at 0.002% DOD; to 581 partial cycles at 0.003% DOD; to 438 partial cycles at 0.005% DOD for the whole of the October 2015. Comparing the number of cycles the BESS endured at each DOD range obtained by simulating EFR-A1, EFR-A2, EFR-A3 for a month, the EFR-A1 produces the highest number of partial charge discharge cycles at each DOD range. This demonstrates that EFR-A1 degrades the battery higher than EFR-A2 and EFR-A3 due to the greatest range of DOD effect on the battery SOH. Comparing the cycling results of EFR-A2 and EFR-A3, both algorithms generate quite similar number of partial cycles experienced by the BESS at each DOD; hence the battery degradation rate caused by EFR-A2 and EFR-A3 does not show a big difference in terms of DOD effect on battery SOH.

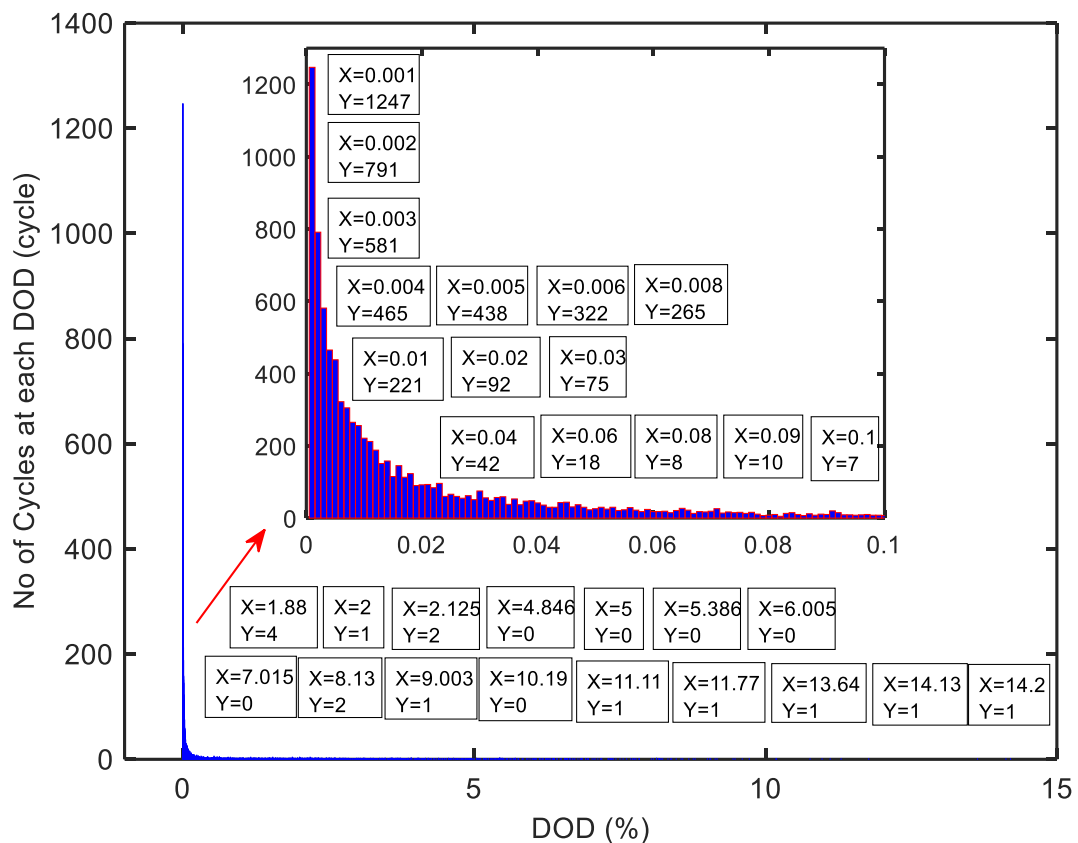


Fig. 5.25 Total number of partial charge discharge cycles at each DOD range extracted from the new fast CCM considering effect of DOD in battery cycling for EFR-A2 for October 2015



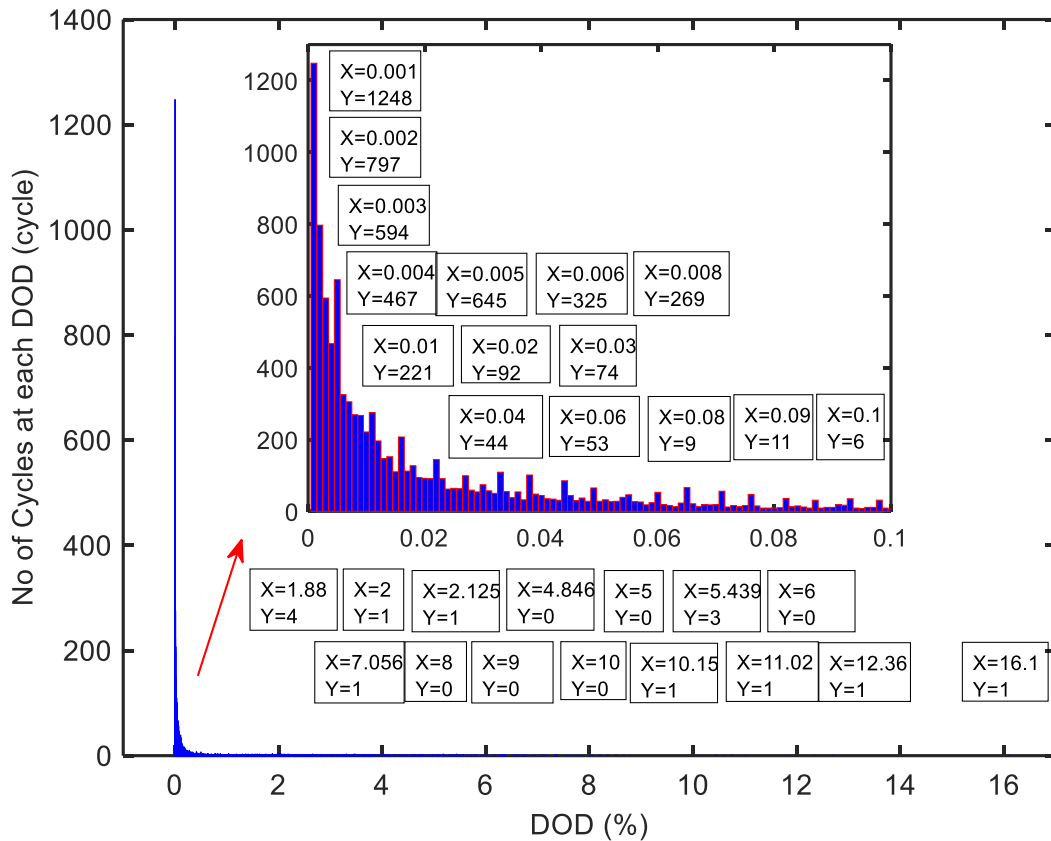


Fig. 5.26 Total number of charge-discharge cycles at each DOD range extracted from the new fast CCM considering effect of DOD in battery cycling for EFR-A3 for October 2015

*C. Simulation Results of the Fast CCM considering the effect of DOD in Battery Partial Charge and Discharge Cycling for EFR-A4*

Using the battery SOC data sets attained by simulating EFR-A4 with the proportional gains of  $K_p = 2000$  for the whole of October 2015, the proposed CCM algorithm considering DOD effect on battery SOH is processed with the results in Fig. 5.27.

As seen from Table 5.11, analysing the proposed CCM algorithm using the EFR-A4 with different  $K_p$  values for October 2015, it is revealed that increasing  $K_p$  gain set in the proportional controller in EFR-A4, the number of partial charge discharge cycles experienced by the BESS increases at each DOD ranges.

Comparing the number of cycles experienced by the BESS at each DOD range obtained by simulating EFR-A1 (Fig. 5.24) with those from EFR-A4 with  $K_p = 2000$  for a month, the partial charge discharge cycles are mostly shifted to lower DOD ranges with EFR-A4 as seen

from Fig. 5.27. This demonstrates that the EFR-A1 degrades the battery higher than the EFR-A4 due to the higher range of DOD effect on the battery SOH.

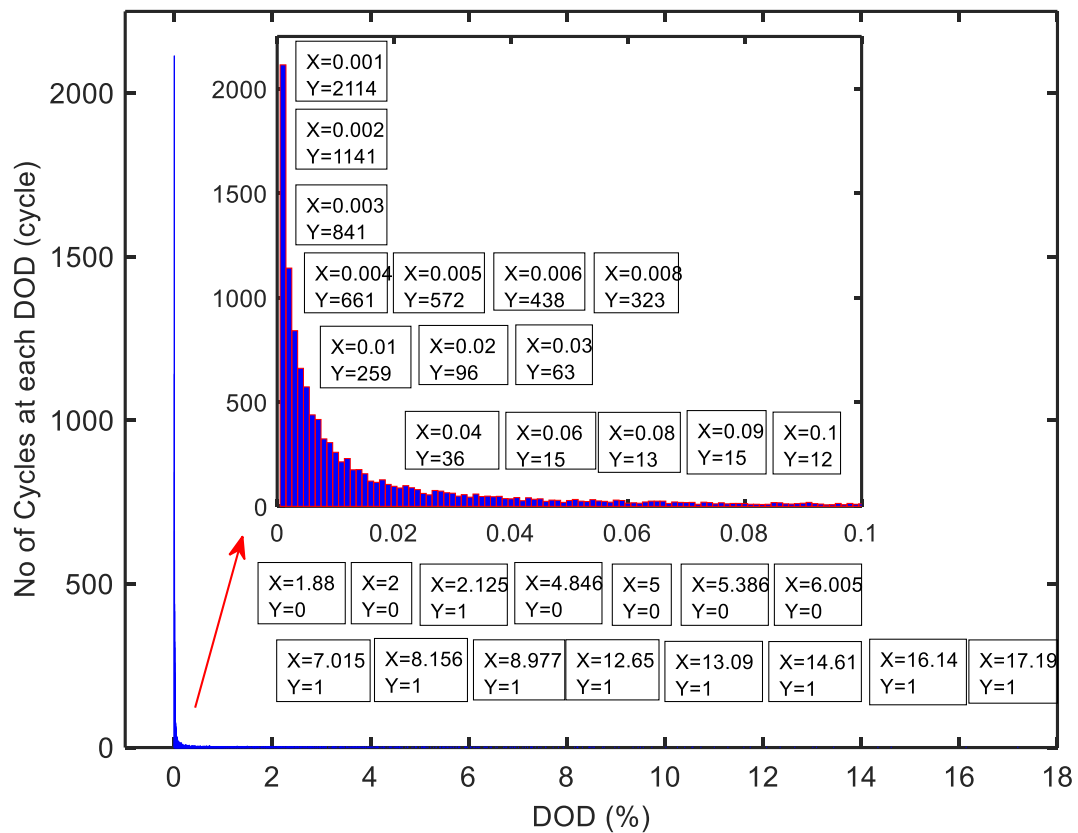


Fig. 5.27 Total number of charge-discharge cycles at each DOD range extracted from the new fast CCM considering effect of DOD in battery cycling for EFR-A4 ( $K_p = 2,000$ ) for October 2015

Table 5.11 Total partial charge discharge cycles at each DOD range extracted from the fast CCM considering DOD effect in battery cycling for EFR-A4 with different  $K_p$  values set.

EFR Control Algorithm for October 2015	Total no of partial charge discharge cycles at each DOD				
	Cycles @ 0.001% DOD	Cycles @ 0.002% DOD	Cycles @ 0.003% DOD	Cycles @ 0.004% DOD	Cycles @ 0.005% DOD
EFR-A4( $K_p = 2000$ )	2114	1141	841	661	572
EFR-A4( $K_p = 10000$ )	7130	1700	1129	738	572
EFR-A4( $K_p = 100000$ )	18880	7404	4665	2666	1764

*D. Simulation Results of the Fast CCM Algorithm considering the effect of DOD in Battery Partial Charge and Discharge Cycling for DFFR Algorithm*

Using the battery SOC data attained by simulating DFFR algorithm for the whole of October 2015 (Fig. 5.8), the proposed CCM algorithm is processed with the results in Fig. 5.28.

As seen from the Fig. 5.28, the BESS is subjected to 2168 partial charge discharge cycles at 0.001% DOD; to 786 partial cycles at 0.002% DOD; to 547 partial cycles at 0.003% DOD; and to 475 partial cycles at 0.005% DOD for the whole of the October 2015.

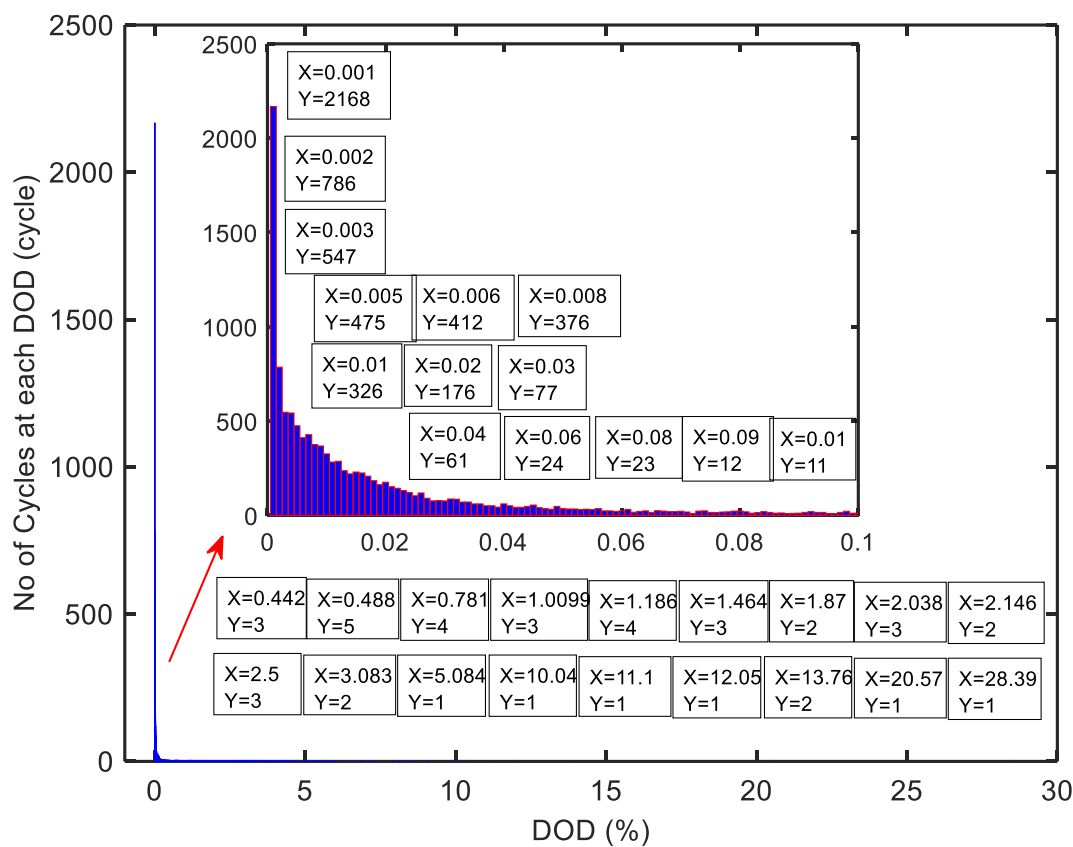


Fig. 5.28 Total number of charge discharge cycles at each DOD range extracted from the new fast CCM considering effect of DOD in battery cycling for DFFR algorithm for October 2015

Analysing the proposed CCM algorithm using the DFFR algorithm for October 2015, it is revealed that, the number of partial charge discharge cycles experienced by the BESS shows a variety at each DOD range. Total partial cycles at  $\geq 0.1\%$  DOD obtained is mostly less than 5 cycles for the whole Oct 2015 (Fig. 5.28). It is clear from the results, the partial charge discharge cycles the BESS experienced at each DOD does not follow a certain pattern; because

there is no battery SOC management in the DFFR algorithm, and hence the battery SOC obtained is exposed to sharp increases (charging) and decreases (discharging) pattern; this degrades the battery quickly. However, changes could be introduced to the NGET provided DFFR service specification to add SOC management in DB.

## 5.4 Conclusion

#1) A basic fast CCM algorithm, for grid-connected BESS, operating in frequency regulation, subjected to microcycles has been developed to achieve an approximation of equivalent battery charge-discharge full cycles. The basic CCM algorithm detects the number of complete charge-discharge cycles endured by the BESS in a given period of time. To demonstrate the performance of the basic CCM algorithm, the EFR and DFFR control algorithms, based on a model of 2MW/1MWh BESS and 1MW/1MWh BESS respectively, have been simulated to obtain a historical SOC data set which is then used by the proposed fast CCM algorithm as an input source. It is revealed that cycle counting for BESS operation in grid frequency regulation is challenging due to the presence of irregular charge and discharge cycles of varying SOC caused by the real grid frequency variability. The battery cycle life varies for different SOC ranges, therefore all microcycles existing in the SOC profile are extracted to estimate the total battery cycle information. Analysis of the results show that the proposed basic fast CCM algorithm detects numerous microcycles existing in the considered SOC profile for October 2015 and extracts them to approximate the total complete battery charge-discharge cycles. It is revealed that the microcycling for the whole of 2015 approximated 553, 375.5, 383.5, 256 and 364 battery charge-discharge cycles, by analysing the EFR-A1, EFR-A2, EFR-A3 and EFR-A4 ( $Kp = 10000$ ) and DFFR algorithm, respectively.

In addition, using the SOC data obtained from simulating the EFR-A1, EFR-A2, EFR-A3 and the DFFR algorithm in analysing the CCM algorithm, microcycling for October 2015 approximates to 49, 34, 35 and 32 full charge-discharge cycles, respectively. Using the SOC data obtained from simulating the EFR-A4 having P controller with different proportional gain values of  $Kp = 2000, 10000, 100000$  in analysing the CCM algorithm, microcycling for October 2015 approximates to 21, 24, 26 full charge-discharge cycles, respectively. These cycles have also been compared to the manufacturer provided degradation data for full cycles to estimate to aid in the prediction of the BESS lifetime. As a results of this, it is revealed that the EFR-A1 degrades the battery much more than EFR-A2 and EFR-A3. It is also revealed that

the higher Kp value set in the proportional controller in EFR-A4, the higher battery degradation rate because of the higher amount of EFR power delivered to the grid responding to the grid frequency events. Using the existing Miner Rule's aging analysis method, these cycles can also be compared to the LTO and NMC battery's manufacturer provided degradation data for full cycles to estimate to aid in the prediction of the BESS SOH.

Comparing with the EFR control algorithms, the DFFR algorithm delivers only half amount of dynamic power (1MW) by the same capacity of battery (1MWh), however it degrades the batteries quite fast in a year under dynamic frequency response operation.

#2) Secondly, the basic CCM algorithm is improved by considering only C-rate effect on battery SOH; and then analysed for the whole of October 2015 data. The proposed algorithm determines the number of charge-discharge cycles experienced by the BESS operating in EFR service at different C-rate values grouped as 0.1C, 0.2C, 0.4C, 0.6C, 0.8C, 1C in October 2015.

Using the constant battery cycling Data-1 which considers same cycling for each C-rate for LTO and NMC battery, the total degradation rate caused by BESS cycling is determined as around 0.4115% for LTO battery and 0.6175% for NMC battery per month (October 2015). However, using battery cycling Data-2 which considers the cycling variable for each group C-rate level, the total degradation rate caused by BESS cycling is calculated as 0.2631% for LTO battery and 0.3354% for NMC battery per month. It is revealed that the effect of C-rate on battery lifetime analysis should be considered for more accurate battery lifetime analysis. In addition, it is also revealed that, the EFR-A1 degrades the LTO battery less than the NMC battery due to the higher LTO cells having lower degradation rates for cycle. Using the Data-2 in the battery degradation analysis, it is demonstrated that the BESS participating in EFR service delivery is mostly operated at 0.2-0.4C with 20.23 cycles, causing 0.1686% and 0.2529% degradation in LTO and NMC battery respectively.

#3) Thirdly, the basic CCM algorithm is improved by considering both C-rate and SOC effect on battery SOH; and then analysed for the whole of October 2015 data. Using the assumed battery cycling data of LTO and NMC batteries for each C-rate for SOC range grouped in the battery degradation analyses, it is revealed that considering the effect of both C-rate and SOC on battery lifetime analysis provides much more accurate degradation analysis rather than that of considering only C-rate.

The proposed algorithm determines the number of charge-discharge cycles experienced by the BESS operating in EFR service at different C-rate values grouped as 0.1C, 0.2C, 0.4C, 0.6C, 0.8C, 1C for each SOC range grouped by 10% in October 2015. It is revealed from the simulation results that thanks to the 15-minute frequency event controller applied into the EFR-A2 and EFR-A3 for increasing BESS availability, the EFR-A1 degrades the battery much higher than the EFR-A2 and EFR-A3, with higher number of battery cycling. However, both EFR-A2 and EFR-A3 have similar controller; the EFR-A3 allows the battery to manage its SOC during the 30-minutes period by charging/discharging itself; therefore EFR-A3 degrades the battery higher than EFR-A2 with the higher number of cycles the battery endured on delivering EFR service to the grid.

Implementing proportional controller into the EFR-A4 which is based on EFR-A1, the amount of EFR power delivered can be decreased without hitting a reduction in the BESS availability. Therefore, using EFR-A4, the number of battery charge-discharge cycles experienced by the BESS and the battery C-rate can be decreased; this will help to extend the lifetime of the battery; however may lead to a reduction in the BESS efficiency.

Comparing the performance of the EFR and DFFR algorithms, it is revealed that the amplitude of second by second battery C-rate obtained from simulating DFFR algorithm is much lower than that of EFR, because only 1MW DFFR power is delivered by the 1MWh BESS to the grid; however 2MW EFR power is delivered with the EFR algorithms. In addition, analysing the EFR algorithms, greater number of cycles experienced by the BESS are mostly obtained at less than 0.4C for 50-60% SOC range; however with the DFFR algorithm, higher number of cycles are attained at  $\leq 0.2C$  for any range of SOC. It is also observed that there is no significant difference in the number of cycle at different C-rate for each grouped SOC range; because DFFR algorithm does not cover a SOC management strategy for maintaining battery SOC. Applying a proper SOC management into the DFFR algorithm, the BESS lifetime can be extended.

**#4)** The last part of the chapter presents a new fast CCM considering effect of DOD in partial charge and discharge cycling. The proposed method approximates the number of partial charge and discharge cycles a battery subjected under different DOD ranges. Analysing the proposed CCM using the EFR and DFFR control algorithms for October 2015, it is revealed that, because the changes in battery SOC are mostly less than 0.1%, causing microcycles due to the variability in the grid frequency, the number of partial charge and discharge cycles experienced

by the BESS is mostly occurred at less than 0.1% DOD ranges. Therefore, the battery degradation is mostly caused by low DOD ranges.

Comparing the number of cycles the BESS endured at each DOD range obtained by simulating EFR-A1, EFR-A2, EFR-A3 for October 2015, the EFR-A1 produces the highest number of partial charge-discharge cycles at each DOD range; this shows that EFR-A1 degrades the battery much higher than the EFR-A2 and EFR-A3 due to the greatest range of DOD effect on the battery SOH. Comparing the battery cycling results of EFR-A2 and EFR-A3, both algorithms generate quite similar number of partial charge discharge cycles experienced by the BESS at each DOD; therefore the battery degradation rate caused by EFR-A2 and EFR-A3 does not show a big difference in terms of DOD effect on battery SOH. In addition, comparing the battery cycling finding of EFR-A1 and EFR-A4, implementing the proper proportional controller into the EFR-A4, the number of partial cycles at each DOD can be decreased without getting a reduction on BESS availability; this helps to reduce the degradation rate on the battery during the EFR service operation.

## 6 Conclusions and Future Work

This Chapter presents a summary of the work carried out in this thesis, examining the role of each chapter in achieving the major objective of the thesis and the contributions made to the body of knowledge as a whole. An overall conclusion is then provided and the scope for the future work which expand on this thesis is also presented.

### 6.1 Conclusion

The primary objective of this thesis was to investigate a control scheme for a large-scale grid-tied battery energy storage system (BESS) for delivery of frequency response services as defined by NGET and to explore ways to maximise its service potential and analyse the effects on degradation. The management of the state-of-charge (SOC) of the BESS is studied to optimize the availability of the system under different scenarios. In addition to releasing and absorbing regulation power during frequency excursion events, the BESS recovers its SOC to a proper level during time when the system frequency is within the nominal range in order to avoid regulation failures in upcoming frequency excursion events. In other words, the BESS is operated in two alternating phases, namely frequency regulation and SOC management (SOC recovery), as shown in Fig. 6.1.

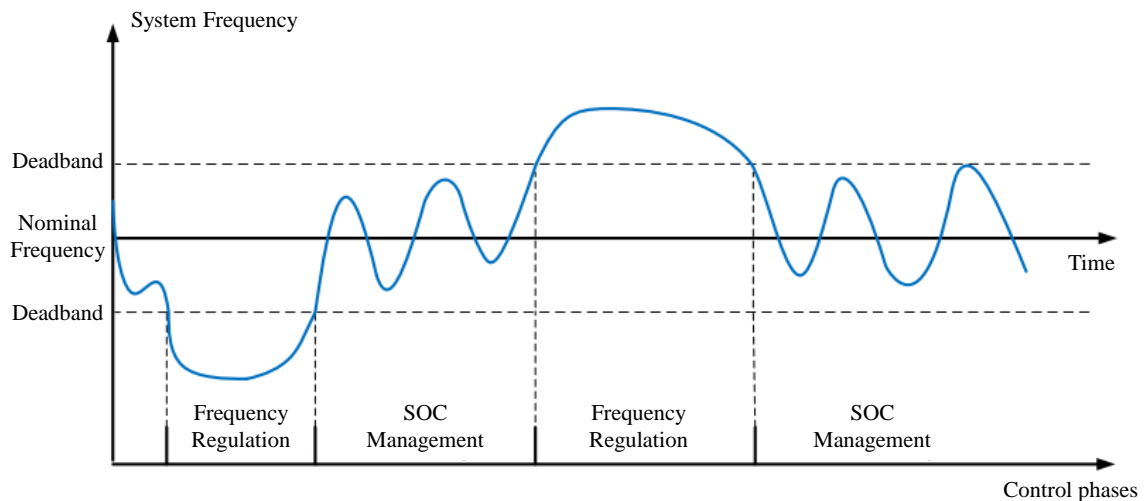


Fig. 6.1 System frequency and proposed control phases in this thesis.

This thesis considers an optimal control of the BESS that maximizes revenue for providing UK frequency response service in the ancillary service market. Regarding the frequency regulation



phase, the control aims to minimize the penalty cost assessed for regulation failure. For the SOC management phase, this thesis aims to maintain the SOC of the BESS at the desired SOC target level. By adjusting the SOC to the target during SOC management phase, the expected regulation failure penalty is minimized for the upcoming frequency failure events. The primary metrics for estimating battery degradation have been explored and an algorithm that can potentially provide an accurate estimate of a BESS under frequency regulation is presented.

### **6.1.1 BESS Control for Dynamic and Static Firm Frequency Response Services**

A dynamic (DFFR) and a static high (SFFR<sub>high</sub>) and low (SFFR<sub>low</sub>) firm frequency response control algorithm based on a model of a 1MW/1MWh BESS was developed to meet the NGET published service requirements. When there is a grid frequency on the grid, the BESS supplies a dynamic power according to a specified DFFR envelope, without managing the battery's SOC. It was shown that the BESS achieved full availability and met the service requirements.

The NGET then updated the DFFR service specifications in April 2018 by requesting a SOC management from the energy storage providers. Therefore, a proportional controller was implemented into the DFFR control algorithm to charge/discharge battery in order to manage the battery's SOC; hence this SOC management will allow the providers reduce the likelihood of unavailability of the BESS on delivering dynamic response service. Applying the SOC-based proportional controller into the DFFR control design will also help to extend the lifetime of the BESS.

It was also demonstrated that, the SFFR control algorithm successfully delivered a non-dynamic service where an agreed amount of power is delivered if the grid frequency reaches a defined trigger point of 49.7Hz (SFFR<sub>low</sub>) or 50.3Hz (SFFR<sub>high</sub>).

Finally, Chapter 3 provided an experimental validation of the DFFR control algorithm without having SOC management with a 2MW/1MWh lithium-titanate based BESS, Willenhall Energy Storage System.

### **6.1.2 BESS Control for Pre Enhanced Frequency Response Services**

In 2015, the NGET prepared a pre enhanced frequency response (pre-EFR) specification to facilitate a tender competition between potential energy storage providers. Using the pre-

published EFR specification, a generalised UK frequency response control algorithm (Pre-EFR) was developed to evaluate control strategies for delivering a real-time response to deviations in the grid frequency. At the time of this work BESS focused frequency response services were still being developed and charge/discharge power constraints in DB were not defined. Therefore, a sensitivity analysis of battery SOC management and a battery charge/discharge management methods were developed in order to maximise BESS availability. It was shown that the best SOC band forecasted is 50-60% with 60kW and 350kW battery charge/discharge powers for a DB range of 0.1Hz and 0.05Hz, respectively. It was demonstrated that the Pre-EFR algorithm met the UK's NGET frequency response specification and successfully manage the BESS's SOC whilst achieving a battery service performance measurement (SPM) requirement (>95%).

### **6.1.3 BESS Control for Enhanced Frequency Response Services**

In Chapter 3, four EFR control algorithms, named EFR-A1, EFR-A2, EFR-A3, EFR-A4, based on a model of a 2MW/1MWh BESS were developed to meet the NGET published EFR requirements and compared. It was shown that the EFR algorithms meet the UK's NGET EFR specifications and successfully managed the SOC by converging towards a desired band of 45-55%. It was shown that for the basic algorithm, EFR-A1, with Service-1, the BESS was available to deliver EFR service on critical days; however, with Service-2, the BESS could not provide 100% availability in the under/over frequency event days, resulting in a service performance penalty. The advanced algorithms EFR-A2 and EFR-A3 which have the 15-minutes frequency event controller provided full BESS availability, meaning no service penalty to the BESS. It also demonstrated that implementing a proportional controller (EFR-A4), the EFR power delivery range is relatively reduced based on the SOC error, without causing a BESS availability penalty in EFR service operation. The EFR-A4 provides an effective performance by decreasing the peak C-rates since there is no requirement to have full power changes, and reduces the rate at which the SOC target band is returned to. Thanks to the SOC-based proportional controller in the EFR-A4 algorithm, working the BESS over long periods of time with lower C-rates will prolong the BESS lifetime, with no performance penalty on EFR service operation; however, this may cause additional efficiency losses on the BESS system depending on the converter design. In Chapter 3, the performance of EFR-A1 was validated experimentally on a 2MW/1MWh BESS with some small variances accounted for.

#### **6.1.4 Triad Avoidance Strategy through Enhanced Frequency Response**

This thesis introduced a strategy to generate additional revenues from other ancillary services such as triad avoidance in the winter season. Chapter 4 investigated using the BESS in order to maximize the system's availability and triad avoidance benefit revenues while layering the UK grid balancing service, EFR. It was demonstrated that with strategic management of the battery's SOC during EFR delivery the BESS could be prepared in order to maximize the available energy to export for Triad Avoidance Benefit (TAB). It was demonstrated that the amount of energy available to export would depend greatly on the grid frequency conditions of the day and the time that a decision is made to commit to preparing for TAB.

#### **6.1.5 Scheduling of Grid Tied BESS Participating in UK Frequency Response Services and Energy Arbitrage**

Using historical UK electricity prices, a balancing service scheduling approach was developed to maximize energy arbitrage revenue by layering different types of UK grid balancing services, FFR and EFR, throughout the day. It was shown that the algorithm delivers both dynamic and non-dynamic FFR and also EFR services to NGET specifications while generating energy arbitrage revenue as well as service availability payments. The advantages of this scheduling method is that it generates arbitrage profit and combines balancing service availability payment revenue through service layering and new SOC management techniques. The revenue generated by the BESS can be maximised using a suitable scheduling scenario that will vary depending on the day/month/season of the year.

#### **6.1.6 Battery State of Health Analysis**

This thesis provided a battery state of health (SOH) analysis based on BESS cycling. In Chapter 5, firstly a basic fast cycle counting method (CCM) for grid-tied BESS operating in frequency response services was developed to achieve an approximation of complete charge-discharge cycles based on microcycling SOC history. Secondly, the basic CCM algorithm was improved by considering the effect of C-rate on battery SOH. Thirdly, the CCM is improved again by considering both C-rate and SOC effects on battery SOH. It was demonstrated that for the EFR-A1, from the basic CCM, the degradation for lithium titanate (LTO) and lithium nickel manganese cobalt (NMC) battery was shown to be 0.4115% and 0.6175% for a month (October 2015); and approximately 4.6% and 6.9% for a year (2015), respectively. However the CCM

grouped by C-rate, this was decreased to 0.26% and 0.34% for a month; and approximately ~3.1% and 4% for the year, respectively. In addition, the CCM with both C-rate and SOC analysis, this was significantly decreased to 0.23% and 0.29% for a month, and approximately ~2.8% and ~3.5% for the year, respectively. It was revealed from the results considering the effect of both C-rate and SOC on battery SOH potentially provides a more useful BESS lifetime analysis and better reflects the degradation for frequency response services compared to standard cycling.

Finally, in this thesis, a new fast CCM considering the effect of depth of discharge (DOD) on battery SOH was developed. The algorithm approximates the number of partial charge and discharge cycles a battery subjected under different DOD ranges. It was demonstrated that, the degradation in battery was mostly caused by low DOD ranges ( $\leq 0.1\%$ ), especially at 0.001%, during frequency regulation operation due to the existence of microcycling on battery SOC. Therefore, the effect of DOD in partial charge discharge cycling must also be considered for an accurate battery SOH analysis.

## **6.2 Scope for Future Works**

Although a conclusive body of work has been presented herein, there are areas which this thesis can expand on. The list below summarises the scope for future work which can lead on from this thesis.

- Applications of the developed frequency response control algorithms to other energy storage systems, e.g flywheel; or to hybrid energy storage system (with battery and supercapacitor).
- Developing new BESS control algorithms for future grid balancing services such as reactive power, voltage control and black start service.
- Efficiency analysis for large scale grid-tied battery energy storage system operating in frequency regulation.
- Improving the proposed battery lifetime analysis technique by having experimental validation of LTO and NMC battery cycling on frequency response operation.

## References

- [ADI99] S. K. Aditya and D. Das, "Application of battery energy storage system to load frequency control of an isolated power system," *Int. J. Energy Res.*, vol. 23, pp. 247–258, 1999.
- [AFF05] A. Affanni, *et al.*, "Battery choice and management for new-generation electric vehicles," *IEEE Trans. Ind. Electron.*, vol. 52, no. 5, pp. 1343-1349, Oct. 2005.
- [ALA16] M. J. E. Alam and T. K. Saha, "Cycle-life degradation assessment of battery energy storage systems caused by solar PV variability," in *IEEE Power Energy Soc. Gen. Meet. (PESGM'16)*, Boston, 2016, pp. 1-5.
- [ALI10] M. H. Ali, B. Wu, and R. A. Dougal, "An overview of SMES applications in power and energy systems," *IEEE Trans. Sustain. Energy*, vol. 1, no. 1, pp. 38-47, Apr. 2010.
- [ALV18] G. Alva, Y. Lin, and G. Fang, "An overview of thermal energy storage systems," *Energy*, vol. 144, pp. 341-378, 2018.
- [AMP17] M. Ampatzis, *et al.*, "Robust optimisation for deciding on real-time flexibility of storage-integrated photovoltaic units controlled by intelligent software agents," *IET Renew. Power Gener.*, vol. 11, no. 12, pp. 1527-1533, 2017.
- [AMZ94] C. Amzallag, J.P. Gerey, J. L. Robert and J. Bahuaud, "Standardization of the rainflow counting method for fatigue analysis", *Int. J. Fatigue*, vol. 16, no. 4, pp. 287-293, Jun. 1994.
- [ANE16] M. Aneke and M. Wang, "Energy storage technologies and real life applications – A state of the art review", *Appl. Energy*, vol. 179, pp. 350-377, 2016.
- [ANV17] A. Moghaddam, *et al.* "Efficient energy management for a grid-tied residential microgrid," *IET Gen. Transm. Distrib.*, 2017, 11, (11), pp. 2752-2761.
- [ARI06] M. Arita, A. Yokoyama, and Y. Tada, "Evaluation of battery system for frequency control in interconnected power system with a large penetration of wind power generation," in *Int. Conf. Power Sys. Technol.*, Chongqing, 2006, pp. 1-7.
- [AST10] K. J. Aström, and R. M. Murray, *Feedback systems: An introduction for scientists and engineers*. Princeton university press, 2010.
- [BAC07] G. Strbac, *et al.* "Impact of wind generation on the operation and development of the UK electricity systems," *Elect. Power Syst. Res.*, 2007, 77, (9), pp.1214-1227.
- [BAH18] M. Bahloul and S. K. Khadem, "Design and control of energy storage system for enhanced frequency response grid service," in *IEEE Int. Conf. Ind. Technol. (ICIT'18)*, Lyon, 2018, pp. 1189-1194.

- [BAH18a] M. Bahloul and S. K. Khadem, "Impact of power sharing method on battery life extension in HESS for grid ancillary services," *IEEE Trans. Energy Convers.*, (early access) Accepted in 2018.
- [BAH18b] M. Bahloul and S. K. Khadem, "Design and control of energy storage system for enhanced frequency response grid service," in *IEEE Int. Conf. Ind. Technol. (ICIT'18)*, Lyon, 2018, pp. 1189-1194.
- [BAK08] J. Baker, "New technology and possible advances in energy storage", *Energy Policy*, vol. 36, no. 12, pp. 4368-4373, 2008.
- [BAR04] P. Barton and D. G. Infield, "Energy storage and its use with intermittent renewable energy," *IEEE Trans. Energy Convers.*, vol. 19, no. 2, pp. 441-448, Jun. 2004.
- [BAR12] E. Barbour, *et al.*, "Towards an objective method to compare energy storage technologies: Development and validation of a model to determine the upper boundary of revenue available from electrical price arbitrage," *Energy & Environmental Sci.*, vol. 5, no. 1, pp. 5425-5436, 2012.
- [BAS11] S. Bashash, S. J. Moura, J. C. Forman, and H. K. Fathy, "Plug-in hybrid electric vehicle charge pattern optimization for energy cost and battery longevity," *J. Power Sources*, vol. 196, pp. 541-549, 2011.
- [BAS17] K. Basaran, N. S. Cetin, and S. Borekci, "Energy management for on-grid and off-grid wind/PV and battery hybrid systems," *IET Renew. Power Gener.*, vol. 11, no. 5, pp. 642-649, 2017.
- [BEL12] H. Beltran *et al.*, "Lithium ion batteries ageing analysis when used in a PV power plant," in *IEEE Int. Symp. Ind. Electron. (ISIE'12)*, pp. 1604-1609, 2012.
- [BEL16] H. Beltran, *et al.*, "Ageing of different types of batteries when enabling a PV power plant to enter electricity markets," in *IEEE Ind. Electron. Soc. Conf. (IECON'16)*, Florence, 2016, pp. 1986-1991.
- [BEV10] H. Bevrani, A. Ghosh, and G. Ledwich, "Renewable energy sources and frequency regulation: survey and new perspectives," *IET Renew. Power Gener.*, 2010, 4, (5), pp. 438-457.
- [BHU12] F. A. Bhuiyan and A. Yazdani, "Energy storage technologies for grid-connected and off-grid power system applications," in *IEEE Elect. Power Energy Conf.*, London, ON, 2012, pp. 303-310.
- [BIS13] J. D. Bishop, C. J. Axon, D. Bonilla, M. Tran, D. Banister, and M. D. McCulloch, "Evaluating the impact of V2G services on the degradation of batteries in PHEV and EV," *Applied Energy*, vol. 111, pp. 206-218, 2013.
- [BOR13] T. Borsche, A. Ulbig, M. Koller, and G. Andersson, "Power and energy capacity requirements of storages providing frequency control reserves," in *IEEE Power Energy Soc. Gen. Meet.*, Vancouver, BC, 2013, pp. 1-5.
- [BOU08] F. Bouffard and F. D. Galiana, "Stochastic security for operations planning with significant wind power generation," *IEEE Trans. Power Syst.*, vol. 23, no. 2, pp. 306-316, May 2008.

- [BOY00] J. D. Boyes and N. H. Clark, "Technologies for energy storage. Flywheels and super conducting magnetic energy storage," in *Power Eng. Soc. Summer Meet.*, Seattle, WA, 2000, pp. 1548-1550.
- [BRA13] F. Braam, *et al.*: "Grid-oriented operation of photovoltaic-battery systems," *Proc. Int. ETG Congress 2013, Symp. 1: Security in Critical Infrastructures Today*, Berlin, Germany, Nov. 2013, pp. 1–6.
- [BRA14] F. Braam, *et al.*, "Peak shaving with photovoltaic-battery systems," in *IEEE PES Inno. Smart Grid Technol. Conf. Europe (ISGT-Europe)*, 12–15 Oct. 2014, pp. 1–5.
- [BUD16] M. Budt, D. Wolf, R. Span, and J. Yan, "A review on compressed air energy storage: Basic principles, past milestones and recent developments", *Appl. Energy*, vol. 170, pp. 250-268, 2016.
- [BYR18] R. H. Byrne, *et al.*, "Energy management and optimization methods for grid energy storage systems," *IEEE Access*, vol. 6, pp. 13231-13260, 2018.
- [CAN17] S. Canevese, *et al.*, "Simulation of enhanced frequency response by battery storage systems: The UK versus the continental Europe system," in *IEEE Int. Conf. Environment Elect. Eng. IEEE Ind. Commercial Power Syst. Euro. (EEEIC / I&CPS Europe)*, Milan, 2017, pp. 1-6.
- [CER05] M. Ceraolo, A. Di Donato, C. Miulli, and G. Pede, "Microcycle-based efficiency of hybrid vehicle batteries," in *IEEE Veh. Power Propul. Conf. (VPPC'05)*, 2005, pp. 233-237.
- [CES15] E. A. M. Cesena, N. Good, and P. Mancarella, "Electrical network capacity support from demand side response: Techno-economic assessment of potential business cases for small commercial and residential end-users," *Energy Policy*, vol. 82, pp. 222-232, Jul. 2015.
- [CET19] T. H. Cetin, M. Kanoglu, and N. Yanikomer, "Cryogenic energy storage powered by geothermal energy", *Geothermics*, vol. 77, pp. 34-40, 2019.
- [CHA10] M. Chawla, R. Naik, R. Burra, and H. Wiegman, "Utility energy storage life degradation estimation method," in *IEEE Conf. Innov. Technol. Efficient Rel. Electricity Supply (CITRES'10)*, Waltham, MA, USA, 2010, pp. 302–308.
- [CHA13] W. Y. Chang, "The state of charge estimating methods for battery: A review," *ISRN Appl. Math.*, vol. 2013, no. 7 pp.1-7, 2013.
- [CHA14] B. R. Chalamala, *et al.*, "Redox flow batteries: An engineering perspective," *IEEE Proc.*, vol. 102, no. 6, pp. 976-999, Jun. 2014.
- [CHA17] L. Chang, W. Zhang, S. Xu, and K. Spence, "Review on distributed energy storage systems for utility applications," *CPSS Trans. Power Electron. Appl.*, vol. 2, no. 4, pp. 267-276, Dec. 2017.
- [CHE09] H. Chen, *et al.*, "Progress in electrical energy storage system: A critical review," *Progress Natural Science*, vol. 19, no. 3, pp. 291-312, 2009.

- [CHE15] Y. Chen, *et al.*, "Energy management method applying in integrated energy system," in *Int. Conf. Elect. Utility Deregul. Restruct. Power Technol. (DRPT'15)*, Changsha, 2015, pp. 1565-1569.
- [CHE16] S. Chen, *et al.*, "Penetration rate and effectiveness studies of aggregated BESS for frequency regulation," *IEEE Trans. Smart Grid*, vol. 7, no. 1, pp. 167-177, Jan. 2016.
- [CHO17] W. Choi *et al.*, "Reviews on grid-connected inverter, utility-scaled battery energy storage system, and vehicle-to-grid application - challenges and opportunities," in *IEEE Transport. Electrific. Conf. Expo (ITEC'17)*, Chicago, IL, 2017, pp. 203-210.
- [CHO17] W. Choi *et al.*, "Reviews on grid-connected inverter, utility-scaled battery energy storage system, and vehicle-to-grid application - challenges and opportunities," in *IEEE Transp. Electrifi. Conf. Expo. (ITEC'17)*, Chicago, 2017, pp. 203-210.
- [COC14] J. Cochran, *et al.*, "Flexibility in 21st Century Power Systems 2014," Available [Online]: <https://www.nrel.gov/docs/fy14osti/61721.pdf>, accessed at 16 Jan. 2019.
- [COL07] M. Coleman, C. K. Lee, C. Zhu, and W. G. Hurley, "State-of-charge determination from EMF voltage estimation: Using impedance, terminal voltage, and current for lead-acid and lithium-ion batteries," *IEEE Trans. Ind. Electron.*, vol. 54, no. 5, pp. 2550-2557, Oct. 2007.
- [COO17] A. Cooke, D. Strickland, and K. Forkasiewicz, "Energy storage for enhanced frequency response services," in *Int. Univ. Power Eng. Conf. (UPEC'17)*, Heraklion, 2017, pp. 1-6.
- [DEA14] J. P. Deane, G. Drayton, and B. P. Ó Gallachóir, "The impact of sub-hourly modelling in power systems with significant levels of renewable generation," *Appl. Energy*, vol. 113, pp. 152-158, 2014.
- [DEH19] A. R. Dehghani-Sanij, E. Tharumalingam, M. B. Dusseault, and R. Fraser, "Study of energy storage systems and environmental challenges of batteries," *Renew. Sustain. Energy Rev.*, vol. 104, pp. 192-208, 2019.
- [DIV09] K. C. Divya and J. Østergaard, "Battery energy storage technology for power systems—An overview," *Electr. Power Syst. Res.*, vol. 79, no. 4, pp. 511–520, Apr. 2009.
- [DIX04] M. Dixon, "Working with the electricity industry in times of rapid change - A telecomms user's experience," in *Int. Telecommun. Energy Annu. Conf. (INTELEC'04)*, 2004, Chicago, pp.100-106.
- [DIX99] M. G. Dixon, "Profitable use of standby generators in a competitive electricity market," in *Int. Telecommun. Energy Conf. (INTELEC'99)*, Copenhagen, 1999, pp. 1-7.
- [DOW82] S. D. Downing and D. F. Socie, "Simple rainflow counting algorithms," *Int. J. Fatigue*, vol. 4, no. 1, pp. 31–40, 1982.



- [DUF08] R. Dufo-Lopez and J. L. Bernal-Agustin, "Multi-objective design of PV–wind–diesel–hydrogen–battery systems," *Renew. Energy*, vol. 33, no. 12, pp. 2559–2572, 2008.
- [DUN16a] A. Dunbar, *et al.*, "Impact of wind power on arbitrage revenue for electricity storage," *IET Gener. Transm. Distrib.*, vol. 10, no. 3, pp. 798-806, 2016.
- [DUN16b] A. Dunbar, A. R. Wallace, and G. P. Harrison, "Energy storage and wind power: sensitivity of revenue to future market uncertainties," *IET Renew. Power Gener.*, vol. 10, no. 10, pp. 1535-1542, 2016.
- [DUR14] E. Durna, *et al.*, "Adaptation of renewable based power plants to the energy market using battery energy storage systems," in *Int. Conf. Renew. Energy Res. Appl. (ICRERA'14)*, 2014, pp. 643-647.
- [ECK14] M. Ecker *et al.*, "Calendar and cycle life study of Li(NiMnCo)O<sub>2</sub>-based 18650 lithium-ion batteries," *J. Power Sources*, vol. 248, pp. 839-851, 2014
- [EGH14] N. Eghtedarpour and E. Farjah, "Distributed charge/discharge control of energy storages in a renewable-energy-based DC micro-grid," *IET Renew. Power Gener.*, vol. 8, no. 1, pp. 45-57, 2014.
- [EIC13] H. R. Eichi, U. Ojha, F. Baronti, and M. Y. Chow, "Battery management system: An overview of its application in the smart grid and electric vehicles," *IEEE Ind. Electron. Mag.*, vol. 7, no. 2, pp. 4-16, Jun. 2013.
- [EKM10] C. K. Ekman and S. H. Jensen, "Prospects for large scale electricity storage in Denmark," *Energy Convers. Manag.*, vol. 51, no. 6, pp. 1140-1147, 2010.
- [FAI12] F. Rahman, S. Rehman, and M. A. Abdul-Majeed, "Overview of energy storage systems for storing electricity from renewable energy sources in Saudi Arabia," *Renew. Sustain. Energy Rev.*, vol. 16, no. 1, pp. 274-283, 2012.
- [FAI18] M. Faisal, *et al.*, "Review of energy storage system technologies in microgrid applications: Issues and challenges," *IEEE Access*, vol. 6, pp. 35143-35164, 2018.
- [FEE16] T. Feehally *et al.*, "Battery energy storage systems for the electricity grid: UK research facilities," in *IET Int. Conf. Power Electron. Mach. Drives (PEMD 2016)*, Glasgow, 2016, pp. 1-6.
- [FER13] H. L. Ferreira, *et al.*, "Characterisation of electrical energy storage technologies," *Energy*, vol. 53, pp. 288-298, 2013.
- [GAL17] E. Gallant, "Lerwick Power Station Shetland Islands Case Study," 2017.
- [GAO17] Yang Gao *et al.*, "Lithium-ion battery aging mechanisms and life model under different charging stresses", *J. Power Sources*, vol. 356, pp. 103-114, 2017.
- [GAO18] Y. Gao *et al.*, "Aging mechanisms under different state-of-charge ranges and the multi-indicators system of state-of-health for lithium-ion battery with Li(NiMnCo)O<sub>2</sub> cathode", *J. Power Sources*, vol. 400, pp. 641-651, 2018.

- [GEE13] A. M. Gee, F. V. P. Robinson and R. W. Dunn, "Analysis of battery lifetime extension in a small-scale wind-energy system using supercapacitors," *IEEE Trans. Energy Convers.*, vol. 28, no. 1, pp. 24-33, Mar. 2013.
- [GIL13] S. Gill, *et al.*, "Maximising revenue for non-firm distributed wind generation with energy storage in an active management scheme," *IET Renew. Power Gener.*, vol. 7, no. 5, pp. 421-430, 2013.
- [GOP15] L. R. GopiReddy, L. M. Tolbert, B. Ozpineci, and J. O. P. Pinto, "Rainflow algorithm-based lifetime estimation of power semiconductors in utility applications," *IEEE Trans. Ind. Appl.*, vol. 51, no. 4, pp. 3368-3375, Aug. 2015.
- [GOU17] R. Gough, C. Dickerson, P. Rowley, and C. Walsh, "Vehicle-to-grid feasibility: A techno-economic analysis of EV-based energy storage," *Applied Energy*, vol. 192, pp. 12-23, Apr. 2017.
- [GRE15] D. Greenwood, *et al.*, "Scheduling power and energy resources on the smarter network storage project," in *Int. Conf. Exhib. Elect. Distrib.*, Lyon, 2015.
- [GRE16] D. Greenwood, *et al.*, "A forecasting, optimization and scheduling system for energy storage systems in distribution networks," in *IEEE Power Energy Soc. Gen. Meet. (PESGM'16)*, Boston, 2016, pp. 1-5.
- [GRE17] D. M. Greenwood, *et al.*, "Frequency response services designed for energy storage," *Applied Energy*, vol. 203, pp. 115-127, Oct. 2017.
- [GUN17a] B. Gundogdu, S. Nejad, D. T. Gladwin, and D. A. Stone, "A battery energy management strategy for UK enhanced frequency response," in *IEEE Int. Symp. Ind. Electron. (ISIE'17)*, Edinburgh, 2017, pp. 26-31.
- [GUN17b] B. Gundogdu, D. T. Gladwin, and D. A. Stone, "Battery SOC management strategy for enhanced frequency response and day-ahead energy scheduling of BESS for energy arbitrage," in *IEEE Ind. Electron. Soc. Annu. Conf. (IECON'17)*, Beijing, 2017, pp. 7635-7640.
- [GUN17c] B. Gundogdu, D. T. Gladwin, and D. A. Stone, "A battery energy management strategy for EFR and day-ahead energy scheduling of BESS for energy arbitrage", in *IEEE Ind. Electron. Soc. Annu. Meeting (IECON'17)*, 2017, Beijing, pp. 1-6.
- [GUN18a] B. Gundogdu, D. T. Gladwin, M. P. Foster and D. A. Stone, "A forecasting battery state of charge management strategy for frequency response in the UK system," in *IEEE Int. Conf. Ind. Technol. (ICIT'18)*, Lyon, 2018, pp. 1726-1731.
- [GUN18b] B. Gundogdu, S. Nejad, D. T. Gladwin, M. P. Foster and D. A. Stone, "A battery energy management strategy for u.k. enhanced frequency response and triad avoidance," in *IEEE Trans. Ind. Electron.*, vol. 65, no. 12, pp. 9509-9517, Dec. 2018.
- [GUN18c] B. Gundogdu, D. Gladwin, and D. Stone, "Battery energy management strategies for UK firm frequency response services and energy arbitrage," *IET J. Eng.*, vol. 2019, no. 17, pp. 4152-4157, 2019.

- [GUN19] B. Gundogdu, D. T. Gladwin, S. Nejad, and D. A. Stone, "Scheduling of grid tied battery energy storage system participating in frequency response services and energy arbitrage," *IET Gener. Transm. Dis.*, early view , published, 26 Feb 2019.
- [HAA17] J. Haas, *et al.*, "Challenges and trends of energy storage expansion planning for flexibility provision in low-carbon power systems – A review", *Renew. Sustain. Energy Rev.*, vol. 80, pp. 603-619, 2017.
- [HAM17] S. Hamdy, T. Morosuk, and G. Tsatsaronis, "Cryogenics-based energy storage: Evaluation of cold exergy recovery cycles," *Energy*, vol. 138, pp. 1069-1080, 2017.
- [HAN14] S. Han, S. Han, and H. Aki, "A practical battery wear model for electric vehicle charging applications," *Applied Energy*, vol. 113, pp. 1100-1108, 2014.
- [HAN17] M.A. Hannan, M.S.H. Lipu, A. Hussain, and A. Mohamed, "A review of lithium-ion battery state of charge estimation and management system in electric vehicle applications: Challenges and recommendations", *Renew. Sust. Energy Rev.*, vol. 78, pp. 834-854, 2017.
- [HAO15] Z. Haoran, *et. al.*, "Review of energy storage system for wind power integration support," *Appl. Energy*, vol. 137, pp. 545-553, 2015.
- [HE12] H. He, R. Xiong, and H. Guo, "Online estimation of model parameters and state-of-charge of LiFePO<sub>4</sub> batteries in electric vehicles," *Appl. Energy*, vol. 89, no. 1, pp. 413-420, 2012.
- [HOK13] A. Hoke *et al.*, "Maximizing lithium ion vehicle battery life through optimized partial charging," in *IEEE PES Innov. Smart Grid Technol. (ISGT'13)*, Washington, DC, 24–27, 2013, pp. 1–5.
- [HOL15] R. Hollinger, L. M. Diazgranados, and T. Erge, "Trends in the German PCR market: Perspectives for battery systems," in *Int. Conf. Euro. Energy Market (EEM'15)*, Lisbon, 2015, pp. 1-5.
- [HOL16] R. Hollinger, *et al.*, "Distributed solar battery systems providing primary control reserve," *IET Renew. Power Generation*, vol. 10, no. 1, pp. 63-70, Jan. 2016.
- [HUE98] F. Huet, "A review of impedance measurements for determination of the state-of-charge or state-of-health of secondary batteries", *J. Power Sources*, vol. 70, no. 1, pp. 59-69, 1998.
- [HUS13] A. A. Hussein and I. Batarseh, "Energy management for a grid-tied photovoltaic-wind-storage system—Part II: Operation strategy," in *IEEE Power Energy Soc. Gen. Meet.*, Vancouver, BC, 2013, pp. 1-5.
- [IBR08] H. Ibrahim, A. Ilinca, and J. Perron, "Energy storage systems—Characteristics and comparisons," *Renew. Sust. Energy Rev.*, vol. 12, pp. 1221–1250, 2008.

- [ISM19] S. M. Ismael, *et al.*, "State-of-the-art of hosting capacity in modern power systems with distributed generation," *Renew. Energy*, vol. 130, pp. 1002-1020, 2019.
- [JAM15] A. A. Jamali, N. M. Nor, and T. Ibrahim, "Energy storage systems and their sizing techniques in power system — A review," in *IEEE Conf. Energy Convers. (CENCON'15)*, Johor Bahru, 2015, pp. 215-220.
- [JEN17] A. M. Jenkins, *et al.*, "Creating virtual energy storage systems from aggregated smart charging electric vehicles," *CIREC - Open Access Proc. J.*, vol. 2017, no. 1, pp. 1664-1668, Oct. 2017.
- [JON11] C. D. Jonghe, B. F. Hobbs, and R. Belmans, "Integrating short-term demand response into long-term investment planning; 2011," Available [Online]: <http://www.econ.cam.ac.uk/research-files/repec/cam/pdf/cwpe1132.pdf>, accessed at 16 Jan. 2019.
- [KAR13] G. Karmiris and T. Tegnér, "Control method evaluation for battery energy storage system utilized in renewable smoothing," in *IEEE Ind. Electron. Soc. Conf. (IECON'13)*, Vienna, 2013, pp. 1566-1570.
- [KAY14] P. Kayal, T. Bhattacharjee, and C. K. Chanda, "Planning of renewable dgs for distribution network considering load model: A multi-objective approach," *Energy Procedia*, vol. 54, pp. 85-96, 2014.
- [KE15] X. Ke, N. Lu, and C. Jin, "Control and size energy storage systems for managing energy imbalance of variable generation resources," *IEEE Trans. Sustain. Energy*, vol. 6, no. 1, pp. 70-78, Jan. 2015.
- [KEL10] S. Kelly and M. Pollitt, "An assessment of the present and future opportunities for combined heat and power with district heating (CHP-DH) in the United Kingdom," *Energy Policy*, vol. 38, no. 11, pp. 6936-6945, Nov. 2010.
- [KHA10] A. Khaligh and Z. Li, "Battery, ultracapacitor, fuel cell, and hybrid energy storage systems for electric, hybrid electric, fuel cell, and plug-in hybrid electric vehicles: State of the art," *IEEE Trans. Veh. Technol.*, vol. 59, no. 6, pp. 2806-2814, Jul. 2010.
- [KHA15] H. Khani, and M. R. D. Zadeh, "Online adaptive real-time optimal dispatch of privately owned energy storage systems using public-domain electricity market prices," *IEEE Trans. Power Syst.*, vol. 30, no. 2, pp. 930-938, 2015.
- [KHA17] Y. Khawaja, D. Giaouris, H. Patsios and M. Dahidah, "Optimal cost-based model for sizing grid-connected PV and battery energy system," in *IEEE Jordan Conf. Appl. Elect. Eng. Comput. Technol. (AEECT'17)*, Aqaba, 2017, pp. 1-6.
- [KIM17] J. Kim, Y. Suharto, and T. U. Daim, "Evaluation of electrical energy storage (EES) technologies for renewable energy: A case from the US Pacific Northwest," *J. Energy Storage*, vol: 11, pp. 25-54, 2017.
- [KNA16] V. Knap, *et al.*, "Sizing of an energy storage system for grid inertial response and primary frequency reserve," *IEEE Trans. Power Syst.*, vol. 31, no. 5, pp. 3447-3456, Sep. 2016.

- [KOL13] M. Koller, T. Borsche, A. Ulbig, and G. Andersson, "Defining a degradation cost function for optimal control of a battery energy storage system," in *IEEE Grenoble Powertech. Conf. Proc.*, Grenoble, France, 2013, pp. 1–6.
- [KOT93] D. Kottick, M. Blau, and D. Edelstein, "Battery energy storage for frequency regulation in an island power system," *IEEE Trans. Energy Convers.*, vol. 8, no. 3, pp. 455–458, Sep. 1993.
- [KYR16] G. L. Kyriakopoulos and G. Arabatzis, "Electrical energy storage systems in electricity generation: Energy policies, innovative technologies, and regulatory regimes," *Renew. Sustain. Energy Rev.*, vol. 56, pp. 1044–1067, 2016.
- [LAN11] E. Lannoye, D. Flynn, and M. O'Malley, "The role of power system flexibility in generation planning," in *IEEE Power Energy Soc. Gen. Meet.*, Detroit, MI, USA, 2011, pp. 1-6.
- [LAR15] I. Laresgoiti, S. Käbitz, M. Ecker, and D. U. Sauer, "Modeling mechanical degradation in lithium ion batteries during cycling: Solid electrolyte interphase fracture," *J. Power Sources*, vol. 300, pp. 112–122, Dec. 2015.
- [LAW14] M. T. Lawder *et al.*, "Battery energy storage system (BESS) and battery management system (BMS) for grid-scale applications," *IEEE Proc.*, vol. 102, no. 6, pp. 1014–1030, Jun. 2014.
- [LI16] X. Li, L. Yao, and D. Hui, "Optimal control and management of a large-scale battery energy storage system to mitigate fluctuation and intermittence of renewable generations", *J. Modern Power Syst. Clean Energy*, vol. 4, no. 4, pp 593–603, Oct. 2016.
- [LIA17] B. Lian, A. Sims, D. Yu, C. Wang, and R. W. Dunn, "Optimizing LiFePO4 battery energy storage systems for frequency response in the UK system," *IEEE Trans. Sustain. Energy*, vol. 8, no. 1, pp. 385–394, Jan. 2017.
- [LU95] C. F. Lu, C.-C. Liu, and C.-J. Wu, "Dynamic modelling of battery energy storage system and application to power system stability," *Proc. Inst. Elect. Eng., Gen., Transm., Distrib.*, vol. 142, no. 4, pp. 429–435, Jul. 1995.
- [LUO15] X. Luo, J. Wang, M. Dooner, and J. Clarke, "Overview of current development in electrical energy storage technologies and the application potential in power system operation", *Appl. Energy*, vol. 137, pp. 511–536, 2015.
- [LUT15] G. Lutzemberger, "Cycle life evaluation of lithium cells subjected to micro-cycles," in *Int. Youth Conf. Energy (IYCE'15)*, Pisa, 2015, pp. 1-5.
- [MAI11] K. Mainka, M. Thoben and O. Schilling, "Lifetime calculation for power modules, application and theory of models and counting methods," in *Proc. European Conf. Power Electron. Appl.*, Birmingham, 2011, pp. 1-8.
- [MAR17] C. Marmaras, A. Javed, L. Cipcigan, and O. Rana, "Predicting the energy demand of buildings during triad peaks in GB," *Energy and Buildings*, vol. 141, pp. 262–273, Apr. 2017.

- [MAS10] T. M. Masaud, K. Lee, and P. K. Sen, "An overview of energy storage technologies in electric power systems: What is the future?," in *North American Power Sympo. 2010*, Arlington, TX, 2010, pp. 1-6.
- [MAT14] H. Matthias, D. Desislava, and H. Thomas, "Integration of wind and solar power in Europe: Assessment of flexibility requirements," *Energy*, vol. 69, pp. 236-246, 2014.
- [MAT68] M. Matsuishi and T. Endo, "Fatigue of metals subjected to varying stress," in *Japan Soc. Mech. Eng.*, pp. 37-40, Dec. 1968.
- [MAT68] M. Matsuishi and T. Endo, "Fatigue of Metals Subjected to Varying Stress," in *Proc. Japan Soc. Mech. Eng.*, Fukuoka, 1968.
- [MBU16] N. T. Mbungu, *et al.*, "Smart SISO-MPC based energy management system for commercial buildings: Technology trends," in *Future Techno. Conf. (FTC'16)*, 2016, pp. 750-753.
- [MBU17] N. T. Mbungu, R. M. Naidoo, and R. C. Bansal, "Real-time electricity pricing: TOU-MPC based energy management for commercial buildings," *Energy Procedia*, 105, pp. 3419-3424, 2017.
- [MEG13] O. Mégel, J. L. Mathieu, and G. Andersson, "Maximizing the potential of energy storage to provide fast frequency control," in *IEEE PES ISGT Europe 2013*, Lyngby, 2013, pp. 1-5.
- [MEH17] J. Meng *et al.*, "An overview of online implementable SOC estimation methods for Lithium-ion batteries," in *Int. Conf. Optim. Electr. Electron. Equip. (OPTIM) & Int. Aegean Conf. Elect. Mach. Power Electron. (ACEMP'17)*, Brasov, 2017, pp. 573-580.
- [MEH18] L. Mehigan, J. P. Deane, B. P. Ó. Gallachóir, and V. Bertsch, "A review of the role of distributed generation (DG) in future electricity systems," *Energy*, vol. 163, pp. 822-836, 2018.
- [MER09] P. Mercier, R. Cherkaoui and A. Oudalov, "Optimizing a battery energy storage system for frequency control application in an isolated power system," *IEEE Tran. Power Syst.*, vol. 24, no. 3, pp. 1469-1477, Aug. 2009.
- [MEY15] Q. Meysam, *et al.*, "Role of power-to-gas in an integrated gas and electricity system in Great Britain," *Int. J. Hydrogen Energy*, vol. 40, no. 17, pp. 5763-5775, 2015.
- [MIL10] A. Millner, "Modeling lithium ion battery degradation in electric vehicles," in *IEEE Conf. Innov. Technol. Efficient Rel. Elect. Supply (CITRES'10)*, Waltham, MA, USA, 2010, pp. 349-356.
- [MIR15] I. Miranda, N. Silva, and A. M. Bernardo, "Assessment of the potential of Battery Energy Storage Systems in current European markets designs," in *Int. Conf. Euro. Energy Market (EEM'15)*, Lisbon, 2015, pp. 1-5.
- [MIS02] S. Mishra, *et al.*, "Remaining life prediction of electronic products using life consumption monitoring approach," in *Proc. Eur. Microelectron. Packag. Interconnect. Symp.*, Kraków, Poland, Jun. 2002, pp. 136-142.

- [MOG17] A. Anvari-Moghaddam, *et al.*, "Efficient energy management for a grid-tied residential microgrid," *IET Gen. Transm. Distrib.*, vol. 11, no. 11, pp. 2752-2761, 2017.
- [MON15] M. A. Monem *et al.*, "Lithium-ion batteries: Evaluation study of different charging methodologies based on aging process", *Applied Energy*, vol. 152, pp. 143-155, 2015.
- [MOU17] S. M. Mousavi, *et al.* "A comprehensive review of flywheel energy storage system technology", *Renew. Sustain. Energy Rev.*, vol. 67, pp. 477-490, 2017.
- [MUL14] C. Mullen, P. C. Taylor, V. Thornley, and N. S. Wade, "Use of standby generation for reduction of transmission network charges for half-hourly metered customers," in *Int. Uni. Power Eng. Conf. (UPEC'14)*, Cluj-Napoca, 2014, pp. 1-6.
- [MUL16] C. Mullen, N. S. Wade, O. Olabisi, and P. C. Taylor, "The impact of the coincidence of STOR and triad events on STOR provider's net-income considering load recovery characteristics," in *CIREN Workshop 2016*, Helsinki, 2016, pp. 1-4.
- [MUS12] M. Musallam and C. M. Johnson, "An efficient implementation of the rainflow counting algorithm for life consumption estimation," *IEEE Trans. Rel.*, vol. 61, no. 4, pp. 978-986, Dec. 2012.
- [MUT19] K. M. Muttaqi, M. R. Islam, and D. Sutanto, "Future power distribution grids: integration of renewable energy, energy storage, electric vehicles, superconductor, and magnetic bus," *IEEE Trans. Appl. Supercond.*, vol. 29, no. 2, pp. 1-5, Mar. 2019.
- [NAD19] F. Nadeem, *et al.*, "Comparative review of energy storage systems, their roles, and impacts on future power systems," *IEEE Access*, vol. 7, pp. 4555-4585, 2019.
- [NEH11] M. H. Nehrir *et al.*, "A review of hybrid renewable/alternative energy systems for electric power generation: configurations, control, and applications," *IEEE Trans. Sustain. Energy*, vol. 2, no. 4, pp. 392-403, Oct. 2011.
- [NEJ15] S. Nejad, D. T. Gladwin, and D. A. Stone, "Enhanced state-of-charge estimation for lithium-ion iron phosphate cells with flat open-circuit voltage curves," in *IEEE Ind. Electron. Soc. Annu. Meeting (IECON'15)*, Yokohama, 2015.
- [NEJ16] S. Nejad, *Adaptive techniques for estimation and online monitoring of battery energy storage devices*. Diss. University of Sheffield, 2016.
- [NEJ16a] S. Nejad, D.T. Gladwin, and D.A. Stone, "A systematic review of lumped-parameter equivalent circuit models for real-time estimation of lithium-ion battery states," *J. Power Sources*, vol. 316, pp. 183-196, 2016
- [NEJ16b] S. Nejad, "Adaptive techniques for estimation and online monitoring of battery energy storage devices". PhD thesis, University of Sheffield, 2016. Available [Online]: <http://etheses.whiterose.ac.uk/17681/>

- [NEW16] D. G. Newbery, "A simple introduction to the economics of storage: shifting demand and supply over time and space," *Cambridge Working Paper in Economics University of Cambridge EPRG*, vol. 1661, pp. 1-24, Oct. 2016.
- [NIN04] G. Ning and B. N. Popov, "Cycle life modeling of lithium-ion batteries," *J. Electrochem. Soc.*, vol. 151, pp. A1584-A1591, 2004.
- [NIN06] G. Ning, R. E. White, and B. N. Popov, "A generalized cycle life model of rechargeable li-ion batteries," *Electrochim. Acta*, vol. 51, no. 10, pp. 2012–2022, 2006.
- [NIR10] N. K. C. Nair and N. Garimella, "Battery energy storage systems: Assessment for small-scale renewable energy integration," *Energy Buildings*, vol. 42, no. 11, pp. 2124-2130, 2010.
- [NUH13] A. Nuhic *et al.*, "Health diagnosis and remaining useful life prognostics of lithium-ion batteries using data-driven methods", *J. Power Sources*, vol. 239, pp. 680-688, 2013.
- [OBA15] Z. A. Obaid, L. Cipcigan, and M. T. Muhsin, "Analysis of the Great Britain's power system with electric vehicles and storage systems," in *Int. Conf. Intell. Syst. Appl. Power Syst. (ISAP'15)*, Porto, 2015, pp. 1-6.
- [ONL15a] National Grid "Enhanced frequency response", Available [Online]: <https://www.nationalgrid.com/uk/electricity/balancing-services/frequency-response-services/enhanced-frequency-response-efr> , 22 Sep. 2015.
- [ONL15b] National Grid, "Invitation for expressions of interest tender prequalification for provision of enhanced frequency response service", Available [Online]: <http://www2.nationalgrid.com/WorkArea/DownloadAsset.aspx?id=42966>, Last access: 22 Sep. 2015.
- [ONL16a] National Grid, "Enhanced Frequency Response, Invitation to tender for pre-qualified parties V2.2", Available [Online]: [https://www.nationalgrid.com/sites/default/files/documents/Enhanced%20Frequency%20Response%20ITT%20v2\\_2%20clean.pdf](https://www.nationalgrid.com/sites/default/files/documents/Enhanced%20Frequency%20Response%20ITT%20v2_2%20clean.pdf) , accessed in 2016.
- [ONL17] Elexon, "System Sell & System Buy Prices," [Online], Available: <https://www.bmreports.com/bmrs/?q=balancing/systemsellbuyprices>, accessed at 20/01/2017.
- [ONL18a] Toshiba Scib rechargeable battery, Available [Online]: <https://www.scib.jp/en/about/index.htm>, accessed 25 Dec. 2018.
- [ONL18b] International hydropower association, Available [Online]: <https://www.hydropower.org/news/2018-hydropower-status-report-shows-record-rise-in-clean-electricity> , accessed 25 Dec. 2018.
- [ONL18d] NGET, "Enhanced Frequency Control Capability (EFCC), Battery Storage Investigation Report 2015," Available [Online]: <https://www.nationalgrideso.com/document/96486/download>, accessed 28 Dec. 2018.
- [ONL18e] Intelligence for Europe's Biggest Storage Project: Leighton Buzzard Battery Park (UK) Availble [Online]: <http://energystorage.org/energy-storage/case->



studies/intelligence-europes-biggest-storage-project-leighton-buzzard-battery, accessed 26 Dec. 2018.

- [ONL18f] US Department of Energy, "Grid energy storage", Available [Online]: <https://www.energy.gov/sites/prod/files/2014/09/f18/Grid%20Energy%20Storage%20December%202013.pdf>, accessed 26 Dec. 2018.
- [ONL18g] National Grid, "Frequency Response Service," Available [Online]: <https://www.nationalgrid.com/uk/electricity/balancing-services/frequency-response-services> , accessed on 10 Aug. 2018.
- [ONL18h] National Grid, "Firm frequency response," <https://www.nationalgrid.com/uk/electricity/balancing-services/frequency-response-services/firm-frequency-response> , accessed at 30 July 2018.
- [ONL18i] National Grid, "Technical guidance and testing procedure for static and dynamic demand response and battery storage providers of frequency balancing services," (Last Seen on 30 July 2018) [Online], Available: <https://www.nationalgrid.com/sites/default/files/documents/DSR%20Battery%20Storage%20Test%20Procedure%20for%20Frequency%20Response.pdf> , accessed at 30 July 2018.
- [ONL18j] National Grid, "Firm frequency response a guide to the services procured by national grid to manage system frequency," [Online], Available: <https://www.nationalgrid.com/sites/default/files/documents/Firm%20Frequency%20Response%201.1.pdf> , accessed at 30 July 2018.
- [ONL18k] National Grid, "Historic frequency data, [Online], Available: <https://www.nationalgrid.com/uk/electricity/balancing-services/frequency-response-services/historic-frequency-data>, accessed at 30 July 2018.
- [ONL18l] National Grid, "Transmission network use of system (TNUoS) charges," Available [Online]: <https://www.nationalgrid.com/uk/electricity/charging-and-methodology/transmission-network-use-system-tnuos-charges>, accessed on 17 Aug. 2018
- [ONL18m] National Grid, "Stage 02: Workshop consultations" Available [Online]: <https://www.nationalgrid.com/sites/default/files/documents/8589937464-Volume%20%20Workgroup%20Consultation%20Report.pdf>, pp. 11, published on 2 Aug. 2016, accessed on 25 Aug. 2018.
- [ONL18n] National Grid, "Firm frequency response interactive guidance" Available: [https://www.nationalgrid.com/sites/default/files/documents/Firm%20Frequency%20Response%20%28FFR%29%20Interactive%20Guidance%20v1%200\\_0.pdf](https://www.nationalgrid.com/sites/default/files/documents/Firm%20Frequency%20Response%20%28FFR%29%20Interactive%20Guidance%20v1%200_0.pdf) , December 2017, accessed at 30 July 2018.
- [ONL18o] National Grid, "Firm Frequency Response frequently asked questions" Available: <https://www.nationalgrid.com/sites/default/files/documents/FFR%20FAQs%20v1.3.pdf> , August 2017, accessed at 10 September 2018.
- [ONL18p] National Grid, "State of charge management guidance for FFR providers" Available: <https://www.nationalgrid.com/sites/default/files/documents/State%20of%20>

Charge%20management%20publication%20-%20EXT\_0.pdf , 23 April 2018, accessed at 10 September 2018.

- [ONL18r] National Grid, "2014-2015 Triads" Available [Online]: <http://www2.nationalgrid.com/UK/Industry-information/System-charges/Electricity-transmission/Transmission-Network-Use-of-System-Charges/Transmission-Charges-Triad-Data/>, accessed on 17 Aug. 2018.
- [ONL18s] National Grid, "Introduction to Triads" Available [Online]: <https://www.nationalgrid.com/sites/default/files/documents/44940-Triads%20Information.pdf>, accessed on 22 Aug. 2018.
- [ONL18u] National Grid, "Triads: why three is the magic number" Available [Online]: <http://nationalgridconnecting.com/triads-why-three-is-the-magic-number/>, accessed on 24 Aug. 2018.
- [ONL18v] National Grid, "Enhanced frequency response," [Online], Available: <http://www2.nationalgrid.com/Enhanced-Frequency-Response.aspx>, accessed at 3 Oct. 2018.
- [ONL18y] Toshiba, "SCiB super charge ion battery" Available [Online]: <https://www.scib.jp/en/download.htm>, accessed at 12 Oct. 2018.
- [ONL19a] "Flexible electricity systems," Available [Online]: <https://researchbriefings.parliament.uk/ResearchBriefing/Summary/POST-PN-0587> , accessed 17 Jan. 2019.
- [ONL19b] National Grid, "Demand side response" Available [Online]: <https://www.nationalgrideso.com/balancing-services/demand-side-response-dsr> ,accessed at 19 Jan. 2019.
- [ONL19c] EPRSC, "Capital for Great Technologies Call: Grid-scale Energy Storage Panel", Available [Online]: <https://epsrc.ukri.org/files/research/capital-for-great-technologies-call-grid-scale-energy-storage-panel/> , accessed 11 Mar. 2019.
- [ONL19e] National grid signs 20MW frequency response contract with battery storage operator, Available [Online]: <https://theenergyst.com/national-grid-signs-20mw-frequency-response-contract-with-battery-storage-operator/> ,accessed 21 Jan. 2019.
- [ONL19f] Available [Online]: <https://www.cornwall-insight.com/> , accessed at 28 Jan. 2019.
- [ONL19g] National Grid "System needs and product strategy", Available [Online]: <https://www.nationalgrideso.com/sites/eso/files/documents/8589940795-System%20Needs%20and%20Product%20Strategy%20-%20Final.pdf> , Accessed 29 Jan. 2019.
- [ONL19h] Two Birds "Future of National Grid Balancing Services - Implications for Storage" "System needs and product strategy", Available [Online]: <https://www.twobirds.com/~media/pdfs/future-of-national-grid-balancing-services--implications-on-storage--july-2017.pdf?la=en> , accessed 27 Feb. 2019.

- [ONL19i] Carbon Brief “Future power system”, Available [Online]: [https://www.carbonbrief.org/uk-needs-a-smart-power-revolution-says-infrastructure-commission/www-gifcreator-me\\_r3xltb-1](https://www.carbonbrief.org/uk-needs-a-smart-power-revolution-says-infrastructure-commission/www-gifcreator-me_r3xltb-1) , accessed 2 Mar. 2019.
- [ONL19j] Energy Storage Association “Hydrogen energy storage”, Available [Online]: <http://energystorage.org/energy-storage/technologies/hydrogen-energy-storage> , accessed 3 Mar 2019.
- [ONL19k] Northern Power Grid, "Generator Connections," [Online]. Available: <http://www.northernpowergrid.com/guide-prices-and-timescales/generation-connection>, Accessed at 02/07/2019.
- [ONL19l] R. Lee "Economics of grid scale lithium-ion battery storage," 2017, [Online] Available: <http://www.energystorage-cdt.ac.uk/outputs-cohort-3> , Accessed on 02/07/2019.
- [ORT14] M. A. Ortega-Vazquez, “Optimal scheduling of electric vehicle charging and vehicle-to-grid services at household level including battery degradation and price uncertainty,” *IET Gener. Transm. Distrib.*, vol. 8, no. 6, pp. 1007–1016, Jun. 2014.
- [OUD06] A. Oudalov, D. Chartouni, C. Ohler, and G. Linhofer, "Value analysis of battery energy storage applications in power systems," in *IEEE PES Power Syst. Conf. Expo.*, Atlanta, GA, 2006, pp. 2206-2211.
- [OUD07a] A. Oudalov, D. Chartouni, and C. Ohler, "Optimizing a battery energy storage system for primary frequency control," *IEEE Trans. Power Syst.*, vol. 22, no. 3, pp. 1259-1266, Aug. 2007.
- [OUD07b] A. Oudalov, R. Cherkaoui and A. Beguin, "Sizing and optimal operation of battery energy storage system for peak shaving application," in *IEEE Lausanne Power Tech.*, Lausanne, 2007, pp. 621-625.
- [OUY15] M. Ouyang *et al.*, “Low temperature aging mechanism identification and lithium deposition in a large format lithium iron phosphate battery for different charge profiles”, *J. Power Sources*, vol. 286, pp. 309-320, 2015.
- [PAP10] S. V. Papaefthymiou, E. G. Karamanou, S. A. Papathanassiou, and M. P. Papadopoulos, "A wind-hydro-pumped storage station leading to high RES penetration in the autonomous island system of Ikaria," *IEEE Trans. Sustain. Energy*, vol. 1, no. 3, pp. 163-172, Oct. 2010.
- [PAT10] C. Patsios, M. Antonakopoulos, A. Chaniotis, and A. Kladas, "Control and analysis of a hybrid renewable energy-based power system," in *Int. Conf. Elect. Mach. (ICEM'10)*, Rome, 2010, pp. 1-6.
- [PAT16] C. Patsios, *et al.*, “An integrated approach for the analysis and control of grid connected energy storage systems,” *J. Energy Storage*, vol. 5, pp. 48-61, 2016.
- [PAT17] H. Patsios, “Hybridizing energy storage systems to improve cost-effectiveness and expand service range”, UKES conference, Dec. 2017, London, Available, [Online]: <https://warwick.ac.uk/fac/sci/eng/research/grouplist/electricalpower/images/>

newsnevents/hies2017/presentations/hies2017\_uninewcastle\_harrispsios.pdf.

- [PEI06] F. Pei, K. Zhao, Y. Luo, and X. Huang, "Battery variable current-discharge resistance characteristics and state of charge estimation of electric vehicle," in *World Cong. Intell. Control Autom.*, Dalian, 2006, pp. 8314-8318.
- [PET10] S. B. Peterson, J. Apt, and J. F. Whitacre, "Lithium-ion battery cell degradation resulting from realistic vehicle and vehicle-to-grid utilization," *J. Power Sources*, vol. 195, no. 8, pp. 2385–2392, 2010.
- [PET10] S. B. Peterson, J. Apt, and J. Whitacre, "Lithium-ion battery cell degradation resulting from realistic vehicle and vehicle-to-grid utilization," *J. Power Sources*, vol. 195, pp. 2385-2392, 2010.
- [PIE14] P. Mancarella, "MES (multi-energy systems): An overview of concepts and evaluation models", *Energy*, vol. 65, pp. 1-17, 2014.
- [PIL01] S. Piller, M. Perrin, and A. Jossen, "Methods for state-of-charge determination and their applications", *J. Power Sources*, vol. 96, no. 1, pp. 113-120, 2001.
- [PIM17] A. J. Pimm, T. T. Cockerill, P. G. Taylor, and J. Bastiaans, "The value of electricity storage to large enterprises: A case study on Lancaster University," *Energy*, vol. 128, pp. 378-393, Jun. 2017.
- [POU06] P. A. Østergaard, "Ancillary services and the integration of substantial quantities of wind power," *Appl. Energy*, vol. 83, no. 5, pp. 451-463, 2006.
- [POU12] P. A. Østergaard, "Comparing electricity, heat and biogas storages' impacts on renewable energy integration," *Energy*, vol. 37, no. 1, pp. 255-262, 2012.
- [POU13] A. Poullikkas, "A comparative overview of large-scale battery systems for electricity storage," *Renew. Sustain. Energy Rev.*, vol. 27, pp. 778-788, 2013.
- [QIA10] H. Qian, J. Zhang, and J. Lai, "A grid-tie battery energy storage system," in *IEEE Workshop Control Model. Power Electron.*, Boulder, CO, 2010, pp. 1-5.
- [QIA11] H. Qian, J. Zhang, J. Lai, and W. Yu, "A high-efficiency grid-tie battery energy storage system," *IEEE Trans. Power Electron.*, vol. 26, no. 3, pp. 886-896, Mar. 2011.
- [RAH16] C. Rahmann, V. Vittal, J. Ascui, and J. Haas, "Mitigation control against partial shading effects in large-scale PV power plants," *IEEE Trans. Sustain. Energy*, vol. 7, no. 1, pp. 173-180, Jan. 2016.
- [RAZ19] S. E. Razavi, *et al.*, "Impact of distributed generation on protection and voltage regulation of distribution systems: A review", *Renew. Sustain. Energy Rev.*, vol. 105, pp. 157-167, 2019.
- [RED15] L. Reddy *et al.*, "Rainflow algorithm-based lifetime estimation of power semiconductors in utility applications," *IEEE Trans. Ind. Appl.*, vol. 51, pp. 3368-3375, 2015.

- [REH15] S. Rehman, L. M. Al-Hadhrami, and M. M. Alam, "Pumped hydro energy storage system: A technological review," *Renew. Sustain. Energy Rev.*, vol. 44, pp. 586-598, 2015.
- [ROB11] B. P. Roberts and C. Sandberg, "The role of energy storage in development of smart grids," *IEEE Proc.*, vol. 99, no. 6, pp. 1139-1144, Jun. 2011.
- [ROH16] P. K. Rohith, J. Priolkar, and G. R. Kunkolienkar, "Hydrogen: An innovative and alternative energy for the future," in *World Conf. Futuristic Trends Res. Innov. Social Welfare (Startup Conclave)*, Coimbatore, 2016, pp. 1-5.
- [ROT05] E. P. Roth and D. H. Doughty, "Development and characterization of Li-ion batteries for the freedom car advanced technology development program," in *IEEE Proc. Veh. Tech. Conf.* Stockholm, Sweden, 2005, pp. 2362-2366.
- [ROY15] N. K. Roy and H. R. Pota, "Current status and issues of concern for the integration of distributed generation into electricity networks," *IEEE Syst. J.*, vol. 9, no. 3, pp. 933-944, Sep. 2015.
- [ROY17] S. J. Royston, *et al.*, "Arc-flash calculation comparison for energy storage systems," in *Int. Univers. Power Eng. Conf. (UPEC'17)*, Heraklion, 2017, pp. 1-6.
- [SAW16] L. H. Saw, Y. Ye, and A. A. O. Tay, "Integration issues of lithium-ion battery into electric vehicles battery pack," *J. Cleaner Production*, vol. 113, pp. 1032-1045, 2016.
- [SAX16] S. Saxena, C. Hendricks, and M. Pecht, "Cycle life testing and modeling of graphite/LiCoO<sub>2</sub> cells under different state of charge ranges", *J. Power Sources*, vol. 327, pp. 394-400, 2016.
- [SCH09] E. Schaltz, A. Khaligh, and P. O. Rasmussen, "Influence of battery/ultracapacitor energy-storage sizing on battery lifetime in a fuel cell hybrid electric vehicle," *IEEE Trans. Veh. Technol.*, vol. 58, pp. 3882-3891, 2009.
- [SHA18] M. Shatnawi, N. A. Qaydi, N. Aljaberi, and M. Aljaberi, "Hydrogen-based energy storage systems: A review," in *Int. Conf. Renew. Energy Res. Appl. (ICRERA '18)*, Paris, 2018, pp. 697-700.
- [SHE15] J. Shen and A. Khaligh, "A supervisory energy management control strategy in a battery/ultracapacitor hybrid energy storage system," *IEEE Trans. Transport. Electrific.*, vol. 1, no. 3, pp. 223-231, Oct. 2015.
- [SIO09] R. Sioshansi, *et al.*, "Estimating the value of electricity storage in PJM: Arbitrage and some welfare effects," *Energy Economics*, vol. 31, no. 2, pp. 269-277, 2009.
- [SMI13] K. Smith, *et al.*, "Models for battery reliability and lifetime," in *Battery Congr.*, 2013, pp. 15-16.
- [SMI19] V. Smil, "Distributed generation and megacities: Are renewables the answer?," *IEEE Power Energy Mag.*, vol. 17, no. 2, pp. 37-41, Mar.-Apr. 2019.

- [SOL14] G. L. Soloveichik, "Regenerative fuel cells for energy storage," *IEEE Proc.*, vol. 102, no. 6, pp. 964-975, Jun. 2014.
- [SOM16] L. Somerville *et al.*, "The effect of charging rate on the graphite electrode of commercial lithium-ion cells: A post-mortem study," *J. Power Sources*, vol. 335, pp. 189-196, 2016.
- [SOO09] K. S. Ng, C. S. Moo, Y. P. Chen, and Y. C. Hsieh, "Enhanced coulomb counting method for estimating state-of-charge and state-of-health of lithium-ion batteries" *Appl. Energy*, vol. 86, no. 9, pp. 1506-1511, 2009.
- [SPI91] W. C. Spindler, "Lead/acid batteries in utility energy storage and power control applications," *J. Power Sources*, vol. 35, no. 4, pp. 395-398, 1991.
- [SPO03] R. Spotnitz, "Simulation of capacity fade in lithium-ion batteries," *J. Power Sources*, vol. 113, no. 1, pp. 72-80, 2003.
- [STR16] D. Stroe, *et al.*, "Degradation behavior of lithium-ion batteries based on lifetime models and field measured frequency regulation mission profile," *IEEE Trans. Ind. Appl.*, vol. 52, no. 6, pp. 5009-5018, Nov.-Dec. 2016.
- [STR16] D. Stroe, M. Swierczynski, A. Stroe, R. Laerke, P. C. Kjaer, and R. Teodorescu, "Degradation Behavior of Lithium-Ion Batteries Based on Lifetime Models and Field Measured Frequency Regulation Mission Profile," *IEEE Trans. Ind. Appl.*, vol. 52, no. 6, pp. 5009-5018, Nov.-Dec. 2016.
- [STR17] D. Stroe, V. Knap, M. Swierczynski, A. Stroe and R. Teodorescu, "Operation of a Grid-Connected Lithium-Ion Battery Energy Storage System for Primary Frequency Regulation: A Battery Lifetime Perspective," *IEEE Trans. Ind. Appl.*, vol. 53, no. 1, pp. 430-438, Jan.-Feb. 2017.
- [STR17] D. Stroe, V. Knap, M. Swierczynski, A. Stroe, and R. Teodorescu, "Operation of a grid-connected Lithium-Ion battery energy storage system for primary frequency regulation: A battery lifetime perspective," *IEEE Trans. Ind. Appl.*, vol. 53, no. 1, pp. 430-438, Jan.-Feb. 2017.
- [SUL76] V. T. Sulzberger and J. Zemkoski, "The potential for application of energy storage capacity on electric utility systems in the United States-Part I," *IEEE Trans. Power App. Syst.*, vol. 95, no. 6, pp. 1872-1881, Nov. 1976.
- [SWI10] M. Świerczyński, *et al.*, "Overview of the energy storage systems for wind power integration enhancement," in *IEEE Ind. Symp. Electron. (ISIE'10)*, 2010, pp. 3749-3756.
- [SWI13a] M. Świerczyński, D. I. Stroe, A. I. Stan, and R. Teodorescu, "Primary frequency regulation with Li-ion battery energy storage system: A case study for Denmark," in *IEEE ECCE Asia Downunder*, Melbourne, VIC, 2013, pp. 487-492.
- [SWI13b] M. Swierczynski, "Lithium ion battery energy storage system for augmented wind power plants," Ph.D. dissertation, Dept. of Energy Technology, Aalborg University, Denmark, 2013.
- [SWI14] M. Świerczyński, D. I. Stroe, A. Stan, R. Teodorescu, and D. U. Sauer, "Selection and performance-degradation modeling of  $\text{LiMO}_2/\text{Li}_4\text{Ti}_5\text{O}_{12}$  and  $\text{LiFePO}_4/\text{C}$  battery cells as suitable energy storage systems for grid integration

with wind power plants: An example for the primary frequency regulation service," *Trans. Sustain. Energy*, vol. 5, no. 1, pp. 90-101, Jan. 2014.

- [TAN13] M. A. Tankari, M. B. Camara, B. Dakyo, and G. Lefebvre, "Use of ultracapacitors and batteries for efficient energy management in wind-diesel hybrid system," *IEEE Trans. Sustain. Energy*, vol. 4, pp. 414-424, 2013.
- [TAN15] A. Tani, M. B. Camara, and B. Dakyo, "energy management in the decentralized generation systems based on renewable energy— Ultracapacitors and battery to compensate the wind/load power fluctuations," *IEEE Trans. Ind. Appl.*, vol. 51, no. 2, pp. 1817-1827, Mar. 2015.
- [TEN17] F. Teng, *et al.*, "Business case for distributed energy storage," *CIREN-Open Access Proc. J.*, vol. 2017, no. 1, pp. 1605-1608, 2017.
- [THO13] E. Thorbergsson, *et al.*, "Primary frequency regulation with li-ion battery based energy storage system - Evaluation and comparison of different control strategies," in *Int. Telecom. Energy Conf.*, Hamburg, Germany, 2013, pp. 1-6.
- [THO13] E. Thorbergsson, V. Knap, M. Swierczynski, D. Stroe, and R. Teodorescu, "Primary frequency regulation with Li-Ion battery based energy storage system - Evaluation and comparison of different control strategies," in *Int. Telec. Energy Conf. (INTELEC'13)*, Hamburg, Germany, 2013, pp. 1-6.
- [TUR03] R. Turvey, "Ensuring adequate generation capacity," *Utilities Policy*, vol. 11, no. 2, pp. 95-102, Jun. 2003.
- [VAC16] S. M. Vaca, C. Patsios, and P. Taylor, "Enhancing frequency response of wind farms using hybrid energy storage systems," in *IEEE Int. Conf. Renew. Energy Res. Appl. (ICRERA'16)*, Birmingham, 2016, pp. 325-329.
- [VAL18] J. A. del Valle, *et al.*, "Analysis of advanced lithium-ion batteries for battery energy storage systems," in *IEEE Int. Conf. Enviro. Electrical Eng. and IEEE Ind Commer. Power Syst. Euro. (EEEIC / I&CPS Euro'18)*, Palermo, 2018, pp. 1-6.
- [VAL18] S. Vazquez, *et al.*, "Energy storage systems for transport and grid applications," *IEEE Tran. Ind. Electron.*, vol. 57, no. 12, pp. 3881-3895, Dec. 2010.
- [VEN09] C. Venu, Y. Rifononau, S. Bacha and Y. Baghzouz, "Battery Storage System sizing in distribution feeders with distributed photovoltaic systems," in *IEEE Bucharest PowerTech*, Bucharest, 2009, pp. 1-5.
- [VET05] J. Vetter *et al.*, "Ageing mechanisms in lithium-ion batteries," *J. Power Sources*, vol. 147, nos. 1-2, pp. 269-281, 2005.
- [WAN11] J. Wang *et al.*, "Cycle-life model for graphite-LiFePO<sub>4</sub> cells," *J. Power Sources*, vol. 196, no. 8, pp. 3942-3948, 2011.
- [WAN14] J. Wang *et al.*, "Degradation of lithium ion batteries employing graphite negatives and nickel-cobalt-manganese oxide + spinel manganese oxide positives: Part 1, aging mechanisms and life estimation", *J. Power Sources*, vol. 269, pp. 937-948, 2014,

- [WAR14] P. Warren, "A review of demand-side management policy in the UK," *Renew. Sustain. Energy Rev.*, vol. 29, pp. 941-951, 2014.
- [WAT14] S. Watanabe *et al.*, "Capacity fade of  $\text{LiAl}_y\text{Ni}_{1-x-y}\text{Co}_x\text{O}_2$  cathode for lithium-ion batteries during accelerated calendar and cycle life tests (surface analysis of  $\text{LiAl}_y\text{Ni}_{1-x-y}\text{Co}_x\text{O}_2$  cathode after cycle tests in restricted depth of discharge ranges)", *J. Power Sources*, vol. 258, pp. 210-217, 2014.
- [WEI14] W. Cao, Y. Du, X. Qi and L. Ji, "Research on operation optimization strategy of grid-connected PV-battery system," in *Int. Conf. Renew. Energy Res. Appl. (ICRERA '14)*, Milwaukee, WI, 2014, pp. 272-279.
- [WHI12] M. S. Whittingham, "History, evolution, and future status of energy storage," *IEEE Proc.*, vol. 100, no. Special Centennial Is., pp. 1518-1534, 13 May 2012.
- [WON19] L. A. Wong, *et al.*, "Review on the optimal placement, sizing and control of an energy storage system in the distribution network," *J. Energy Storage*, vol. 21, pp. 489-504, 2019.
- [WU19] Y. K. Wu, and K. T. Tang, "Frequency support by BESS – Review and analysis," *Energy Procedia*, vol. 156, pp. 187-191, 2019.
- [XIN17] H. Xing, *et al.*, "Distributed algorithm for dynamic economic power dispatch with energy storage in smart grids," *IET Control Theory Appl.*, vol. 11, no. 11, pp. 1813-1821, 2017.
- [XU16] X. Xu, M. Bishop, D. G. Oikarinen, and C. Hao, "Application and modeling of battery energy storage in power systems," *CSEE J. Power Energy Syst.*, vol. 2, no. 3, pp. 82-90, Sept. 2016.
- [XU18] B. Xu, *et al.*, "Modeling of Lithium-Ion Battery Degradation for Cell Life Assessment," *IEEE Trans. Smart Grid*, vol. 9, no. 2, pp. 1131-1140, Mar. 2018.
- [XU18a] B. Xu, J. Zhao, T. Zheng, E. Litvinov, and D. S. Kirschen, "Factoring the cycle aging cost of batteries participating in electricity markets," *IEEE Trans. Power Syst.*, vol. 33, no. 2, pp. 2248-2259, Mar. 2018.
- [YAN14] Y. Yang, H. Li, A. Aichhorn, J. Zheng and M. Greenleaf, "Sizing strategy of distributed battery storage system with high penetration of photovoltaic for voltage regulation and peak load shaving," *IEEE Trans. Smart Grid*, vol. 5, no. 2, pp. 982-991, Mar. 2014.
- [YUK07] K. Yukita, K. Ichiyanagi, Y. Goto, and K. Hirose, "A study of electric power quality using storage system in distributed generation," in *Int. Conf. Elect. Power Quality Util.*, Barcelona, 2007, pp. 1-4.
- [ZAK15] B. Zakeri and S. Syri, "Electrical energy storage systems: A comparative life cycle cost analysis," *Renew. Sustain. Energy Rev.*, vol. 42, pp. 569-596, 2015.
- [ZAL13] M. Z. Daud, A. Mohamed, and M. A. Hannan, "An improved control method of battery energy storage system for hourly dispatch of photovoltaic power sources," *Energy Convers. Manag.*, vol. 73, 2013, pp. 256-270.



- [ZHA08] Q. Zhang and R. E. White, "Capacity fade analysis of a lithium ion cell," *J. Power Sources*, vol. 179, no. 2, pp. 793–798, 2008.
- [ZHA15] H. Zhao, *et al.*, "Review of energy storage system for wind power integration support," *Appl. Energy*, vol. 137, pp. 545-553, 2015.
- [ZHA17] Q. Zhai, K. Meng, Z. Y. Dong, and J. Ma, "Modeling and analysis of lithium battery operations in spot and frequency regulation service markets in australia electricity market," *IEEE Trans. Ind. Informat.*, vol. 13, no. 5, pp. 2576-2586, Oct. 2017.
- [ZHA18] C. Zhang, Y. L. Wei, P. F. Cao, and M. C. Lin, "Energy storage system: Current studies on batteries and power condition system", *Renew. Sustain. Energy Rev.*, vol. 82, no. 3, pp. 3091-3106, 2018.
- [ZHO11] C. Zhou, K. Qian, M. Allan, and W. Zhou, "Modeling of the cost of EV battery wear due to V2G application in power systems," *IEEE Trans. Energy Conv.*, vol. 26, pp. 1041-1050, 2011.
- [ZHU19] D. Zhu and Y. A. Zhang, "Optimal coordinated control of multiple battery energy storage systems for primary frequency regulation," *IEEE Trans. Power Syst.*, vol. 34, no. 1, pp. 555-565, Jan. 2019.
- [ZHU65] S. N. Zhurkov, "Kinetic concept of the strength of solids," in *Proc. ICFI*, Sendai, Japan, 1965, pp. 1167–1184.

## Appendix A General Definitions

### A.1 Important Components of the UK Electricity System

**Generators** produce electricity and then sell it in the wholesale market. In 2017, 40% of UK electricity provided from gas, 29.5% from renewables and 21% from nuclear. In winter, peak power demand is approximately 50 gigawatts (GW) [ONL19a].

**The transmission network** is the network of high voltage lines which carries power over long distances, from large generators (e.g. gas power stations) to large industrial consumers and distribution networks [ONL19a].

**The distribution networks** is the low voltage network which has traditionally carried power from the transmission network to consumers. 14 distribution networks cover separate areas of UK. 6 distribution network operators (DNOs) own and they are responsible for operating and maintaining these [ONL19a].

**Suppliers** buy electricity in the wholesale market and sell it to consumers. They provide and fit smart electricity meters\*.

**\*Smart electricity meters:** According to UK Government rollout programme, all UK householders are being offered a smart electricity meter by 2020. The smart meters provide consumers with real time information on their electricity usage and enable more accurate electricity billing and energy saving. Smart electricity meters could aid to facilitate automated residential demand side management (DSM) and allow suppliers to make more precise demand forecasts and provide time-of-use pricing that is more responsive to demand [ONL19a].

**Aggregators** are companies that have contracts with several users who can increase/decrease their demand. They can adjust the demand of these users to sell grid balancing services. Some existing suppliers perform as aggregators [ONL19a].

### A.2 Definition of Demand Side Sources

**Turn-down demand side response (DSR):** Users decrease power consumption, reducing the power system demand.

**Turn-up demand side response (DSR):** Users increase demand at times of excess supply.

**Demand Side Response (DSR) by on-site Generation:** Many consumers use on-site generates such as combined heat, storage and power systems to provide for their own needs, reducing the system demand.

**Demand Side Management (DSM):** Users adjust the timing of the energy using to shift demand away from peak times [WAR14], [ONL19a], [ONL19b].

### **A.3 Definition of Distribution Network Operator (DNO) and Distribution System Operator (DSO)**

DNOs have traditionally held a passive role in maintaining the distribution network. Currently, they are undergoing a transition towards a DSO role. DSOs will take a more active role in monitoring network and are improving a plan for using flexibility services to manage power flows over their networks [ONL19c], [ONL19d].

## Appendix B Simulation Findings of Fast CCM

### B.1 Fast Battery CCM Considering No Other Effect

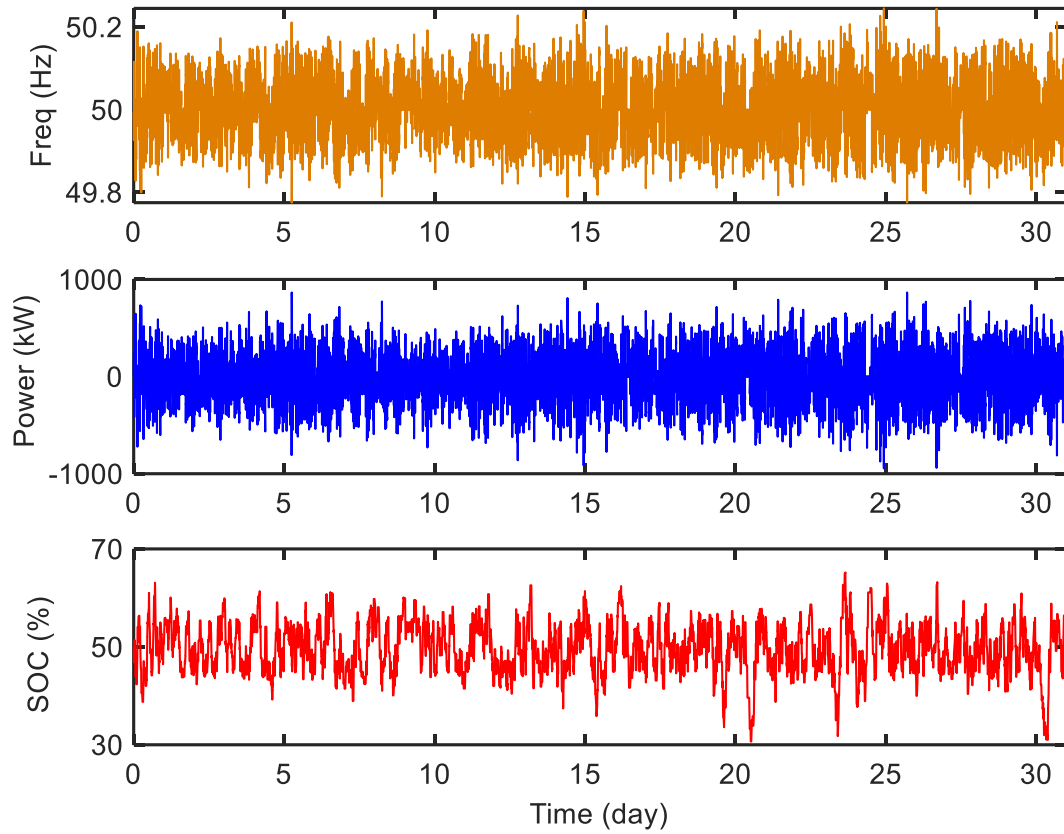


Fig. B.1 Simulation results of the EFR-A2 with Service-2 for October 2015.

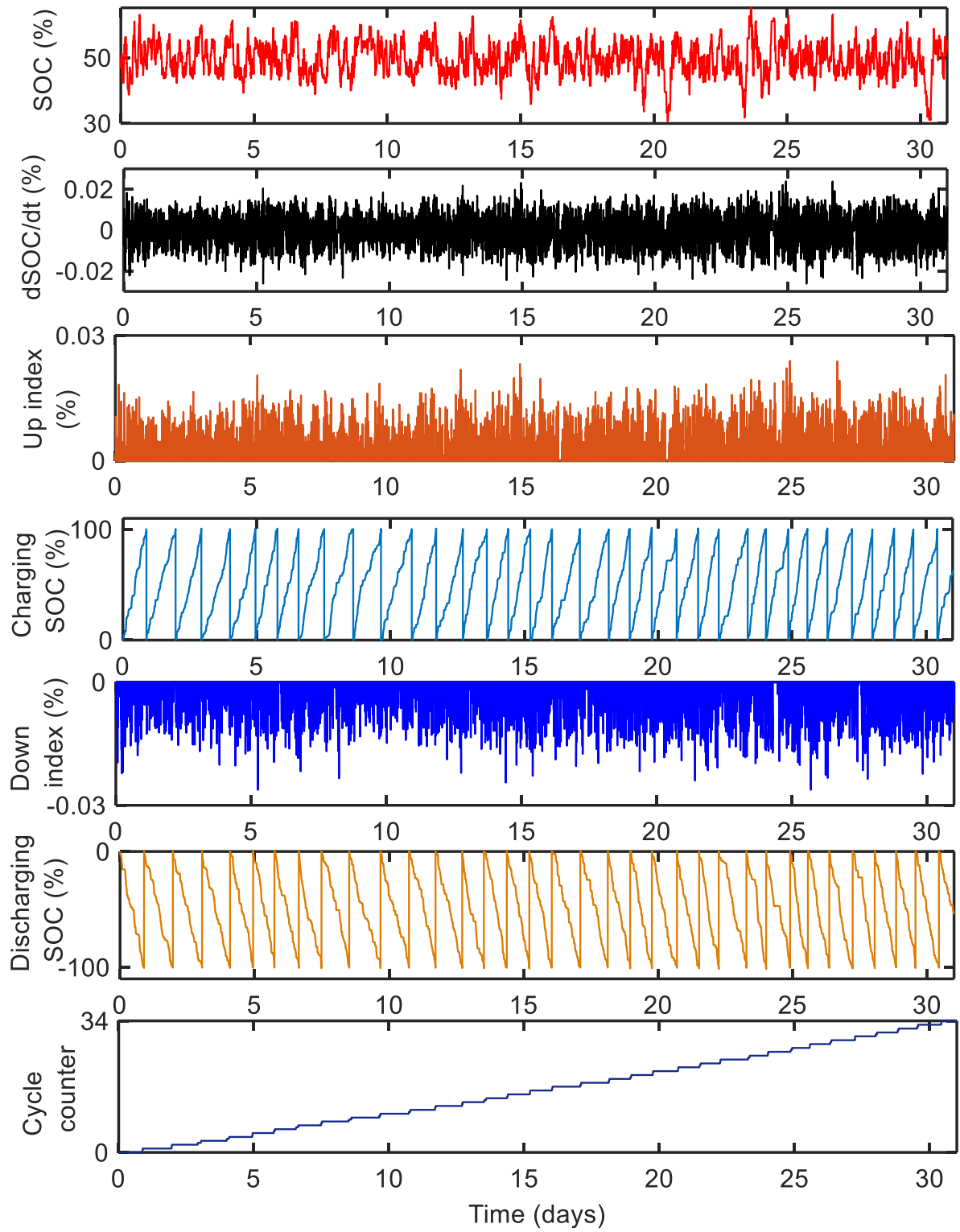


Fig. B.2 Demonstration of the basic CCM on 1-month profile of a battery SOC data set obtained by simulating the EFR-A2 for whole October 2015 frequency data.

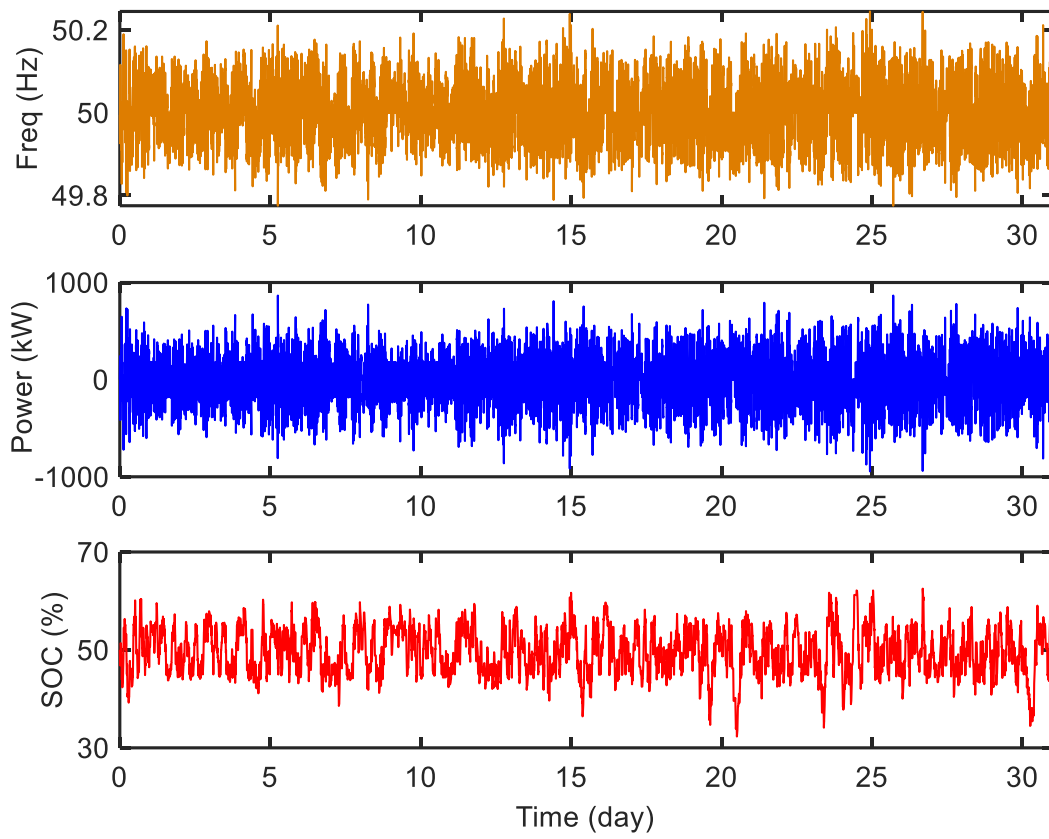


Fig. B.3 Simulation results of the EFR-A3 with Service-2 for October 2015.

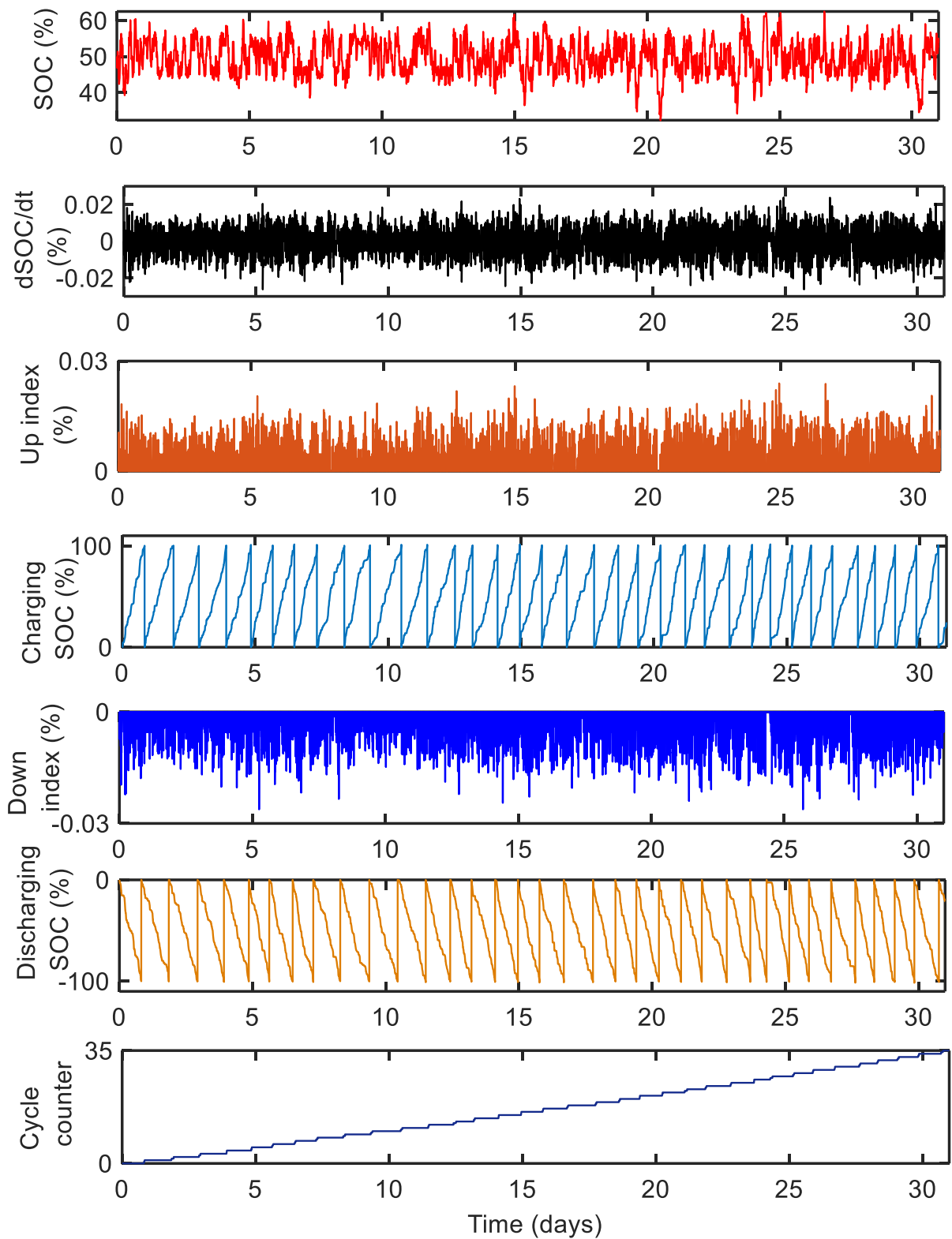


Fig. B.4 Demonstration of the basic CCM on 1-month profile of a battery SOC data set obtained by simulating the EFR-A3 for whole October 2015 frequency data.

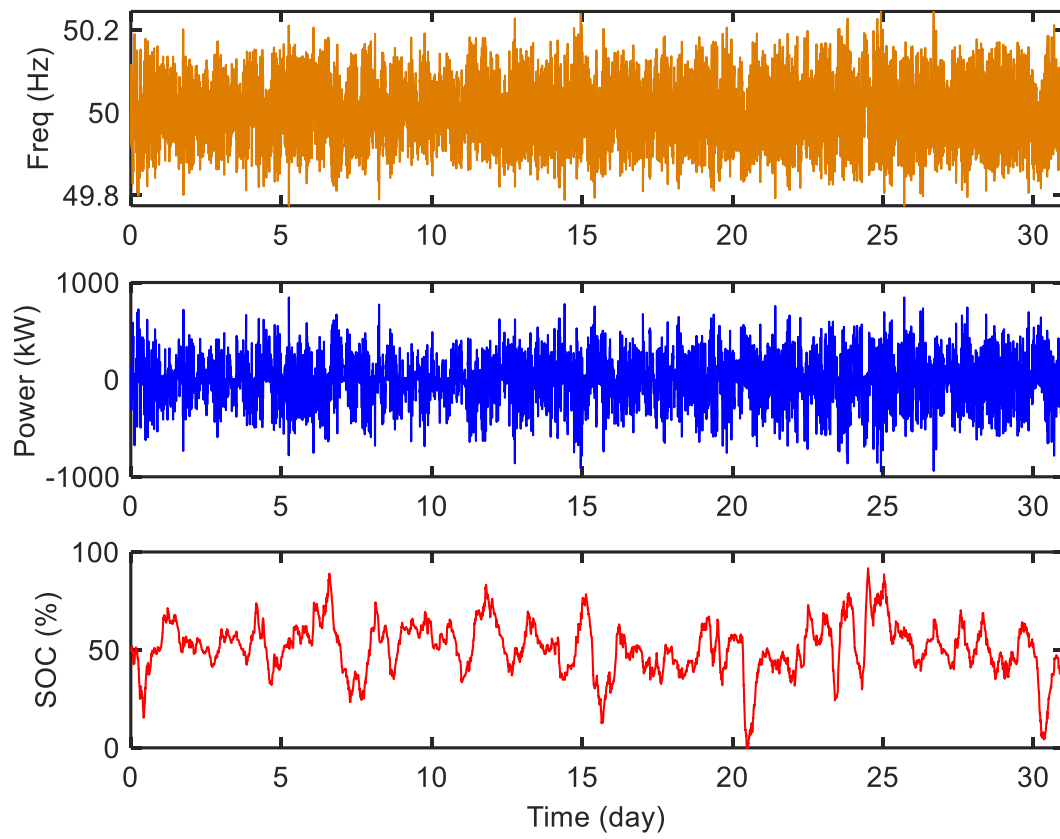


Fig. B.5 Simulation results of the EFR-A4 ( $Kp = 2000$ ) with Service-2 for October 2015.



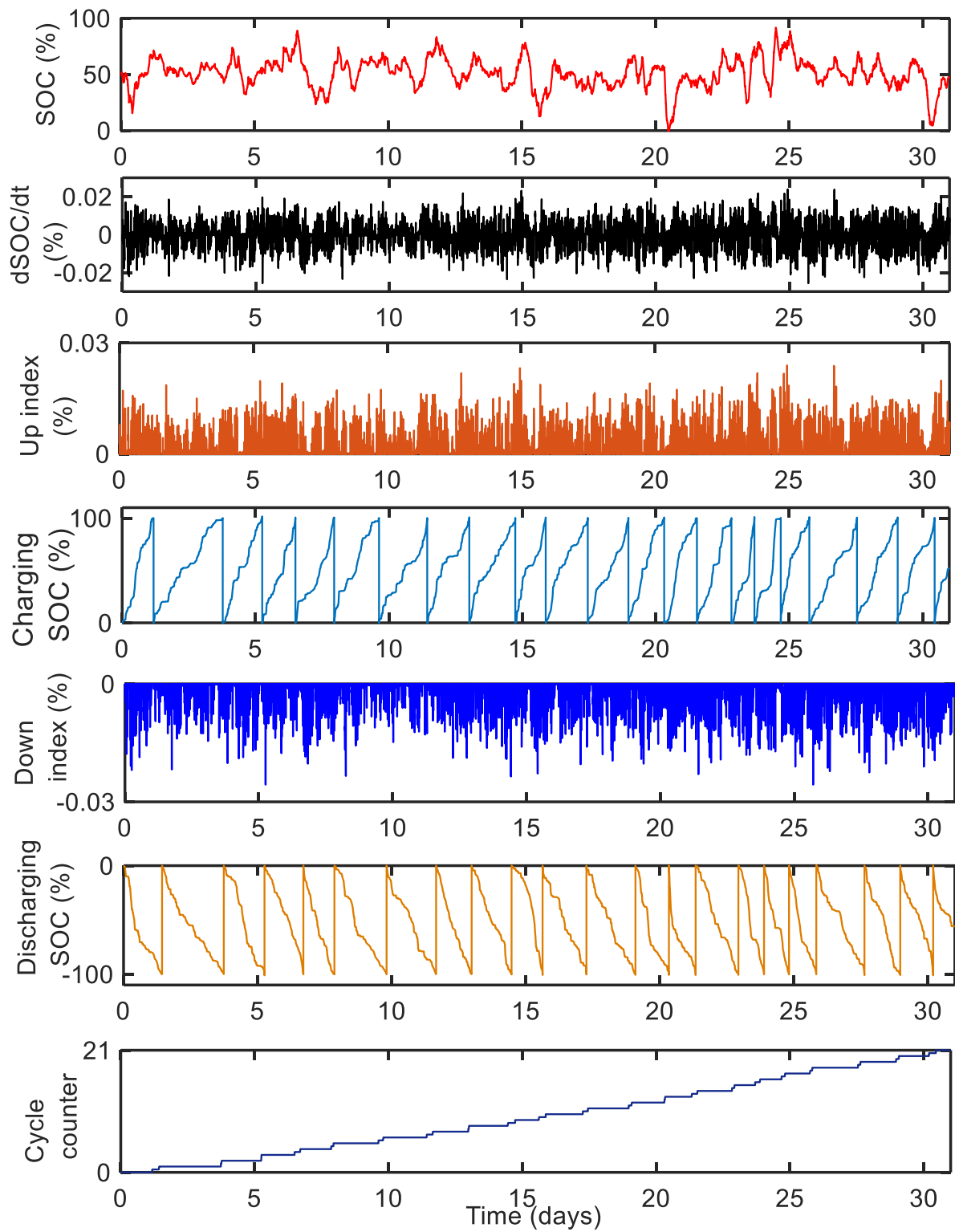


Fig. B.6 Demonstration of the basic CCM on 1-month profile of a battery SOC data set obtained by simulating the EFR-A4 ( $Kp = 2000$ ) for whole October 2015 frequency data.

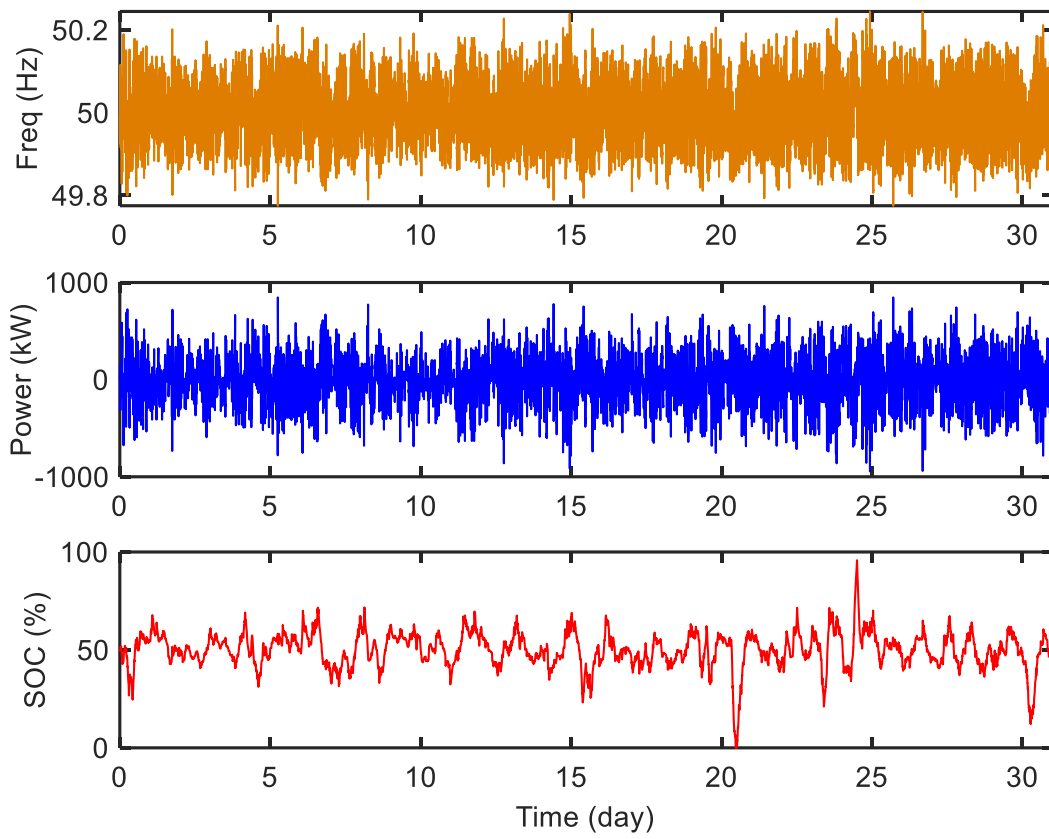


Fig. B.7 Simulation results of the EFR-A4 ( $Kp = 10000$ ) with Service-2 for October 2015.

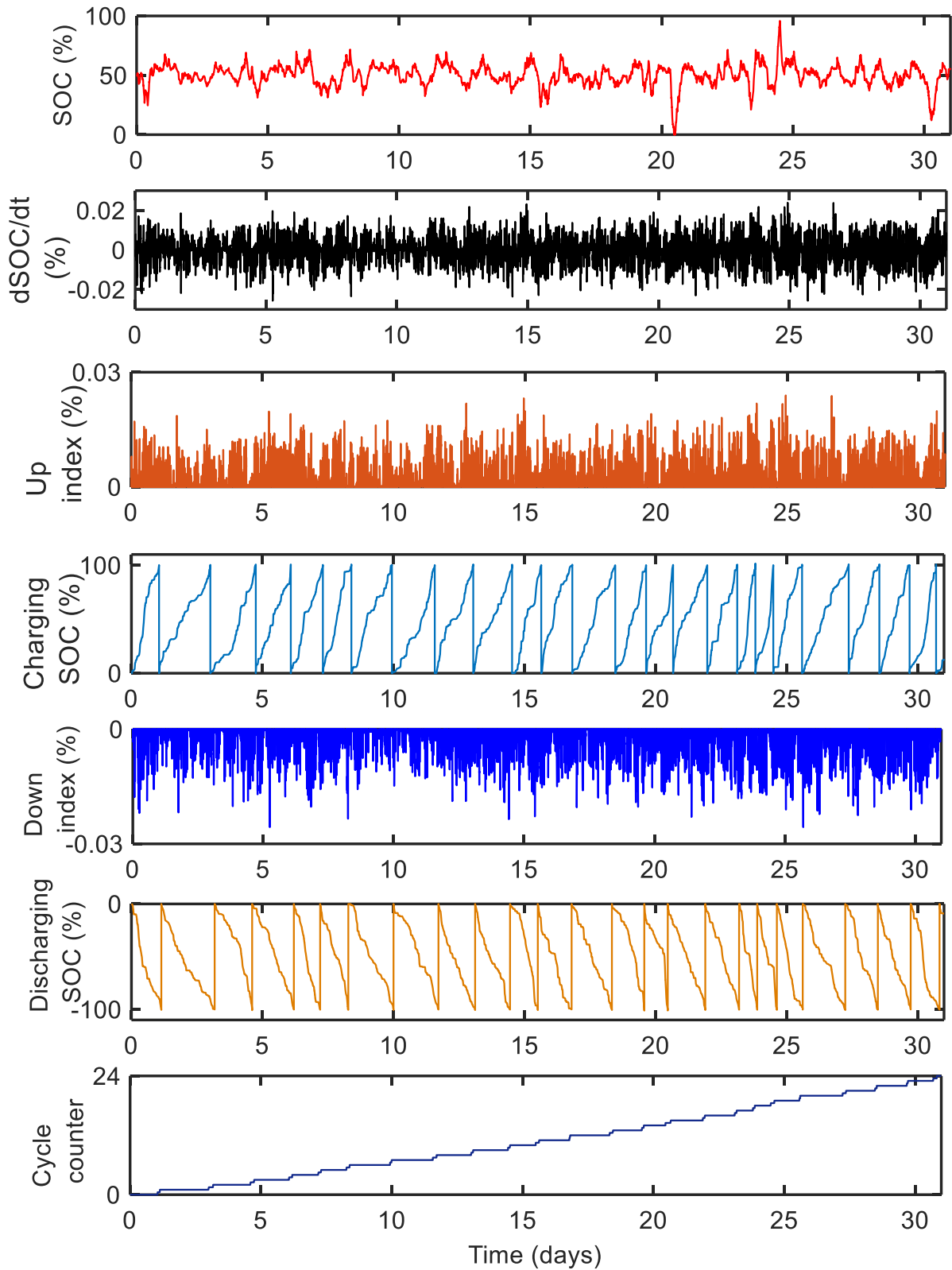


Fig. B.8 Demonstration of the basic CCM on 1-month profile of a battery SOC data set obtained by simulating the EFR-A4 ( $Kp = 10000$ ) for whole October 2015 frequency data.

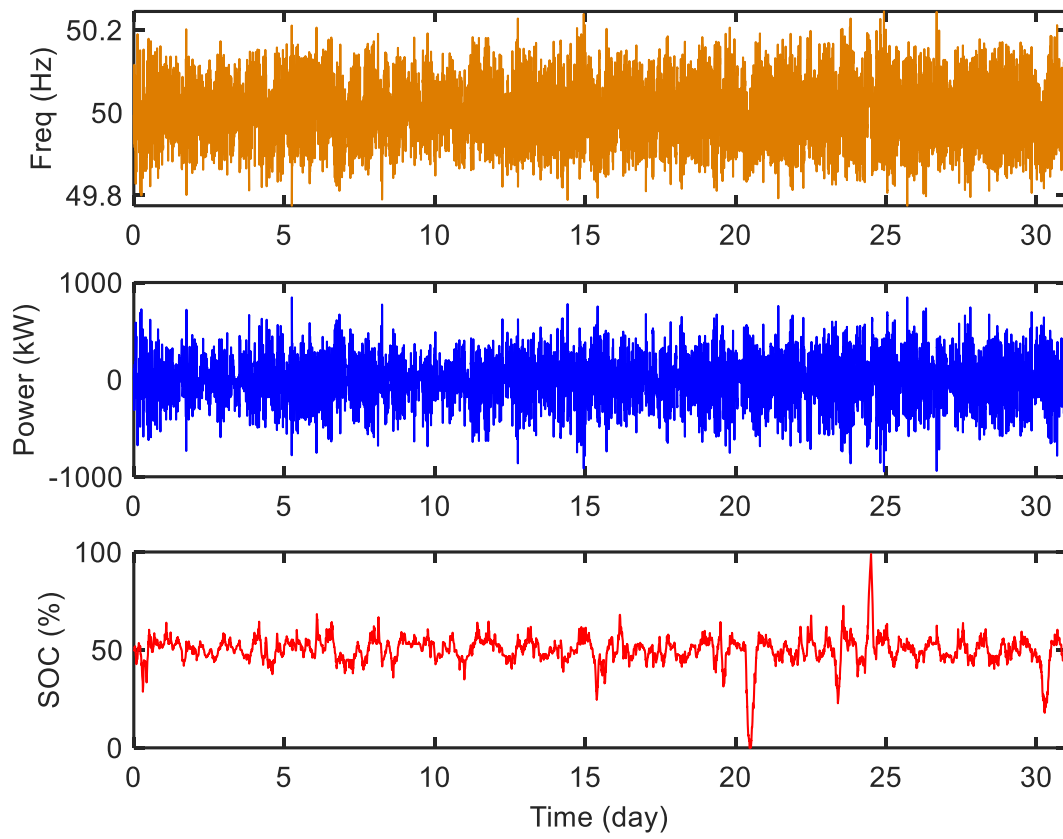


Fig. B.9 Simulation results of the EFR-A4 ( $Kp = 100000$ ) with Service-2 for October 2015.

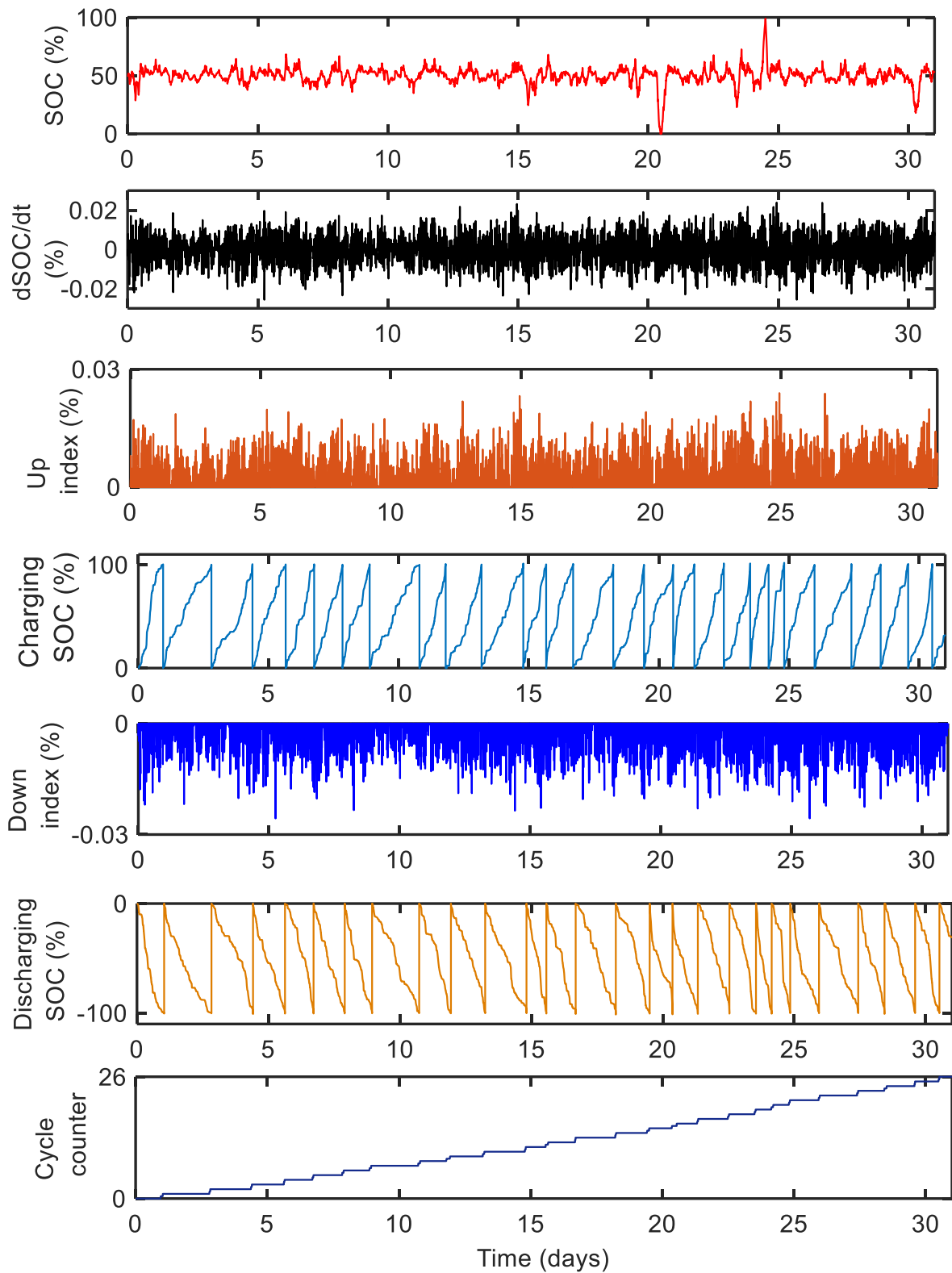


Fig. B.10 Demonstration of the basic CCM on 1-month profile of a battery SOC data set obtained by simulating the EFR-A4 ( $Kp = 100000$ ) for whole October 2015 frequency data.

## B.1 Fast Battery CCM Considering SOC and C-rate effect on Battery Lifetime

### A. EFR-A1 Results for October 2015

Table B.1 Number of cycles obtained from the fast cycle counting method considering SOC and C-rate effect for EFR-A1 for October 2015 frequency data

		C-rate					
		0.1	0.2	0.4	0.6	0.8	1
SOC (%)	10	0.03176	0.08897	0.05415	0.003499	0	0
	20	0.009354	0.02281	0.0738	0.00559	0	0
	30	0.07636	0.2257	0.2241	0.06883	0.00216	0
	40	0.1782	0.6087	0.723	0.2022	0.01163	0.0005625
	50	3.186	8.626	9.047	2.23	0.1693	0.003902
	60	2.409	7.226	9.249	2.508	0.2179	0.01754
	70	0.1026	0.4928	0.665	0.2053	0.02576	0.003105
	80	0.01563	0.04898	0.1061	0.02974	0	0
	90	0.009212	0.04938	0.03559	0.01201	0.005155	0
	100	0.0114	0.02604	0.0555	0	0	0

### B. EFR-A2 Results for October 2015

Table B.2 Number of cycles obtained from the fast cycle counting method considering SOC and C-rate effect for EFR-A2 for October 2015 frequency data

		C-rate					
		0.1	0.2	0.4	0.6	0.8	1
SOC (%)	10	0	0	0	0	0	0
	20	0	0	0	0	0	0
	30	0	0	0	0	0	0
	40	0.07812	0.2915	0.3179	0.09971	0.003971	0
	50	2.321	6.439	7.114	1.773	0.1569	0.00729
	60	1.739	4.943	6.891	2.015	0.1798	0.01164
	70	0.03111	0.1356	0.1763	0.03994	0.009931	0.003105
	80	0	0	0	0	0	0
	90	0	0	0	0	0	0
	100	0	0	0	0	0	0

C. EFR-A3 Results for October 2015

Table B.3 Number of cycles obtained from the fast cycle counting method considering SOC and C-rate effect for EFR-A3 for October 2015 frequency data

		C-rate					
		0.1	0.2	0.4	0.6	0.8	1
SOC (%)	10	0	0	0	0	0	0
	20	0	0	0	0	0	0
	30	0	0	0	0	0	0
	40	0.05715	0.2567	0.201	0.07425	0.003886	0
	50	2.374	7.006	7.149	1.8	0.151	0.005948
	60	1.799	5.624	6.739	1.891	0.1637	0.01152
	70	0.008685	0.07292	0.04351	0.01832	0.01006	0.003105
	80	0	0	0	0	0	0
	90	0	0	0	0	0	0
	100	0	0	0	0	0	0

D. EFR-A4 Results for October 2015

Table B.4 Number of cycles obtained from the fast cycle counting method considering SOC and C-rate effect for EFR-A4 ( $Kp = 2000$ ) for October 2015 frequency data

		C-rate					
		0.1	0.2	0.4	0.6	0.8	1
SOC (%)	10	0.2043	0.07024	0.09051	0.01362	0	0
	20	0.1452	0.08897	0.1765	0.05661	0.00546	0
	30	0.3135	0.2092	0.3616	0.06746	0	0
	40	0.7645	0.6639	1.064	0.3093	0.02765	0.001137
	50	0.9541	1.523	2.199	0.5923	0.07313	0.0006767
	60	1.067	1.564	2.238	0.5408	0.05314	0.002857
	70	1.31	0.9027	1.374	0.4065	0.04811	0.004883
	80	0.6628	0.2893	0.5515	0.1617	0.04635	0.004157
	90	0.172	0.05476	0.135	0.04978	0.009987	0
	100	0.009928	0.001223	0.006523	0	0	0

Table B.5 Number of cycles obtained from the fast cycle counting method considering SOC and C-rate effect for EFR-A4 ( $Kp = 10000$ ) for October 2015 frequency data

		C-rate					
		0.1	0.2	0.4	0.6	0.8	1
SOC (%)	10	0.03026	0.08572	0.05565	0.006381	0	0
	20	0.0436	0.1072	0.1458	0.0198	0.001908	0
	30	0.09054	0.3691	0.185	0.06464	0.002418	0.0005625
	40	0.9854	0.6803	0.7674	0.234	0.009956	0
	50	1.915	1.962	2.967	0.7287	0.1016	0.002049
	60	2.428	2.214	3.049	0.7792	0.06264	0.003147
	70	1.213	1.076	1.031	0.3479	0.08531	0.007951
	80	0.02155	0.08788	0.07411	0.01284	0	0
	90	0.006609	0.04343	0.05115	0.004684	0	0
	100	0.01039	0.02119	0.03217	0	0	0

Table B.6 Number of cycles obtained from the fast cycle counting method considering SOC and C-rate effect for EFR-A4 ( $Kp = 100000$ ) for October 2015 frequency data

		C-rate					
		0.1	0.2	0.4	0.6	0.8	1
SOC (%)	10	0.03299	0.08907	0.04997	0.006381	0	0
	20	0.01071	0.02924	0.09107	0.004952	0	0
	30	0.07966	0.2282	0.2215	0.06652	0.002332	0
	40	0.1313	0.4996	0.6424	0.1509	0.004221	0.0005625
	50	2.434	3.121	3.31	0.8153	0.1014	0.001827
	60	2.781	4.104	4.532	1.048	0.1351	0.00903
	70	0.09885	0.4343	0.6156	0.2037	0.02345	0.002291
	80	0.006182	0.03111	0.07945	0.01462	0	0
	90	0.009212	0.0489	0.03588	0.01221	0.005155	0
	100	0.0114	0.02653	0.05643	0.0009971	0	0



*E. DFFR Algorithm Results for October 2015*

Table B.7 Number of cycles obtained from the fast cycle counting method considering SOC and C-rate effect for DFFR Algorithm for October 2015 frequency data

		<b>C-rate</b>					
		0.1	0.2	0.4	0.6	0.8	1
<b>SOC (%)</b>	10	0.4621	0.7223	0.3843	0.001698	0	0
	20	0.6574	1.278	0.5824	0.004454	0	0
	30	0.9776	1.854	0.7466	0.001886	0	0
	40	1.097	1.766	0.8723	0.003599	0	0
	50	1.491	2.522	1.207	0.01542	0	0
	60	1.411	2.383	0.9675	0.006787	0	0
	70	1.043	1.613	0.5797	0.001308	0	0
	80	0.9255	1.507	0.5563	0.007388	0	0
	90	0.9291	1.372	0.6237	0.006254	0	0
	100	0.6695	0.9592	0.4217	0.002303	0	0

## Appendix C LabVIEW Software Coding of EFR-A1 used in WESS

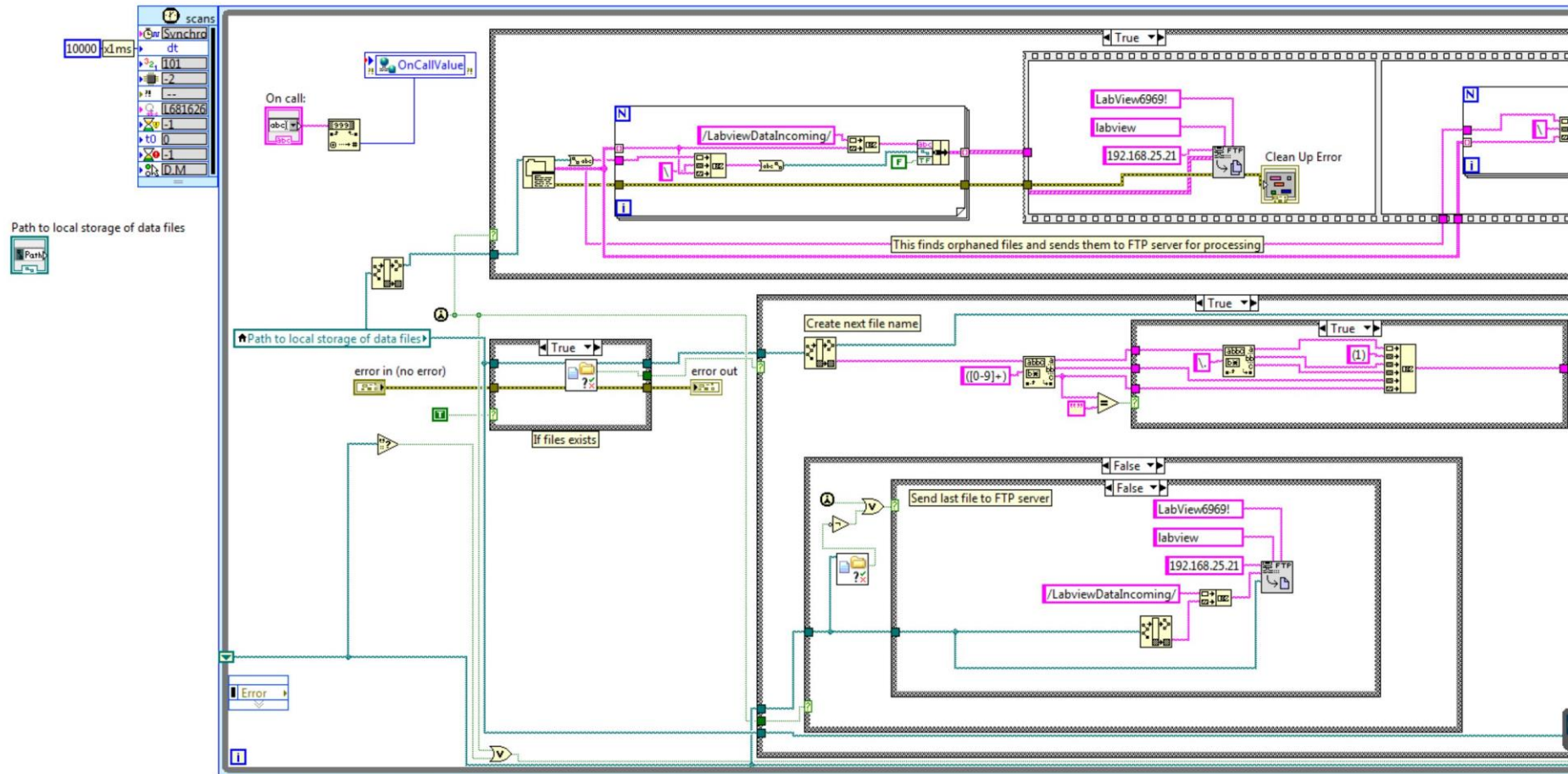


Fig. C.1 Demonstration of LabVIEW code of EFR-A1 (oneA)

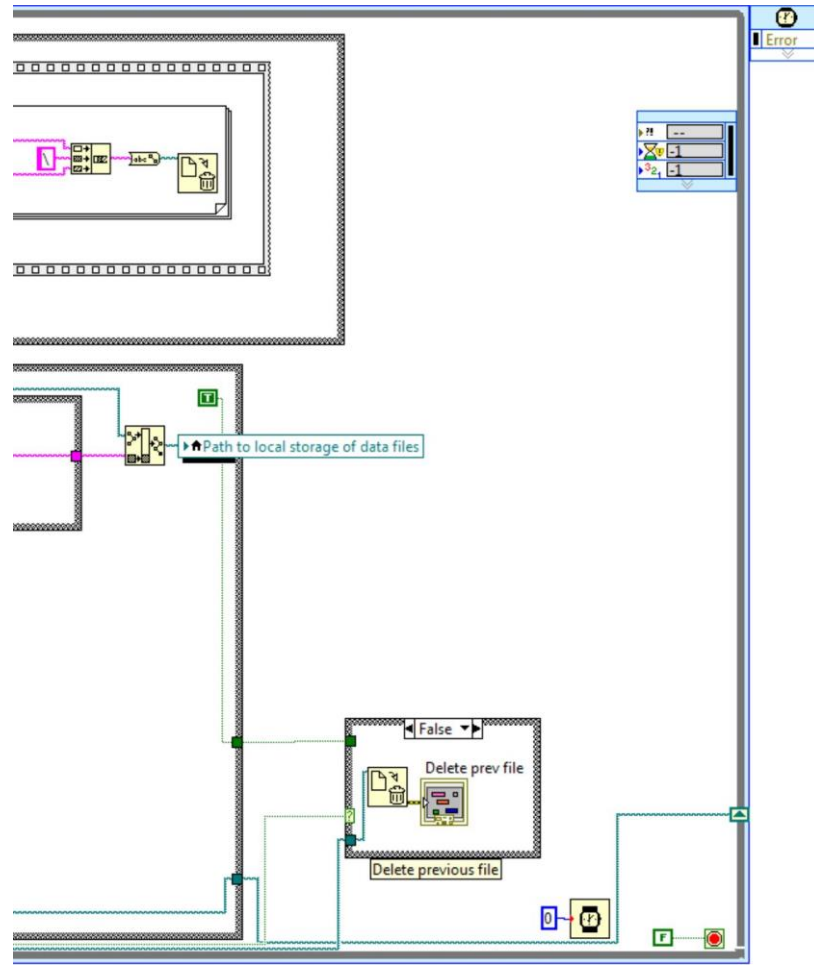


Fig. C.2 Demonstration of LabVIEW code of EFR-A1 (oneB)

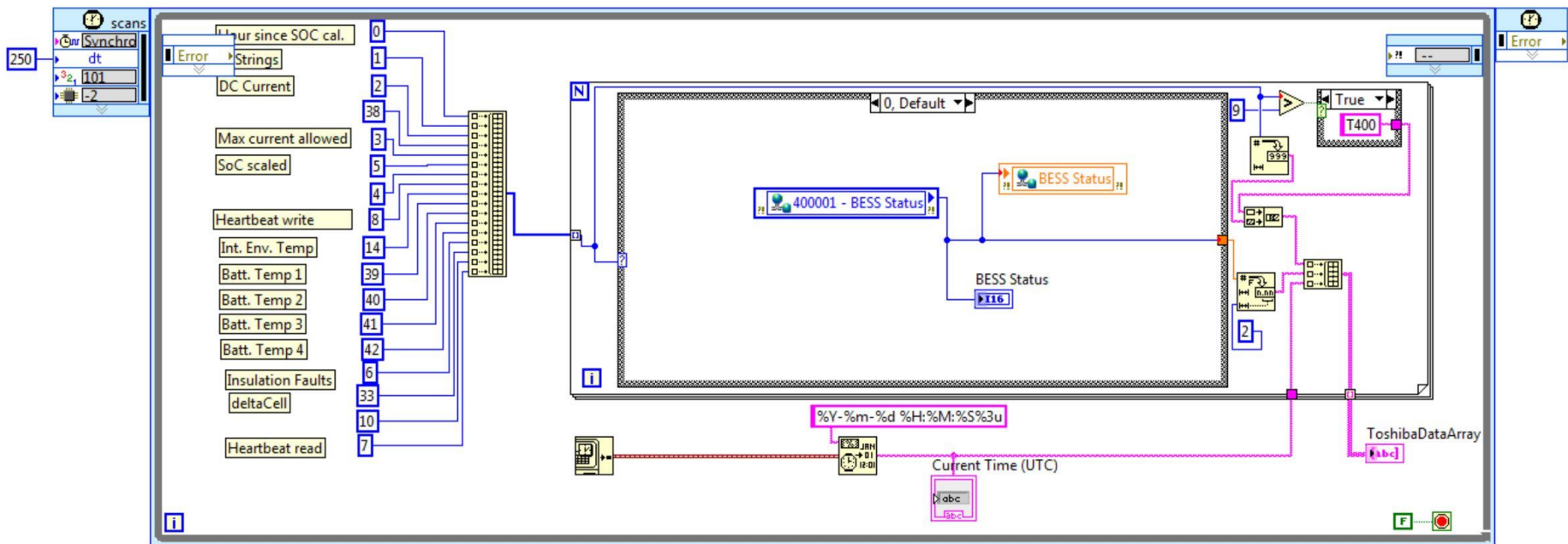


Fig. C.3 Demonstration of LabVIEW code of EFR-A1 (two)

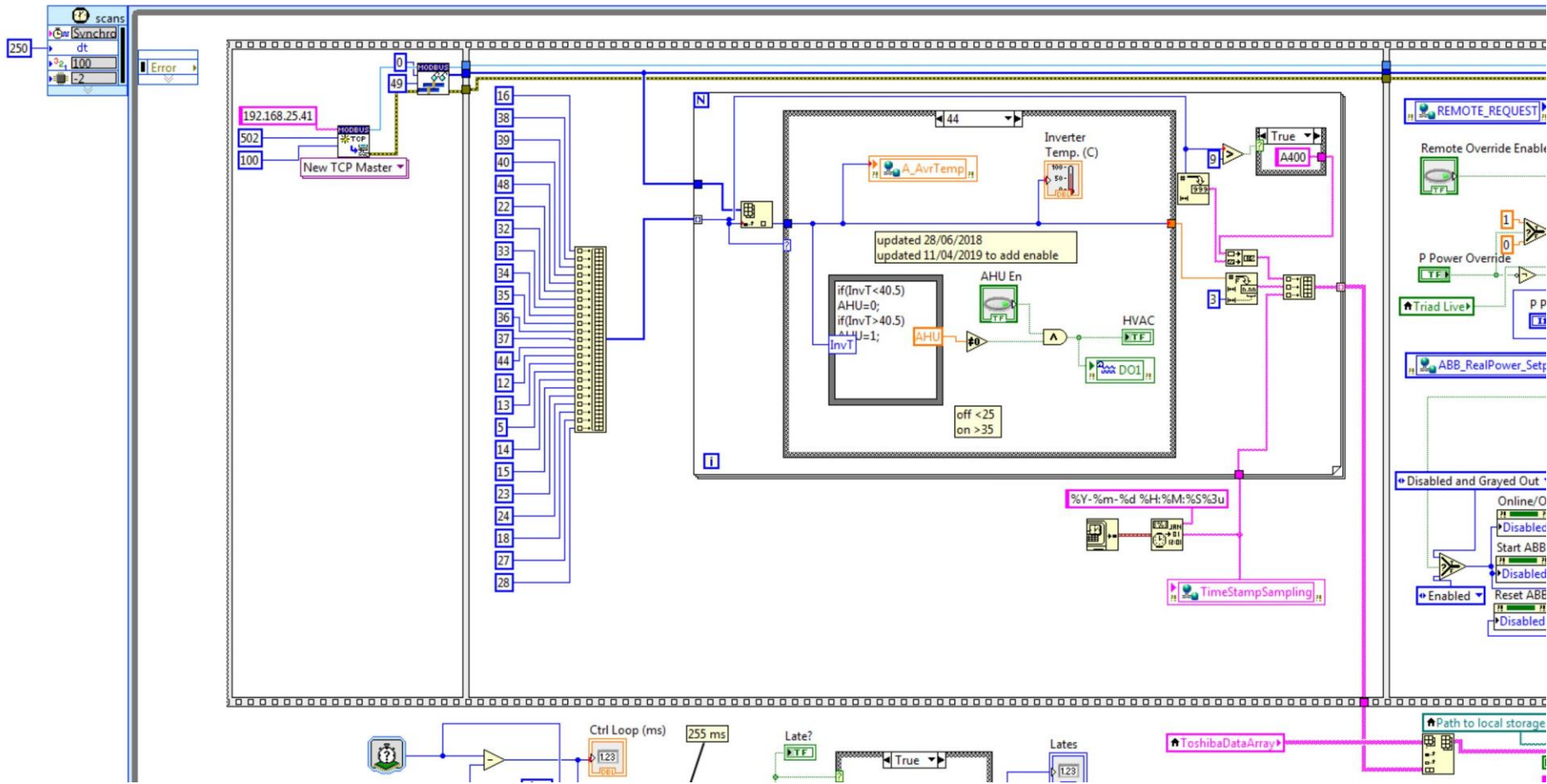


Fig. C.4 Demonstration of LabVIEW code of EFR-A1 (threeA)

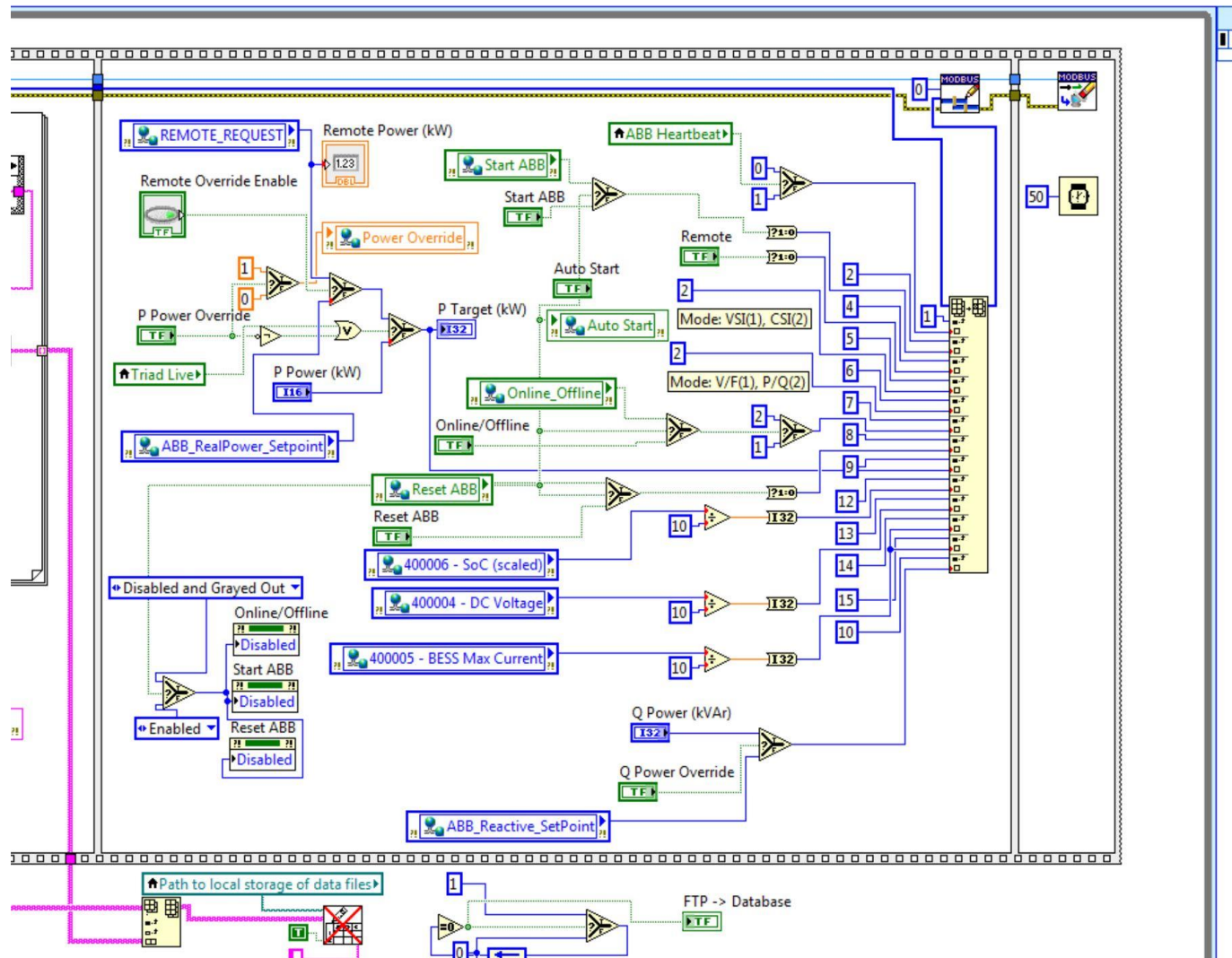


Fig. C.5 Demonstration of LabVIEW code of EFR-A1 (threeB)

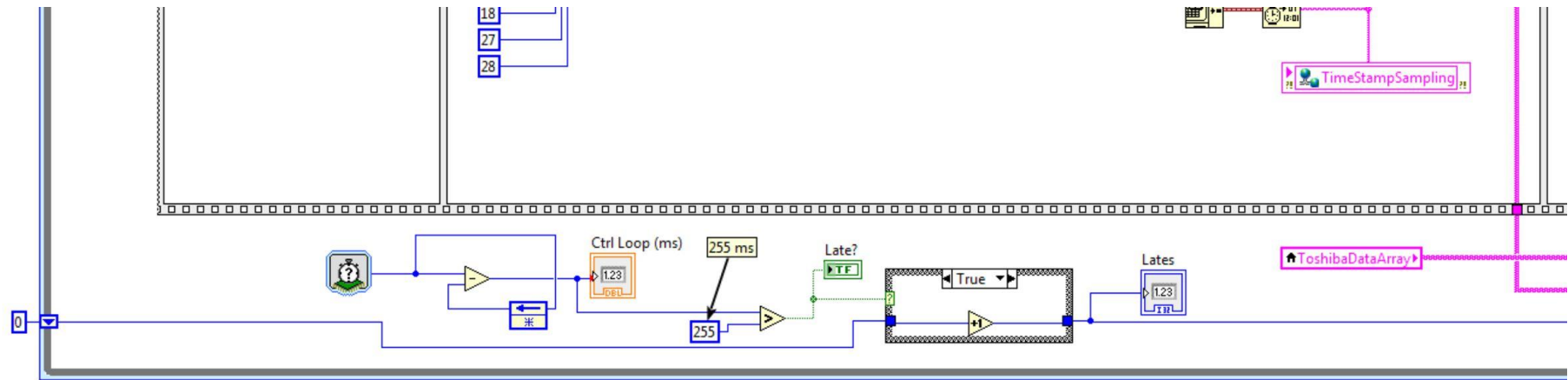


Fig. C.6 Demonstration of LabVIEW code of EFR-A1 (threeC)

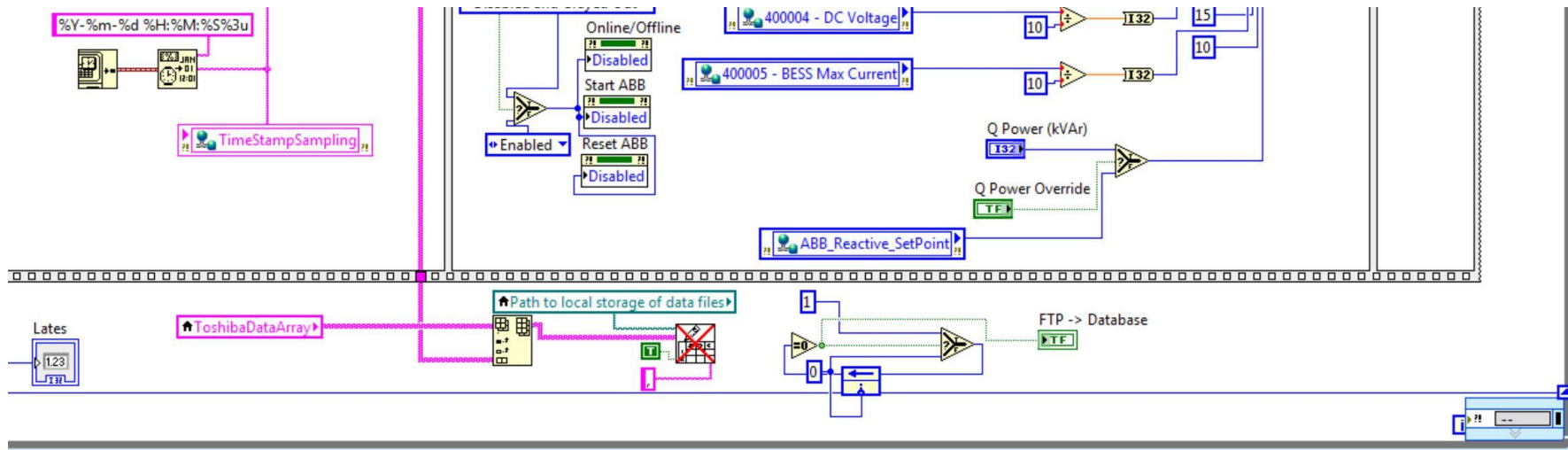


Fig. C.7 Demonstration of LabVIEW code of EFR-A1 (threeD)

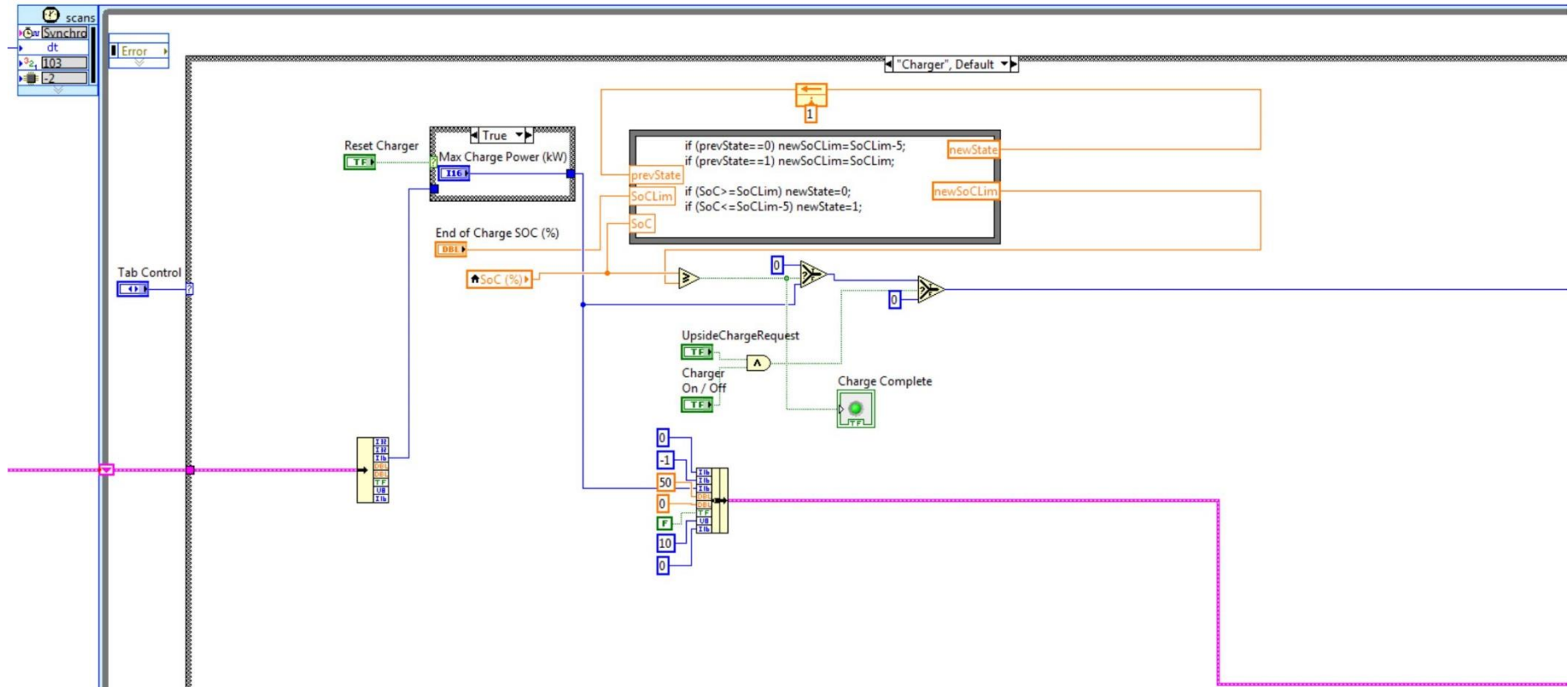


Fig. C.8 Demonstration of LabVIEW code of EFR-A1 (fourA)



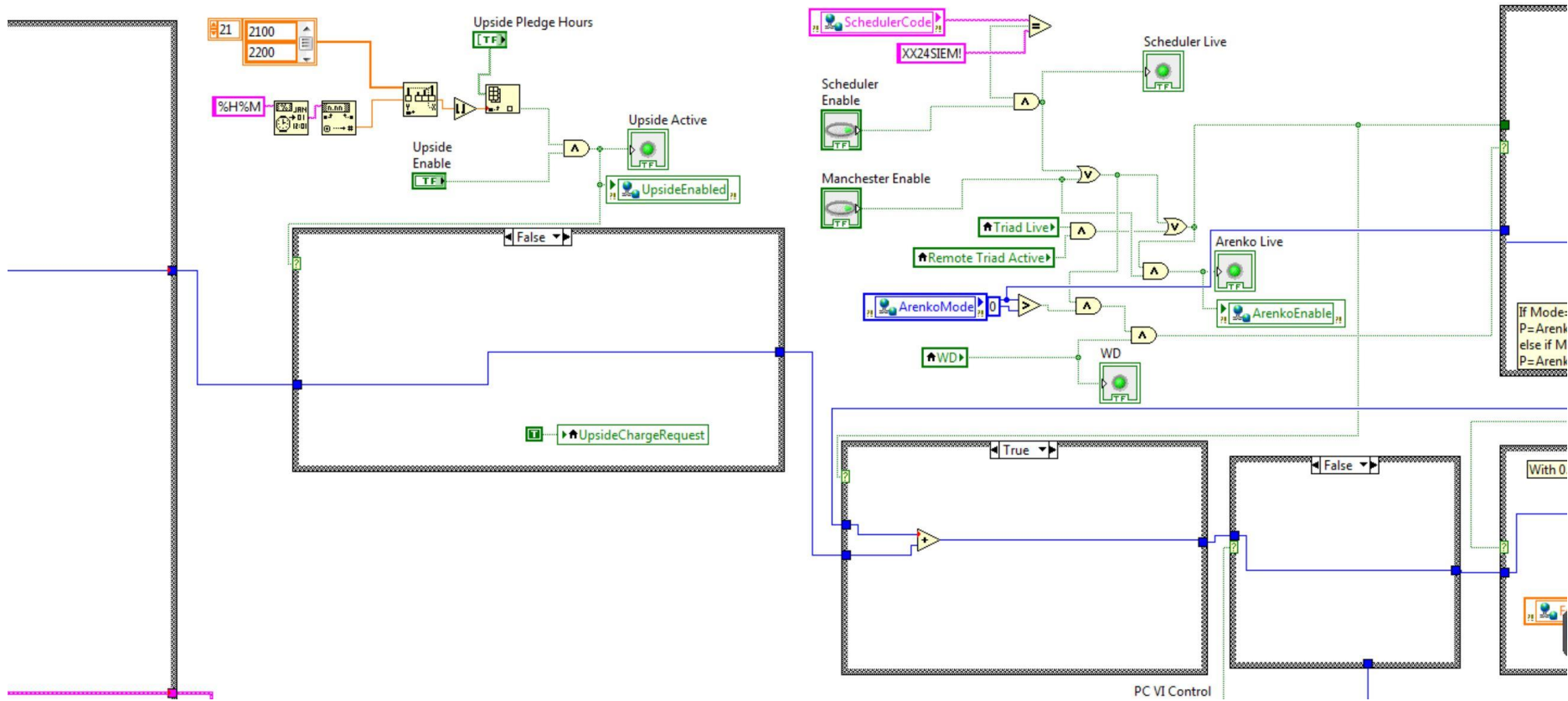


Fig. C.9 Demonstration of LabVIEW code of EFR-A1 (fourB)

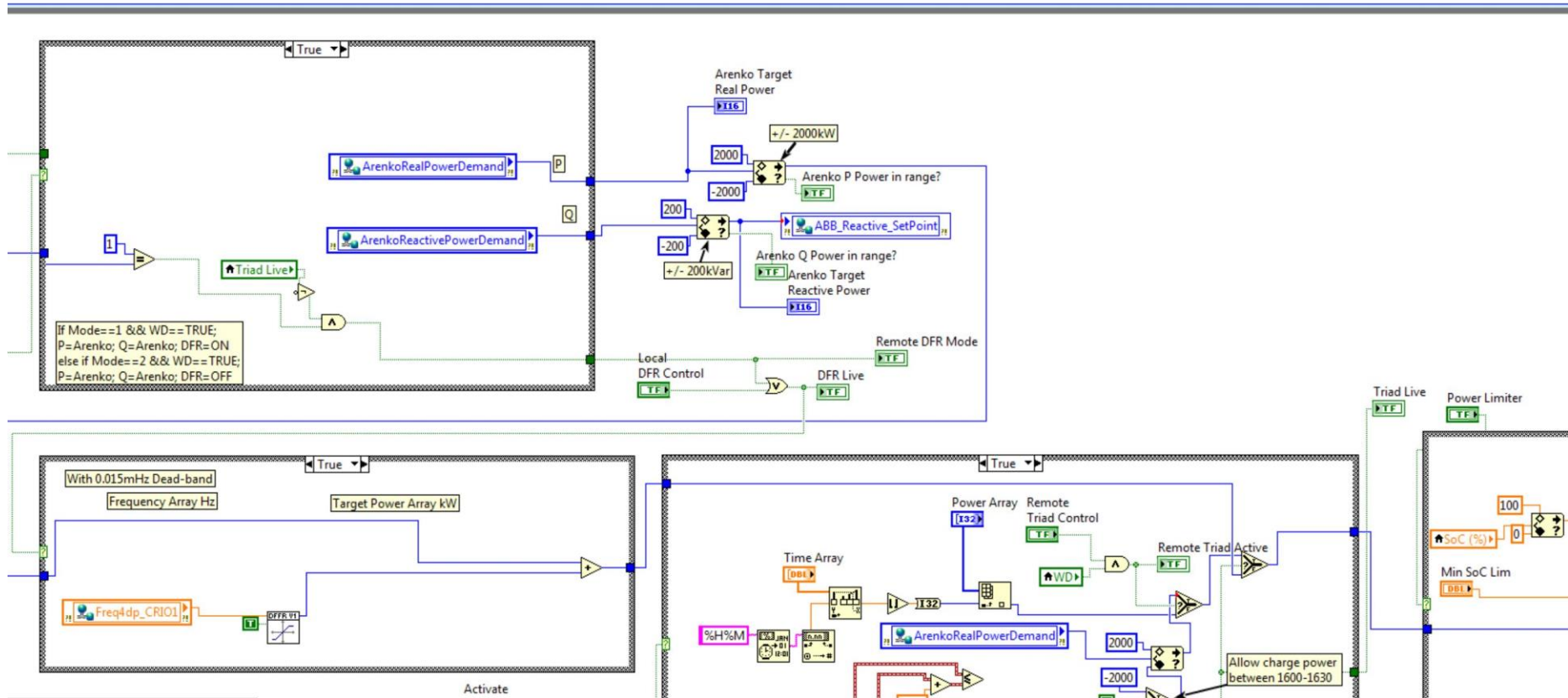


Fig. C.10 Demonstration of LabVIEW code of EFR-A1 (fourC)

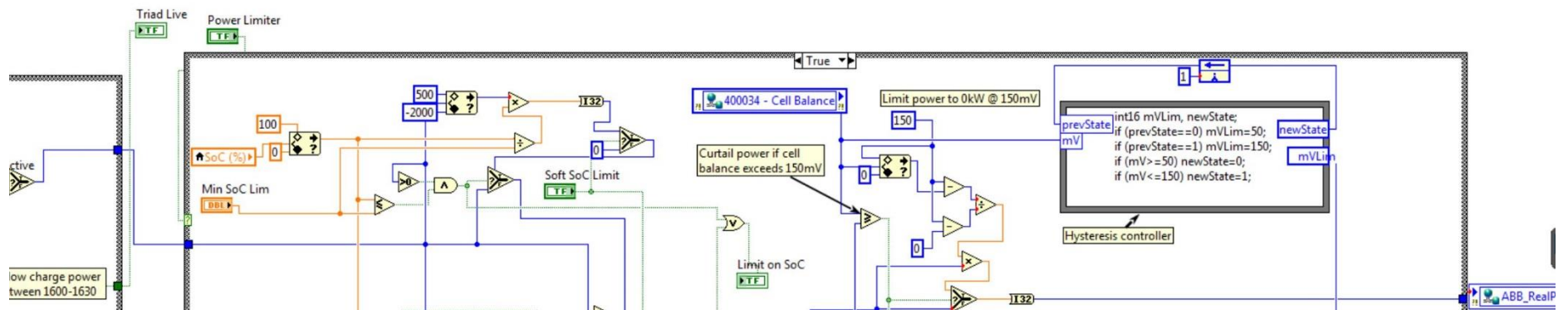


Fig. C.11 Demonstration of LabVIEW code of EFR-A1 (fourD)

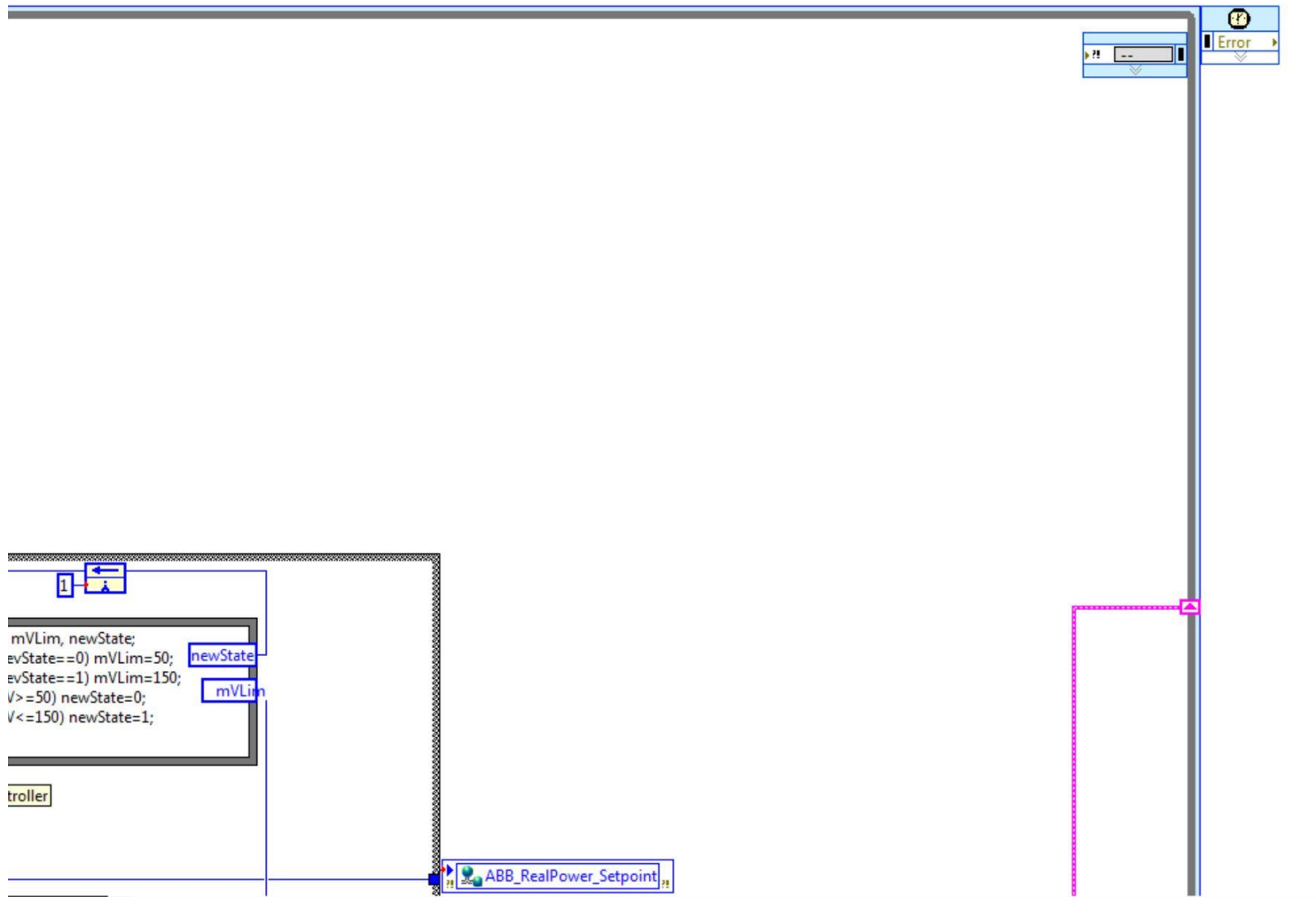


Fig. C.12 Demonstration of LabVIEW code of EFR-A1 (fourE)

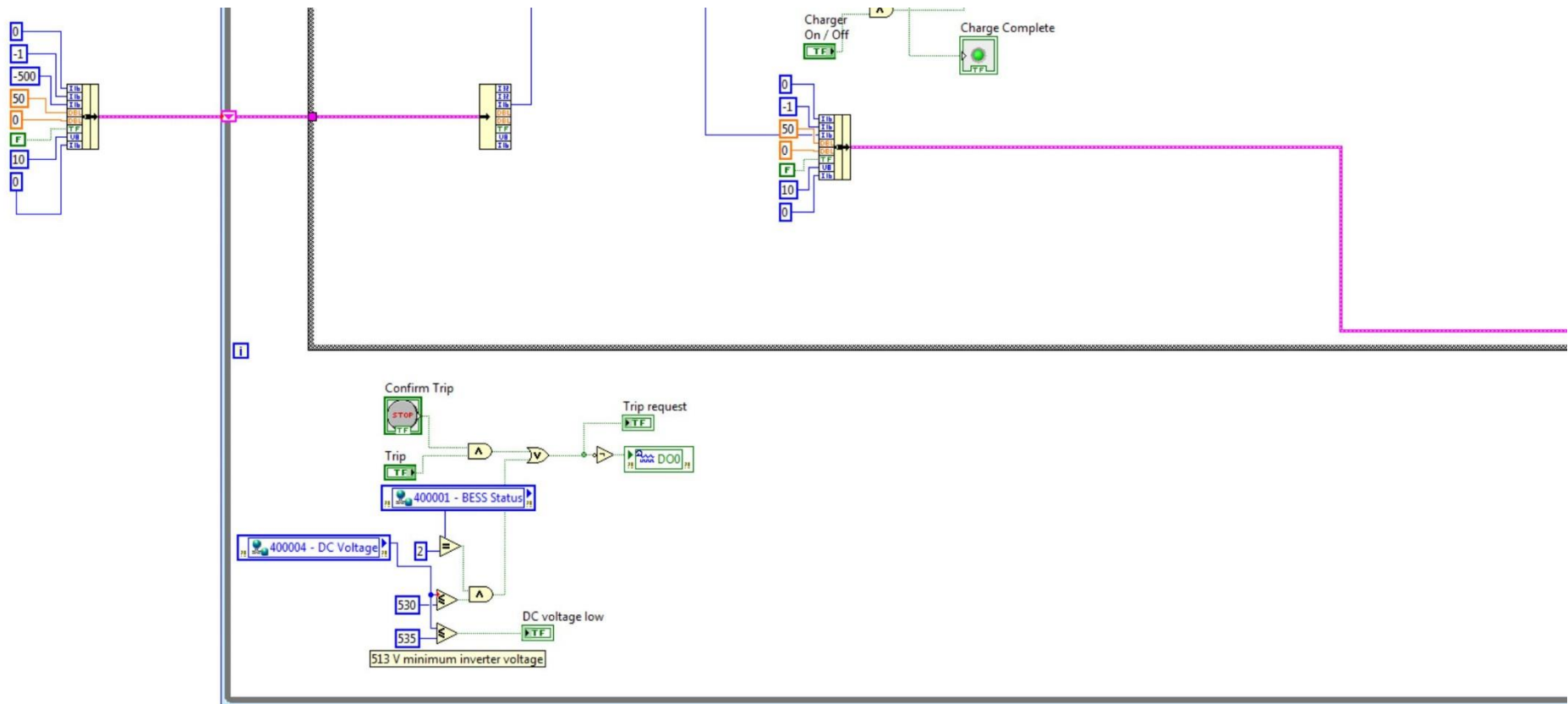


Fig. C.13 Demonstration of LabVIEW code of EFR-A1 (fourF)

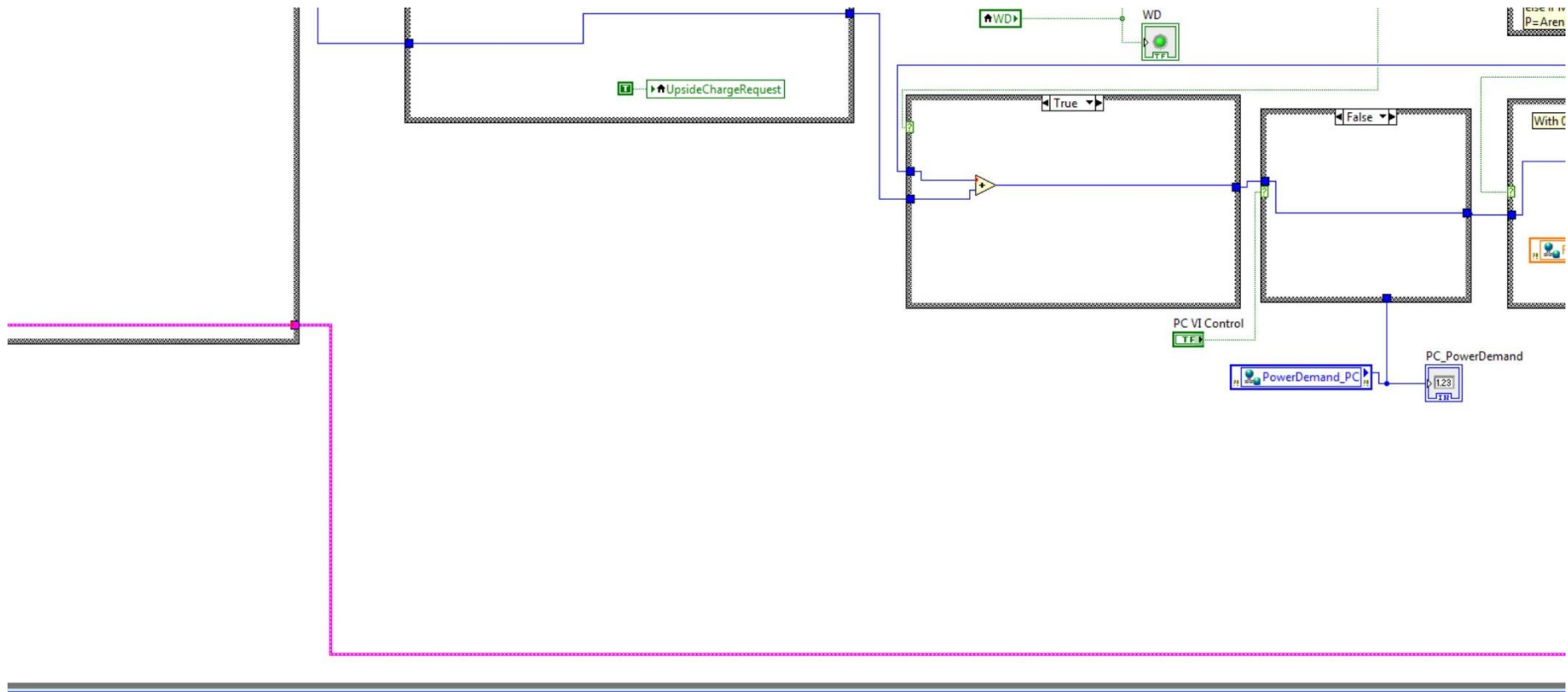


Fig. C.14 Demonstration of LabVIEW code of EFR-A1 (fourG)

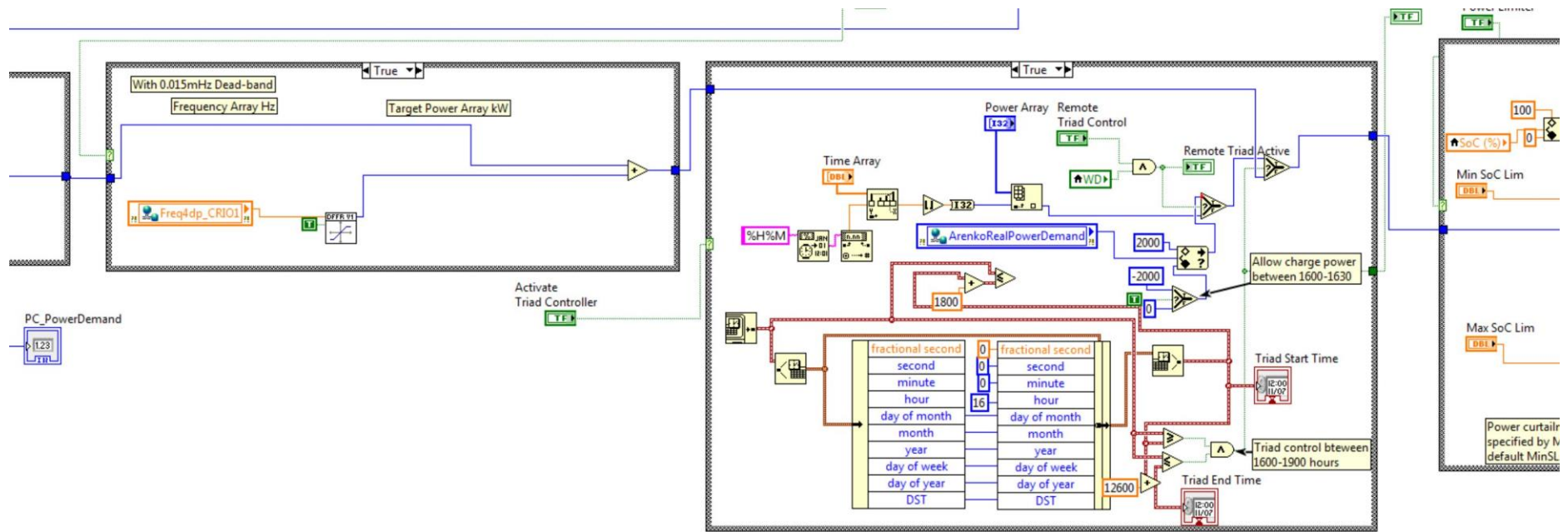


Fig. C.15 Demonstration of LabVIEW code of EFR-A1 (fourH)

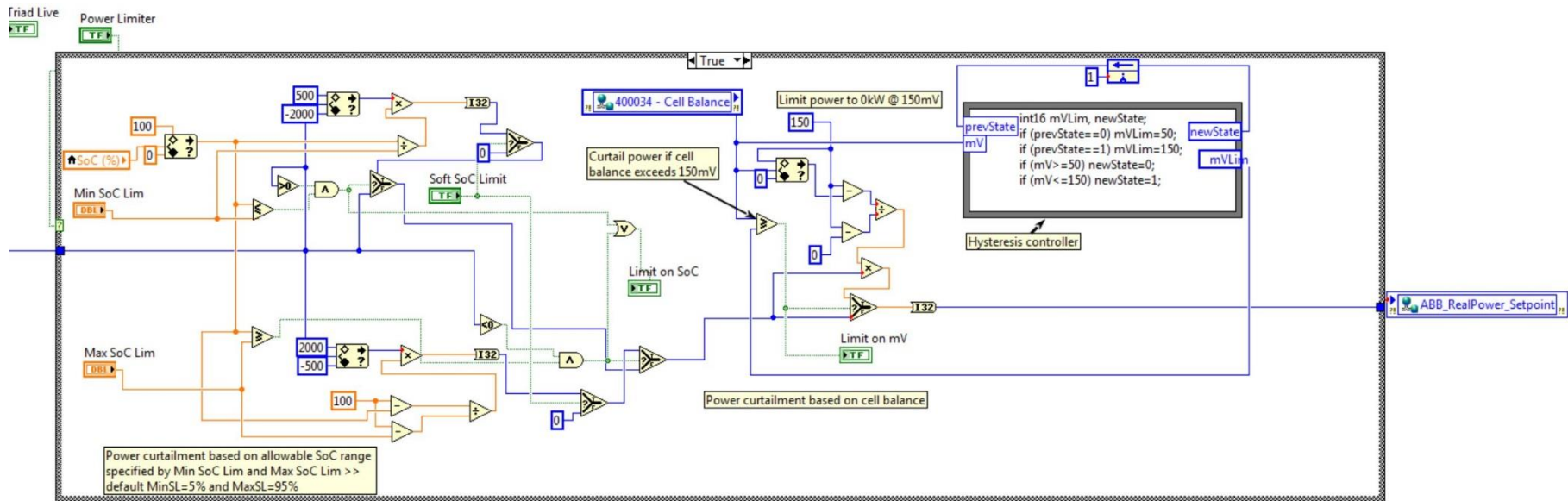


Fig. C.16 Demonstration of LabVIEW code of EFR-A1 (fourI).



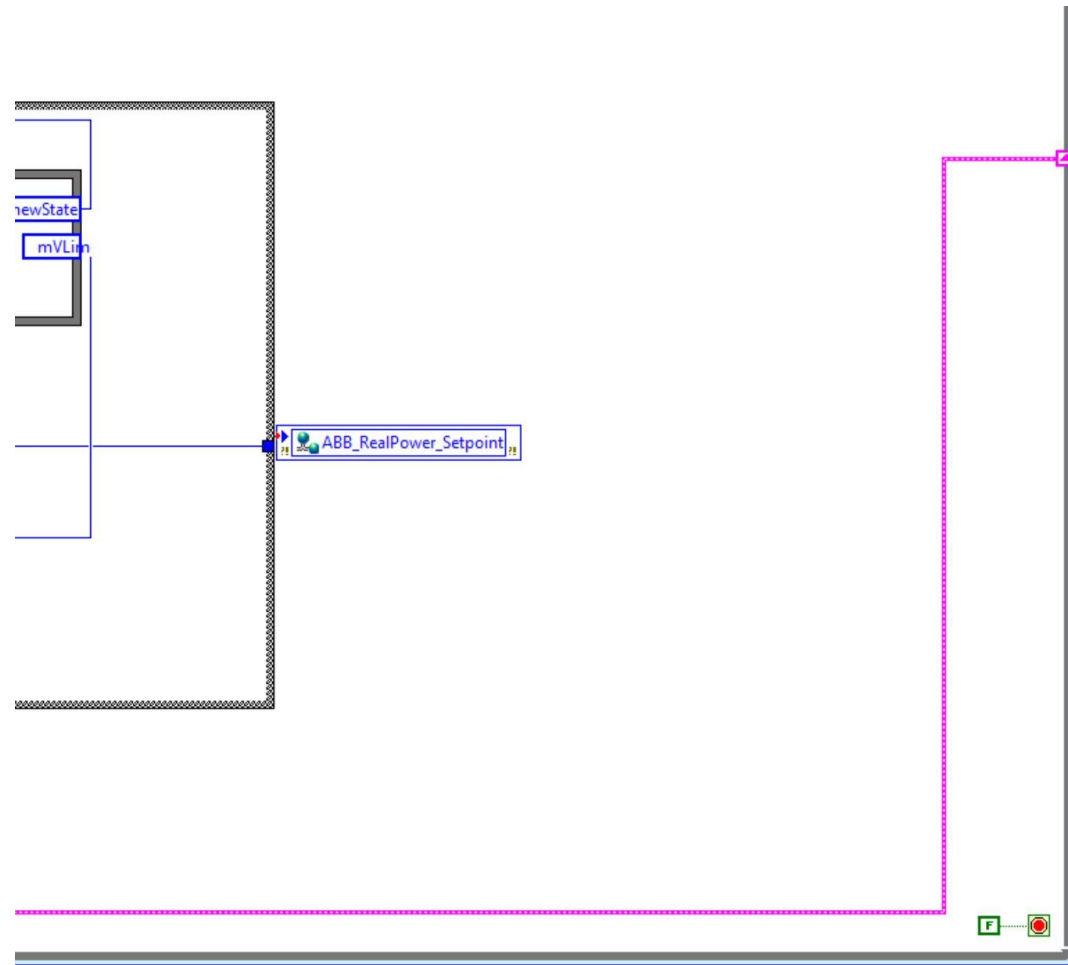


Fig. C.17 Demonstration of LabVIEW code of EFR-A1 (fourJ).

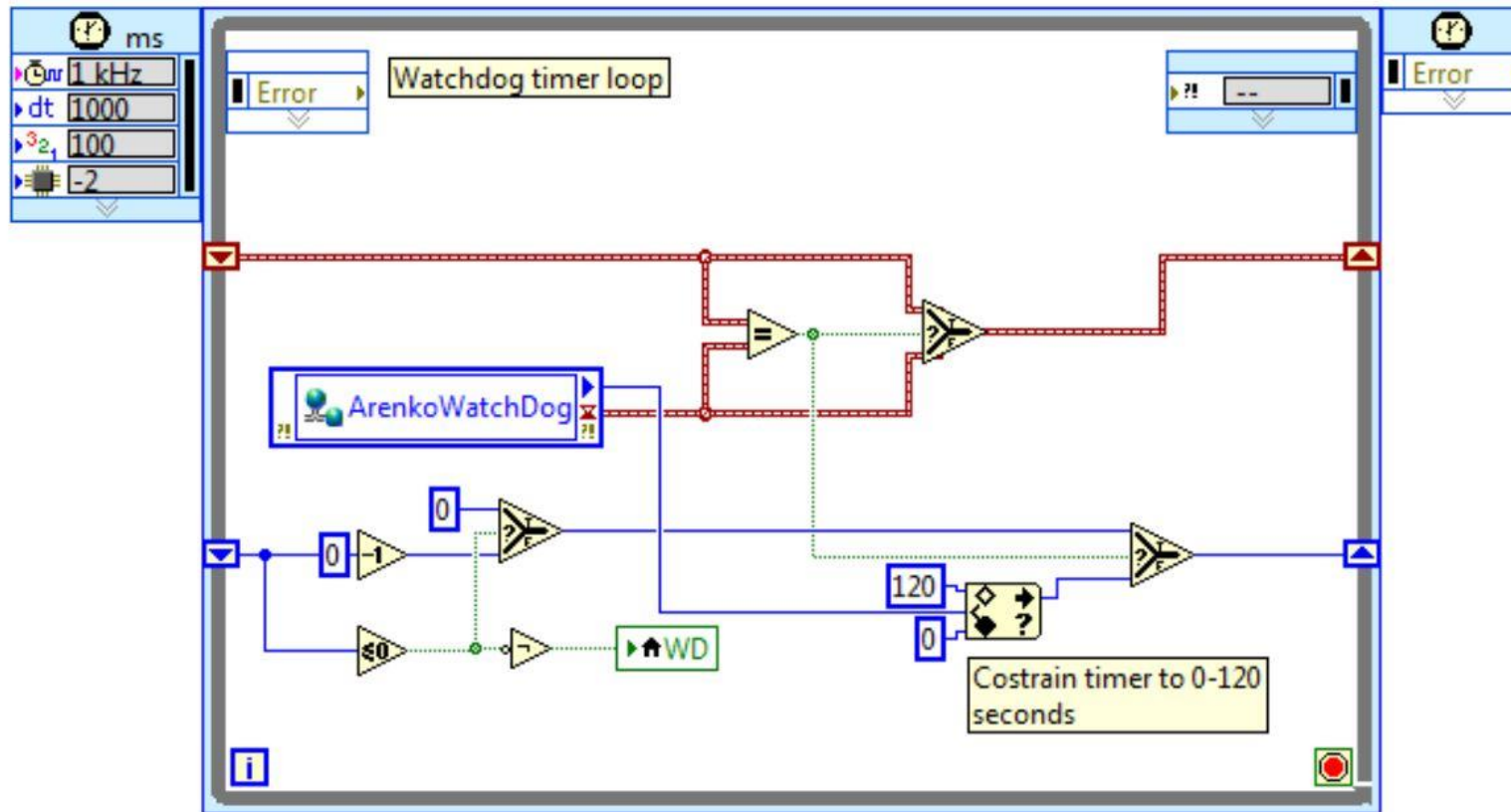


Fig. C.18 Demonstration of LabVIEW code of EFR-A1 (five).